

Diss. ETH Nr. 13182

Chemical and Nanotopographical Substrate Design for AFM Analysis of Proteins in Supported Biomembranes

A dissertation submitted to the
SWISS FEDERAL INSTITUTE OF TECHNOLOGY ZURICH
for the degree of
Doctor of Natural Sciences

presented by

FRANK G. ZAUGG
Dipl. Nat. Sciences, ETH Zürich

Born January 3, 1972
Citizen of Röthenbach i.E., Switzerland

Prof. Dr. N. D. Spencer, examiner
Prof. Dr. G. Semenza, co-examiner
Prof. Dr. U. W. Suter, co-examiner

Zürich, 1999

Contents

CONTENTS	1
ABBREVIATIONS	5
SUMMARY	8
ZUSAMMENFASSUNG	10
<u>INTRODUCTION</u>	<u>12</u>
GETTING A VISIBLE UNDERSTANDING OF BIOLOGY AT THE MICRO AND NANOSCALE	12
ATOMIC FORCE MICROSCOPY (AFM) FOR BIOLOGICAL APPLICATIONS	14
BIOLOGICAL MEMBRANES	17
SURFACE DESIGN FOR THE PROPER PRESENTATION OF BIOLOGICAL MEMBRANE/PROTEIN SYSTEMS FOR ATOMIC FORCE MICROSCOPY	19
THE AIM AND OUTLINE OF THE WORK	23
LITERATURE ON THE TOPIC “AFM OF BILAYER MEMBRANES“	26
<u>MATERIALS AND METHODS</u>	<u>29</u>
CHARACTERIZATION METHODS	30
GENERAL PROCEDURES	35
<u>MICRO- AND NANOSTRUCTURING OF SURFACES</u>	<u>42</u>
A) MICROSTRUCTURING	42
PHOTOLITHOGRAPHY	42
MICRO-CONTACT PRINTING (μ CP)/ETCHING	47
B) NANOSTRUCTURING	52
NANOSPHERES	54
POLYCARBONATE FILTERS	66

CHEMICAL MODIFICATION OF SURFACES	68
SELF-ASSEMBLED MONOLAYERS	69
ALKANETHIOLS ON GOLD	69
MIXED SAMs	74
OCTADECYLPHOSPHATES	77
HYDROSILANES	78
OTHERS	80
SILANIZATION	80
PASSIVATION	81
OXYGEN-PLASMA TREATMENT	83
PIRANHA TREATMENT	83
CHEMICAL PATTERNING	85
OVERVIEW OF TECHNIQUES	85
MICROFLUIDIC PATTERNING	85
MICRO-CONTACT PRINTING	87
THE TECHNIQUE	87
USING MICRO-CONTACT PRINTED SUBSTRATES FOR THE COVALENT IMMOBILIZATION OF BIOLOGICAL OBJECTS	90
LATEX BEADS ON CHEMICALLY PATTERNED SURFACES	92
IMMOBILIZATION OF VIRUSES ON THE PATTERNED SURFACES	94
COLLAGEN V IMMOBILIZATION	95
IMMOBILIZATION OF PEROXIDASE	96
DETERMINATION OF THE AMOUNT ALKANETHIOL TRANSFERRED BY μ CP ONTO A SUBSTRATE	100
GENERATION OF ETCH-PATTERNED SURFACES WITH IMMOBILIZED BIOMOLECULES: SAM EXCHANGE TECHNIQUE AND COLLAGEN V IMMOBILIZATION.	102
CONCLUSIONS FOR THIS CHAPTER	105
BILAYER FORMATION	107
BLACK LIPID MEMBRANES (BLM)	107

LANGMUIR BLODGETT FILMS (LB)	109
LIPOSOME FUSION	117
THE TECHNIQUE	119
REQUIREMENTS ON THE SAMPLE-HOLDER	121
VESICLE-FUSION ONTO DIFFERENT SUBSTRATES	122
BILAYER FIXATION	131
INHOMOGENEITIES ON THE SUPPORTED BILAYERS	132
BEHAVIOR OF LIPOSOMES OBTAINED BY VORTEXING AND SONICATION: MULTIWALLED VESICLES	136
CREATION OF BILAYERS AT DEFINED AREAS ON A SURFACE	138
OOCYTE MEMBRANES	140
<u>PROPERTIES OF LIPID BILAYERS ON SURFACES</u>	<u>143</u>
THE PHASE STATE AND MORPHOLOGY OF BILAYERS ADSORBED ON SUBSTRATES	143
CONTROL OF BILAYER FLUIDITY AND HEAT INDUCED MORPHOLOGIES	147
SUSPENDED BILAYERS	151
<u>INSERTION OF PROTEINS IN BILAYERS</u>	<u>159</u>
STREPTOLYSINE (SLO) AS A MODEL PROTEIN	159
REACTIVITY TESTS	162
TESTING THE RING-STRUCTURE FORMATION CAPABILITY	162
TESTING THE PORE-FORMATION CAPABILITY	167
INSERTION OF SLO IN A SUPPORTED BILAYER	169
TOPOGRAPHY OF SLO INSERTED IN THE BILAYER	172
INSERTION OF SLO IN A BILAYER BEFORE BILAYER FORMATION	178
<u>SUMMARY AND OUTLOOK</u>	<u>184</u>
<u>APPENDIX</u>	<u>188</u>
HYDROSILANE THIN FILMS	188
HYDROSILYLATION IN ORGANIC CHEMISTRY	189

METHODS	190
OPTICAL EVALUATION OF THE AU SAMPLES AFTER REACTION WITH ODSIL, AND CONTACT ANGLE MEASUREMENTS	191
FT-IR-SPECTRA OF OCTADECYLSILANE IN CHCl ₃	191
COMPARISON OF IR SPECTRA OF ODSIL, OCTADECANETHIOL AND OCTADECYLTRICHLOROSILANE	193
THICKNESS'' OF ADSORBED LAYERS AND ADSORPTION KINETICS	195
ELEMENTARY COMPOSITION OF THE ODSIL FILMS: CONFIRMATION OF THE PRESENCE OF OXYGEN IN THE ORGANIC LAYERS.	196
SUMMARY	199
RELATED PAPER:	200
ATOMIC FORCE MICROSCOPY DETECTS CHANGES IN THE INTERACTION FORCES BETWEEN GROEL AND SUBSTRATE PROTEINS.	200
REFERENCES	223
<hr/>	
A CKNOWLEDGMENTS	232
CURRICULUM VITAE	233

Abbreviations

Å	Ångström
2-D	two-dimensional
3-APTS	3-aminopropylsilane
3-D	three-dimensional
AFM	Atomic Force Microscope
asym.	asymmetrical
ATP	adenosine triphosphate
BHF	buffered hydrofluoric acid
BLMs	Black-Lipid Membranes
BODIPY	a fluorescently labelled lipid-analog
DBSP	cis-dichlorobis(styrol)platinum (II)
DCC	N,N'-dicyclohexylcarbodiimide
DDT	dodecanethiol
dest.	“distilled“
DODAB	Dioctadecyldimethyl-ammoniumbromide
DP	dicetylphosphate
DPPC	dipalmitoyl-phosphatidylcholine
DSC	Differential Scanning Calorimetry
DSU	11,11'-dithiobis(succinimidylundecanoate)
EC	erythrocytes (blood cells)
EDTA	ethylenediamine tetraacetic acid
eV	electron volt
FT-GIR	Fourier-Transform Grazing-Angle Infrared Spectrophotometer
GA	glutaraldehyde
GroEL	a chaperonin (protein)
HDT	hexadecanethiol
HMDS	hexamethyldisilazane
HUT	11,11',-Dithiobis(undecanol)
Hz	Hertz

IUVs	intermediate unilamellar vesicles
kD	kilo Dalton
LB	Langmuir-Blodgett
Lip	designates a liposome fraction (see Table 2)
LSM	Laser Scanning Microscope
LUV	large unilamellar vesicles
MDCK	madine-darby canine kidney cells
MHA	16-mercaptohexadecanoate
MW	molecular weight
NBD-PE	fluorescently labelled PE
NHS	N-hydroxy-succinimide
NMR	Nuclear Magnetic Resonance
Nr.	number
ODP	octadecylphosphate
ODSil	octadecylsilane
OWLS	Optical Waveguide Lightmode Spectroscopy
PBS	phosphate buffered saline
PC	phosphatidylcholine
PDMS	polydimethylsiloxane
PE	phosphatidyl-ethanolamine
POD	peroxidase
PTFE	Teflon
PVC	poly(vinylchloride)
Q-tip	Cotton swab
Ra	mean roughness
SAM(s)	Self-Assembled Monolayers
SDS	sodium dodecyl sulfate
SEM	Scanning Electron Microscope
SFV	semliki-forest virus
Si	Silicon
SiO ₂	Silicon-oxide

SLO	Streptolysine O
SPM	Scanning Probe Microscope
SPR	Surface Plasmon Resonance
STM	Scanning Tunneling Microscope
sym.	symmetrical
T _c	Transition temperature of lipids
TEM	Transmission Electron Microscope
THF	tetrahydrofuran
TMB	3,3'-5,5'-tetramethylbenzidine
Tris	Tris(hydroxymethyl)aminomethane
TSG	template-stripped gold
TWEEN	polyoxyethylenesorbitane
UAc	Uranylacetate
UV	ultra-violet
XPS	X-Ray Photoelectron Spectroscopy
μCP	Micro-contact Printing
μFP	Micro Fluidic Patterning

Summary

The goal of this thesis was the development of a suitable support to render protein-containing artificial membranes accessible to scanning probe microscopy (SPM) under physiological conditions. Bilayer membranes directly supported on flat substrates as well as bilayer membranes suspended over topographically and chemically defined nanocavity surfaces were produced and studied.

A method based on thin-film technology and etching has been devised for the production of a flat gold/silicon substrate containing a defined density of round nanohole structures with diameters ranging from 50 - 200 nm and a depth varying between 5 and 300 nm. The geometry of a single nanohole consisted of a hydrophilic silicon cavity covered by a thin Au layer containing a hole.

These, as well as flat and ultraflat gold substrates, were then chemically modified using alkanethiols. We were able to tune the physical and/or chemical properties of the substrates—hydrophilic or hydrophobic, positively- or negatively charged, and inert or amino-reactive—by the formation of self-assembled monolayers with different end-group functionalities. Based on micro-contact printing (μ CP), a method was then developed to direct an aminoreactive crosslinker molecule to predefined, micrometer-sized areas on a gold surface. By exposing such substrates to collagen V, semliki forest virus (SFV) or peroxidase (POD) it could be shown, that biomolecules do selectively bind to the reactive SAM areas and that they retain their functionality. A new route was then studied for the chemical modification of metal- and metal-oxide surfaces, based on hydrosilanes and a catalyst. This chemistry did lead to stable, organic thin films with a linear growth rate over time and of a molecular order inferior to alkanethiol SAMs.

In the next step, the deposition of bilayer membranes on the chemically modified and structured substrates were investigated. Three techniques were compared for the formation of homogeneous supported membranes: the black lipid membrane (BLMs) technique, the Langmuir-Blodgett technique (LB) and the direct fusion of lipid vesicles onto hydrophilic surfaces. Homogeneous bilayers were obtained very reproducibly on amine-terminated, self-assembled monolayers and on SiO_2 substrates using the lipid vesicle method. The phase behavior of these supported bilayers was then investigated using photobleaching experiments and fluorescently labeled lipids. On SAM-modified gold surfaces, mainly crystalline lipid bilayers were obtained, whereas on SiO_2 surfaces, the bilayers retained their fluidity. By fine-tuning the lipid composition of liposomes containing cholesterol, the crystalline-to-fluid phase transition temperature of the supported bilayers could be varied from below room temperature to 60°C . This allows the bilayer-state to be switched from solid to liquid by means of small temperature

changes in an experimental setup, making it possible to control the lateral diffusion of inserted membrane proteins.

The insertion of a model pore-forming protein (Streptolysine O (SLO)) into the supported bilayers was then studied and optimized to finally test the resolution that can be obtained with the atomic force microscope (AFM) on such systems. High-resolution images of the round-shaped membrane pores were obtained in an aqueous environment and without fixation, showing that the retrieval of molecular information from native membrane samples is possible.

Finally, after chemical modification of a substrate containing 100 nm nanocavities, the suspension of a bilayer membrane over these structures was achieved. AFM images revealed the presence of a lipid bilayer spread across the small holes, which under certain conditions was stable enough not to be indented by the AFM tip. These membrane/cavity substrates are ideal supports for the accommodation of large membrane proteins making them accessible to SPM.

Zusammenfassung

Das Ziel dieser Dissertation war die Entwicklung eines geeigneten Substrats, das Proteine in künstlichen Phospholipid Membranen dem Raster Sonden Mikroskop zugänglich macht. Es wurden einerseits direkt auf flachen Oberflächen gespreitete Membranen hergestellt und untersucht, als auch solche, die über chemisch definierte Nanokavitäten gespannt waren.

Basierend auf einer Dünnschichttechnik und auf Ätzen wurde ein Silizium/Gold Substrat mit kleinen Nanolöchern entwickelt. Diese „Nanokavitäten“ hatten Durchmesser von 50 bis 200 nm und eine Tiefe von wahlweise 5 bis 300 nm. Grob beschrieben bestanden diese kleinen Löcher aus einer in Silizium geätzten, hydrophilen Kavität, bedeckt von einer dünnen aber stabilen Goldschicht, in der ein Loch eingelassen ist.

Diese strukturierten Oberflächen sowie flaches und ultraflaches Gold wurden dann mittels Alkanthiolen chemisch modifiziert. Es gelang, durch die Wahl von entsprechenden ω -terminierten Thiolen, diese Oberflächen wasseranziehend oder -abstossend, positiv- oder negativ geladen oder inert oder aminoreaktiv zu gestalten. Durch Anpassung einer neuen, chemischen Strukturierungsmethode - dem sogenannten „micro-contact printing (μ CP)“ - an die Bedürfnisse einer in unserem Labor synthetisierten, aminoreaktiven Substanz, gelang es dann, reaktive, sich selbst organisierende Schichten (SAMs) gezielt im Mikrometermassstab auf Goldoberflächen zu deponieren. Auf solcherart „chemisch“ strukturierten Oberflächen war es möglich, Collagen V, Semliki Forest Viren und das Enzym Peroxidase gezielt und ausschliesslich an jenen Stellen zu binden, die das aminoreaktive Alkanthiol enthielten. Mittels Peroxidase konnte dann im Weiteren gezeigt werden, dass Proteine (einen Teil) ihrer Aktivität bewahren, wenn sie kovalent an das Gold gebunden werden.

Parallel zu den Bestrebungen, Gold chemisch zu modifizieren, wurde auch ein neues hydrosilan/katalysator system auf seine Fähigkeit untersucht, auf Metall oder Metalloxid Oberflächen dünne Organische Schichten auszubilden. Es zeigte sich, dass langkettige Hydrosilane in einer katalysierten Reaktion sehr wohl zu stabilen organischen Filmen auf Gold führen, dass diese aber nicht so dünn und geordnet wie Alkanthiolschichten sind.

In einem nächsten, wichtigen Schritt wurde dann die Spreitung von Lipid-Membranen auf den verschiedenen Oberflächen untersucht. Drei Techniken wurden diesbezüglich

erwogen: Die „Black Lipid Membrane“ Methode, Die Langmuir-Blodgett Technik sowie das direkte Fusionieren von Lipidmembranen auf Oberflächen. Die letztere Methode führte schliesslich zu sehr reproduzierbaren, homogenen Membranen auf SiO₂ Oberflächen und auf gold modifiziert mit einem aminofunktionalen SAM. Mittels Photobleaching Experimenten wurde das Phasenverhalten dieser Membranen untersucht. Hier zeigte sich, dass auf SAM modifizierten Oberflächen die Membranen in den allermeisten Fällen in einer kristallinen Phase vorlagen, während sie sich auf SiO₂ wie eine zweidimensionale Flüssigkeit verhielten. Durch die Wahl geeigneter Lipidzusammensetzungen der Liposomen, konnte der Schmelzpunkt der Membranen zwischen unterhalb der Raumtemperatur und 60° eingestellt werden. Dies erlaubt es, die Diffusion von membran-integrierten Proteinen zu steuern.

Schliesslich wurde die Insertion eines porenformenden Modell-Proteins (Streptolysin O) in die gespreiteten Membranen untersucht. AFM Bilder sehr hoher Auflösung konnten nach dem Optimieren der Insertionsbedingungen bekommen werden, die die kringelförmige Gestalt dieser Löcher zeigen. Das Besondere dabei war, dass diese molekulare Auflösung beim Messen in wässriger Lösung und ohne die Probe zu fixieren, erhalten wurde.

Schlussendlich wurden die Anfangs erwähnten, nanostrukturierten Si/Au Oberflächen mit einer Alkanthiolschicht modifiziert und Liposomen darüber gespreitet. Mit dem AFM konnte gezeigt werden, dass mit dieser Methode Membranen hergestellt werden können, die zwischen dem Wasser in der Nanokavität und dem restlichen Wasservolumen aufgehängt waren. Von diesen hängenden Membranen wird erwartet, dass sie Membranproteinen eine besonders naturgetreue Umgebung Schaffen, damit diese in ihrer natürlichen Art Raster-Sonden Mikroskop Untersuchungen unterzogen werden können.

INTRODUCTION

Getting a visible understanding of biology at the micro and nanoscale

Today, scientific research in the biological sciences is still very concerned with understanding the components nature is built of and it aims to discover how these parts interact to produce the marvelous, highly complex living species on our planet. Recently, developments in microscopy have opened new possibilities for studying the microscopic world beyond human vision, giving the opportunity to get a visual impression of the full width of what is termed “biology“: Namely the field ranging from the “ecosystem“ down to the “molecular biology“, from where the bridge to the organic and inorganic chemistry could be drawn.

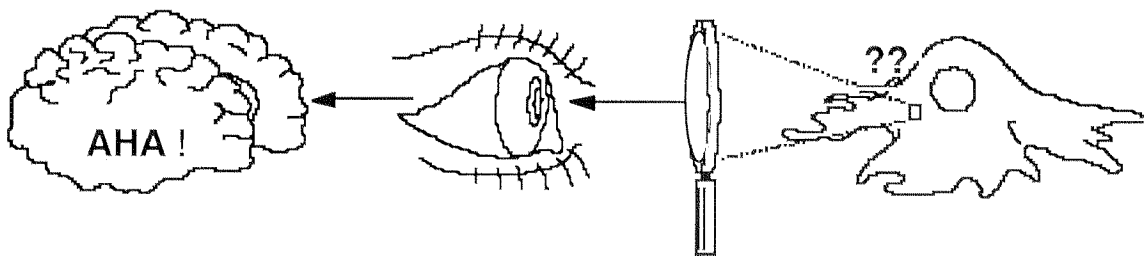


Figure 1: “Seeing is understanding“ - or in other terms - “Vision gives the most extensive information about a system“.

Fast advances in the field of the biology were very often related to the invention of a new technique, making a previously invisible object or system accessible to human vision (Table 1). In the 17th century, light-microscopy showed that life does extend far beneath the 100 μm dimension and that on this scale everything is in motion. The concepts of “cells“ and “microorganisms“ were introduced. Very soon thereafter, as the magnification of and the preparation techniques for the microscopes were optimized, the highly complex subcellular building blocks of life were discovered, of which the structural and functional organization relied on even smaller, yet not visible structures. The invention of the electron microscope in the 1960s finally revealed the nanometer-size world to the biological community making it possible to visualize the basic building blocks of life: DNA, proteins and other macromolecules.

Device	Resolution	Measurement conditions and obtained information.	Time * needed
Human eyes	$\pm 50 \mu\text{m}$	Only objects emitting or reflecting light between 380 - 800 nm are visible. 3-D vision.	real-time
Light microscopy	200 nm (0.6λ) (UV: 100 nm) (2000 \times magnified)	Same as for human eyes. Native biological samples measurable.	real-time
Laser scanning microscopy (fluorescence)	200 nm (0.6λ) UV: 100 nm	3-D reconstruction of transparent, fluorescently labeled objects. Native biological samples measurable.	real-time - hours
Scanning electron microscope (SEM)	$\pm 10 \text{ nm}$	High vacuum for high resolution needed. Sample must be electrically conducting.	30 min.
Transmission electron microscope	0.3 nm (1'000'000 \times magnified)	High vacuum needed; ultrathin, dried samples only (semi-transparent for electrons). Organic samples have to be contrasted with heavy metal salts.	30 min.
SNOM (Scanning Near-Field Optical Microscope)	20 - 100 nm	Sample must be flat. Still very difficult to get images in solution and very difficult handling.	real-time in intervals of 1-10 min.
AFM (Atomic Force Microscope)	$\pm 0.01 \text{ nm}$ (height) $\pm 0.1 \text{ nm}$ (lateral) $\pm 0.7 \text{ nm}$ (soft material in solution)	Only surface topography, but native biological samples can be measured with submolecular resolution in buffer solutions. Sample must be flat.	real-time in intervals of 1 sec.-10 min.
STM (Scanning Tunneling Microscope)	0.01 nm	Samples need to be conductive. The image is a mixture between the surface topography, the electron density distribution- and work function of the surface. Sample must be flat.	real-time in intervals of 1 sec.-10 min.
NMR (Nuclear Magnetic Resonance)	atom-position resolution in 3-D	The interatomic distances of small molecules to proteins of about 15 kD (soon 60 kD) can be determined in solution. The 3-D structure has to be computed. Some dynamic processes can be studied.	days-month
x-ray Crystallography	near-atomic resolution in 3-D	3-D electron density map of molecules of any size can be obtained with near atomic resolution. Only crystalline samples can be investigated	days-years

Table 1: Comparison of techniques giving structural information of sub-millimeter biological samples. *Time needed for the preparation of a standard sample and acquisition of one image or structural map.

Along with methods giving a visual impression of a biological object, of course many other, indirect techniques were also used to answer questions about the motion, interaction and behavior of the biological molecules. Some examples are the use of spin relaxation experiments or optical dichroism studies to measure molecular motion, and fluorescence quenching experiments to get information about the interaction of proteins. But obviously, all of the methods have the drawback, that they only give information about a few, very specific aspects of the system under study and that the biological system must be prepared (and often denatured) in order to make it accessible to a certain analysis method. Examples for sample preparation can be found in microscopy too: Drying of the samples is necessary for TEM investigations, a conductive coating is needed in the case of SEM imaging, the need for large crystals of a molecule for X-ray structure determination and the limitation to “low” molecular weights in the case of NMR structure determination. For a very long time, a gap existed concerning imaging of native biological systems in the nanometer dimension (0.1-100 nm). This gap was filled in 1986 by the invention of the atomic force microscope (AFM) by Binnig, Quate and Gerber (Binnig et al., 1986).

Atomic Force Microscopy (AFM) for biological applications

The AFM belongs to the family of scanning probe microscopes (SPM). These SPMs record a 3-D image of a surface by measuring the direct interaction of an extremely small and sharp probe-tip with the substrate, which is scanned over the surface. The precise scanning is achieved by mounting the tip or the substrate on a special piezo-tube, which can be moved with sub-nanometer precision in 3 dimensions. Depending on the type of microscope, a different interaction is used to reconstruct a digital image of the substrate. In the case of a scanning tunneling microscope (STM), the tunneling current flowing between the scanning tip and the conductive substrate is detected. In the case of an AFM, an extremely sharp tip fixed at one end of a long cantilever (spring) is scanned over the substrate in direct contact: The tip will exert a certain force on the sample, and vice-versa. To detect the deflection of the cantilever at every position on the substrate, a laser is projected onto the back of the cantilever and then reflected into a 4-segment photodiode, which transforms the deflection into an electrical signal. By choosing cantilevers with very small spring constants and by scanning at minimal forces, damaging of the substrate can be minimized. The latter can be achieved by a feedback loop, which constantly readjusts the z-height of the sample in order to keep the deflection of the cantilever constant. In the case of an AFM, the image obtained corresponds to a force map of the sample, containing the topographical information.

A schematic of the AFM is displayed in Figure 2.

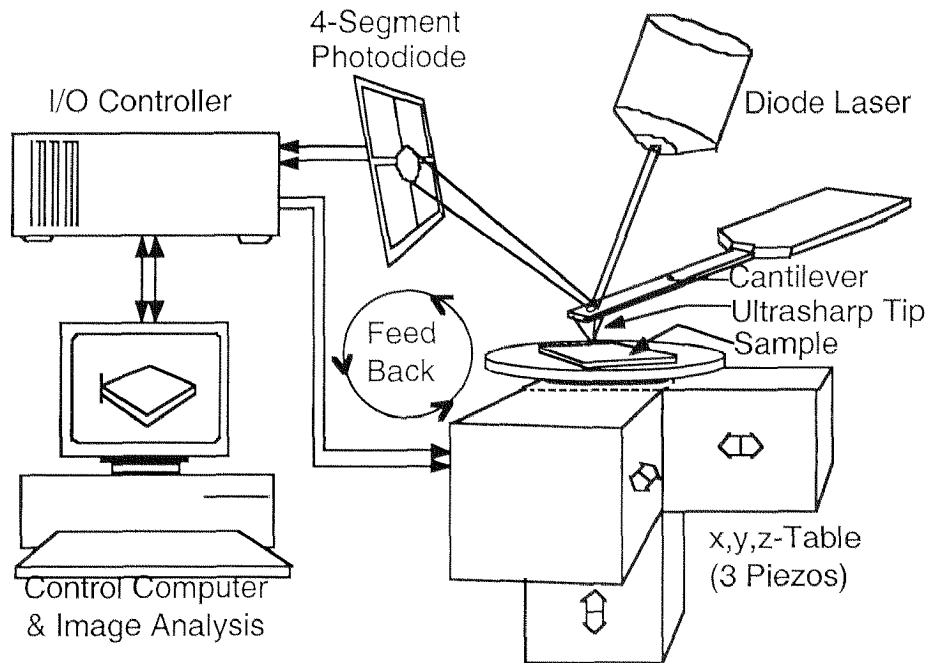


Figure 2: Scheme of the Atomic Force Microscope (AFM).

The AFM has one big advantage over other techniques giving visual information in the nanometer dimension: Due to its purely mechanical principle, the measurement can be performed not only in a vacuum, but also in ambient air or even in liquids including water and organic solvents. The possibility to perform measurements under liquids is very interesting for biological applications, as most of the molecular processes do happen in the liquid environment of cells or organs. The possibility to obtain molecular resolution on native, “living“ samples was therefore very exciting for the biological community and it did not take long before the first images of biomolecules were published using this technique. Soon, however, it was noticed, that to get nanometer or even Å resolution, the sample preparation becomes very crucial when working in air or in solution. The resolution obtained with an AFM is related to the sharpness of the scanning probe, but also the sample needs to be immobilized properly as else the biological species are simply swept away by the lateral forces of the scanning AFM tip. Therefore, over a period of several years, the immobilization conditions for molecules were optimized. Different strategies were followed:

a) A first approach was based on physisorption of the biological species onto a substrate. However, there are only a few substrates available that were flat enough to allow molecular resolution. Most often, mica and highly oriented pyrolytic graphite

(HOPG), glass or silicon wafers were used. Unfortunately, the immobilization strength of the biomolecules can only be poorly controlled. Adhesion forces that are too strong can lead to denaturation of the species on the substrate, resulting in loss of activity.

b) Another possibility is the chemical modification of the molecules in order to attach them by an additional functional group to a surface. E.g.: thiol groups were introduced on proteins to make them adhesive to Au surfaces ((Leggett et al., 1993)). The drawback of this approach is the chemical modification of the protein (molecule) itself. Therefore not really “native“ molecules are obtained and loss of their activity can occur.

c) The third approach was the chemical activation of a surface using molecules that would strongly bind to an inorganic surface and on the other hand also bind to a functional group on the protein or molecule to be immobilized. In our laboratory, among others, an alkanethiol was synthesized with a terminal succinimidyl group which covalently binds primary amino-groups. This, as well as other long-chain alkanethiols form well ordered, self-assembled monolayers (SAMs) on gold with a thickness of less than 2 nm, on which proteins do bind strong enough to allow good AFM imaging (see Figure 3). By making SAMs using alkanethiols with different functional endgroups, the surface chemistry can be tuned at will, making an Au surface compatible with the requirements of a protein to preserve its activity.

Another approach, in this case for the immobilization of proteins on silicon substrates, is based on the production of an aminomodified silane layer onto which the proteins are covalently bound by the mediation of glutaraldehyde ((Weetall, 1976)).

The establishment of immobilization protocols and the possibility to obtain high-resolution images of native (but immobilized) proteins paved the way to make dynamic biological processes visible on a molecular scale. This had never been possible before. In the very beginning, the polymerization of fibrin was monitored in real time (Drake et al., 1989) as well as the interaction of ribonucleic-acid (RNA) polymerase with desoxyribonucleic acid (DNA) (Guthold et al., 1994). In our group, real time images of the disassembly process of clathrin cages were obtained (Wagner et al., 1994b).

Then, the possibility to measure mechanical properties in the nanoscale with the AFM on biological substrates was explored. The interaction of proteins with molecules or other proteins were measured (Vinckier et al., 1998, Dammer et al., 1995, Florin et al., 1994, Lee et al., 1994, Ros et al., 1998), elastic- and plastic properties of cells and molecules determined in the nanoscale ((Vinckier and Semenza, 1998)) and the allosteric vibration of catalytic proteins during their reaction cycle was visualized

(Radmacher et al., 1994). Very high resolution images of proteins can be obtained if the proteins are arranged in a two-dimensional lattices on a substrate (Karrasch et al., 1994, Schabert et al., 1995).

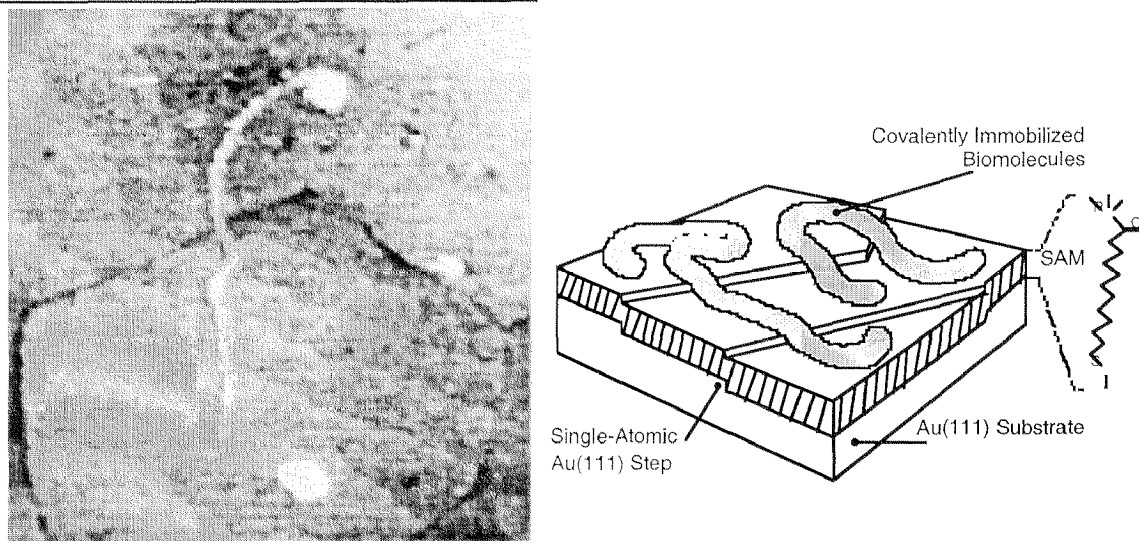


Figure 3: Left: Single collagen V molecule imaged by contact-mode AFM in buffer solution. The filamentous protein is covalently bound to a reactive SAM covering the ultraflat gold substrate. The step-like structure in the lower half of the image are single (Au) atomic steps on the surface of a small Au(111) crystallite. Dimensions of the image: 350 × 350 nm. Right: Schematic drawing of the situation in the left image.

Biological Membranes

The positive results with proteins encouraged the search for AFM applicability in the field of molecular and cellular biology. The possibility to address and measure single molecular events showed that, indeed, information that could not be obtained by other methods could be obtained by SPM. Studying biological systems of higher complexity was therefore the next challenge. One of the most central and interesting systems, are biological membranes.

These tiny, but highly complex architectures - apart from being the main components of the cellular envelope - are building blocks of many intracellular organelles (Figure 4). The biological membranes are composed of a lipid bilayer with inserted and attached (glyco-)proteins which are in constant motion and which constantly interact with each other. Figure 5 shows an illustration of a molecularly resolved plant chloroplast membrane including the most important proteins responsible for photosynthesis.

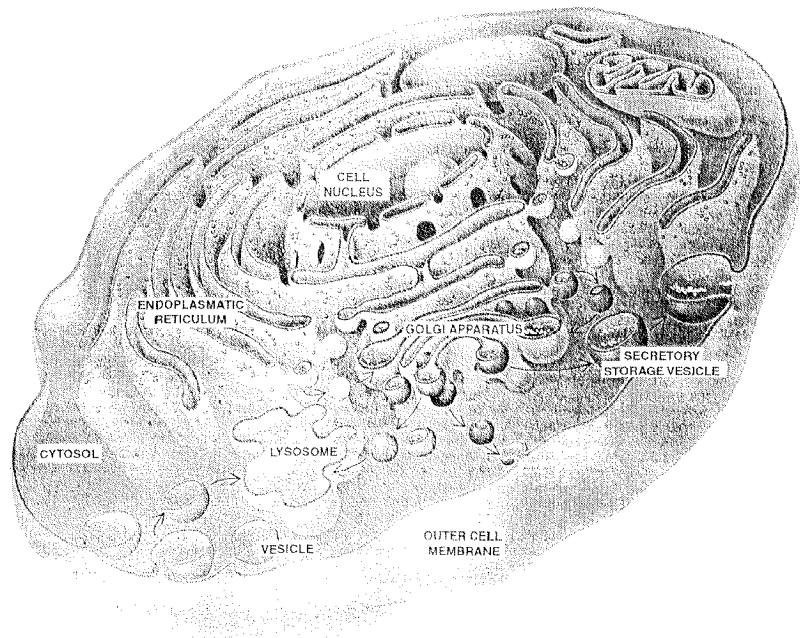


Figure 4: Scheme of a cross-section through an animal cell showing the complex interior organization in organelles composed of phospholipid bilayer membranes. The membranes include complex, attached or inserted protein systems, these are the sites where the most important cellular reactions take place. Round-shaped membrane vesicles are responsible for the transport of substances from the golgi apparatus to other organelles or the exterior of the cell. But they can also be formed at the cellular membrane taking up substances from the exterior and bringing them to predefined organelles in the cell. Source: (Rothman and Orci, 1996).

Many things are known about the integrated proteins and also about the physical properties of phospholipid membranes. The combined system however,—the interplay of the bilayer and the proteins or of the proteins among each other—is still very poorly understood. The possibility to visualize these processes would be of big significance. Based on the ability of the AFM to allow the study of molecules in their natural environment, such processes may be visualized.

First approaches have been done by studying cells and membrane patches. However, this is not always such a straight-forward approach, as the natural cellular membranes are highly complex structures which are poorly accessible to the AFM probe. Therefore we decided to produce suitable supports for the reconstruction of artificial membranes, where proteins can be inserted. This is the main topic of this dissertation.

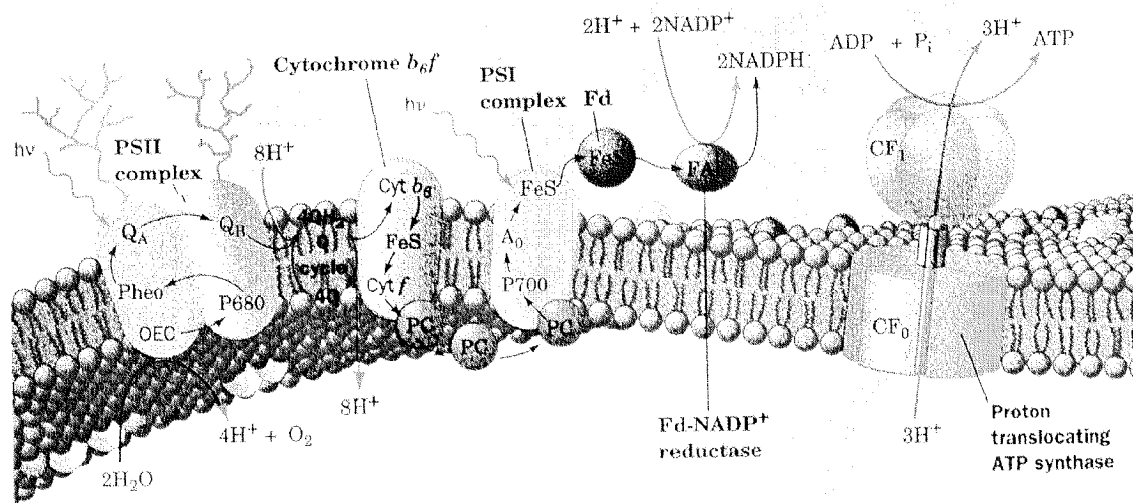


Figure 5: Schematic model of a plant thylacoid membrane showing the complex interplay of inserted and attached proteins. The proteins can (probably) freely diffuse within the 2-D phospholipid “liquid-like phase“. This image corresponds to magnification of about 3’000’000 times and shows the reactions taking place during photosynthesis: Light is absorbed by the photosystems (PS) I and II, leading to complex electron transfer reactions which finally split water, produce energy for the cell (ATP) and regenerate the cellular reducing agent nicotinamide hypoxanthine dinucleotide (NADPH).

Surface design for the proper presentation of biological membrane/protein systems for atomic force microscopy

Membrane proteins in their natural environment are strongly embedded in a fluid, two-dimensional phospholipid bilayer membrane. They can freely diffuse, as long as they are not hindered by cytoskeletal components like actin strands or microtubuli etc., which stabilize the membrane, or as long as they are not held in place by crosslinkers binding them to other cellular structures. Almost all the membrane proteins do have extramembraneous domains which are often responsible for the interaction with other proteins and molecules like drugs and hormones. These domains extend freely into the water-based solutions of the interior and the exterior of the membrane-enclosed compartment. The dimensions of these extramembraneous protein-domains is very variable, ranging from 0 nm (the protein does not exceed the width of the membrane) to for example approximately 10 nm for axonin.

Therefore, if a protein is inserted in an artificial membrane which is supported by an artificial substrate the following requirements are important: the membrane must be fluid, secondly the protein must be surrounded with water on both sides of the membrane and thirdly its extramembraneous domains should not be touching any substrate structures. These requirements can obviously not be fulfilled by an artificial

membrane which consists of a bilayer membrane directly immobilized on a flat support (see Figure 6).

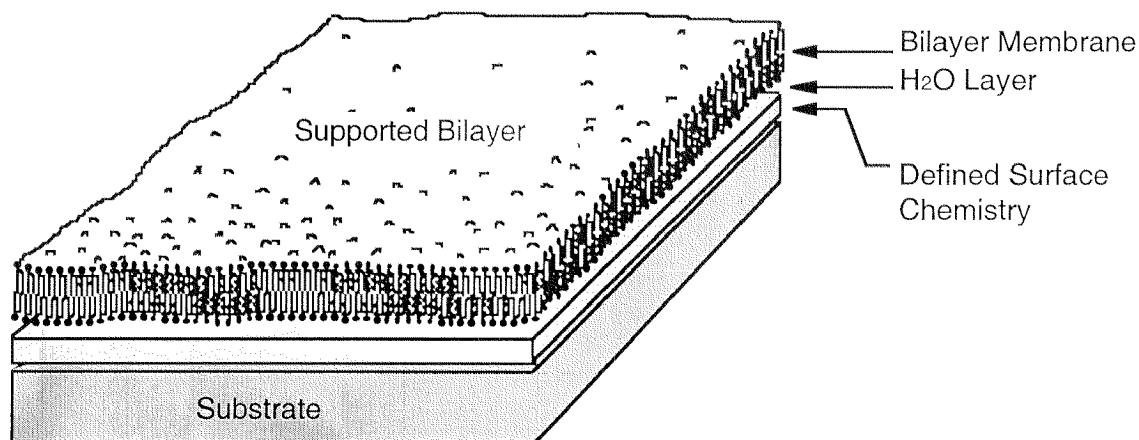


Figure 6: Supported bilayer membrane immobilized on a flat and chemically defined support.

In such a setup, the bilayer membrane can be separated from the substrate by a very thin water layer by choosing an appropriate surface chemistry. This can be enough to accommodate a protein in such a bilayer. However, if the inserted membrane proteins have very small extramembraneous domains, they will be disturbed by the presence of the nearby substrate.

An improvement in this regard is the modification of the substrate with organic monolayers of different thickness as shown in Figure 7. Vogel et al. (Heyse et al., 1998b) did use such a setup to spatially control the localization of proteins in a membrane. Using alkanethiol-based SAMs, the maximum depth of the water-cavities is however restricted to less than the thickness of the thicker SAM, which typically cannot exceed 1-2 nanometers. For many membrane proteins, this is not enough to accommodate their extramembraneous domains.

Alkanethiols of higher complexity have been synthesized containing a long, hydrophilic spacer arm between the alkyl chains of the SAM and the bilayer binding domain (Figure 8A) (Bunjes et al., 1997). Using this SAM in a similar approach as described before, larger “cavity” depth could possibly be achieved. But, bilayers immobilized on a spacer exceeding 5 nm in length are probably very difficult to form and the still close proximity of the substrate may influence the behavior of the membrane-inserted proteins through long range forces. If on the other hand, instead of using SAM-domains with differing thickness, diluted, long-chain and lipid-adhesion promoting SAMs are used (Figure 8B), the diffusion of the proteins is probably hindered compared to the natural state.

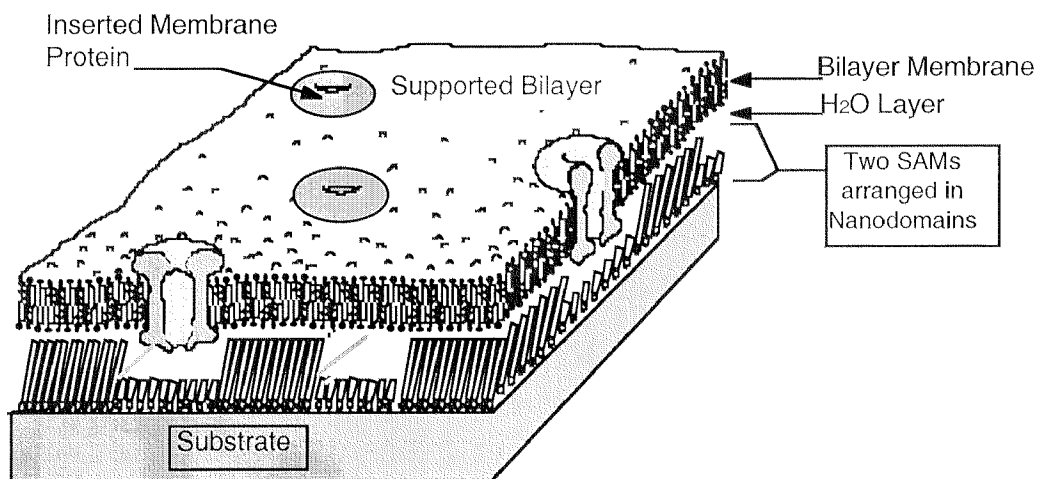


Figure 7: Au surface structured in the nm dimension with two SAMs of different thickness. Small extramembraneous domains of membrane proteins can be accommodated within the cavities formed by the short-chain nanodomains.

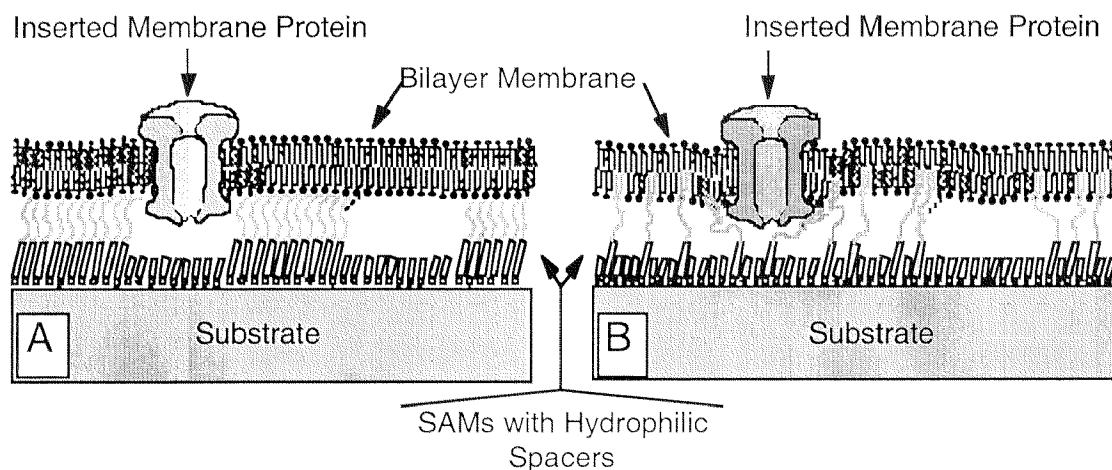


Figure 8: Special SAMs containing hydrophilic spacer arms between the supported bilayer and the substrate bound alkyl-chain domains. As in Figure 7, these SAMs could be combined with short-chain SAMs organized in Nanodomains (A) or in a “mixed-monolayer“ approach (B).

For all the reasons mentioned above, we did finally chose an approach based on the production of freely suspended membranes over nanocavities (nanoholes) (see Figure 9). Natural biological membranes, which are stabilized by cytoskeletal components can be excised from a cell by means of a patch pipette of several microns in diameter - the membrane then being freely suspended within the glass rim of the pipette. Such a suspended membrane is usually stable for hours and has already been imaged by AFM (Hoerber et al., 1995) (It was however not possible to resolve single proteins on such preparations). But also black-lipid membranes (BLMs), which consist exclusively of an

artificial phospholipid bilayer suspended over a teflon hole of up to 4 mm (!) in diameter, are very stable as long as they are kept in a vibration free environment. (see chapter “Black Lipid Membranes (BLM)”) Therefore there were good reasons, that optimal conditions for preserving the integrity of the proteins as well as for AFM imaging would be obtained, if one would succeed to produce membranes suspended over cavities having nanometer dimensions (50 - 300 nm).

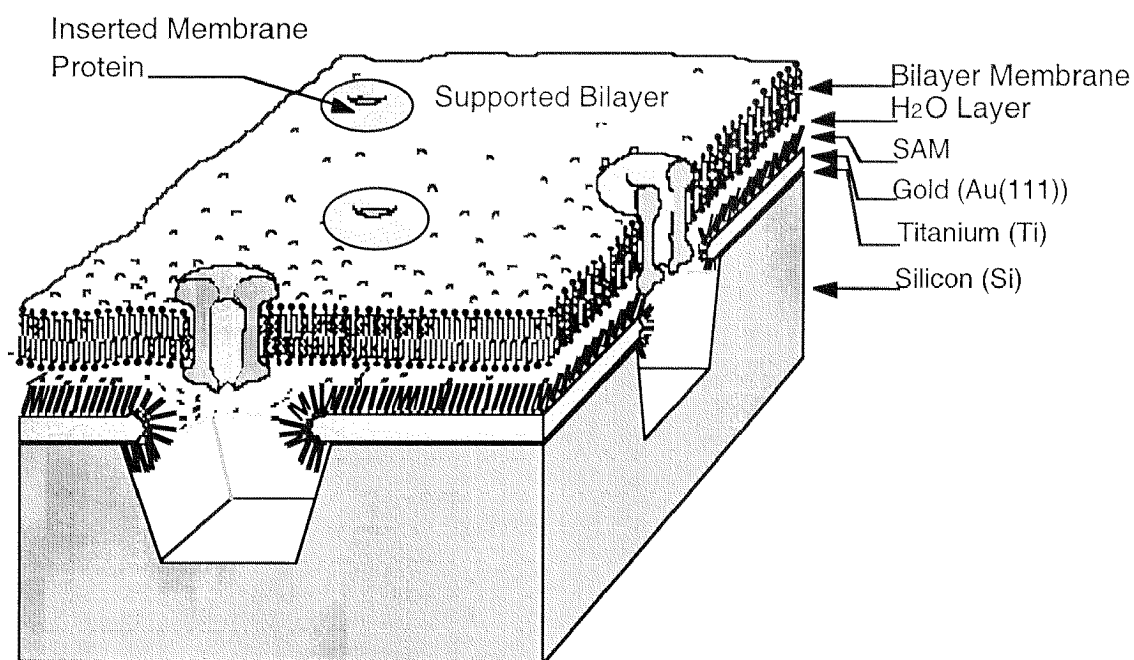


Figure 9: Structured Au/Si substrate with chemically well-defined nanocavities. This setup creates a membrane nanoenvironment for the proteins which best mimics the conditions in their natural biological system. Proteins with extramembraneous domains of any size can be accommodated and the presence of a water compartment below the suspended membrane can be used to create non-symmetric solution conditions. In this thesis, different approaches are discussed to obtain such structures.

Proteins inserted in the membrane over the nanocavities have large water volumes on both sides around their extramembraneous domains and their radius of activity is confined within the perimeter of the holes. This characteristic may be of great advantage for AFM investigations to study protein interactions, because the proteins will not be able to escape from a predefined, scanned area. The elasticity of the membranes as well as the diffusion of the proteins in the membrane can be influenced by choosing lipids of different transition temperatures (T_c) or by small temperature changes applied to a membrane sample having a T_c around room temperature (see chapter “Control of bilayer fluidity and heat induced morphologies”). Very importantly, by reducing the temperature under the T_c of the lipid bilayer, the motion of the inserted proteins can be frozen, whereas the water surrounding the proteins is still liquid.

The chemical definition of the substrate becomes a very important topic, when it is intended to produce such nanostructured surfaces for the immobilization and suspension of bilayer-membrane systems. The surface chemistry should allow the deposition of a bilayer membrane on the surface (see chapter “BILAYER FORMATION“). At the same time, the surface can be designed to covalently bind the membrane, to strongly adsorb it such that the bilayer fluidity is lost, or to exert a short-range repulsive force, leading to a supported, fluid bilayer. The interior of the nanocavity must be hydrophilic, in order to allow entrapment of water, but the affinity of the membrane to the interior of the cavity should be kept small, as else the membrane would get sucked into the hole. These are topics which were addressed in this dissertation.

The aim and outline of the work

The aim of this thesis was to work out a methodology which would make processes happening on a molecular scale in and on biological membranes accessible for AFM investigation. This involved the combination of methods coming from very distinct areas of technology including silicon photolithography, thin-film technology, organochemical surface modification, membrane- and protein biochemistry and surface analysis.

A strategy was developed to produce nanostructured, chemically defined substrates for the controlled immobilization of artificial membranes. Defined areas on these substrates had to be designed such, that the supported membrane would stretch over a nanocavity in the support, leading to small membrane areas suspended between the water in the cavity and the bulk solution.

In a first step we studied the chemical modification of the substrate.

We decided to use materials coated with a thin gold film as substrates for all the further experiments. These substrates are easily amenable to chemical modification using alkanethiols, which form self assembled monolayers on gold. Alkanethiols with different ω -functionalities were available in our laboratory, some of which had the potential to covalently bind other molecules (proteins, lipids). For the chemical patterning of the substrates, we decided to use a recently developed method called μ CP which was known to be useful to produce micropatterns of hydrophobic alkanethiols. For our applications we were more interested in patterning hydrophilic SAMs. Therefore, this method was modified making it suitable for the transfer of a reactive, hydrophilic alkanethiol SAMs.

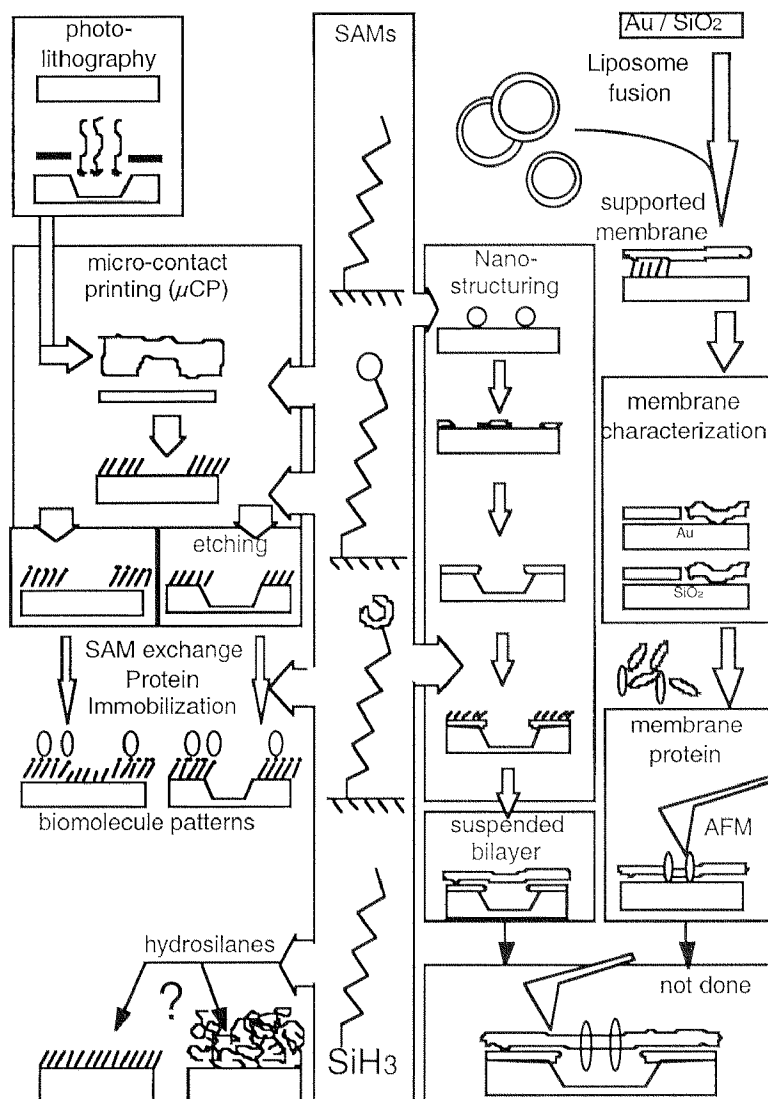


Figure 10: Flow-chart showing a graphical outline of this thesis

These surfaces were then tested in terms of their capability to covalently bind molecules using different proteins as well as lipid containing virus particles. By using peroxidase, it could be shown, that biological species can retain their functionality upon immobilization on these structured substrates, making this method also interesting for protein-based biosensor applications.

Related to this chemical patterning, we have used silicon photolithography methods to produce the microstructured polymer masters needed for μ CP, and a new, promising method based on hydrosilanes, which were expected to lead to SAMs on oxide surfaces, was investigated. Chemical patterning was not only important for the site-directed immobilization of proteins, but also to control the substrate parameters related to the formation of supported membranes.

Once the chemical patterning had been optimized, different strategies to produce the supported and/or suspended planar bilayers on our substrates were evaluated. Both a technique based on black-lipid membranes (BLMs), as well as the Langmuir-Blodgett (LB) technique were tested, but did not lead to reproducible supported bilayers. Therefore we changed to a method based on the spreading and fusion of liposomes onto the substrates, which did lead to well defined bilayer membranes.

The (i) production of unilamellar liposomes of different lipid composition, (ii) the conditions which are needed to induce their spreading and (iii) the requirements on the surface chemistry for this process were then optimized. These experiments were made by using fluorescent vesicles in order to have the possibility to check the shape and homogeneity of the supported membrane, optically.

Then, the influence of the substrate on the bilayer fluidity was investigated followed by the development of a method which allows the fluidity of a membrane to be controlled at temperatures around body temperature. This makes it possible to control the lateral mobility of a protein inserted in a suspended membrane, making it amenable to high resolution AFM.

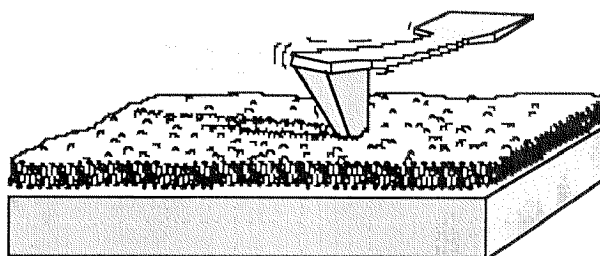
The insertion of a model pore-forming protein into SiO₂-supported bilayers was then studied. This was done with the aim to get familiar with the behavior of membrane proteins in artificial membranes and it also served as pre-test for the later incorporation of this and similar proteins into membranes suspended over nanocavities. At the same time, we were seeking to get an idea of the resolution which can be attained on artificial membrane preparations including proteins, using the AFM. The choice of the SiO₂ substrate for these tests was due to the fact that the lipid bilayers retained their fluidic state on this substrate - similar condition therefore, the proteins would encounter if integrated in suspended membrane systems. To learn more about protein interactions, additional experience in the preparation and AFM imaging of native proteins immobilized on substrates was acquired: The interaction forces between GroEL, a bacterial chaperonin, and two substrate proteins were determined using AFM. This work is reproduced in the Appendix under “Related paper:“.

In a further, major part of this thesis, strategies to produce suitable, 50-200 nanometer diameter holes (nanocavities) in a flat gold substrate were evaluated. Two approaches based on polymer-nanospheres and polycarbonate filters were investigated experimentally. The combination of thin-film technology and silicon etching techniques finally led to the desired nanocavity substrate, which was chemically modified using SAMs as previously described.

In the last step, the formation of suspended membranes over the nanostructured, chemically defined gold/silicon substrates was studied and the mechanical properties of such architectures evaluated with the AFM. These substrates were then ready to be used as platforms for the investigation of biomolecular events in membranes by means of scanning probe techniques.

Literature on the topic “AFM of bilayer membranes“

In this chapter, a short overview over publications related to “phospholipid bilayer membranes“ and “scanning probe microscopy“ is given. For reviews about “AFM in biological applications“ in general including membrane related topics, the reader is referred to (Lal and John, 1994, Shao and Yang, 1995, Hansma and Hoh, 1994, Kasas et al., 1997).



Living, cultured cells were addressed by AFM at an early stage. First results showed, that it is possible to scan the cellular membrane without destroying it, although it was noticed that the tip is very much indented into the cell (with only occasional penetration) due to the softness of the native membrane structure. The elastic property of the membrane reduces the attainable resolution on the cells as does also the presence of microvilli (small membrane protrusions) which interfere with the AFM tip (Hoh and Schoenenberger, 1994, Zachee et al., 1996).

Compared to pure phospholipid bilayers, membranes from living species are stabilized by the cytoskeleton, which is strongly attached to the membrane at several points and which, web-like, spans the interior side of the cellular membrane. These structures can either be seen as filaments of higher strength through the membrane on flat cellular areas (Kuznetsov et al., 1997, Lesniewska et al., 1998, Oberleithner et al., 1996) or with higher resolution directly on membrane patches obtained after squirting of the cells attached to a glass (Ziegler et al., 1998b). On such a substrate stabilized membrane patches, single membrane proteins can be resolved. Large, suspended membrane patches of several microns in diameter excised by the patch-clamp technique from oocytes did appear to be stable enough for AFM imaging, but no high resolution images

were obtained (Hoerber et al., 1995). Molecular resolution on a natural membrane was achieved on patches of the double-bilayer nuclear membrane, on which the large nuclear pores could be resolved and some functional studies performed ((Lärmer et al., 1997)).

More suited for high resolution applications are artificial, spread membranes on ultrasmooth substrates. Such supported bilayers are often produced by the spreading of lipid vesicles on freshly cleaved mica substrates. A very early report is (Singh and Keller, 1991), in which the difficulty to obtain homogeneous bilayers is reported. At temperatures below the T_c of lipids, molecular resolution of the head groups of membrane lipids has been obtained, and at naturally occurring defect sites or through scratching with the AFM tip, the thickness of protein-free bilayer could be determined to be about 5 nm in height, in perfect agreement with data obtained from X-ray diffraction (Beckmann et al., 1998). Membrane structure and phase transitions including the induction of a ripple-phase (Mou et al., 1994b), the formation of interdigitated domains (Mou et al., 1994a, Fang and Yang, 1997) and the formation of Ca^{2+} -induced domains (Czajkowsky, 1996) on such membranes have been monitored

An alternative method which has been used to produce supported bilayer membranes is the Langmuir-Blodgett technique. The influence of AFM imaging on the structure and stability of such films has been studied [Hii, 1995 #144], molecular resolution of the lipids was obtained and the adsorption of membrane binding proteins could be monitored with high resolution or in real time: (Egger et al., 1990)(Structure of an immobilized Fab'-Fragment of a monoclonal antibody with lipid-anchor) and (Tamm et al., 1996) (Binding process of the influenza virus). Only poor resolution was obtained on LB membranes including the photosynthetic protein complex from *Rhodospseudomonas viridis* (Yamada et al., 1994).

Groups interested in biological membranes soon went over to study combined protein/bilayer systems. Different aspects of such systems were soon addressed: Aggregated protein layers were described after the LB transfer of cytochrome f onto a gold coated mica substrate (Tazi et al., 1996) and diffuse objects of the expected size were visible in the AFM after LB transfer of an acetylcholine receptor/lipid mixture (Fare et al., 1992) or of the photosynthetic membrane complex of a bacterium. The heptameric quaternary structure of the α -Hemolysin prepore in an egg-PC bilayer could be very nicely resolved by (Fang et al., 1997), showing that stable protein imaging in supported membranes is also possible in bilayers above T_c . Pictures of the

degradation of a bilayer by phospholipase A₂ were first produced by (Grandbois et al., 1998), and Takeyasu and colleagues reported the presence of ring-like protein domains on mica after drying of a F₀F₁-ATPase micelles suspension (Takeyasu et al., 1996). But these results should be carefully interpreted because it is very tricky to dry lipid samples and also because “tip-effects“ are visible in some of their images. On natural, supported nuclear envelopes, (Rakowska et al., 1998) was able to show dynamic protein binding events on well resolved, nuclear pore complexes. These pores do nearly completely cover the double-bilayer membrane of the nuclear envelopes of *xenopus laevis* oocytes.

The best resolution of native membrane proteins under physiological conditions has however been obtained so far on 2D crystalline protein array structures supported on mica. This technique can be applied to proteins which are already arranged in 2D-crystalline domains in their native environment, or to proteins, which form such aggregates if concentrated after extraction. Subnanometer resolution was obtained on 2D-crystalline bacteriorhodopsin HPI layers (Mueller et al., 1995b) , and even the closing and opening of the central pore of this protein could be visualized (Mueller et al., 1996) as well as AFM-tip induced conformational changes monitored (Mueller et al., 1995a).

Using the same approach, high resolution images of native Cholera Toxin B layers (Shao and yang, 1995), of gap junctions (John et al., 1995) (Hoh 93 to be copied) and of aquaporin (Walz et al., 1996) were obtained. The orientation of purple membrane protein patches was determined by in-situ measurement of antibody adsorption, showing that molecular reactions can be monitored on such preparations (Müller et al., 1996).

On single proteins inserted in a lipid bilayer it will probably be very difficult to attain the same resolution as obtained on 2D-protein crystals. However, the crystals can only be used for studying the structure-function relationship of proteins including ligand binding, but not for studies dealing with the interaction of proteins with other molecules in the plane of the bilayer and for mobility studies. For such applications, the suspended membranes architectures prepared in this dissertation may be the ideal supports.

This short literature review shows, that the dynamics of native membrane proteins can be addressed in biological or artificial bilayers by AFM. The use of more sophisticated scanning techniques as e.g. electrochemical nanosensor tips or combined near field optical cantilevers with high tapping-resolution capabilities will provide additional information together with structural data from native membrane/protein systems. These developments will also make new demands on the presentation and immobilization of the bilayer membranes.

Materials and Methods

Chemicals: If not otherwise stated, chemicals of the highest available purity were used, purchased from Fluka, Aldrich or Sigma (Switzerland). 18 M Ω ultrapure water was prepared by passage through a Barnstead purification system.

The “piranha” solution consists of 30% H₂O₂/conc. H₂SO₄ (3:7). The acid is rapidly poured into the peroxide in a clean glass beaker. Much care has to be taken because this reaction is extremely exothermic and the solution may explode if the sulfuric-acid concentration is too low or if it comes into contact with organic material. Piranha solution should be used hot and be discarded immediately after use (carefully neutralize with KOH).

Buffer solutions: PBS: (137 mM NaCl, 2.7 mM KCl, 8 mM NaH₂PO₄, 1.5 mM K₂HPO₄, pH adjusted using diluted HCl or KOH). SLO-Tris: (137 mM NaCl, 25 mM Tris, 5 mM KCl, 1 mM NaH₂PO₄, pH 7.4).

Lipids: Cholesterol, L- α -Phosphatidylcholine (from fresh egg-yolk)(PC), L- α -Dipalmitoyl-phosphatidylcholine (C 16:0, synthetic)(DPPC), Dihexadecyl phosphate (Dicetylphosphate)(DP) and L- α -Phosphatidyl-DL-glycerol (from egg-yolk)(PG) were purchased from Sigma (Switzerland). Phosphatidyl-ethanolamine (PE; Grade 1) was from Lipid Products (Surrey, England) and NBD-PE and BODIPY from Molecular Probes (Eugene, USA). These lipids (except the fluorescently labeled) were solubilized in chloroform containing 5 % methanol to a final concentration of 100 mg/ml. BODIPY is soluble in ethanol.

Alkanethiols and substances for SAMs: 11-Hexadecanethiol (95%) was purchased from Fluka (Buchs, Switzerland) and the dodecanethiol (98%) from Aldrich (Switzerland). The synthesis of 11,11'-dithiobis(succinimidylundecanoate) (DSU) was carried out as previously described by (Wagner et al., 1996a). 11,11',-Dithiobis(undecanol) (HUT) was synthesized according to Bain et al. (Bain et al., 1989a) and the synthesis and properties of 11-mercapto-4-nitrobenzyl-undecanoate are described in (Wagner et al., 1996b). 11,11',-dithiobis(undecanoate) and 11,11'-dithiobis(1-aminododecane) were synthesized according to (Wagner, 1995). For the organic monolayers on metal-oxide surfaces, octadecylphosphate obtained from Novartis was used and in the hydrosilane project, octadecylsilane (98%) from Aldrich and dimethyloctadecylsilane (>97%) from Fluka were used.

Biological species: Lyophilized bovine uterus collagen V (800 $\mu\text{g}/\text{ml}$ in 0.1 M acetic acid, purified according to a protocol from Miller et al. (Miller and Rhodes, 1982) was a gift from Dr. Beat Trüeb, Maurice E. Mueller Institute for Biomechanics, Berne (Switzerland). Horseradish Peroxidase (POD, type II, EC 1.11.1.7) was purchased from Sigma (Buchs, Switzerland). Streptolysin O from *Streptococcus pyogenes* was bought from Sigma (Buchs, Switzerland) (1 mg solid (25'000 units/mg solid) were solubilized in 1 ml Tris buffer pH 7.4, aliquoted and stored at - 70°C). A suspension of semliki-forest virus (SFV; 0.8 mg protein in 1 ml 13% sucrose solution) was a gift from Dr. P. Durrer, Biochemistry II, ETHZ, Zürich, Switzerland).

Substrates: Silicon wafers (Si(100), n-type, 2-50 Ω cm) were purchased from Faselec AG (Zürich, Switzerland) and oxidized wafers with an field-oxide layer of \pm 500 nm were a gift from E. Hollaender, Philips Semiconductors, Zürich. Gold (99.99%) was from Cendres and Metaux SA (Biel, Switzerland), titanium and chromium from Balzers, Liechtenstein, and muscovite mica was obtained from Bal-Tec (Liechtenstein).

Others: The yellow-green (505/515) fluorescent polystyrene microspheres were purchased from Molecular Probes (Eugene, USA): We did use 3 types: 200 nm diameter, amine-modified; 100- and 40 nm diameter carboxylate-modified. The nucleopore polycarbonate filters with pore diameters of 100 and 200 nm were from Costar Scientific Corporation. Sephadex G-50 was purchased from Pharmacia LKB, Uppsala, Sweden.

Characterization Methods

Atomic force microscopy (AFM): The AFM images were obtained either on a Bioscope or a NanoScope III equipped with a fluid cell and a "J-type" piezoscanner with a maximum scan range of 140 μm (Digital Instruments, Santa Barbara, CA). Monocrystalline silicon cantilevers (Lot, Darmstadt, Germany) or silicon-nitride cantilevers (NanoProbes, DI, Santa Barbara, USA) were used with force constants ranging from 0.06 to 0.58 N/m (13-100 N/m for tapping-mode). In contact mode, the z-feedback loop was frequently adjusted to guarantee minimal forces between tip and substrate, and the feedback speed was maximized setting it close to the point where the cantilever begins to oscillate. Force-versus-distance curves were recorded with tips having very small force constants, at a sampling rate of 1 Hz. For measurements in buffer solutions, a fluid-cell was used, and the cantilevers were allowed to equilibrate in

the measurement buffer for some hours prior to the experiment (in a beaker). This was particularly important in the case of alumina back-coated Si cantilevers, because they would not reach a bending equilibrium for up to 1 hour due to slow oxidation of the metal coating.

Scanning electron microscopy (SEM): Prior to scanning electron microscopy (Philips SEM 505, equipped with a digital data acquisition system), 8-nm-thick gold layer was deposited on the dried and etched samples in a sputtering device (Balzers Union, Balzers, Lichtenstein), to avoid electrostatic charging of the surface. Images were obtained at high-tensions ranging from 20 to 30 kV, and with spot-sizes of 5-20 nm.

Transmission electron microscopy (TEM): The transmission electron images were acquired on a Philips CM 100 (Bio) microscope at a high tension setting of 80 kV. The samples were prepared as follows: 200 Mesh copper grids coated with a thin PVC membrane and 7-8 nm carbon were first exposed to an air plasma for 20 sec. to increase the charge-density of the carbon coating and thus making it more sticky for molecules. Then, the grids were incubated for 1-3 min. on a buffer drop containing the liposomes or molecules to be imaged. After sucking the grid dry by touching a cellulose filter with its edges, the grid was shortly dipped into a water drop, dried again and then lied onto a water drop containing 1% uranyl-acetate for 120 sec. (contrasting solution). In order to fix proteins, the sample was then exposed to a 1% glutaraldehyde solution for 60 sec. and finally air-dried prior to the insertion into the TEM.

Laser scanning microscopy (LSM): For the visualization of fluorescent beads and fluorescently labeled bilayer membranes or liposomes, a Laser Scanning Microscope 310 from Zeiss, Oberkochen, Germany was used. The fluorochromes were excited with an Ar laser at 488 nm and the fluorescence collected between 520 and 570 nm. The images of supported bilayers were performed at constant contrast, pinhole and brightness settings. For photobleaching, the fluorescent samples were first imaged using a 20 × objective (magnification 200 ×). Then, the surface area scanned by the laser was reduced to 1/4, the sample bleached 64 times and then an image was recorded after zooming back to 200 × magnification. Imaging the same substrate area in intervals of 5 minutes gave information about the fluidity (fluorescence recovery) of the membrane. The bleached area had dimensions of 120 × 185 μm.

X-Ray photoelectron spectroscopy (XPS): The XPS spectra were recorded using an ESCA 5400 instrument (Physical Electronics, Eden Prairie, MN) with MgK α radiation at 300 W (15 kV). Measurements were taken at a take-off angle of 45° with respect to the sample surface. The analyzed area was 3.5 mm². Survey scans were taken for each sample with a constant detector pass energy range of 50 eV, followed by high resolution XPS measurements (Pass energy 17.9 eV) between 528 and 738 eV. Electron binding energies were calibrated to the Au 4f (84.0 eV) line.

XPS can also be used to determine the thickness of an adsorbed thin layer (d_2) on a surface. This was done by comparing the change of intensity of a substrate peak (I_s) at two different electron take-off angles (α_1, α_2) using equation A. But the inelastic mean free path of the photoelectrons (λ) in the adlayer must be known (α : electron take-off angle).

Equation A:
$$d_2 = \lambda * \ln(I_s^{\alpha_1}/I_s^{\alpha_2}) / ((1/\sin\alpha_2) - (1/\sin\alpha_1))$$

If the substrate intensity (I_s^1) is known for a reference sample coated with an adlayer of defined thickness (d_1) (e.g. Alkanethiol SAM coated Au(111)), the thickness of a similar, unknown surface coating (d_2) can be determined by relating its substrate intensity (I_s^2) to the one of the reference according to the equation B. In this case, only one measurement at a fixed angle is needed.

Equation B:
$$d_2 = d_1 + \sin\alpha * \lambda * \ln(I_s^1/I_s^2);$$

On evaporated gold surfaces covered with SAMs, however, the approach based on angle variation did not lead to correct thickness calculations. After a series of experiments, the roughness of the gold could be identified as the source for this problem: AFM measurements of evaporated gold shows nanocrystalline domains at very high AFM magnifications. These round shaped domains give rise to a less reduced electron emission at grazing take-off angles (relative to the intensity at large take-off angles) as compared to the same relation on flat samples, leading to an underestimation of the real layer thickness. Example: Octadecanethiol was incubated on ultraflat (TSG) Au(111)- and on normally evaporated Au(111). Using the same XPS settings and the same mathematical model, for the SAM on the flat substrate, a thickness of 18.7 Å was obtained compared to 14.3 Å obtained on the “rough“ gold. Even on optically flat substrates like evaporated gold care has therefore to be taken when determining the thickness of an organic layer using the varying angle approach. On gold it is therefore

better to proceed according to the needs of equation B, and grazing angles should be avoided.

A further point which has to be taken into consideration when applying XPS to thin organic films is the slow degradation of organic layers caused by the strong x-ray radiation. This is specially important when long-time measurements are made on the sample, for example when atomic ratios are to be determined. The degradation of the organic layer can easily be detected by a decreasing peak-integration area of a selected adlayer-peak, coming along with longer exposure to x-ray radiation of the sample. To minimize this effect, high-resolution spectra of the most important elements should therefore be measured at the beginning, or, the power of the x-ray gun can be reduced.

Fourier-transform grazing-angle infrared spectroscopy (FT-GIR): The fourier-transform, grazing-angle infrared spectroscopy was performed on a Bruker IFS 66v photospectrometer operated in a vacuum of ca. 0.5 mbar. For the detection of organic coatings in the thickness range of only one or less than a monolayer, prior to measuring the coated samples, a very clean reference sample without an adlayer has to be measured. This reference spectrum is then subtracted from the spectra of the coated samples. Especially in the case of gold as a substrate, the reference IR spectrum must be measured immediately after the gold preparation, because gold adsorbs organic molecules very fast, leading to contamination. Compared to nitrogen-purged or ambient-air spectrometers, the measurement in a vacuum leads to the best discrimination of spectral adsorption bands stemming from adsorbed water. Using such a machine it is also important to acquire the spectra by keeping the time interval between the insertion of the sample into the measurement chamber and the measurement itself constant.

Ellipsometry: The thickness of the stamped DSU layers was measured using a Plasmos SD 2300 ellipsometer at a wavelength of 623.8 nm. The angle of incidence was 70° and the layer thickness measured relative to non-modified areas of bare gold on the same sample, assuming a refractive index of 1.44 for organic thin films. For a measurement, first the refractive index n and the extinction coefficient k were determined for a clean reference substrate without a layer. These data were then used as settings for the complex index of refraction of the substrate. The roughness of the substrate has a big influence on k , which makes it extremely important to use a reference substrate which was produced under exactly the same conditions as the substrates with the adlayers. The best is to measure (various locations) on samples containing both, coated and non-coated areas. Gold reference surfaces should be

measured immediately after evaporation, as contamination from the air will change the n and k of this substrate. In the experiment which was done to determine the amount of DSU transferred to a gold sample by stamping, 20 mM DSU in dioxane was used for inking the stamp.

Contact-Angle goniometry: Advancing contact angle measurements were carried out on a G-I contact angle meter (Krüss, Hamburg, Germany) by applying a 3- μ l drop of ultrapure water to a freshly prepared surface. A second drop was centered on the first, and the advancing contact angle was measured within 30 seconds. A set of six locations was averaged per sample.

Thin film deposition: Metal films of Au, Cr and Ti were deposited on flat substrates using a vacuum coating system BAE 370 from BAL-Tec (Liechtenstein) with integrated quartz crystal deposition controller Inficon XTC/2 from Leybold (Switzerland). This large evaporator was equipped for thermal (Au) as well as electron-beam (Ti) metal deposition. The large distance (30 cm) between the metal source and the target led to metal coatings of homogeneous thickness. On the other hand, due to the size and design of the vacuum chamber, the freshly evaporated samples could not be removed without exposing them to ambient air - leading to contamination.

For the coating of small samples, a PST 170 E (Bal-Tec, Liechtenstein) tabletop evaporator was used, which could be ventillated with argon but which led to inhomogeneous metal coatings due to a distance between the tungsten filaments and the substrates of less than 10 cm.

The conductive gold coating on samples for SEM imaging was sputter-coated in a Balzers Union SCD 010 sputtering/etching device in a 0.06 mbar argon atmosphere. Typically, 5 nm gold were deposited.

Langmuir Blodgett Technique (LB): The transfer of lipid bilayers by LB deposition was done using a 10 x 40 cm teflon trough equipped with a Lauda filmlift, model FL-1E (Lauda, Königshofen, Germany) and a surface pressure tensiometer from NIMA Technology, model PS3 (Coventry, UK). The lipids were dissolved to a total concentration of 1 mg/ml in CHCl_3 and 30 μ l of this solution were then applied to the air/water interface of the trough. The solvent was allowed to evaporate for 10 min., after which the film was compressed with a speed of 20 cm^2/min . until the desired transfer pressure was attained. The lipid monolayer was then allowed to equilibrate for 15 min.. The first LB monolayer was then deposited by withdrawal of the substrate through the

air/water interface at a dipper speed of 0.5 cm/min.. The sample was then allowed to dry in air for 5 - 15 min., after which it was pushed back through the interface at the same dipper speed. Ultrapure water or buffer solutions were used as subphase, and the depositions were made at $24 \pm 1^\circ\text{C}$.

Others: The plasma cleaning of surfaces was performed in an old Edwards High Vacuum LTD carbon-coating device equipped with two circular high-tension electrodes. The plasma was produced in an argon, nitrogen, air or oxygen environment, depending on the application.

General procedures

Preparation of Gold Surfaces: Two main, different gold substrates have been used in this thesis :

(a) A 200-nm Au layer was deposited by thermal evaporation using the BAE 370 vacuum coating system onto silicon wafers coated with an adhesion layer consisting of 8 nm of Ti (electron-beam). These substrates were placed under an argon atmosphere immediately after the preparation in order to avoid contamination of the gold from the ambient. In the present work we always refer to this type of gold, if not otherwise stated.

(b) Ultraflat, template-stripped gold (TSG) with a mean roughness of 0.2 - 0.5 nm over $25 \mu\text{m}^2$ was prepared as described previously (Hegner et al., 1993, Wagner et al., 1996b). These surfaces are protected from contamination by the mica template itself, which can easily be lifted off mechanically with the help of tweezers immediately before use. One can reproducibly obtain bare TSG samples without remaining mica pieces by cutting the edges of the glued sample with a sharp knife prior to the mica template removal.

Chemically patterned surfaces: The monolayer patterns in chapter “Using micro-contact printed substrates for the covalent immobilization of biological objects“, are composed of different alkanethiolates (dodecanethiol, hexadecanethiol (HDT), 11-hydroxyundecanethiol (HUT), and 11,11'-dithiobis-(succinimidylundecanoate) (DSU)). The patterns were prepared according the μCP method discussed in chapter “Micro-Contact Printing“ (Wilbur et al., 1994, Kumar et al., 1994). For route A (Figure 48), the stamp was exposed to a solution of DSU (1 mM in dioxane). After drying with nitrogen and one minute in air, the stamp was lightly pressed onto the gold sample: alkanethiol was thereby transferred to the gold, forming an adsorbed layer. The DSU-pattern was

then rinsed with HUT (5 mM in ethanol) for 30 seconds in order to cover the residual bare gold surface with a defined chemical functionality. For route B (Figure 48), the gold was patterned with a monolayer of hexadecanethiolate (1 mM in ethanol) by μ CP and then subjected to chemical etching to create topographically patterned surfaces.

Physically patterned surfaces: The preparation of topographically (physically) patterned substrates using the alkanethiol-resist method is discussed in detail in chapter “Micro-contact printing (μ CP)/etching“. The Au/Si structure described in chapter “Generation of etch-patterned surfaces with immobilized biomolecules: SAM exchange technique and collagen V immobilization.“ was produced by first creating a patterned hexadecanethiol SAM on gold by μ CP. Afterwards, the gold areas which were not covered by monolayers were selectively etched by immersion in an aqueous solution of 2 mM $K_3Fe(CN)_6$, 20 mM KCN and 1 M KOH at 3°C for 10 min. while stirring. The titanium layer and the underlying thin silicon oxide layer were then removed by etching with 1 % HF. Subsequent boiling in 4M KOH in 15 % v/v isopropanol for 4 min. at 60°C resulted in V-shaped, anisotropic etching of the silicon. These substrates were then washed with 1 M KOH and water, dried under nitrogen and exposed to “piranha” solution consisting of 30% H_2O_2 /conc. H_2SO_4 (3:7), at 60 °C for 2 min., to remove the organic monolayer etch-resist from the gold surface. Finally, after washing with water and drying, these substrates were incubated in a solution of 1 mM DSU in dioxane for 2 hours, washed with dioxane and were then ready for immobilization of proteins.

Peroxidase activity test: 1 ml of a solution of horseradish peroxidase (POD type II, 200 U/mg) in PBS (pH 7.5, activity 30 mU/ml) was applied to different DSU- and/or HUT-monolayer substrates and kept for 4 hours at room temperature under gentle shaking. These surfaces were washed three times with a stream of PBS containing 0.1 % (v/v) Tween-20 and further soaked for 20 min. in the same buffer. The enzymatic activity of the chemisorbed peroxidase was quantified as follows: After washing (as described) the samples were incubated individually at 24°C in 1 ml of a 0.42 mM solution of 3,3'-5,5'-tetramethylbenzidine (TMB) in PBS (pH 6, containing 1% dimethyl-sulfoxide DMSO and 0.004 % H_2O_2). After 45 min. the blue supernatants were transferred into disposable cuvettes, the reaction stopped by adding 100 μ l of 2 M H_2SO_4 and the absorption measured at 450 nm (JASCO 7800 UV/Vis Spectrophotometer). For the high-resolution AFM samples, POD (12.5 U/ml, 10 h at 4°C) was used and the sample dried under nitrogen after rinsing with water.

Immobilization of latex microspheres: A droplet of a suspension of yellow-green fluorescent, amino-modified latex microspheres (4.5×10^{13} spheres/ml in PBS buffer; diameter: 200 nm) was applied to the surface of DSU/dodecanethiol patterned gold and incubated in a chamber with 100 % humidity at room temperature. After 2 hours, the surface was washed with buffer solution, then subjected to a very strong stream of water for several seconds (sonication removes all latex beads, whether covalently bound to DSU or physisorbed on HUT), and examined in a confocal laser scanning microscope.

Immobilization of biological samples on the aminoreactive SAM:
Immobilization of Semliki Forest viruses: The stock solution containing Semliki Forest virus (0.8 mg protein/ml) was diluted 1:20 with PBS pH 7.9 and applied to a DSU/dodecanethiol patterned gold surface for 6 hours at room temperature. The surface was then rinsed with fresh high-salt buffer and then with PBS pH 7.5.

Immobilization of collagen: The acidic collagen V solution (800 μ g/ml) was diluted 1:4000 with high-salt buffer (PBS, pH 7.9, supplemented with 500 mM NaCl) and then applied to a 1 cm² HUT/DSU patterned surface for 2 hours at room temperature. After washing with 15 ml of the buffer, the surface was again incubated in high-salt buffer for 2 hours under gentle shaking. In some cases, non-specifically adsorbed protein had to be removed by brief sonication in NaCl-supplemented buffer with 0.05 % Tween 20, followed by rinsing with PBS. The collagen pattern was examined by AFM either in PBS or after air-drying. This strategy was also used for the immobilization of collagen V on the 3D-patterned surfaces.

Liposome production: A large variety of unilamellar liposomes of different phospholipid compositions were produced according to the method described by MacDonald et al. (MacDonald et al., 1991). In short, CHCl₃ solutions of the different lipids were mixed together in a long reagent-tube (total lipid content was approx. 25 mg) and then the CHCl₃ was removed under reduced pressure in a rotavap. A film of dry lipids on the walls of the flask is obtained which is then further dried for 1 hour in high-vacuum to remove all the entrapped solvent. Then, the lipid film is rehydrated by addition of approximately 1 ml of buffer solution and thoroughly vortexed at maximum speed until no more lipid sticks to the walls and a turbid solution is obtained.

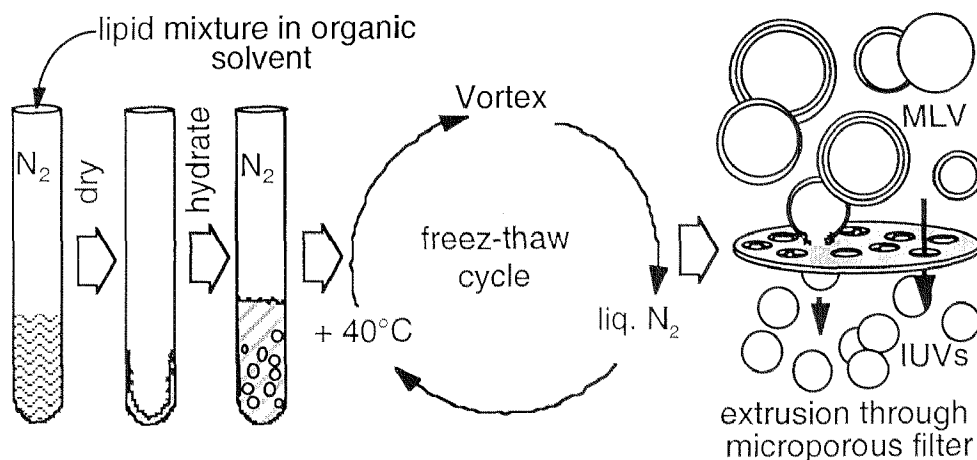


Figure 11: Preparation of liposomes by lipid rehydration/freezing-thawing and extrusion (MLV = Multi-Lamellar Vesicles, IUVs = Intermediate Unilamellar Vesicles).

Some lipid mixtures dissolve very badly and have to be heated in order to get dissolution. During this step, multiwalled liposomes of all sizes are produced. If a fluorescent marker is included into the lipids, the wonderful small spheres can be observed in a fluorescent microscope. The brownian motion keeps everything in motion and also changes in surface tension produced by altered buffer conditions lead to large morphology changes of the lipid structures. Very spectacularly, if small amounts of microscope-immersion oil are added to the water phase, long tubular structures are formed which seem to have inherent life (Figure 12) .

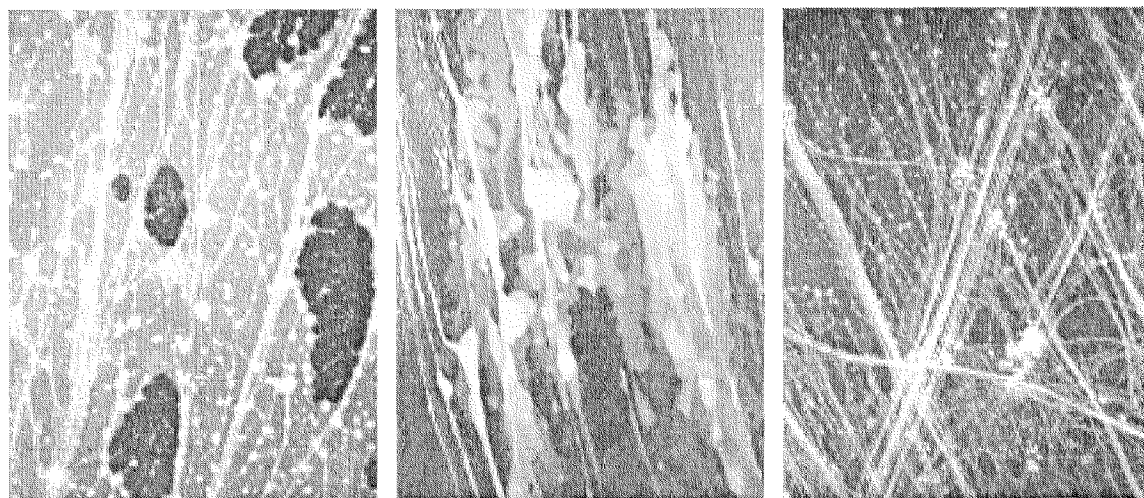


Figure 12: 3-D networks of moving, fluorescent lipid structures obtained after addition of oil to a lipid solution. LSM image.

To obtain intermediate unilamellar vesicles (IUVs), the liposome solution after hydration is first freeze-thawed 5 times in order to make the liposomes smaller and less rigid (Lasic, 1993). This is achieved by repeating the following sequence for 5 times:

- freezing of the lipid solution for 30 sec. in liquid nitrogen
- thawing of the solution in a water-bath at 36°C ($T > T_c$ lipids) for 2 min.
- strong vortexing for 1 min.

After this step, unilamellar vesicles of fairly homogeneous size are obtained by passing the lipid solution through a polycarbonate filter with defined, round shaped holes. This was done by either using a desk-top extruder driven by N_2 gas pressure, or using the hand-extruder from Avestin, Inc., Ottawa, Canada which is described in MacDonald et al. (MacDonald et al., 1991). Due to its simplicity and due to the fact, that never liposome volumes larger than 1 ml were needed, the hand driven extruder proved to be best suited for our applications. Moreover, this extruder can simply be immersed in a thermostated water-bath at higher temperature, which must be done to extrude liposomes having a transition temperature higher than room temperature. Usually, 2 polycarbonate filters were laid into the extruder with the opaque sides facing each other and 21 passes through the filters were run. Polycarbonate filters from Sterico AG, Dietikon, Switzerland with pore diameters of 100, 200 or 400 nm were used. Extrusion through 400 nm pore-size filters does lead to a large particle size distribution for which the use of larger diameters is not worth trying (except for sterilization). Usually, filters with pores of 100 or 200 nm diameter were used.

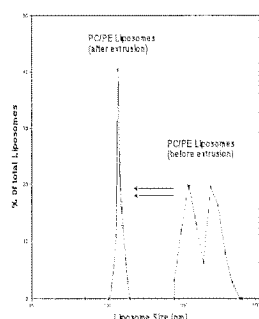


Figure 13: Size distribution of PC/PE/fluorophore liposomes determined by Right Angle Photocorrelation Spectroscopy. The broad twin-peak on the right comes from an only freeze-thawed liposome preparation. On the left, the narrow size distribution of a freeze-thawed liposome preparation is shown, which was additionally extruded through a 100 nm polycarbonate filter.

The large unilamellar vesicles (LUVs) solution was then transferred into small storage vials and kept at 4°C prior to further use. Freezing will destroy the homogeneity of the liposomes. The liposome solutions can be used for about 1 month and should be kept under nitrogen to avoid oxidation of unsaturated lipids.

Name	Composition	Size-distribution (nm)	Comments
Lip01	PC/PE, 8:2; NBD-PE	105-225	PE for covalent binding to DSU-SAM
Lip02	PC/PG, 8:2, NBD-PE	105-225	Negatively charged liposomes
Lip03	PC/PE, 9:1, NBD-PE	85-160	
Lip04	PC/PE, 6:4, NBD-PE	50-340	
Lip05	PC/Chol/DP, 30:15:3, NBD-PE	110-230	Lipid composition according to (Duncan and Schlegel, 1975a). For SLO insertion.
Lip06	PC/PE, 8:2, BODIPY	120-180	New fluorescent dye
Lip07	PC/Chol/DP, 30:15:3, BODIPY	100-250	
Lip08	PC/Chol/DP, 30:15:3, BODIPY	-	
Lip09	DPPC/Chol/DP, 30:15:3, BODIPY	-	Synthetic DPPC
Lip10	PC/Chol/DP, 30:15:3, BODIPY	-	
Lip12	DPPC/Chol/DP, 20.62:1.87:1.5, BODIPY	-	Cholesterol conc. 1/4 compared to Lip10
Lip13	DPPC/Chol/DP, 22.12:0.37:1.5, BODIPY	-	Cholesterol conc. 1/20 compared to Lip10
Lip14	PC/Chol/DP, 30:15:3, BODIPY	-	Not freeze-thawed nor extruded. Vortexed and exposed to U-sound (Duncan and Schlegel, 1975a).
Lip15	PC/Chol/DP, 30:15:3, BODIPY	-	Not freeze-thawed nor extruded. Vortexed and exposed to U-sound (Duncan and Schlegel, 1975a).
Lip16	PC/Chol/DP, 30:15:3, BODIPY	-	
Lip17	PC/Chol/DP, 30:15:3, containing 0.1 M K_2CrO_4	-	For chromate release assay
Lip18	PC/Chol/DP, 30:15:3, containing 0.3 M Glucose	-	For glucose release assay
Lip19	PC/Chol/DP, 30:15:3	-	Negative reference for release assays
Lip20	PC/Chol/DP, 30:15:3, BODIPY	140-310	Large LUVs for membrane suspension over nanocavities
Lip21	PC/PE/Chol/DP, 10:5:7.5:1.5, BODIPY	130-280	Large LUVs for membrane suspension over nanocavities
Lip22	PC, BODIPY	77-360 (3× extruded)	Large LUVs for membrane suspension
Lip23	PC/PE, 30:6, BODIPY	95-360 (2× extruded)	Large LUVs for DSU-bound, suspended membranes
Lip24	DPPC, BODIPY	1050-1800	Large, crystalline LUVs for membrane suspension

Table 2: Liposome preparations made during this Ph. D. thesis.

Table 2 lists the different liposomes which were produced. The concentration of the fluorescently labeled phospholipids NBD-PE and BODIPY was always 1%. Liposomes were hydrated in PBS buffer pH 7.4 and size distribution after extrusion was determined by Right Angle Photocorrelation Spectroscopy (Figure 13).

MICRO-AND NANOSTRUCTURING OF SURFACES

A) Microstructuring

Microstructuring of silicon and gold substrates was important for two kinds of applications in this dissertation: (i), appropriate silicon masters had to be produced by standard silicon-photolithography for subsequent casting of PDMS stamps (in this chapter). These stamps were then used for the creation of chemically micropatterned substrates (see chapter “CHEMICAL PATTERNING“) and (ii), for the production of microetched Au/silicon structures using the SAM-resist method (see „Micro-contact printing (μ CP)/etching“).

Photolithography

Photolithography became the standard structuring method for chip-technology and it is used for the production of most of the highly integrated electronic devices in use nowadays ((Glockner and Shah, 1995, Vossen and Kern, 1978, Menz and Bley, 1993)).

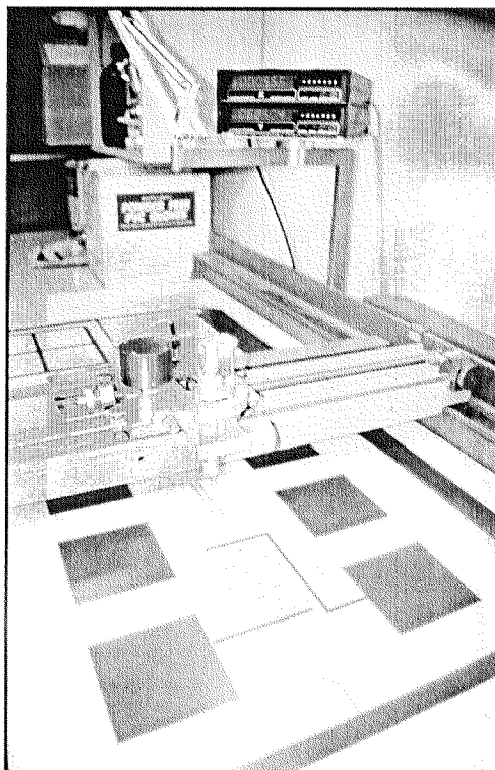


Figure 14: Hand-driven “coordinatograph“ with attached rubilith-foil mask which is being cut with a precision of 10 μ m.

Based on this technology, we used monocrystalline silicon wafers which could easily be structured in a controlled and anisotropic manner. The sharply defined structures which were obtained together with their very flat surfaces are very well suited for the production of masters for the subsequent micro-contact printing (μ CP) pattern transfer.

The following steps were performed to produce the microstructured Si(100) wafer: Firstly, a mask containing the desired patterns for downscaling had to be designed. For the production of features down to $5\ \mu\text{m}$, the “rubilith-foil mask“ technique was applied: a 50-fold magnified version of the desired patterns was cut manually into the foil using a coordinatograph (Figure 14). Usually, the mask is designed using “computer aided design“ (CAD) tools and then the foil is cut automatically on a knife-plotter. For our case however, this plotter could not cut the foil sharp enough, so we had to proceed manually which gave a positioning accuracy of $10\ \mu\text{m}$.

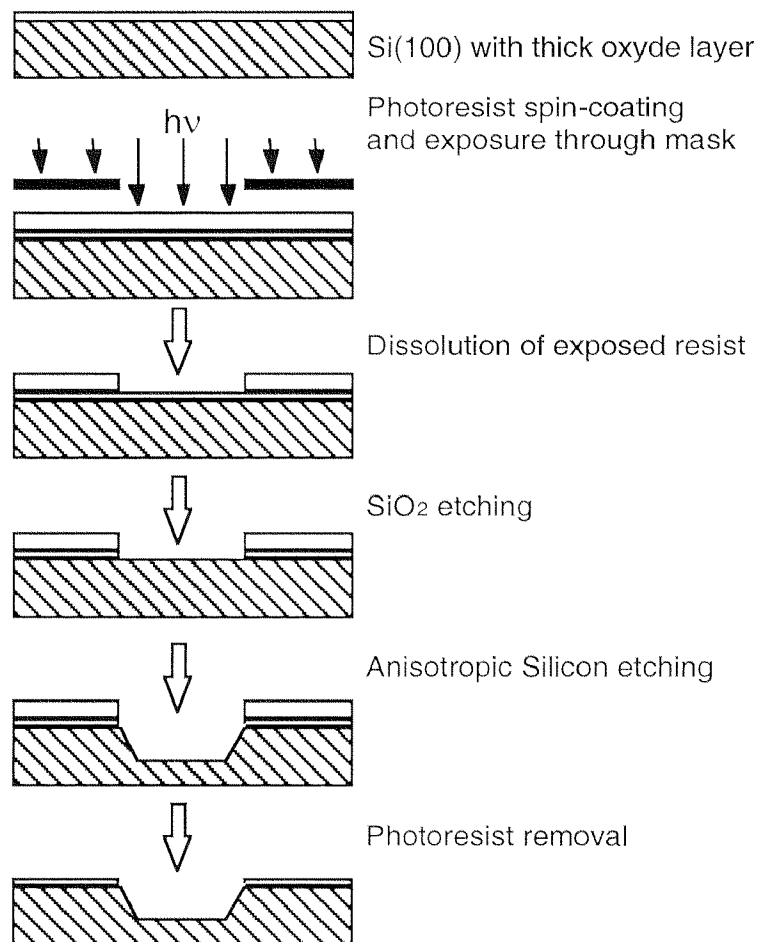


Figure 15: Scheme of the steps which were followed to perform the lithography and the etching steps.

After carefully peeling off the cut, red foil areas, the mask with a size of 1 m² was reduced by a factor of 5 by using a high resolution photoreproduction process (SPEICH, Zurich), followed by a photographic, 10-fold reduction step at the IFH (ETHZ). This led to a 4.5 cm glass mask through which the resist-coated wafers can be exposed in a photoaliner.

The following processes (Figure 15) were performed in a cleanroom (at the IFP, ETHZ): Si(100) wafers were coated with 500 nm “field-oxide“, cut into halves and then into pieces of appropriate size (3 × 3 cm). After rinsing with water and drying, they were ultrasonic-cleaned using acetone and isopropanol. After a dehydration-bake at 180°C, the wafers were silanized in a gas-phase reaction using hexamethyldisilazane (HMDS) in order to enhance the adhesion of the photoresist, which was then spin-coated to a thickness of 3,1 μm. The unwanted resist on the back-side of the wafer was removed using an ear cotton swab (Q-tip) and acetone before softbaking at 90°C on a hotplate.

Prior to exposure with the patterned mask, the thick resist-bulges at the edges of the wafers had to be removed by a long exposure of a darkfield-mask to guarantee a subsequent tight-fit of the mask to the wafer in the photoaliner. The subsequent exposure of the photomask was done using a high-pressure UV lamp with an intensity of 150 mJ/cm² (the mask was aligned parallel to the Si(111) orientation). After development (removal of the light-exposed resist parts), the wafers were qualitatively examined in a binocular and then post-bake to smoothen the photoresist patterns.

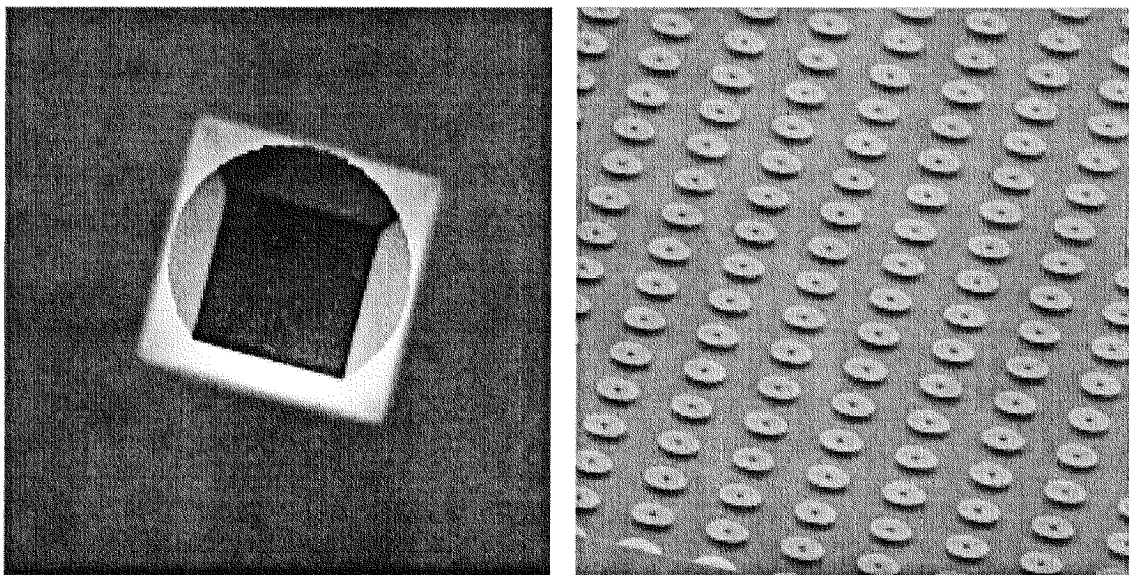


Figure 16: Si(100) microstructures produced by etching through a SiO₂ mask: Strong underetching at a circular hole in the SiO₂ (left) and under circular SiO₂ islands (right). (SEM, the circles have a diameter of 60 μm)

The etching steps were performed in the chemistry-lab under non-cleanroom conditions: Firstly, the not protected oxide layer was removed by etching with BHF until the nonprotected areas turned hydrophobic (clean Si is hydrophobic compared to SiO₂). After water-rinsing and drying, the remaining photoresist was removed by short dipping in acetone. The wafer then exposed the structured, protecting SiO₂ layer which acts as a resist through which the silicon could be etched using a stirred, aqueous hydroxyl-ion solution at 60°C.

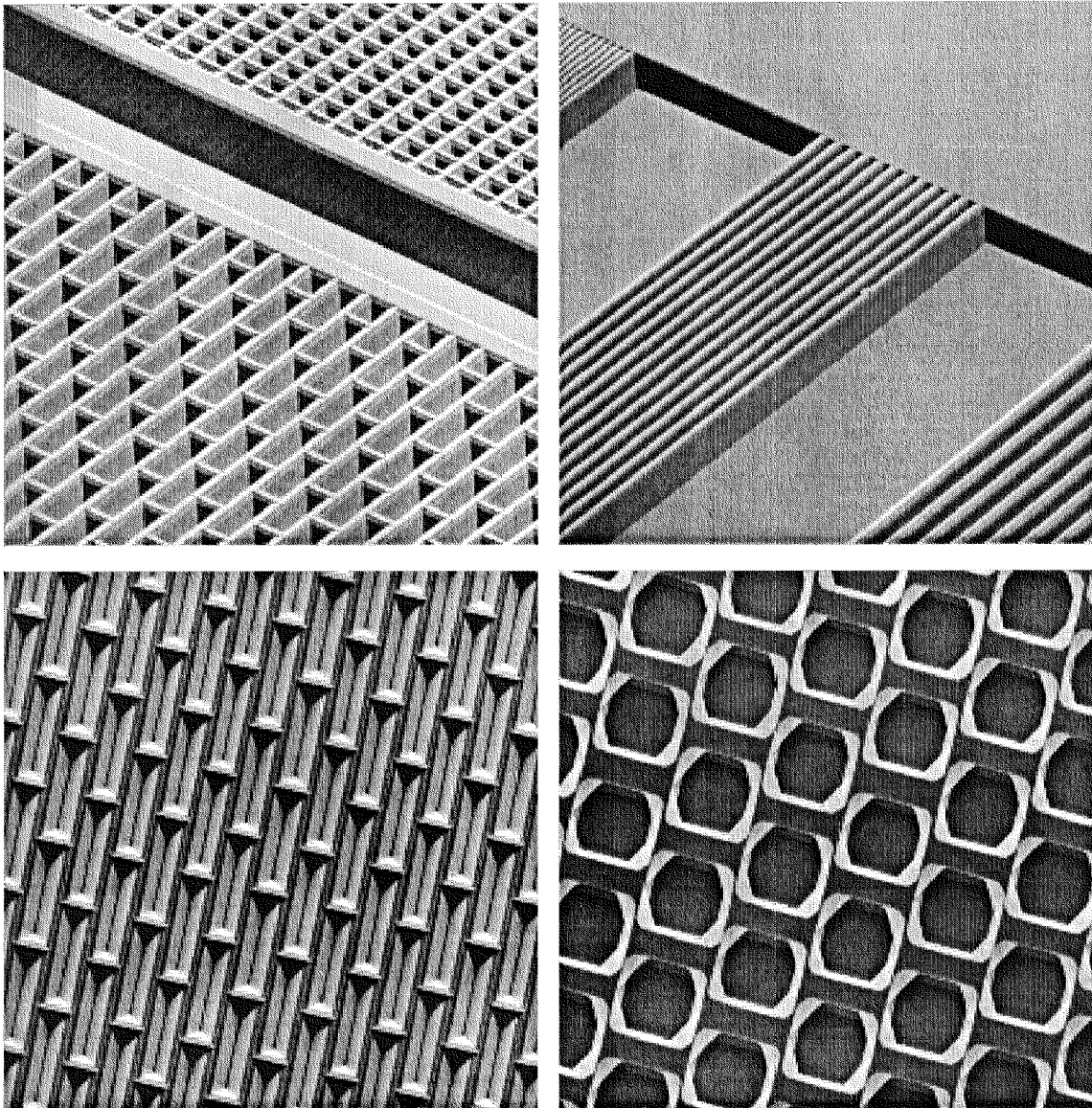


Figure 17: SEM images of microstructures obtained after KOH etching of Si(100) through a SiO₂ mask. The periodicity of the structures in the middle of the upper-right figure is 40 μm .

The depth of etching could accurately be controlled by varying the etching-time, the KOH concentration or the bath-temperature. KOH based solutions etch the Si(100)

anisotropically (not at the same rate in the different crystalline lattices). This makes it impossible to obtain round-shaped structures or slim lines parallel to the Si(010) direction (non-orthogonal structures), due to strong underetching. The strong underetching obtained on such structures is shown in the SEM images of Figure 16 For crystallographic reasons, not orthogonal but V-shaped etch-grooves are obtained by etching Si(100). This is due to the fact that the slowest-etching Si plane (Si(111)) is oriented at an angle of 54.7° relative to the surface plane Si(100) (See Figure 23). Figure 17 shows four details of the microstructures which were obtained after etching. In a last step (if required) the remaining SiO_2 resist was removed by etching in BHF and then different surface-coatings were produced on the structured Si masters depending on the latter use.

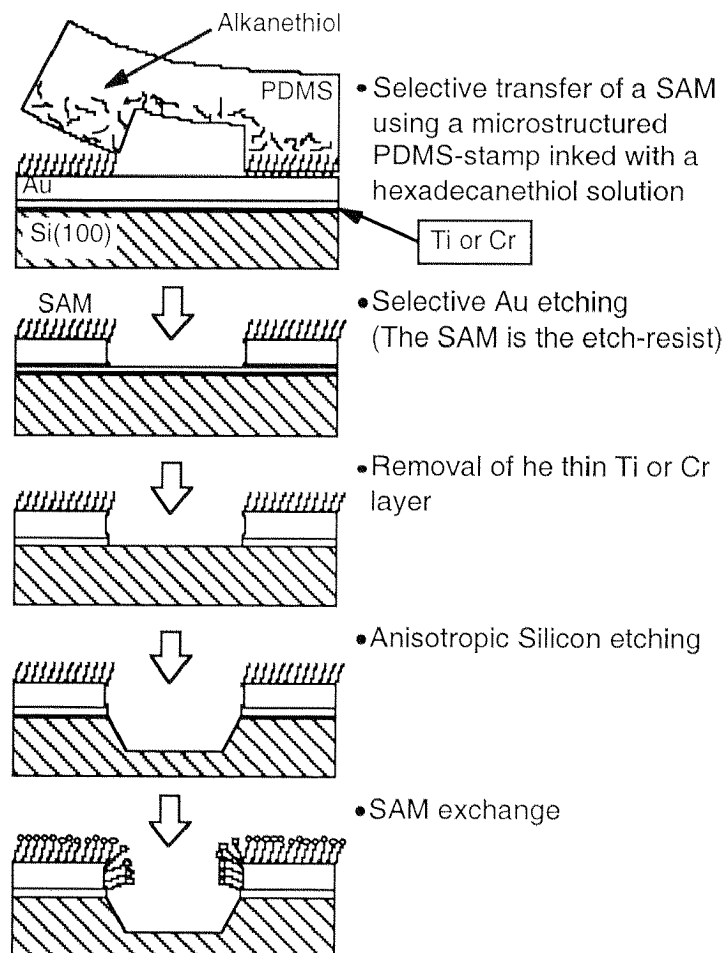


Figure 18: A scheme of the μCP /etching technique.

Micro-contact printing (μ CP)/etching

Microstructured (etched) gold surfaces (which can be modified chemically) can be produced by sputtering or evaporating gold on the structured Si-wafers described in the previous chapter. These were however first in line used as masters for the production of stamps because far less equipment and time is needed to obtain structured gold surfaces using the μ CP/etching method ((Xia and Whitesides, 1998, Wilbur et al., 1994, Kumar et al., 1994, Mrksich and Whitesides, 1996)). This technique consists in transferring locally a hydrophobic and extremely ordered self-assembled monolayer (SAM) of hexadecanethiol by means of a PDMS stamp on a gold substrate. The SAM then acts as an etch-resist, protecting the underlying gold from being etched. A scheme of this method is given in Figure 18.

Manufacturing of PDMS stamps

In order to cast PDMS stamps using microstructured Si masters, the silicon has first to be rendered hydrophobic in order to avoid the PDMS to adhere strongly to clean Si or SiO₂ surfaces upon polymerization (it is in fact not surprising that a silicon-based material (PDMS) adheres well to a silicon surface). Three approaches were found to be efficient:

- The substrate can be silanized using octadecyltrichlorosilane in an organic solvent: The substrates are immersed in an 1% octadecyltrichlorosilane solution in CHCl₃ for 5 min. at room temperature and then thoroughly rinsed in CHCl₃ followed by drying with nitrogen.
- Secondly, the substrates can be exposed to hexamethyldisilazane (HMDS) in the vapor-phase. This small silane-compound is also used to render silicon wafers hydrophobic prior to photoresist spin-coating. Several ml of HMDS are poured into a big, flat beaker containing a stirrer covered by a teflon holder. The beaker is covered with a large petri-dish and then heated to 40°C (irritant fumes and stench !). The wafers are then exposed to this atmosphere for 15 min., dried under nitrogen and then rinsed with water.
- The wafers can also simply be passivated in BHF. This gives rise to Si-H bonds on the surface which are hydrophobic in nature. However, this surface is not very stable and reconverts slowly to SiO₂.

Any of these treatments render Si non-adhesive for the PDMS, but the third method finally was preferred.

PDMS based-solution and crosslinker are weighed in a ratio of 10:1 w/w in a disposable beaker and then extensively mixed for several minutes. Thousands of air bubbles form in the viscous solution during this process which then have to be removed by exposing the polymer to a vacuum for 30 min. This solution is then carefully poured over the silicon master for which a small flat-bottom aluminum-foil basket has been folded. The polymerization is allowed to proceed during 5 hours at 80°C, after which the aluminum-foil is peeled off, overhanging PDMS is carefully cut away with a sharp, solvent-cleaned knife-blade (cutter-blade) and then the stamp is peeled off from the master (wafers are extremely brittle !).

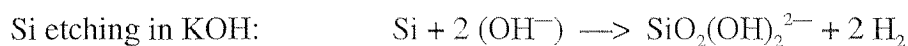
Micro-Contact Printing

Micro-contact printing is performed as follows : First the stamps must be thoroughly cleaned to avoid contamination from previous experiments. This is done by sonication in a good solvent for the alkanethiols previously stamped. PDMS will swell more or less strongly depending on the solvent used. This swelling can be measured by determining the weight difference before and after exposure to the solvent. Such a study as well as a measurement of the evaporation kinetics (of different solvents out of PDMS) can be found in (Lehmann et al., 1998b). According to these data, after cleaning, the stamps have to be allowed to dry for half an hour in a dust-free atmosphere prior to stamping.

Then, a stamp is exposed to a solution of hexadecanethiol (1-10 mM in ethanol) with the help of a Q-tip. After wetting, the Q-tip must be shaken out intensively in order to get rid of an excess alkanethiol solution. After drying in air for 60 sec, the stamp is carefully deposited with one edge on the Au substrate and then allowed to fall onto the Au under its own weight. Using this technique, it is possible to avoid lateral movement of the stamp on the substrate which would negatively affect the resolution. Afterwards, the stamp is lightly pressed onto the gold sample, beginning in the middle of the stamp and proceeding towards the corners (in order to avoid to entrap air). Often optically visible, the stamp is thereby sucked at the gold leading to a nanoscopic solvent bridge between the stamp and the surface, through which the alkanethiol molecules can reach the gold by diffusion - where they self-assemble, forming an adsorbed (resist)monolayer. After 120 sec., the stamp is vertically lifted off the surface without squeezing it (which could lead to alkanethiol solution leaking).

Etching

The creation of etch-structured gold/silicon surfaces is achieved by a multistep etching procedure: Nonprotected - i.e. monolayer-free - gold areas are selectively etched by immersion in an aqueous cyanide-solution consisting of 2 mM $K_3Fe(CN)_6$, 20 mM KCN and 1 M KOH at 3°C for 10 min. under stirring. The titanium layer and the underlying thin native silicon oxide layer are then removed by etching with 1 % HF. Subsequent boiling in 4M KOH in 15 % v/v isopropanol for 4 min. at 60°C results in V-shaped, anisotropic etching of the silicon. The gold areas act in this case as resist-layer, and the depth of the grooves can be chosen varying the etching time or temperature. Subsequently, the substrates are washed with 1 M KOH, water and then dried under nitrogen. This results in flat, elevated micrometer-sized gold islands on the silicon support. No changes in the Au(111) morphology could be observed due to the etching.



By exposure of these samples to “piranha” solution consisting of 30% H_2O_2 /conc. H_2SO_4 (3:7), at 60 °C for 2 min., the organic etch-resist monolayer can be removed from the gold surface. The topographically structured substrates can then be chemically modified as described in the chapter „SAM exchange technique“.

On the other hand, using “Aqua Regia“ (HNO_3/HCl 1:3), the Au can be completely removed leading to structured Si surfaces.

It is quite remarkable that an only nanometer-thick resist is capable of preventing chemical etching of the underlying substrate. This phenomenon can be understood in terms of the very strong intermolecular van der Waals forces which tightly hold together the alkanethiol side-chains in the SAM (See „Introduction“). However, not all the existing gold etching solutions can be prevented from attacking the gold. It is indeed very difficult to find suitable etching solutions and -conditions which allow good etching selectivity. Table 3 summarises the Au-etching tests which were performed and the etching results. Several etching solutions were also tested for the Si-etching step (Table 4).

Au etching solutions

Many other etching tests were performed varying different parameters like temperature or concentrations etc. But these results were not very meaningful, for with hindsight it

was discovered that the absolute cleanness of the Au substrate prior to stamping had an enormous effect on the stamping efficiency. In some laboratory-rooms it was even completely impossible to produce micro-contact printed surfaces. In those rooms there must have existed some air-pollutants which were quickly and strongly adsorbed by the gold surfaces making them badly accessible for alkanethiols. Freshly evaporated gold surfaces are usually kept under nitrogen (5.0) before use and can be cleaned with hexane to remove weak contaminants.

Etch-solution	Composition	Result
Etch 1	100 mM NaCN in 1 M NaOH room temperature, until dark Si appears	Bad etching selectivity leading to extremely rough Au after etching
Etch 2	100 mM NaCN in 1 M NaOH, O ₂ bubbling. room temperature, until dark Si appears	Somewhat better selectivity but still not very reproducible.
Etch 3	Au-etch obtained by Mr. Hollaender from Faselec. Unknown composition. room temperature, 30' to 3 hours	Good selectivity but extremely low etching rate.
Etch 4	2 mM K ₃ Fe(CN) ₆ 20 mM KCN in 1 M KOH 3°C, ±10 min.	Good selectivity at 3°C.

Table 3: Au etching solutions. A recent publication listing different etching solutions is: (Xia and Whitesides, 1998).

More contaminated gold can be cleaned by exposing it to piranha solution for several minutes. The best strategy however is to directly perform the stamping after the Au-evaporation step. (It is important not to ventilate the evaporator high vacuum (HV) chamber with ambient air but with nitrogen (5.0) or argon. Also due to oil contamination, oil-diffusion HV pumps have proven completely incompatible with Au evaporation techniques even using high-quality, PTFE-based oils.)

Silicon etching solutions

Etch-solution	Composition	Result	Ref.
Etch "A"	4 M KOH 15% Isopropanol 60°C, 5 min.	Au not attacked. Si bright and flat at short etching-times/ slightly dull at longer etching-times.	(Vossen and Kern, 1978), p. 441
Etch "B"	100 ml HNO ₃ (65%) 40 ml H ₂ O 6 ml HF (40%) room temperature, 5 min.	Au is strongly attacked. Underetching (Ti is etched).	(Vossen and Kern, 1978), p. 439
Etch "C"	Hydrazine-H ₂ O equimolar ! Poisonous ! 120°C, reflux.	Au is not attacked, but Si is rough after etching.	(Vossen and Kern, 1978), p. 443
Etch "D"	5.5 g ethylenediamine 4.5 ml H ₂ O 85°C, 2 min.	Au not attacked, Si well etched but very rough. Defects etch as rectangles.	(Walker and Tarn,), p. 1034
Etch "F"	100 ml H ₂ O 10 g NH ₄ F 0.2 ml H ₂ O ₂ room temperature, 10 min.	Au is not attacked. Flat, bright Si. Some Ti etching. Low etch-rate.	(Vossen and Kern, 1978), p. 440

Table 4: Etching solutions which were tested to etch Si(100) protected by an Au or SiO₂ resist-mask. The etching solutions were heated in a stirred glass beaker immersed in a temperature-controlled oil-bath, and the samples were hold using tweezers.

Simple KOH-based Si-etching solutions were finally chosen for Si etching in general. Etching rates for such systems can be found in (Heuberger, 1991). Sometimes, an additional smoothening of the etched Si surfaces was achieved using isotropic Si-etching (not described). However, in the presence of small amounts of contaminants on the Si surface (due to non-cleanroom conditions in our chemistry laboratory) this can also lead to additional roughening of the surface.

B) Nanostructuring

Nanostructuring is probably the most topical science in nanotechnology. Thanks to new developments in electron-beam- or X-ray lithography as well as scanning-probe techniques it is becoming more and more possible to create structures in these small dimensions. Nevertheless, the substrates which are amenable to such techniques are still very few and it is thus not seldom that other approaches have to be worked out for a specific nanostructuring problem. In our case we were looking for possible routes for nanostructuring Au substrates in order to profit from the very good chemical modifiability of this element. Figure 19 gives an overview over possible routes which were taken into consideration. Many of them are completely new approaches which have never been studied before.

Route A: Micro-contact printing has been described in the chapters above and can indeed also be used to structure substrates in the nm dimension. However a master with the desired nm-patterns is needed in a first place. This master has to be written by using electron-beam lithography. Secondly, a PDMS stamp of higher strength has to be used in order to obtain good pattern reproduction. The latter technique was discussed very recently by Delamarche et al. (Delamarche et al., 1998).

Route B, based on the use of polycarbonate filters is described below in chapter “Polycarbonate Filters“.

Route C is based on the nanostructured porosity which is inherent of some aluminumoxide membranes produced by anodic spark deposition ((ANOTEC, 1998, Wirtz et al., 1991)). The honeycomb-like structures can have diameters ranging from a few to hundreds of nm and have a depth of several hundreds of microns. These ceramic-based materials are being used commercially as high-tech filters. As substrates for bilayer immobilization after coating with a gold layer these surfaces however were not used in this thesis. Firstly, the honeycomb surface is too rough and secondly one had to expect that the liposomes would hardly find enough surface-contact to induce spreading. Furthermore it is preferably to have a few holes embedded in a defined, flat plane instead of having holes all over the surface.

Route D, based on nanometer-scale polymer beads and evaporation techniques is the one best suited for our application and is described in detail further below in chapter “Nanospheres“.

Route E: Embossing is a technique by which a hard, micro- or nanostructured masterpiece is indented (embossed) into a thermoplastic material upon heating. It is possible to produce hundreds of copies (negative form) of the masterpiece surface-structure by this means.

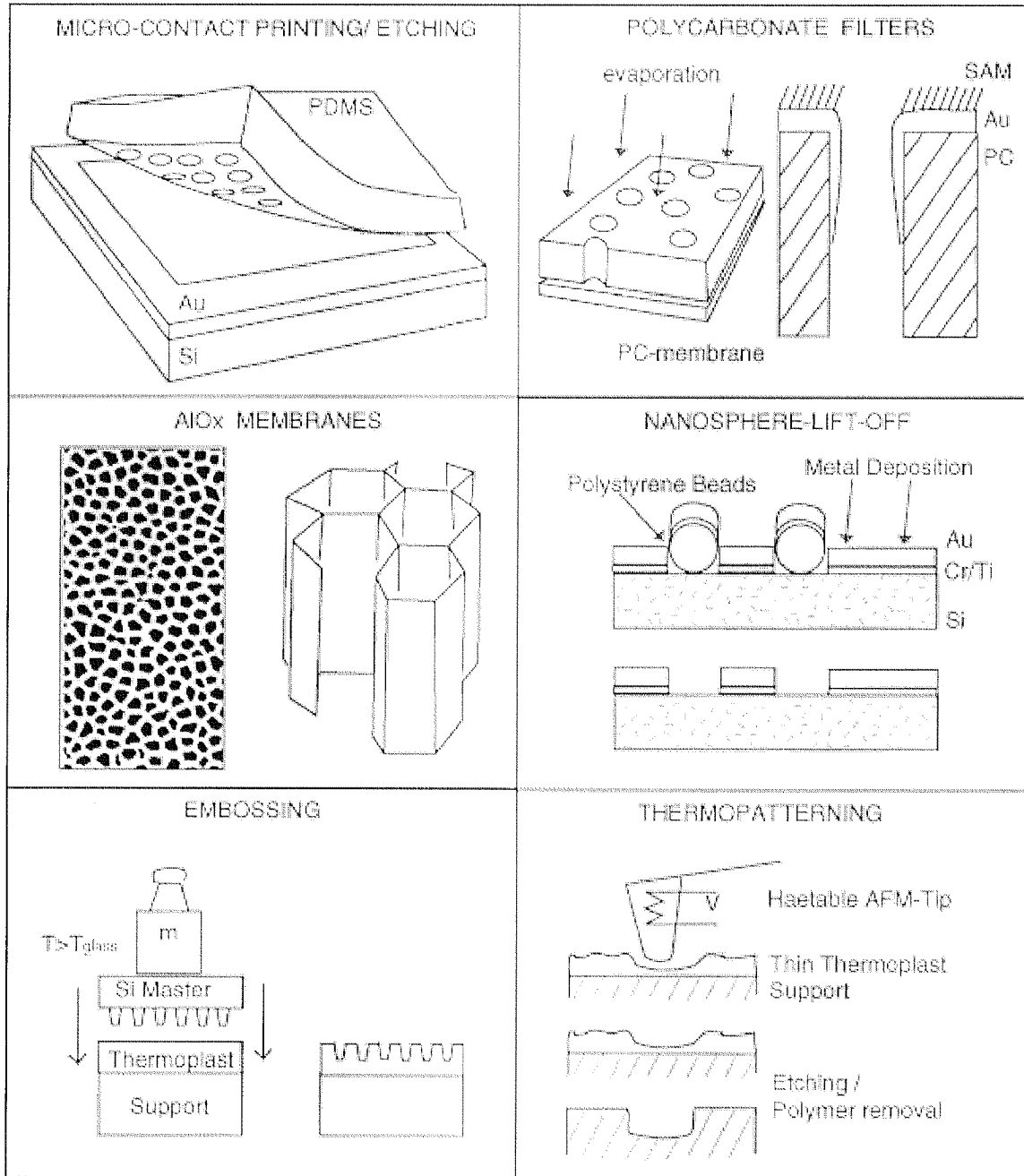


Figure 19: Schematic of possible routes to obtain chemically defined nanostructures in flat substrates. Numbering: A→B/↓/C→D/↓/E→F.

This would have been a possible approach but again a nanostructured master is needed which had to be written using electron-beam lithography. Plastic nanohole devices for

membrane research based on this technology are presently being developed in collaboration with Dr. L. Tiefenauer at PSI Villingen.

Route F: Scanning-probe thermopatterning is being developed at IBM Rueschlikon to reach the 7 gigabit/cm² field of data storage devices. By means of a heatable cantilever tip it is possible to write nanometer sized indentations into a surface coated with a very thin thermoplast-layer. These substrates can then be etched and the polymer-coat be removed if necessary. Nanometer sized indentations are very well obtained using this strategy, but further research would be needed to be done to produce well-defined pattern edges.

Nanospheres

It is possible to produce nanometer-sized features making use of nanometer-sized particles from which the dimensions are translated to the other material. Micro- or nanometer-sized polymer spheres can be bought in different sizes ranging from 20 nm to 15 μm . These “beads“ are immobilized on a flat surface which is then vertically coated with a thin metal layer by evaporation.

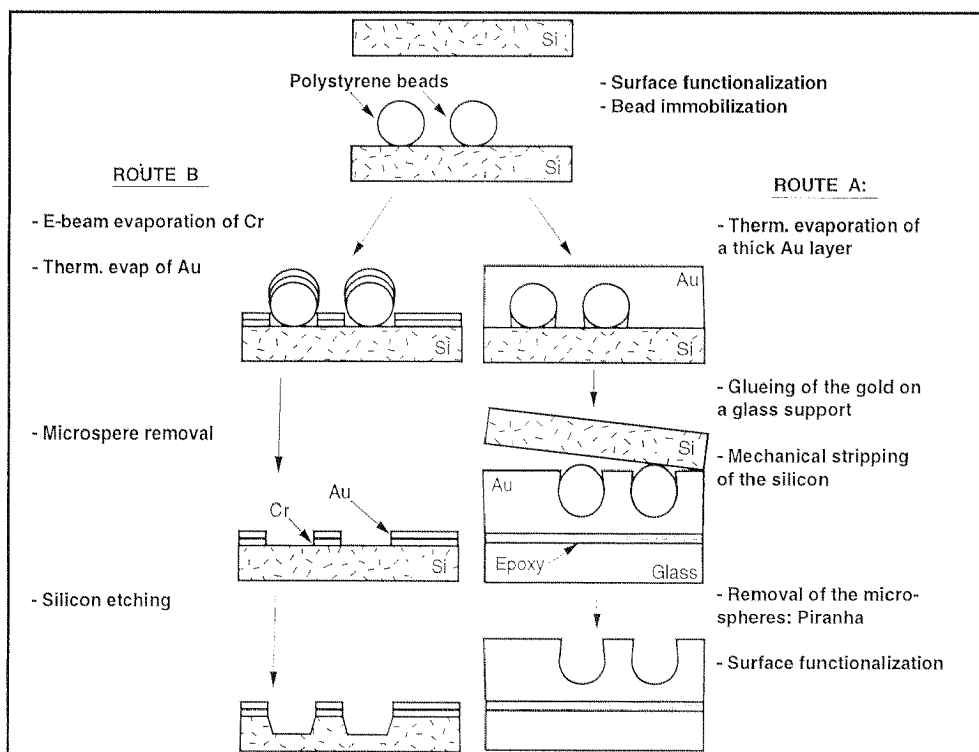


Figure 20: Scheme of two possible routes to produce nanoholes using polymeric nanospheres combined with metal-evaporation techniques.

After removal of the beads, round shaped metal-features are obtained which can be further processed via etching and surface modification. Two routes were followed in this work which are schematically illustrated in Figure 20 A and B:

Route A: Reversed silicon stripping method. After the immobilization of the beads, a thin 2-3 nm layer of chromium is deposited on the sample by electron-beam evaporation followed by deposition of an extremely thin layer of Au (typically 10-30 nm). The metal-coated beads can then be removed by lift-off. Nanometer sized silicon islands embedded in a flat gold surface are produced. Using a short silicon-etching step, the depth of the holes can be varied.

Route B: In order to obtain even smoother gold-surfaces and holes which are completely made of gold, a “stripping“ technique is applied: After the immobilization of the beads, a thick gold layer is thermally evaporated on the surface which completely covers the beads. The Au side is then glued to a small glass plate using epoxy-glye. Because there is no adhesion promoter between the gold and the silicon, the silicon plate can be then “stripped off“ the gold by applying a small shear-force. After removal of the entrapped beads, nanometer sized, round-shaped holes in the gold are obtained which are again accessible to chemical surface modification using alkanethiols.

A more detailed discussion of these techniques is given below:

Bead immobilization

Four factors were found to be important in the bead immobilization step: a) a flat substrate, b) a strong attachment of the beads to the substrate, c) a clean surface prior to evaporation, and d) a homogeneous distribution of the beads.

A flat substrate is needed in order to get a flat gold surface after evaporation for high resolution AFM imaging. We tested silicon wafers and mica, but finally we decided to use silicon because we were familiar with this material and also because silicon can be etched. Prior to any immobilization step, the silicon substrates were cleaned in piranha solution in order to remove hydrophobic, organic contamination. The substrates are then completely wetting.

Very importantly, a strong adhesion between the nanospheres and the substrate was necessary in order to be able to wash the substrate after the immobilization of the beads. This washing step was necessary when buffer solutions were used in the immobilization step which could lead to salt-crystallization on the substrate upon drying. Such crystals

and other possible contaminations would negatively affect the adhesion of the Ti or Cr layer. In our case, two different immobilization strategies had to be optimized because the available nanospheres had different surface chemistries.

Due to their positive charge in aqueous solution, the amino-modified, 200 nm latex spheres did attach extremely strongly to the negatively charged silicon surface.

On the other hand, the 50 and 100 nm spheres did not at all attach to the silicon surface due to the fact that they were carboxylate-modified (they are not available with amino-modification). At neutral pH these spheres are negatively charged and hence are strongly repelled by the Si surface. Several approaches were made to counteract this behavior. Firstly, it was tried to force the beads onto the surface by simply drying a solution containing a small amount of beads directly on the Si surface. This led to an optically homogeneous distribution of the beads on the surface displaying a centrosymmetric arc-like iridescence. But, AFM images of the same surface showed very large aggregates of beads which were arc-like organized on the surface (Figure 21, left).

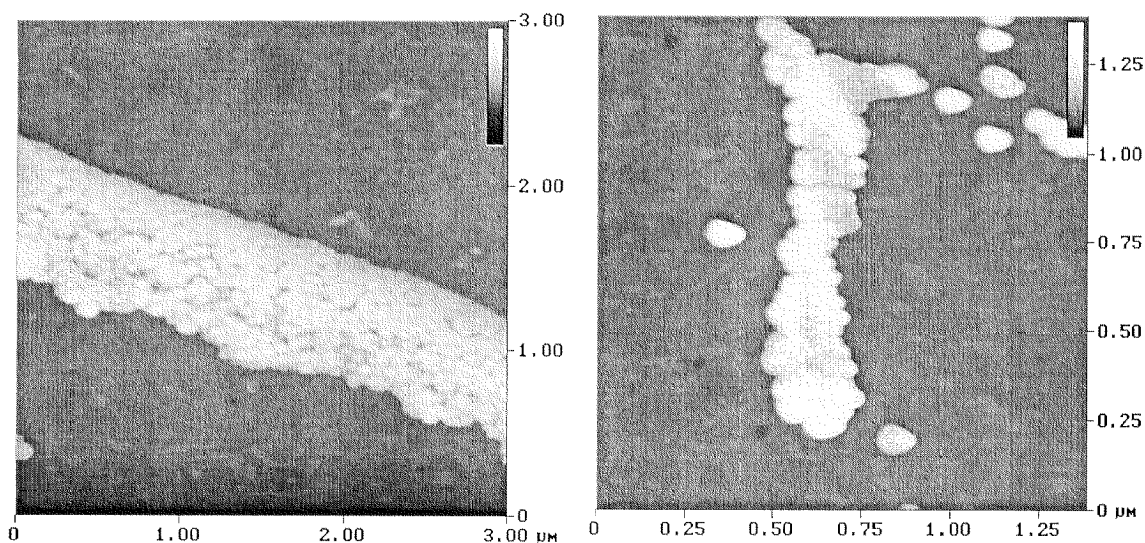


Figure 21: Left: AFM image of huge, arc-like aggregates of 100 nm, carboxylate-modified beads resulting from drying a bead solution in air. Right: AFM image of a SiO₂ surface after Ca²⁺ induced immobilization of carboxylate-modified beads. Large and small aggregates of spheres are visible due to Ca²⁺ mediated crosslinking of beads with each other.

Probably the beads do have a high affinity for the interface between air and water and did therefore accumulate on the surface of the drying drop, where then they were

stepwise transferred to the silicon surface at the drying front between the liquid and the silicon.

In a second essay, the divalent anion calcium was used to bridge together electrostatically the negatively charged surface and beads. Upon addition calcium, the beads rapidly and strongly attached to the Si substrate. However, the surface looked optically inhomogeneous and the AFM revealed the presence of small groups of aggregated beads with only very few single beads (Figure 21, right) Ca^{2+} as expected did also lead to aggregation of the beads in solution. The same would probably also happen with other coupling agents due to the interaction being of the same kind between the surface and a bead and between two beads respectively. For our application it is important to avoid aggregates as they lead to enlarged feature sizes.

Finally strong immobilization and non-aggregated beads could be achieved through aminofunctionalization of the Si surface: The Si was silanized using 3-APTS leading to positive charges on the surface which led to strong adhesion of the beads. Since the beads are negatively charged, they strongly repulse each other leading to a perfect distribution on the surface with nearly no aggregation. The thin organic silane-layer surprisingly did not prevent a strong adhesion of the latter evaporated Cr layer, probably due to the fact that only an extremely short silanization time was applied leading to incomplete silanization film.

Metal evaporation

For route B it is mandatory to control accurately the thickness of the thin metal films transferred. At a given bead-size, the total thickness of the metal layer must be kept far below one half of the nanosphere-radius in order to obtain a non-continuous metal-film which allows bead lift-off (Figure 22). A thickness of 2-3 nm Cr or Ti and 7-10 nm Au proved to work well for 50 nm diameter beads. Some 20 nm thick metal layers can be used for 100 nm beads and 30-50 nm for 200 nm beads (it is important to carefully calibrate the thickness monitoring device in the evaporator !). The evaporation was done at room temperature and at 0.05 nm/sec for Ti/Cr and 0.04 - 0.4 nm/sec for Au. No difference in roughness was detected depending on different evaporation rates for Au. On the other hand, although a thicker gold layer was evaporated onto the samples of route A, these substrates had a smaller roughness after lifting-off gold, compared to the route B substrates (see Table 5).

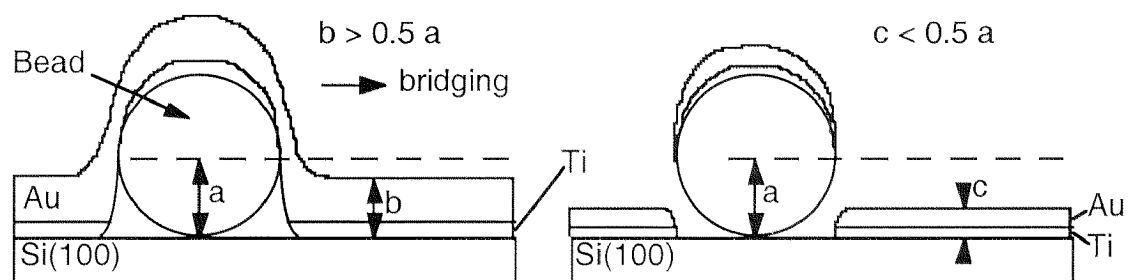


Figure 22: The thickness of the evaporated Ti and Au film must be kept below one half the radius of the beads in order to be able to remove the beads by lift-off, afterwards.

Substrate	Surface roughness (Ra) (for a $2 \mu\text{m}^2$ area, not including bead-holes)
Si(100) wafer	0.1 nm
Au, Route A (after Si stripping, 300 nm Au)	0.25 nm
Au, Route B (8 nm Au)	0.55 nm

Table 5: Surface roughness comparison between the two different Au substrates. AFM contact-mode measurement.

Bead lift-off and removal

After the evaporation step, the beads have to be removed from the gold surface. In route B, due to electrostatic forces, the beads strongly adhere to the silicon surface and it was not possible to remove them by sonication in distilled H₂O (10 min., room temperature) nor by sonication in PBS buffer. A substantial improvement of the bead removal efficiency in the case of aminomodified beads was achieved using sonication in Tris-buffer. Tris contains amino-groups which compete with the amino-groups of the beads for binding to the negative charges on the Si-surface, leading to desorption of the beads. Similarly, carboxylate-modified beads can more efficiently be removed from the surface using a buffer solution containing negative species (phosphate-group in PBS) which enter in competition with the negatively charged carboxylates for binding to the aminosilane-surface coating. Many other strategies presented in Table 6 were also tested to promote bead-desorption including the use of EDTA-containing buffers in the case of Ca-immobilized beads or removal of beads by dipping in strongly alkaline solutions. However, none of these methods proved to be superior to the mechanical method:

All the beads can very efficiently be removed by soft, “mechanical“ wiping of the gold-surface using a paint-brush and 2% SDS solution. A very soft paint-bush must be used to avoid scratching or even removing the gold. Afterwards, the surface has to be thoroughly rinsed with water followed by cleaning with ethanol to remove all the detergent from the surface.

Table 6: A selection of the different bead-removal strategies which were tested for route B.

200 nm NH ₃ -beads	sonication in H ₂ O dest., 10’.	Removal of 50% of the beads
	sonication in PBS pH 7.4, 10’.	Removal of 50 % of the beads
	sonication in 10 times concentrated Tris pH 7.4, 2’.	All the beads were removed.
50 nm COOH-beads	sonication in Tris pH 7.4, 5’	Not all the beads were removed.
	BL7b Au exposed to hexadecanethiol, then PDMS was polymerized on this substrate, lift-off.	Beads were not removed! But AFM scanning removes the beads.
	sonication in 5 times concentrated PBS, 30’.	Nearly all the beads removed
	10 M KOH, 100°C, 2 sec.	Beads were not removed.
	sonication in 25 mM EDTA, pH 7, 2’ (Ca attached beads).	No removal of the beads
	sonication after long exposure to CHCl ₃ : swelling of the beads.	Beads were not removed
	sonication in 5% TWEEN 20, 5’.	Only a few beads removed.
	sonication in 2% SDS	Not all the beads removed
	soft wiping using a paint-brush and 2% SDS solution.	All the beads were removed ! Best method.
100 nm COOH-beads	soft wiping using a paint-brush and 2% SDS solution.	All the beads were removed !

In the case of surfaces produced according to route A, the beads are extremely strongly embedded in the gold which makes it impossible to remove them using sonication or detergent-brushwiping. These beads can only be removed using hot piranha solution (dipping of the substrates for 3 min.) which completely oxidizes the organic beads transforming them into H₂O and CO₂ (see Table 7). Care has to be taken not to excessively expose the organic epoxy-glye between the gold and the small glass plate to piranha solution.

Table 7: A selection of the different bead-removal strategies tested for route A.

200 nm NH ₃ -Beads	Piranha solution, hot, 2 min.	Beads were well removed (by oxidation)
50 nm COOH-Beads	Piranha solution, hot, 2 min.	Beads were well removed (by oxidation)

Etching

The 50- and 100 nm holes obtained through route B were etched using boiling 10 M KOH for 3 sec. A scheme of this step including theoretical etching rates ((Heuberger, 1991)) are given in Figure 23. Due to anisotropic etching of the Si(100), V-shaped, rectangular holes are obtained covered by a circular Au openings.

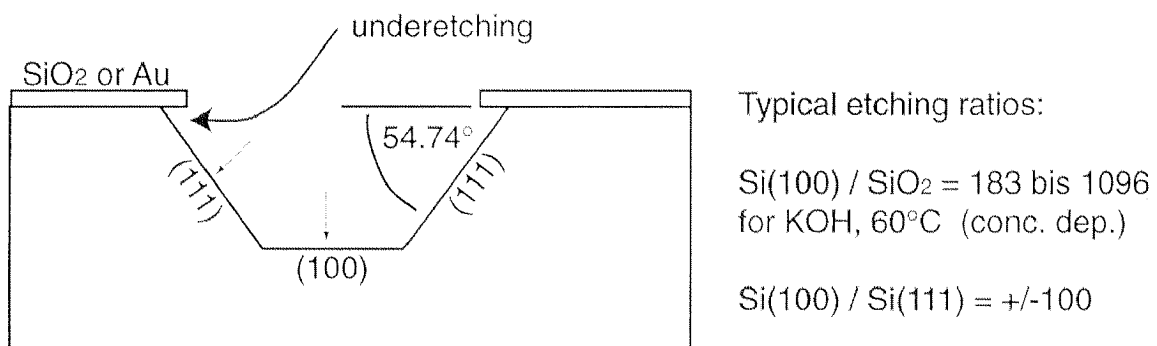


Figure 23: Scheme of the etching behavior of Si(100) in KOH solutions. The silicon is etched anisotropically depending on the respective etching rates of each crystallographic direction. Approximate, relative etching-ratios are written at right. Figure 16 shows a SEM image of a KOH etched structure.

Hole-geometries

Following route A, after lifting-off the Si plate, AFM images reveal small, round protrusions on the gold surface stemming from the entrapped 200 nm beads which seem to expand slightly when the Si is removed (Figure 24). After removal of the beads, round shaped holes can be seen in the gold (Figure 25) embedded in large and very flat Au crystallites (Figure 26). The border of the holes show small gold extending from the flat gold plane due to the swelling of the beads as described in Figure 26. In the case of the 50 nm beads (Figure 27), not very well defined, round shaped holes are obtained. In this case, the crystallite growth-pressure during evaporation seems to be stronger than

the elasticity of the polystyrene beads leading to a strong deformation of the beads. Hole structures with strange and angular features are obtained which are not suited for our applications.

Holes produced according to route B show nice, round shaped geometries for all three bead-sizes: 200 nm (Figure 28), 100 nm (Figure 29) and 50 nm (Figure 30). The Au surface shows much smaller crystallites compared to route A gold, but the roughness of these substrates is larger.

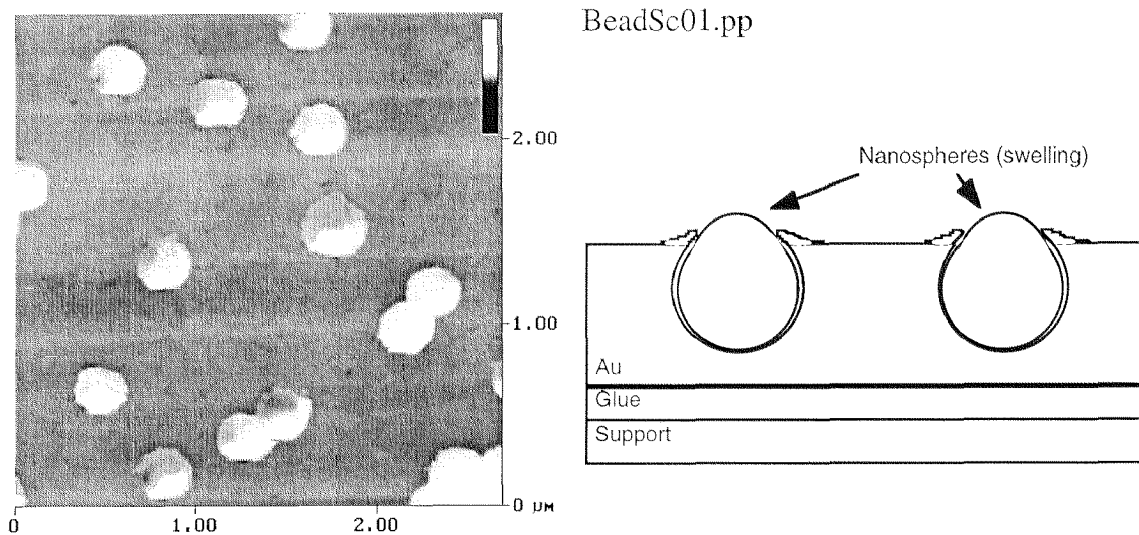


Figure 24: The surface with completely gold-entrapped beads after stripping-off the silicon wafer (route A): The beads unexpectedly rise above the gold surface probably due to swelling in the presence of air humidity (They were gold coated in the vacuum and therefore were completely dry during the embedding process)(left: AFM image).

These small crystals which have diameters in the range of 1/5 of the hole diameter can be well-distinguished on the sample with the 50 nm holes. They are responsible for the fact that the production of even smaller holes will lead to poor geometrical definition of the hole-shape and also sets limits to the minimal surface roughness which can be obtained using this method (Table 5). Mainly the 50 nm holes suffer from a bad edge definition. Therefore we mainly used 100 nm holes for further experiments including bilayer membranes.

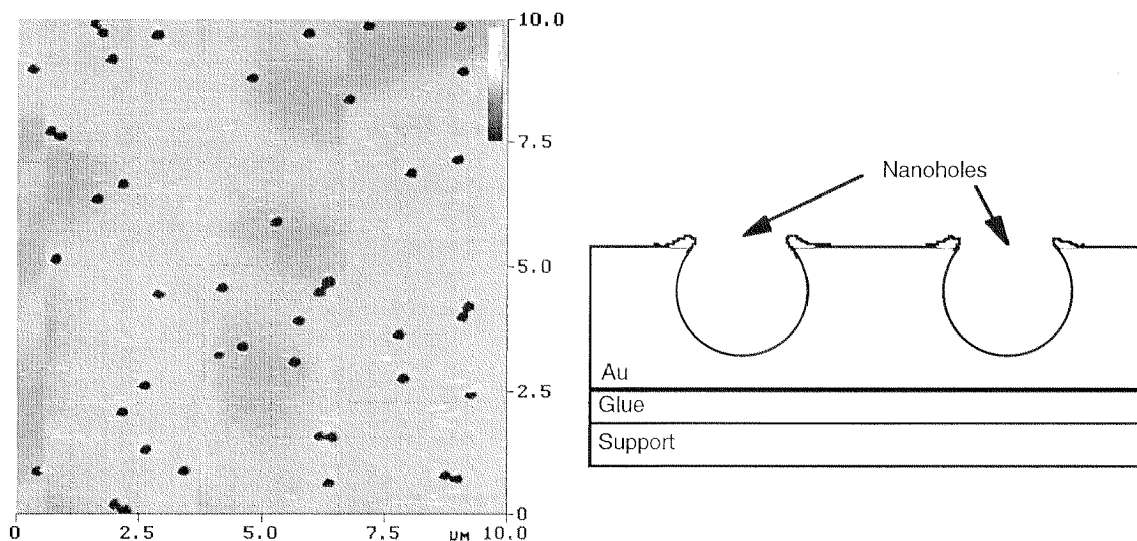


Figure 25: Au surface after removal of the entrapped 200 nm beads by piranha treatment (route A) (left: AFM image).

After etching,, the depth of the holes increases to about 100 nm and the AFM-tip can crash into the underetched gold regions in scanning direction leading to squeezing of the gold (elevated Au structures on the AFM image in Figure 29). These phenomena can be avoided by optimizing the scanning conditions and will probably not happen as soon as a bilayer covers the holes.

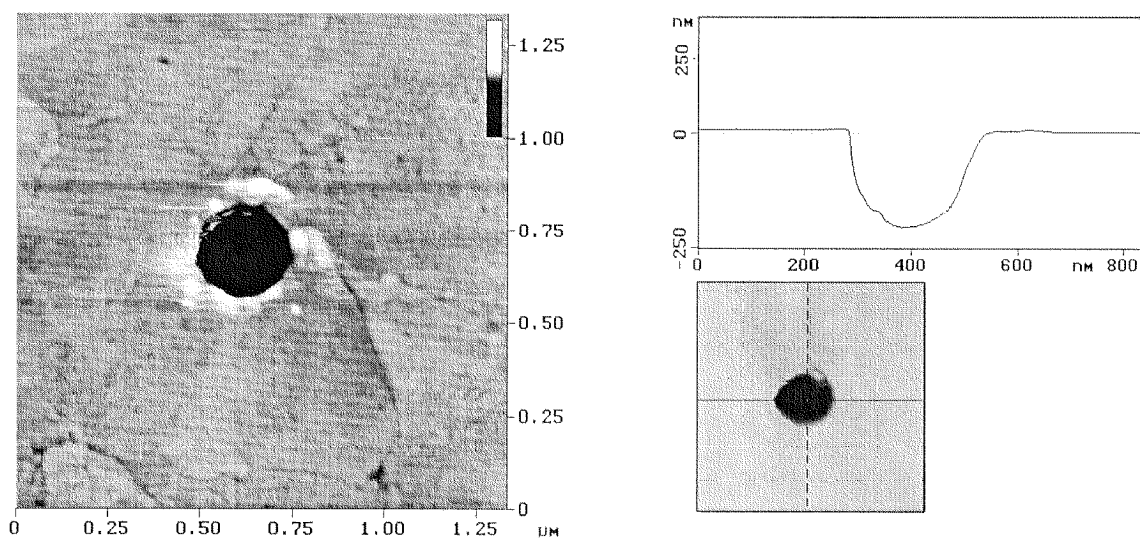


Figure 26: Left: Magnification of one nanohole after Si-stripping and piranha treatment (route A). Due to the swelling mentioned in Figure 24, the Au borders of the hole were partially lightly pushed upwards. The very large and extremely flat Au crystallites are nicely visible surrounding the hole. Right: AFM section through the 200 nm deep hole. The round shape of the previously entrapped bead was transferred to the gold.

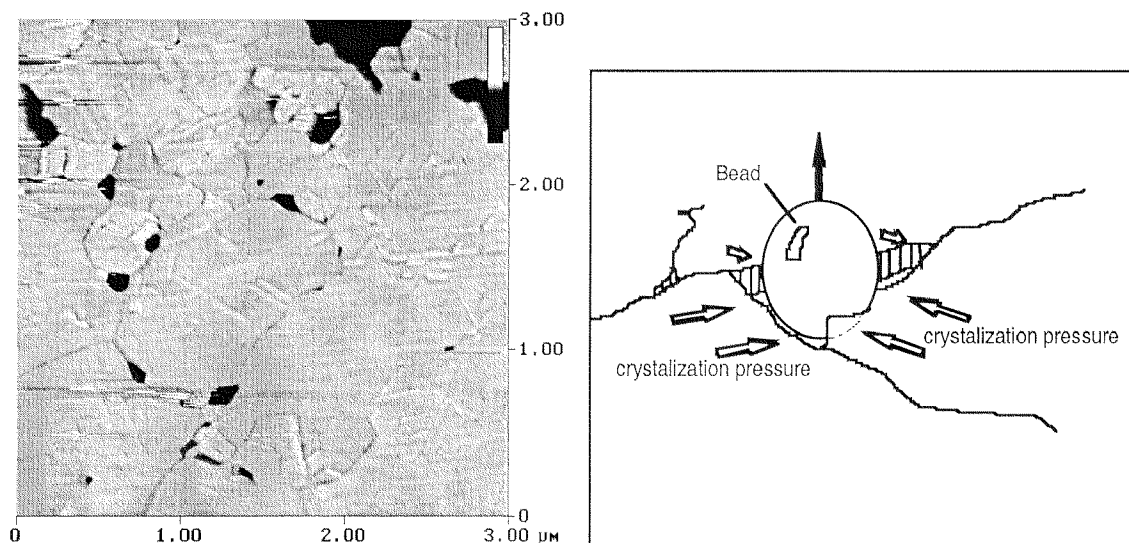


Figure 27: Left: AFM image of the “route A” Au surface after Si-stripping and removal of the remaining 50 nm beads by piranha treatment. Some holes are visible, but the beads could not impart their round shape to the holes. These beads seem to be too small to withstand the crystallization pressure of the growing Au crystals during evaporation and are pushed out of place. Furthermore the Au crystallites are big compared to the beads for which rather the crystallization fronts of each crystallite define the final shape of the holes (scheme on the right).

It must further be reminded and emphasized that the holes which were produced have extremely small dimensions. E.g., the 50 nm holes do not exceed 180 Au atoms in diameter! In these dimensions even the SEM fails to resolve features and one is compelled to use the AFM to get information about the structures produced. However, AFM tips have a radius in the range of 10 to 50 nm which leads to AFM images being superpositions of the hole- and the tip geometries. This artifact can easily be recognized if all the holes on an AFM image display the same morphological features in the same orientation.

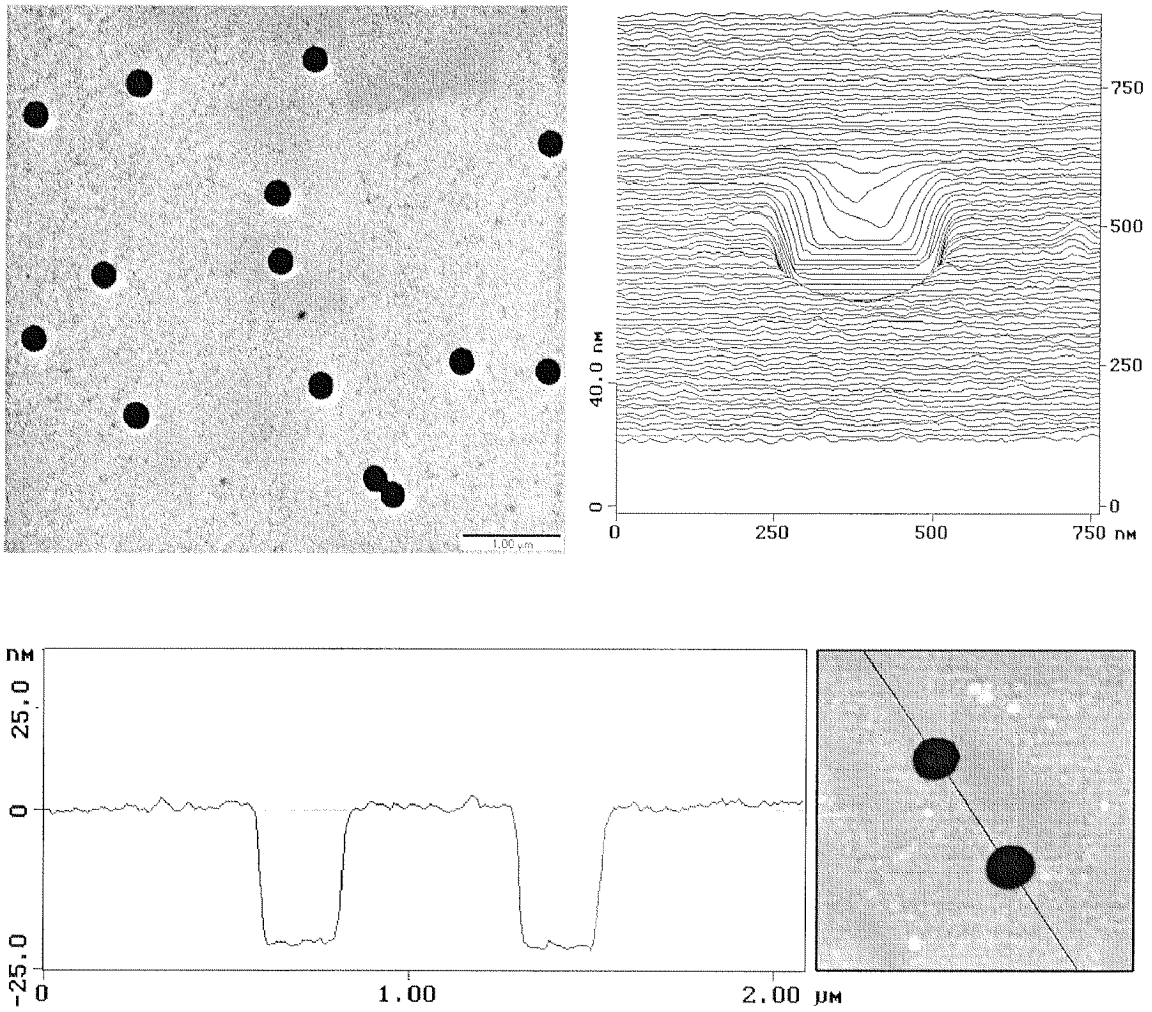


Figure 28: Left: TEM image of round-shaped Au/Si holes produced following route B, after removal of the 200 nm beads. The holes are randomly distributed over the surface. Right: 3D-image of a hole according to AFM data and section (bottom). The Silicon-bottom of the holes is very flat and the depth corresponds to the thickness of the evaporated Au/Ti layer (21 nm).

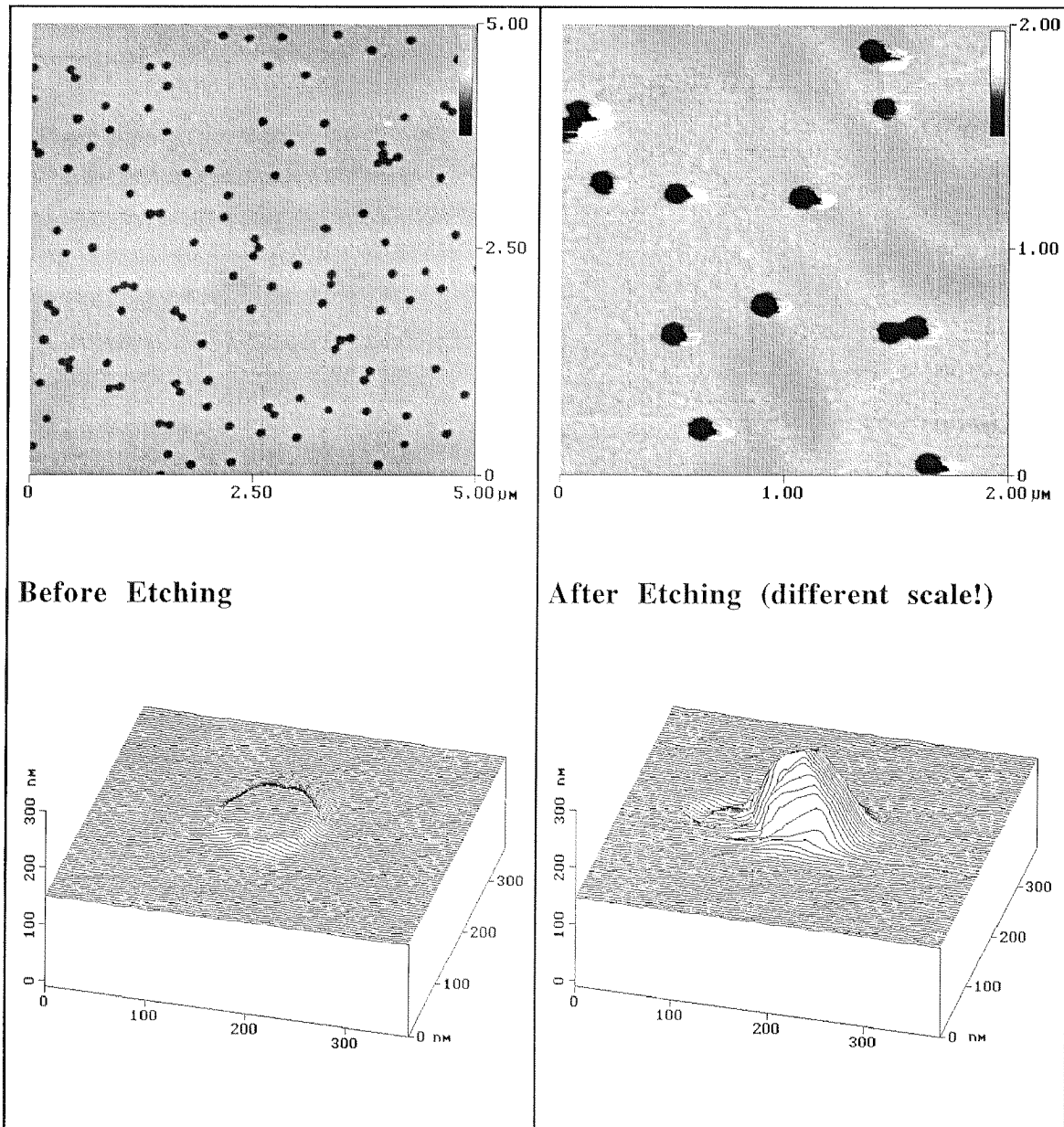


Figure 29: Left: Route B nanoholes produced using 100 nm, carboxylate-modified beads. The inverted 3-D projection of the holes shows their flat Si(100) bottom. Right: After a very short KOH etch, the shape of the holes is not affected (except that the AFM tip -due to overhanging, underetched Au areas- injures the hole-edges in scanning direction). The inverted 3-D projection of an etched hole reveals the increased depth of the hole and at a closer look the inverted shape of the tip is visible.

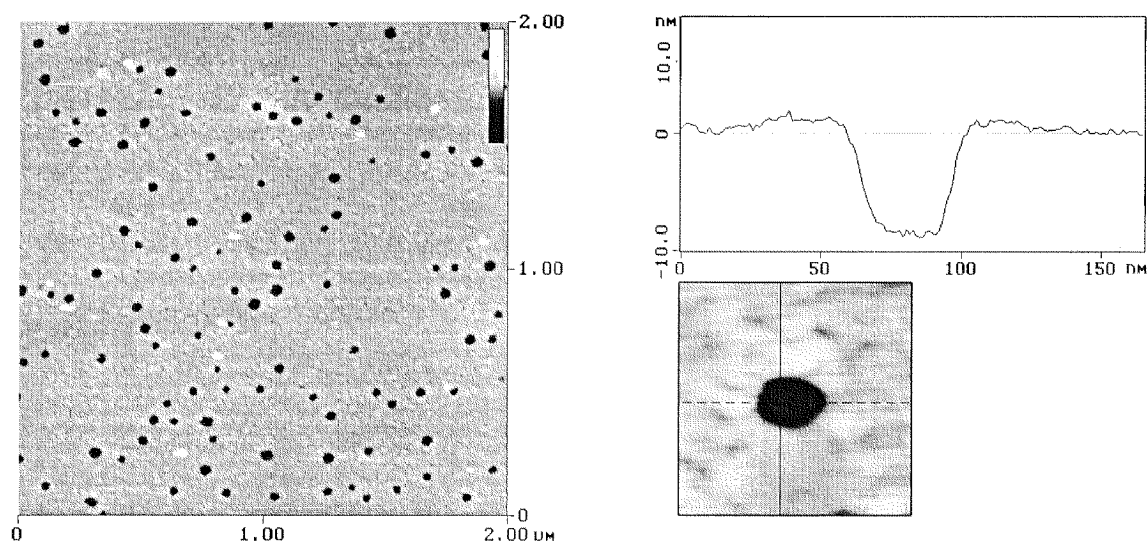


Figure 30: Left: Holes produced using 50 nm nanospheres according to route B: The shape of these holes is not any more very spherical due to the growth kinetics of the Au-crystals which have nearly the same size as the holes themselves. According to the section on the right, the Si-bottom of the holes is still flat. In these dimensions - the diameter of these structures does not exceed 180 Au-atom diameters (!) - it is very important to use sharp AFM tips during scanning as else a superposition of the tip and the hole geometries is obtained.

The “nanosphere/evaporation“ method did lead to reproducible and well defined nanohole structures which are easy to produce. The surface coverage as well as the diameter and the depth of the depressions can be controlled making it a handy substrate for the bilayer suspension experiments described in “Suspended bilayers“.

Polycarbonate Filters

The second approach which was investigated for the production of gold nanoholes was based on the use of polycarbonate filters (but finally this method proved less useable than the nanobeads method):

Nanoporous polycarbonate-membranes are commonly used as sterilizing filters in biosciences. These polymeric membranes contain round shaped pores of well defined diameter and cylindrical section spanning the whole membrane thickness of about 6-11 μm (Figure 31). Pore sizes ranging from 15 nm up to 12 μm can be bought. Due to their polymeric nature, these membranes are not suited as substrates for AFM measurement as they are too soft (image not shown): Even under minimal forces applied in contact mode, the surface is distorted under the scanning force.

However, this behavior can completely be circumvented by coating the polymer with a thin layer of metal. In our case the membrane was glued onto a SEM holder using epoxy-gluce and then 6 nm of gold were sputtered onto the surface. AFM measurement

of these coated surfaces exhibit stable scanning conditions and the 80-95 nm diameter holes could be well resolved.

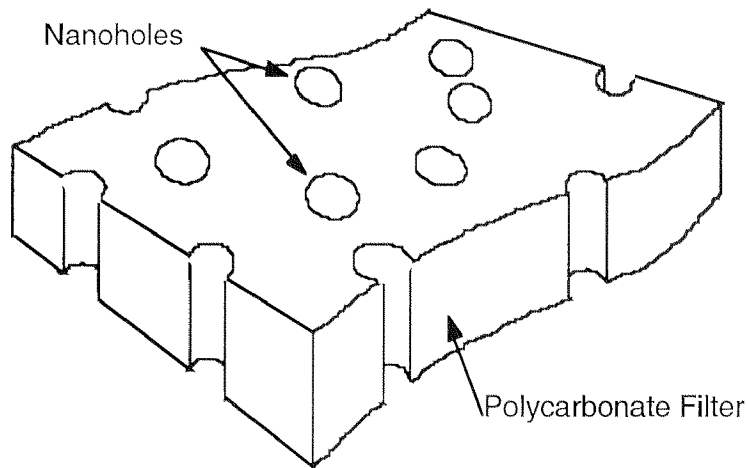


Figure 31: Structure of a polycarbonate filter membrane with vertical holes of defined diameter. Filter-thickness: approx. 10 μm .

Interestingly, the Au coating did strongly adhere to the polycarbonate substrate. No adhesion promoter was needed. The roughness of these gold coated polymer membranes is higher than the roughness of the gold coated silicon substrates, for which this approach was not further pursued. Si has also the advantage, that it is much harder than PC-membranes and it is not prone to swelling in solvents.

CHEMICAL MODIFICATION OF SURFACES

The chemical modification of a surface can be achieved through different approaches. The probably oldest technique is based on coating a specific surface with a fairly thick layer of a material having the required surface properties. Examples are Anti rust paintings, polymer-film coatings and metallization. Unfortunately, these techniques are always accompanied by changes in surface morphology and they also modify the physical properties of the surface. very often it is sufficient to modify the surface with a depth of a few \AA to nm because mostly only the outermost layers effects the interface properties of the material towards ist environment. Such a modification can be achieved by using covalent chemistry based on compounds which bind to a surface and which do prevent the adsorption of further molecules after a monolayer covers the surface. Examples of such methods are (i) silanizations - based on the covalent linkage of low molecular, organic silicon compounds on oxygen containing surfaces (Mittal, 1992) and on the other hand, (ii) coatings based on macromolecules which do have the capacity to adsorb onto a surface, but which do not show aggregation or chemical polymerization among each other (Hirayama, 1997, Swalen et al., 1887). Such coatings are extremely thin and do therefore neither substantially alter the surface micro-topography nor the physical properties of the materials.

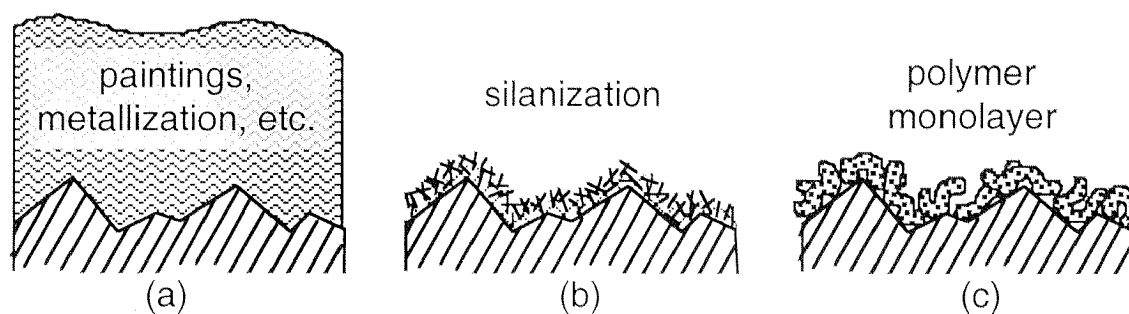


Figure 32: Three standard surface modification methods

The modification of nanostructured surfaces still has other requirements on the chemical surface modification: The surface topography should even not be altered in the atomic scale and the functional groups of the coating should extend from the surface with a defined orientation and be arranged in a two-dimensional lattice of defined periodicity. These requirements are achieved by self-assembling systems (Bishop and Nuzzo, 1996, Ulman, 1996).

Self assembling surface coating systems are based on molecules which have different domains including a) a binding site for a specific surface, b) sites which define the

interaction and orientation with respect to molecules of the same species and d) a chemical functionality which does imparts a desired chemical or physical property to the assembled state of the system. With “self -assembly“ it is meant that these systems self-organize into an ordered state of lower entropy without need for a higher, controlling authority. The best known molecules prone to self-assembly are alkanethiol-based systems which form monomolecular, ordered „carpets“ on gold surfaces (see below). However, there are many other systems which also show a similar behavior (Swalen et al., 1887): Very importantly, life would not be possible without the self-organization (and self-assembly) of lipid-molecules forming the cellular walls (Fuhrhop and Koenig, 1994), and also certain proteins as e.g. microtubuli self-assemble into long tubular structures which are responsible for intracellular trafficking (distribution of cellular components within the cell).

Self-Assembled Monolayers

Alkanethiols on Gold

In 1983, Nuzzo and Allara (Nuzzo and Allara, 1983) discovered the strong attachment of organosulfur species to gold surfaces forming SAMs. The structure and formation of such self-assembled monolayers (SAMs) based on alkanethiols and dialkyldisulfides has since then been studied intensively (Bain et al., 1989b, Porter et al., 1987, Sellers et al., 1993) (for recent reviews see: (Bishop and Nuzzo, 1996, Ulman, 1996)). The chemical models of alkanethiol and alkyldisulfide molecules are given in Figure 33.

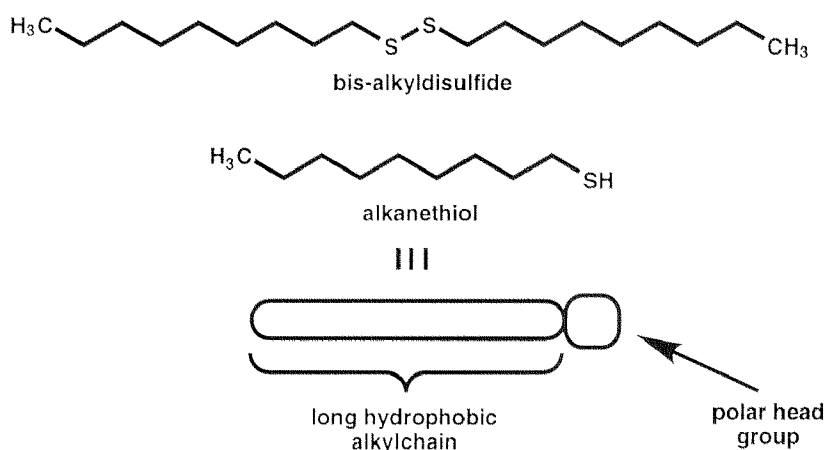
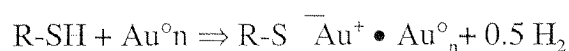
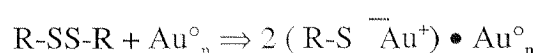


Figure 33: The basic structure of non-functionalized alkanethiol- and alkanedisulfide molecules which do form homogeneous SAMs on gold substrates.

Such molecules dissolved in a proper solvent (mostly EtOH) will completely coat a gold surface with a monolayer of alkanethiols within seconds of immersion. This chemisorption reaction has now been shown to produce thiolate species on the gold according to the equation (Ulman, 1996):



Self assembly of dialkyldisulfides leads to indistinguishable SAMs as compared to alkanethiols. The chemical mechanism here is assumed to be:



The strength of the Au-S bond with ~184 kJ/mole (Sellers, 1990) has about half the strength of a covalent C-C bond (~347 kcal/mole) and is much stronger than hydrogen bonding (10-40 kJ/mole). Additional stabilization of the SAMs results from strong Van der Waals interactions between adjacent alkyl-chains in the order of 110 kJ/mol (Sellers et al., 1993), which are also responsible for the SAM orientation. SAMs are stable up to about 100°C (Sellers, 1990, Delamarche et al., 1994) but the thiolates can be converted into alkylsulfonates by photolysis with UV-light which makes them water soluble (Huang et al., 1994). The partially electrostatic nature of the Au-S bond as well as the good conductivity of gold make thiolate-SAMs accessible to electrochemical manipulation. In diluted electrolyte solutions, monolayers are only stable in the potential range between -400 and +1400 mV (Finklea et al., 1987, Yang et al., 1997).

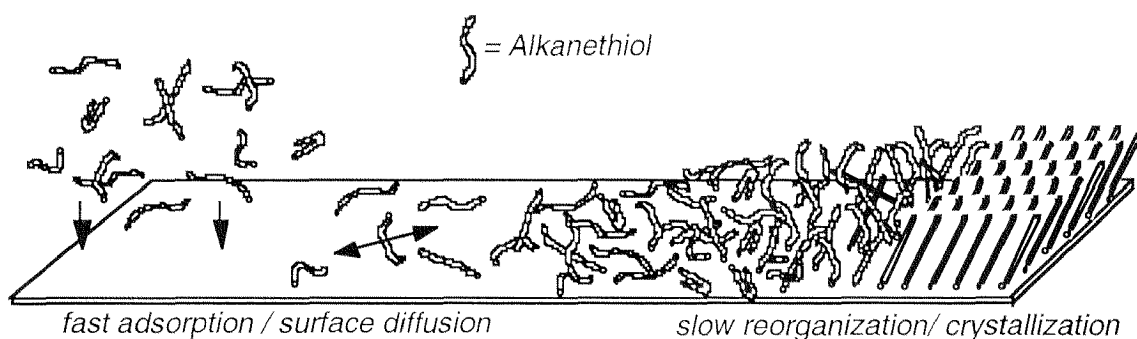


Figure 34: Scheme of the SAM formation process: Alkanethiols dissolved in ethanol adsorb on an Au(111) surface and cover it within seconds, after which a slower reorganization process takes place, leading to a well ordered SAM with hexagonal packing of the alkanethiolates.

The formation of the ordered SAM has been studied in detail by monitoring a gas phase adsorption process of alkanethiols by ultra high vacuum AFM: At low coverages, the alkanethiols lie flat on the gold surface and are free to diffuse over it. As the packing gets denser, the alkanethiols exert a pressure on each other, which forces the hydrophobic tails to stretch into the third dimension, away from the substrate. Crystalline domains in which the alkyl-chains are in an all-trans conformation begin then to appear, and in which the alkanethiols are arranged in a hexagonal array. The last rearrangement step which may take hours for completion, is much slower than the initial adsorption (seconds to minutes). This is due to sterical hindrance in the nearly fully developed SAM. Figure 34 illustrates the adsorption process and, in Figure 35, the domain-like formation of a functionalized SAM on ultraflat Au(111) is shown: After less than 1 sec., crystalline domains (bright areas) appear meander-like within areas of still disordered alkane chains (darker areas). After one hour, the whole SAM is crystalline .

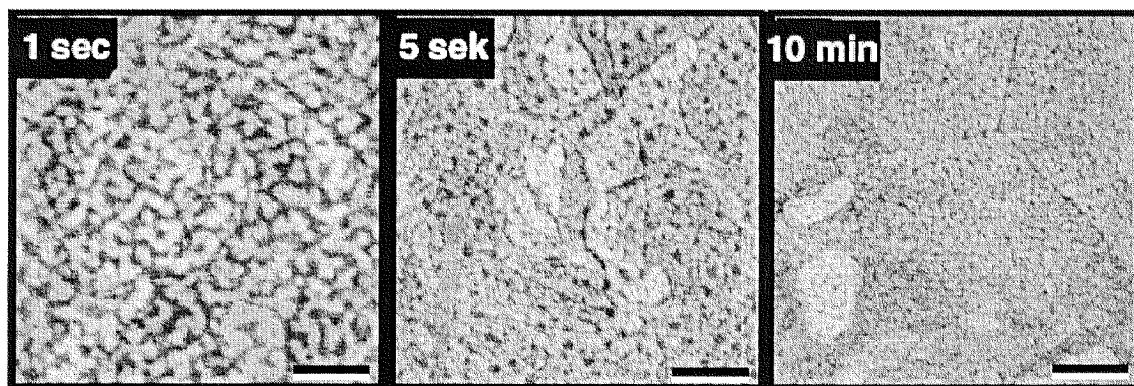


Figure 35: Kinetics of monolayer formation monitored by AFM on air dried DSU-SAM. The times indicated refer to the immersion length of ultraflat gold samples in 1 mM DSU in 1,4-dioxane. The large areas of different brightness correspond to one atom high Au(111) planes (Wagner et al., 1996a) (bar = 100 nm).

Due to the fact that the sulfur atoms are larger than the gold atoms, the hollow sites on the gold - which are supposed to be the binding site of the thiol (Ulman, 1996) - cannot be all occupied by a sulfur atom and therefore a $\sqrt{3}\times\sqrt{3}R 30^\circ$ overlayer is formed (see Figure 36 (left)). The density of the alkyl chains in such an arrangement is too small, leading to tilting of the alkyl tails, by which the chains come into closer contact following the van der Waals attraction (see Figure 36 (right)) (Fenter et al., 1993).

A broad range of applications of such systems has arisen from the synthesis of alkanethiols having functional groups in the ω -position. These make it possible to impart virtually any chemical property to a gold surface, and thus parameters such as wettability (Bain and Whitesides, 1989a, Drelich et al., 1994) , and reactivity

(Delamarche et al., 1996, Rozsnyai and Wrighton, 1995, Wagner et al., 1996b, Wagner et al., 1996a) can be controlled on such a surface. Monolayers on gold have been used to bind selectively and/or covalently cells (Lopez et al., 1993a, Singhvi et al., 1994, Herbert et al., 1997, Mrksich et al., 1997), proteins (Delamarche et al., 1996, Wagner et al., 1996a, Prime and Whitesides, 1991, Lopez et al., 1993b, Sigal et al., 1998), membranes (Lang et al., 1994b), and other subcellular structures (Wagner et al., 1994a) (for a review see: (Mrksich and Whitesides, 1996)).

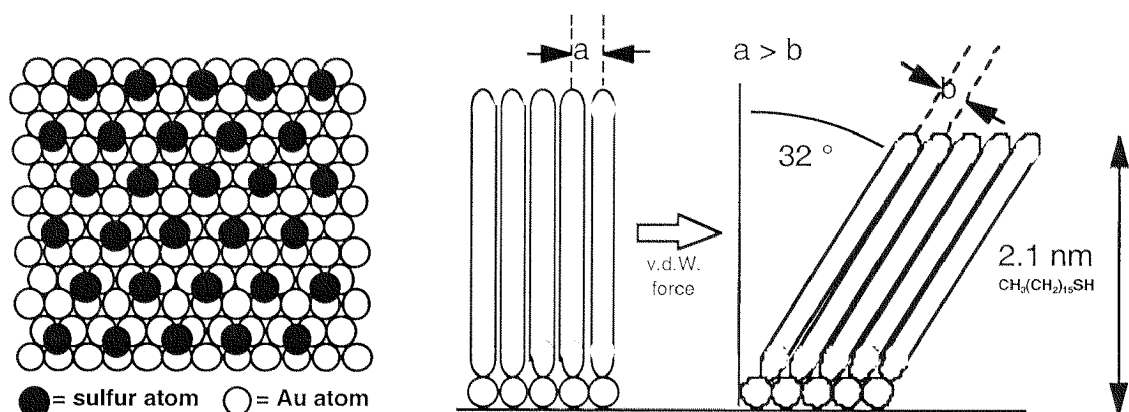
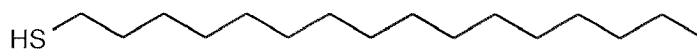
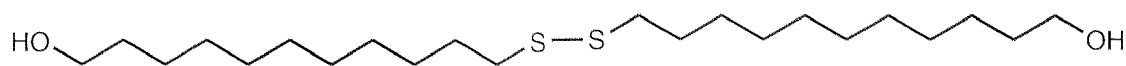


Figure 36: Left: Scheme of the arrangement of the thiolates on an Au(111) surface. The hexagonal overlayer lattice is designated $(\sqrt{3} * \sqrt{3})R30^\circ$. In other words, the spacing between the thiol molecules is $\sqrt{3}$ times larger than the distance between two Au atoms (0.288 nm). Right: Due to the fact that the perpendicular area needed by the alkyl moiety is smaller than the surface area occupied per sulfur atom, the chains have to tilt by about 30° relative to the surface normal giving in to the van der Waals attraction between the long alkane chains.



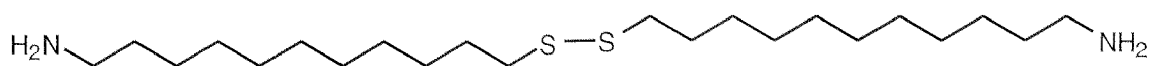
Hexadecanethiol (HDT)



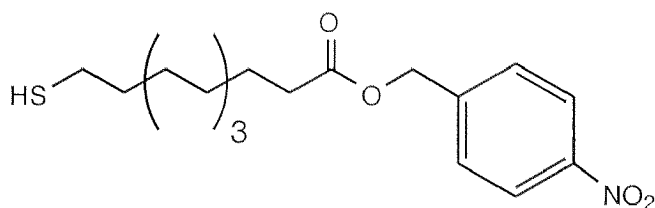
11,11'-dithiobis(undecanol)



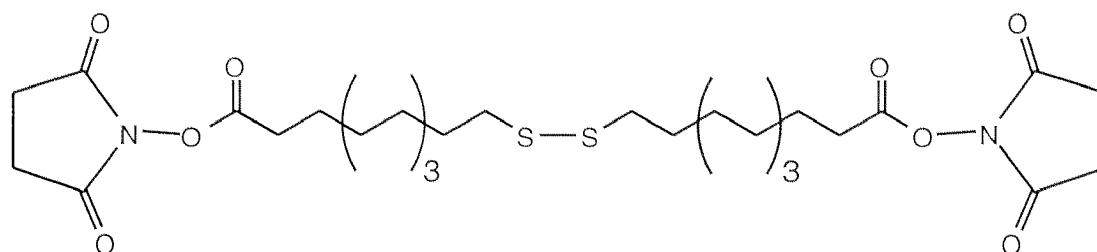
11,11'-dithiobis(1-undecanoate)



11,11'-dithiobis(1-aminododecane)



11-mercapto-4-nitrobenzylundecanoate



dithiobis(succinimidylundecanoate) (DSU)

Figure 37: SAM-forming molecules which were available in our laboratory.

For the chemical modification of gold surfaces, the alkanethiols listed in Figure 37 were available in our laboratory. They were either commercially available or were synthesized in our laboratory. The following table gives more information concerning their provenience, properties and applications:

Hexadecanethiol (HDT)	HDT is usually used to produce a completely hydrophobic surface (advancing contact angle around 115°). It can well be used for μ CP and it gives the best surface protection against gold etching solutions. This compound is commercially available. solvent: ethanol
11,11'-dithiobis(undecanol)	This compound leads to SAMs exposing hydroxyl-groups to the environment, leading to a highly polar but not charged substrate. This surface is completely wetting (contact-angle of 0°). Proteins do not strongly immobilize on such a surface and can (often) be washed off ((Wagner, 1995)). solvent: ethanol or 1,4-dioxane
11,11'-dithiobis(undecanoate)	This thiol leads to very hydrophilic surfaces which are negatively charged around neutral pH. The carboxyl-group is readily accessible to chemical modifications as e.g. through activation with N,N'-dicyclohexylcarbodiimide (DCC). solvent: 1,4-dioxane
11,11'-dithiobis(1-aminododecane)	This thiol leads to a surface exposing amino functionalities. It is positively charged at pH < 9 and is also hydrophilic. Primary amines can easily be activated using glutaraldehyde for later, covalent protein immobilization. This compound was synthesized as described in (Wagner, 1995) and was used without further purification. solvent: water
11-mercapto-4-nitrobenzylundecanoate	The nitroaryl-group of this compound can be activated in two steps, leading to a reactive diazo-compound which binds covalently molecules containing phenols or imidazoles (e.g. proteins containing the aminoacids tyrosine and histidine). The synthesis and properties of this compound can be found in (Wagner et al., 1996b). solvent: 1,4-dioxane
dithiobis(succinimidylundecanoate) (DSU)	The properties of a SAM composed of these molecules are discussed in detail in (Wagner et al., 1996a). Any molecules or objects having primary amines on their surface are readily, covalently bound by this SAM at neutral pH, leading to good protein immobilization for AFM microscopy applications. solvent: 1,4-dioxane or acetone

Mixed SAMs

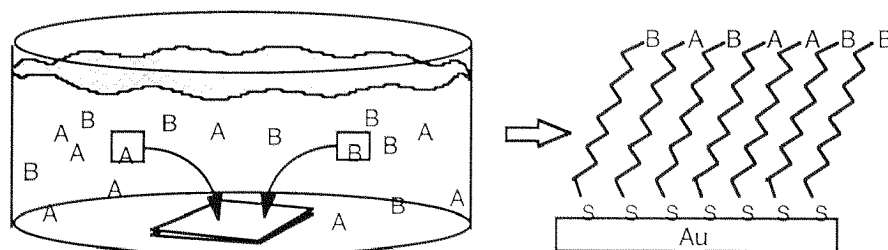


Figure 38: Simultaneous incubation of two different alkanethiols leads to mixed SAM.

By coating of an Au surface with one kind of an alkanethiol of defined ω -functionality, the physical and chemical properties of the surface can only roughly be tuned. In special cases, more precisely tuned surface-characteristics may be needed, e.g. a very defined isoelectric point, a defined wettability (surface tension) or a specific surface activity (reactivity). This can be achieved by the simultaneous adsorption of different alkanethiols leading to surface properties within the extremes of the two pure compounds (Figure 38).

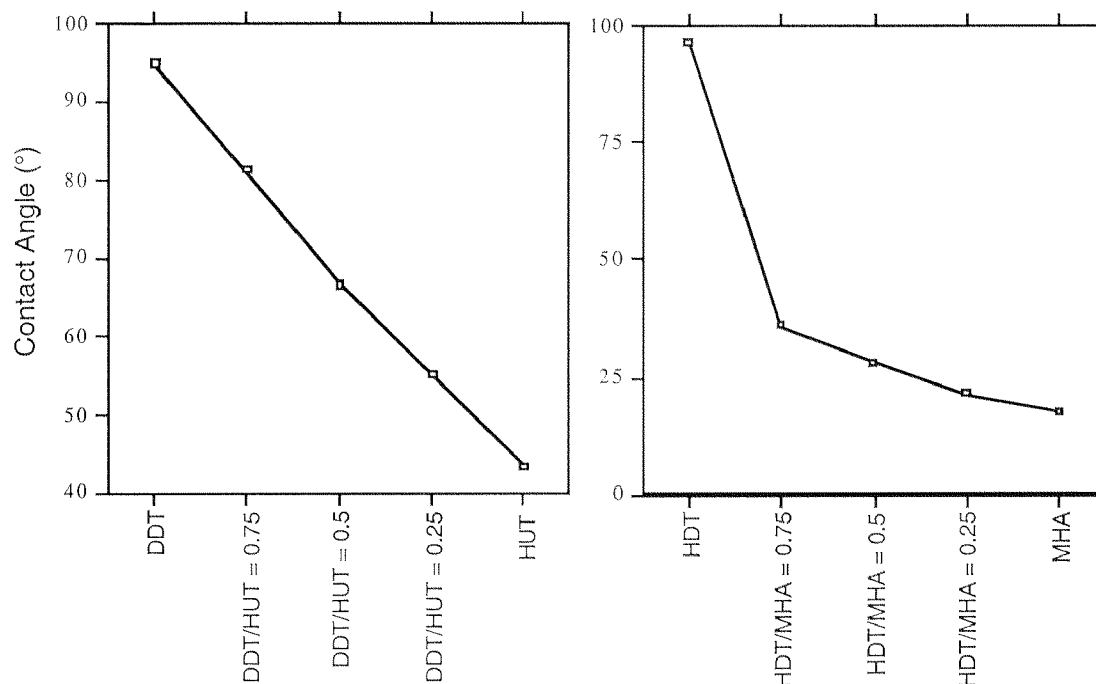


Figure 39: Water contact-angle measurements on gold surfaces exposed to THF solutions containing different amounts of two alkanethiols with different ω -functionalizations, but equal chain length (total thiolate concentration: $10 \mu\text{M}$). Left: Coadsorption of dodecanethiol (DDT) and 11-mercaptoundecanol (HUT); Right: Coadsorption of hexadecanethiol (HDT) and 16-mercaptohexadecanoate (MHA). The standard errors are smaller than the symbols used.

Figure 39 shows such a behavior: two kinds of alkanethiols were allowed to self-assemble competitively onto a gold surface out of a solution composed of different molar ratios of the two compounds. The y-axis of the curves represent the contact angles of the surfaces after a short incubation time. In the first case, a quasi-linear relationship between the molar ratio and the final contact angles was obtained, indicating that the amount of alkanethiols which adsorb to the gold is proportional to the molar ratio in solution.

In the second case (coadsorption of HDT and MHA), the apparent relative amount of molecules on the surface is not any more proportional to the molar concentrations in the solution. These following reasons may explain these different behaviors:

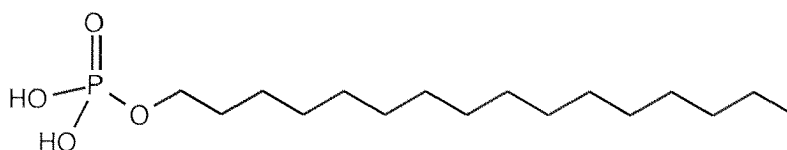
- Firstly, the ratio of the two compounds on the surface has been shown to reflect the relative solubilities of the compounds in the assembly-solvent: In a competitive adsorption assay (Figure 39, right) in the relatively nonpolar solvent THF, more carboxylate-terminated alkanethiols will adsorb than methyl-terminated alkanethiols of the same chain length, due to worse solubility of the hydrophilic molecule in THF [compare with Bain, 1989 #54].
- Secondly, although thiols and disulfides adsorb with the same rate, the replacement of a pre-formed SAM by disulfides in solution is much slower than by thiols (Biebuyck et al., 1994).
- Thirdly, it has been shown (Offord et al., 1994, Bain and Whitesides, 1989b) that contrary to what would be expected with diffusion laws, long chain thiols adsorb with much greater efficiency compared to short analogues. This can be understood in terms of the smaller stabilizing contribution of the inter-chain Van der Waals interaction in an advanced adsorption scenario for short thiols (Bain et al., 1989a). Additional effects on the adsorption ratios may also result from the stabilization of the SAM molecules among each other through ω -functional groups (e.g. hydrogen-bonding etc.). Thermodynamic aspects therefore play a major role in the final composition of the SAM. Much longer incubation times (days to weeks) would allow the SAM to completely reach its thermodynamic equilibrium with the surface covered exclusively with the more stable thiol.
- Finally, the measured contact-angles on mixed SAMs proved to nearly, but not perfectly, reflect the concentration ratio of the components in the SAM (as measured by XPS). This could in fact be expected since e.g. the accessibility for hydration of a polar group in a fully formed SAM is sterically hindered compared to in a SAM where these groups are diluted - leading to additional effects influencing the contact angle. On the other hand, the interactions between adjacent functional groups in the SAM can also influence the wettability, e.g. by hydrogen bonding between neighboring head -groups in the SAM.

Interestingly, despite intensive research, the conditions which lead to phase segregation of a mixed SAM into nanometer sized domains have not yet been clearly elucidated. While in SAMs composed of hexadecanethiol and $\text{CH}_3\text{O}_2\text{C}(\text{CH}_2)_{15}\text{SH}$, nano-domain formation has been observed by STM after short alkanethiol incubation times (Stranick et al., 1994), no such segregation was observed in very similar undecanethiol/11-mercaptoundecanoate or mixed alkyl-/fluoroalkyldisulfide SAMs (Imabayashi et al., 1998, Schoenherr et al., 1996). If very large chain length- and end-group chemistry differences exist in a binary SAM, phase separation was observed (Imabayashi et al.,

1998). Bain et al. concluded, that if domains are formed in SAM of similar chain length, these would more likely resemble molecular clusters of maximum some tens of Å across (Bain and Whitesides, 1989b).

Octadecylphosphates

In order to have more flexibility in the choice of the substrate (e.g. Si wafers or TiO₂ instead of Au), self-assembling systems different from alkanethiols were of big interest for this project. As will be presented further in “Vesicle-fusion onto different substrates“, none of the functionalized sulfur-based SAMs led to adsorbed bilayer membranes in the fluid state on gold. On the other hand, fluidity was reproducibly achieved on SiO₂ substrates. To influence the surface chemistry and to pattern these substrates, two routes based on novel self-assembling chemistries were tested. In the first place, long chain alkanephosphates or -phosphonates, which are known to produce well ordered monolayers on oxide surfaces ((Gao et al., 1996)) were used to test whether they can be patterned via μ CP. The second approach based on hydrosilane chemistry is presented in the next section.



Octadecylphosphoric-acid (ODP)

On titaniumoxide, octadecylphosphoricacid produces ordered SAMs of 21 Å thickness (XPS) with an adv. contact angle of $107 \pm 2^\circ$. But unlike alkanethiols on Au, phosphoric acids have very slow chemisorption kinetics which makes it tricky and time consuming to transfer them onto a surface using μ CP. Prolonged stamping times and carefully chosen stamping-solvents finally led to micro-contact printed layers with a contact angle of $82 \pm 4^\circ$ and a thickness of 10 -11 Å. Patterning of the SAMs was therefore possible, but the quality of the transferred layers was inferior to micro-contact printed, non-functional alkanethiol SAMs (Lehmann et al., 1998a). Figure 40 shows lateral (friction) force images of ODP molecules deposited in lines by μ CP on a substrate. The AFM tip senses large friction differences between the bare regions.

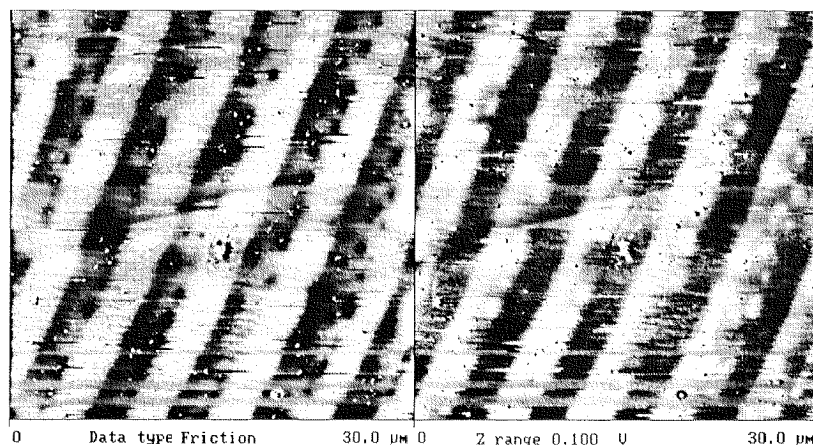


Figure 40: Trace and retrace lateral force microscope images of a SiO₂ substrate which has been structure-stamped with ODP molecules.

Very similar results were obtained for the self-assembly and micro-contact printing of ODP on alumina substrates (Michel-Choi, 1998).

Chemical patterning based on alkanephosphate or alkanephosphonate chemistry could probably be improved using polymer masters and microfluidic techniques which are more suited for the long incubation time required by this system. Suitable micropatterned stamps for microfluidic applications based on novel polymers (for the use with organic solvents) are now being developed and a more detailed study of the binding mechanism of long chain phosphates or -phosphonates will soon be published by R. Hofer et al.

Hydrosilanes

A second approach for organochemical modification of surfaces based on a novel hydrosilane chemistry was investigated in collaboration with M. Hirayama. During her thesis she discovered that polymers containing Si-H groups could strongly be attached to most metal surfaces ranging from metals without any oxygen layer (Au) to oxidized aluminum, in the presence of a catalyst (Hirayama, 1997). More recent results even showed that these compounds can also be used to coat wood and stone etc.. Some investigations have been performed to see whether hydrosilanes derivatized with a long alkyl chain would lead to a novel self-assembling system. Using such a hydrosilane was very challenging, mainly due to the above mentioned many modifiable substrates. Until now, such generally applicable systems are not known.

The two commercially available alkylsilanes “Octadecylsilane (A)” and “Dimethyloctadecylsilane (B)” were allowed to react with gold coated silicon substrates in the absence and presence of the catalyst (Figure 41). Different reaction conditions as

well as reaction times were studied and the coated surfaces were then analyzed by XPS, grazing-angle FT-IR, ellipsometry and contact angle measurements. A detailed description of these experiments can be found in the appendix under “Hydrosilane thin films”.

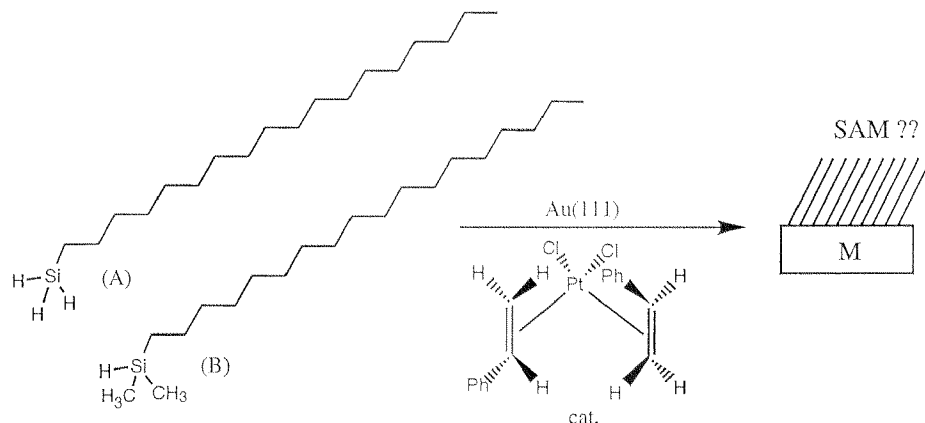


Figure 41: Scheme of the catalyzed reaction of alkylhydrosilanes with Au(111).

Summarizing the results: According to contact angle measurements, long chain alkylsilanes do form strongly immobilized, ultrathin and very hydrophobic layers on gold. However, the thickness of the growing coating does not stop at the monolayer level, but stands in a linear relationship to the incubation time. FT-IR measurements show, that the Si-H bond is not any more detectable after binding to the substrate, proving, that not only physisorption of molecules is taking place but rather kind of a polymerization reaction. On having a closer look at the chemistry of the supported layer, large amounts of oxygen are found in the layers according to XPS and FT-IR data. As neither the gold, the catalyst nor the hydrosilanes contain oxygen, this fact implies, that either water-impurities in the organic solvent or oxygen coming from the air must play an important role in the reaction mechanism. This hypothesis was additionally supported by the finding that the reaction kinetics strongly varied in different experiments although the silane concentration was kept constant (chloro-silane contamination in the hydrosilane batch could also be acquitted as the source of the polymerization, as no difference in the adsorption behavior could be detected before- and after deactivation and distillation of compound A). From these and FT-IR results it had to be concluded, that siloxane-like structures are at least partly responsible for the observed polymerization process on the surface. The atomic ratios found for hydrosilane thin films as determined by XPS, showed the presence of amounts of oxygen larger than would correspond to a stoichiometry of 3 oxygens per silicon atom. This may be an indication for the participation of a yet unknown, oxygen-containing molecule in the binding of the hydrosilanes (the catalyst or part of it ?).

To understand better the binding mechanism of the silane to the gold as well as the role of the oxygen, a ^{29}Si -NMR study of the behavior of the silanes in solution was made. In the absence of catalyst, dimethylsilane showed to be very stable within a period of a week without loss of the Si-H bond, whereas in the presence of the catalyst, dozens of silicon species were produced in different amounts of which any (or many) could be the surface-active species. Some possible alternative reactions-paths for the H-Si bond can be found in (Merciniec, 1992).

From these results, the conclusion had to be drawn, that long-chain alkyl hydrosilanes, in the presence of the Pt-catalyst, do not form SAMs on gold. More likely thin, but not monolayer coatings are produced on this metal, having a similar chemical composition as silane layers produced by chloro-, methoxy- or ethoxysilanes. Getting better and more knowledge about the binding mechanism of siloxane-polymers containing Si-H groups is actually the topic of a dissertation. Results being obtained therein will hopefully also shed light on the behavior of the low-molecular weight compounds tested in this dissertation. Again, the reader is referred to the Appendix “Hydrosilane thin films“, where the hydrosilylation is discussed in more detail.

Others

Silanization

Silanization of oxygen containing surfaces is one of most applied and best studied systems for surface modification. This technique is also being used for industrial-scale surface modification. Materials like glass, stone, many polymers, tissues, metals and many others are accessible to this kind of treatment (Mittal, 1992). The underlying chemistry is based on a hydrolysis reaction between a silanol-group and surface hydroxyl-groups leading to a covalent $(\text{R})_m\text{-Si-(O-Surface)}_n$ ($n=1,2,3$; $m=4-n$) bond configuration (Ulman, 1996) (Figure 42). Today, hundreds of substituents are commercially available, attached to the organic moiety of the silanes which can be used to tailor the properties of a given substrate according to specific demands. Silanization agents are most commonly used in the form of chloro-, methoxy-, or ethoxysilanes which then hydrolyze to silanols in the presence of traces of water and subsequently undergo the covalent linkage to the surface. If compounds with more than one chloro-, methoxy-, or ethoxy group are used, polymerization of the silanes on the surface and in the solvent can occur leading to thick surface siloxane coatings. Here it is important to mention, that - probably due to the presence of contamination-traces of higher oxidized species - even monochloro-, -methoxy-, or -ethoxy silanes undergo most often

polymerization reactions which make it nearly impossible to obtain monomolecular layers using the silanization approach.

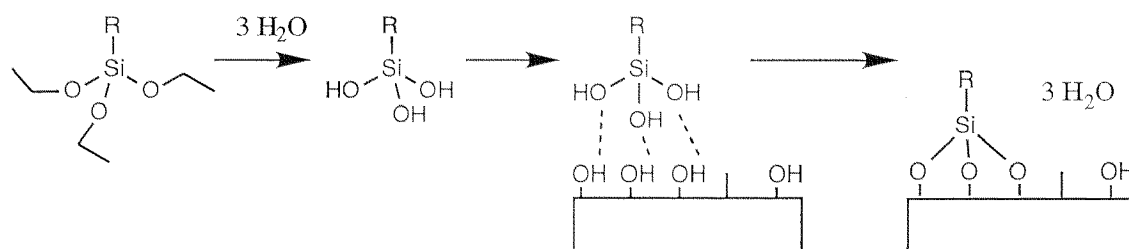


Figure 42: A typical silanization reaction between a triethoxysilane compound and a hydroxyl containing surface.

A very big drawback of the silane-chemistry is therefore the bad reproducibility in terms of achievable surface-coating densities. This is mostly due to the fact that it is extremely difficult to control the amount of water present on either the surface which will be coated or in the silanization solution. However, if the surface coverage is not critical, silanization is a very fast and reliable method and it has the big advantage of being directly applicable to silicon surfaces. Some silanes can furthermore be transferred by μ CP using PDMS stamps, (St. John and Craighead, 1996, Wang et al., 1997a, Xia et al., 1995) and it is also worth mentioning, that non-oxidized surfaces like gold have successfully been modified using silanes (Finklea et al., 1986). If Au and Si areas on a very same sample are to be chemically modified each with a different chemistry, silanization and alkanethiol SAM formation can be combined under certain conditions (Kossek et al., 1996).

We used either a 1 mM octadecyltrichlorosilane solution in toluene, into which the samples were immersed for several minutes or hexamethyldisilazane (HMDS), which was applied in the vapor phase. After silanization, the substrates were dried in an oven at 160°C for 90 min.

Passivation

The word “passivation“ is very widespread in surface science and means that a surface is modified in a way that its tendency to undergo reactions is reduced. In the chemical sense this is equivalent to reacting the surface with another species to lower the surface free energy (thermodynamic passivation) or a reaction which leads to an enlarged activation energy ΔG^{\ddagger} of the passivated surface compared to the non-passivated surface

(reaction-kinetics passivation)(Figure 43). Of course, also thick coatings, by merely inhibiting reactants to reach the protected surface can be called passivation layers in the “physical“ sense.

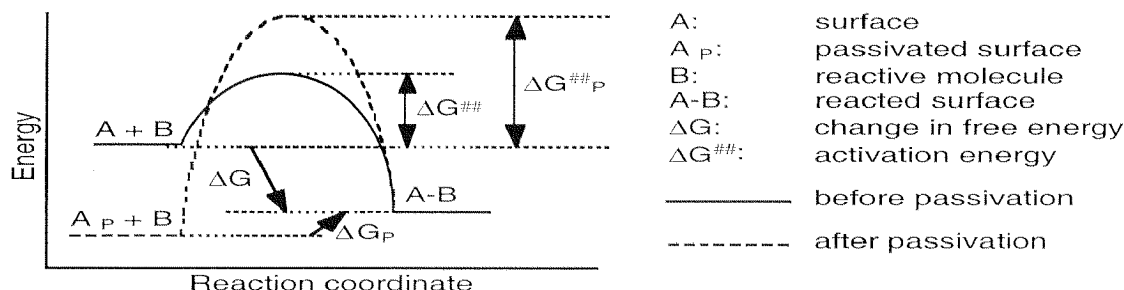


Figure 43: Energy plot for the reaction for a substrate A with a reactive species B before and after passivation.

Oxidation of Si

A silicon surface in ambient air readily builds up a passivating SiO₂ layer which constantly grows over time. This reaction occurs spontaneously which is already an indication for a process with negative ΔG (Δ_fH°_{SiO₂} = -911 kJ/mol !). The oxidation of silicon can be accelerated using oxidizing agents (piranha solution, KOH etc.) or by thermal oxidation in the presence of steam at about 900-1200°C. The latter can be used to produce up to 2 μm thick oxide layers for masking applications (Buettgenbach, 1991). Piranha and KOH treatment lead to very thin, weak and hydrated oxide layers, which are useful for making Si surfaces hydrophilic (e.g. for liposome spreading leading to fluid supported membranes).

Often it is desired to obtain hydrophobic, passivated silicon surfaces. In this project this was important in order to reduce the affinity of the PDMS polymerization solution to silicon during stamp-production. The same process is also a tool to influence the interaction of the silicon with biological species, without need for silanization.

Hydrophobic passivation is obtained by exposing the surface to HF or related solutions. HF etches away the natural oxide-layer effectively and gives rise to Si-H bonds on the surface which are very inert towards further modifications. In contact with air, these surfaces very slowly reconvert to SiO₂. By applying highly buffered HF solutions to Si(111), due to anisotropic etching, a very flat Si-H surface topography is obtained (Higashi et al., 1990), having potential applications for scanning-probe microscopy (Wagner et al., 1997).

Si-H passivation:

- Clean Si substrates were incubated in 40% NH_4F until the surfaces turned hydrophobic (no more wetting by the etching solution). Longer incubation times lead to flattening of the Si surface.
- A standard receipt for buffered HF (BHF) is: 90% v/v 40% NH_4F + 10% v/v HF. This solution can be used to hydrogen-passivate silicon wafers in the same manner as described above.

Oxygen-Plasma treatment

Exposing samples to a gas plasma is a very effective means to remove organic contamination from inorganic surfaces or to make organic substrates more hydrophilic by oxidation. To create a plasma, ambient air or a gas (O_2 , Argon etc.) is ionized at reduced pressure (between 5 and 20 Pa - the optimal pressure is reached when the plasma light emission reaches its maximum) by either a high tension which is applied between two electrodes in the proximity of the samples or by a high-frequency magnetic field produced by a coil around the vacuum chamber. Within the plasma, some gas molecules are converted into radicals which attack and break-up organic bonds on the substrate. If oxygen is used, organic surface contaminations are removed by oxidation ($\rightarrow \text{CO}_2$, H_2O). Usually, silicon wafers or AFM tips were exposed for 2 minutes to a faintly purple-glowing plasma, after which they were completely wetting. Oxygen-plasma was also used to render PDMS stamps, PTFE-foils, and polycarbonate filters hydrophilic (see corresponding chapters).

Piranha treatment

Another means to render Si or Au surfaces hydrophilic or to remove organic contamination is to use highly oxidizing solutions. Such a solution is obtained by mixing sulfuric acid and hydrogen peroxide together in a ratio of 7:4, (Attention: The solution gets very hot !)(Coles, 1976). According to the following mechanism, peroxisulfuric-acid is formed, which instantly and completely oxidizes organic species at high temperatures (near-boiling solution)(Figure 44).

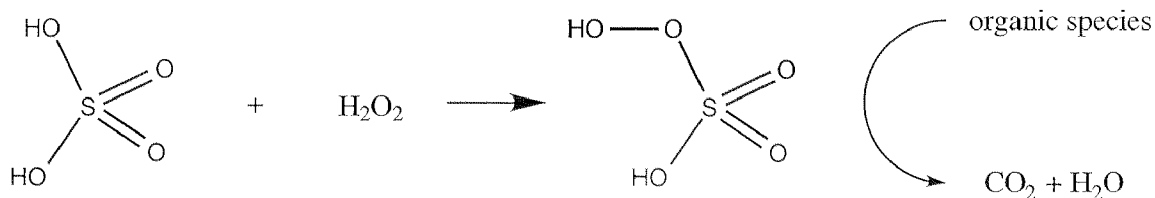


Figure 44: Formation of a peroxide-acid in the presence of hydrogen-peroxide.

It is now probably comprehensive, why this solution is commonly called “piranha solution“. Obviously, one has to take care when working with this solution, as it will readily destroy glove-material. Piranha solution should not be allowed to evaporate as it will explode if the sulfuric-acid content is reduced under a certain limit (Johnson, 1967, Coles, 1976).

Prior to liposome-spreading, silicon- and silicon-oxide surfaces were always cleaned in piranha solution (5 minutes dip followed by extensive rinsing with 18 MΩ water). Also contaminated gold substrates can be cleaned using this approach, but freshly evaporated samples are preferred.

CHEMICAL PATTERNING

Overview of techniques

Chemical patterning means the transfer of different chemical functionalities on predefined areas on the two-dimensional surface of a substrate. Such structurization has had little importance in the microelectronics sector compared to topographical (etch-) patterning and ion implantation techniques. However, many of the topics which are crucial for the development of the upcoming interdisciplinary technologies combining modern biology (biotechnology, genetics, biochemistry, molecular biology etc.) with the traditional scientific fields (chemistry, physics, engineering etc.) are directly dependent on the development of chemically patterned and tailoring surfaces. As for topographical nanopatterning, only a few techniques have been developed so far for this purpose, and those which exist can often not be applied in general, but are limited to a very special kind of surface and application. In this chapter we will present two techniques which can be used to pattern a substrate based on chemical compounds which have already been introduced in the chapter “CHEMICAL MODIFICATION OF SURFACES“. First, we will present “micro-fluidic patterning (μ FP)“, and then go to “micro-contact printing (μ CP)“. Both techniques are based on the use of micro- or nanostructured polymeric masters which can repeatedly be used to transfer organochemical compounds to defined sites on a surface.

Microfluidic patterning

The microfluidic patterning technique can be used to pattern any chemical surface modification agent which can be applied from a solution. Figure 45 gives an illustration of this technique:

A polymer-form (master) with structured channels running from one liquid reservoir to another is carefully pressed onto the substrate to be chemically patterned. Then, a solution containing the molecules for the surface modification is applied to one of the liquid reservoirs upon which it is sucked into the channels by the action of the surface tension or by gravitation. The molecules are then allowed to assemble or bind to the surface in a steady flow, or if highly concentrated solutions are used, by diffusion. After the required incubation time, the channels are flushed using clean solvent, dried under nitrogen and then the master is carefully removed. This process can be repeated several times, each time applying different surface modifications, or following the first

modification, the substrate can be rinsed with a second compound which will only modify not yet occupied areas. This technique has been used to produce micropatterns by molding of polymeric microspheres (Kim et al., 1996), for the patterned immobilization of immunoglobulins (Delamarche et al., 1997) and for protein patterning in general (Bernard et al., 1998).

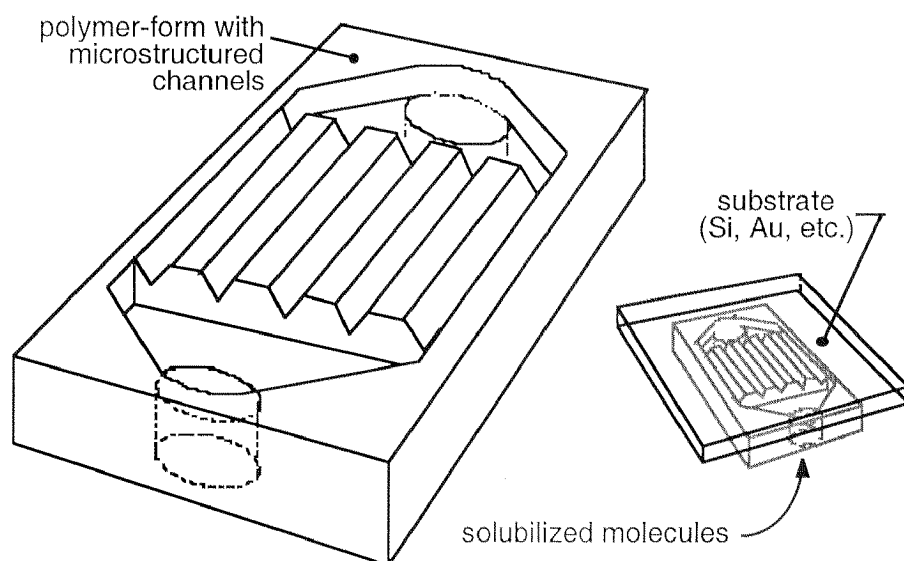


Figure 45: Scheme of the microfluidic-patterning technique and the microstructured polymer forms needed for the chemical patterning of flat substrates..

PDMS masters can be fairly well used for the application of water-based solutions. If the depth of the micro-channels is chosen deep enough (several microns), the water readily flows through them although PDMS in principle is very hydrophobic and thus not wetting. In case that water does not flow through the channels, the master has either to be conceived in a way that vacuum can be applied to it or the PDMS has to be rendered more hydrophilic by exposure to oxygen plasma. In the latter case, it has to be carefully tested whether no liquid is being sucked between the PDMS and the substrate, which would lead to bad pattern definition. In combination with organic solvents, PDMS μ FP can only be used if the master is not being swollen by the solvent or if the immobilization step is extremely fast (within seconds). Otherwise, masters made out of other polymeric-materials have to be used, but nothing in this respect has been published so far. If special functionalities are necessary on the PDMS master, these can be introduced via silanization after oxygen-plasma treatment of the stamp.

We have produced PDMS masters for microfluidics by casting of silicon structures produced by photolithography Figure 46. The depth of the channels were varied between 5 and 60 μm .

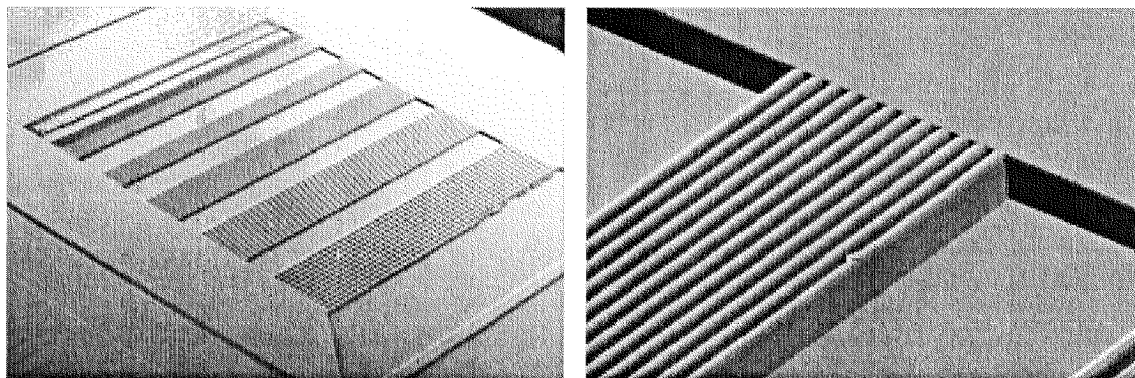


Figure 46: SEM images of silicon templates for casting of polymer masters for microfluidic patterning. The width of the channels is 5-50 μm and their depth can be adjusted by varying the KOH etching time.

The major disadvantage of this method is the restriction to patterns which have channel-like character and join two liquid compartments. The realization of small, island-like patterns would be very difficult.

Micro-Contact Printing

The technique

In the days when alkanethiol self-assembled monolayers gained more and more popularity in the scientific community, a method was introduced by Whitesides and coworkers, which allowed the micropatterned transfer of these self-assembled monolayers by means of a simple stamping technique. If a structured polymeric stamp is exposed to an alkanethiol solution, dried and then pressed onto a gold substrate, alkanethiols are transferred to the gold substrate, forming a well-packed, self-assembled monolayer where the stamp touches the gold surface. This technique has been used to provide monolayer surfaces with spatially resolved head-group functionalities, for the transfer of multiple SAMs on one surface, for the production of resist layer patterns (see Chapter “Micro-contact printing (μCP)/etching“), for cell patterning, for protein patterning and to control the wetting properties on substrates. A lot of methods for micro-or nanostructuring derived from the basic stamping approach were then discovered in the years that followed. A good summary is given by Xia and Whitesides (Xia and Whitesides, 1998).

For our project, this technique was very promising as we aimed to control the spreading of liposomes, the fluidity of the resulting supported bilayer as well as the stabilization of the suspended bilayers using alkanethiol-SAMs. The patterned, local application of such SAMs would permit to control the behavior of the SAM in the micro to nanometer dimensions, which is already the first step in direction of gaining control over proteins inserted in the supported membranes. The experiments described below were performed to find answers to the following main five questions:

- Can μ CP be used to transfer the reactive alkanethiols which were synthesized in our laboratory? (Answer: yes. see “Using micro-contact printed substrates for the covalent immobilization of biological objects“)
- Are the reactive SAMs, which have been applied as described in the previous question, still able to covalently bind proteins? (Answer: yes). How good is the discrimination of the proteins between binding- and non-binding SAM areas?
- How active are the proteins after the immobilization step compared to on SAMs which have been formed by solution immersion? (Answer: they are active)
- How can etched Au/Si surfaces produced by micro-contact printing (see chapter “Micro-contact printing (μ CP)/etching“) be further processed in order to covalently bind proteins (or membranes) onto them ?
- Does the μ CP technique work on the ultraflat, template-stripped gold substrates which were developed in our laboratory? (Answer: yes)

Answers to these questions are found throughout this thesis and are positive.

Although in the end we aimed to use the described technology for the immobilization of bilayer membranes, proteins were used in the first place to test the reactivity of the patterned DSU-SAM. The reason for this was that we were more familiar with proteins and that they are more accessible to surface analysis. The “how to do“ micro-contact printing is explained in detail in chapter “Micro-contact printing (μ CP)/etching“, on page 47. Here, before going into experimental details, a closer look at the mechanism of stamping is appropriate. Unexpectedly, μ CP appeared to be dependent on lots of factors and a series of variables which influence the efficiency of patterning. Figure 47 illustrates graphically the processes which are involved in the stamping process and which have to be mutually suited for optimal SAM transfer to the substrate.

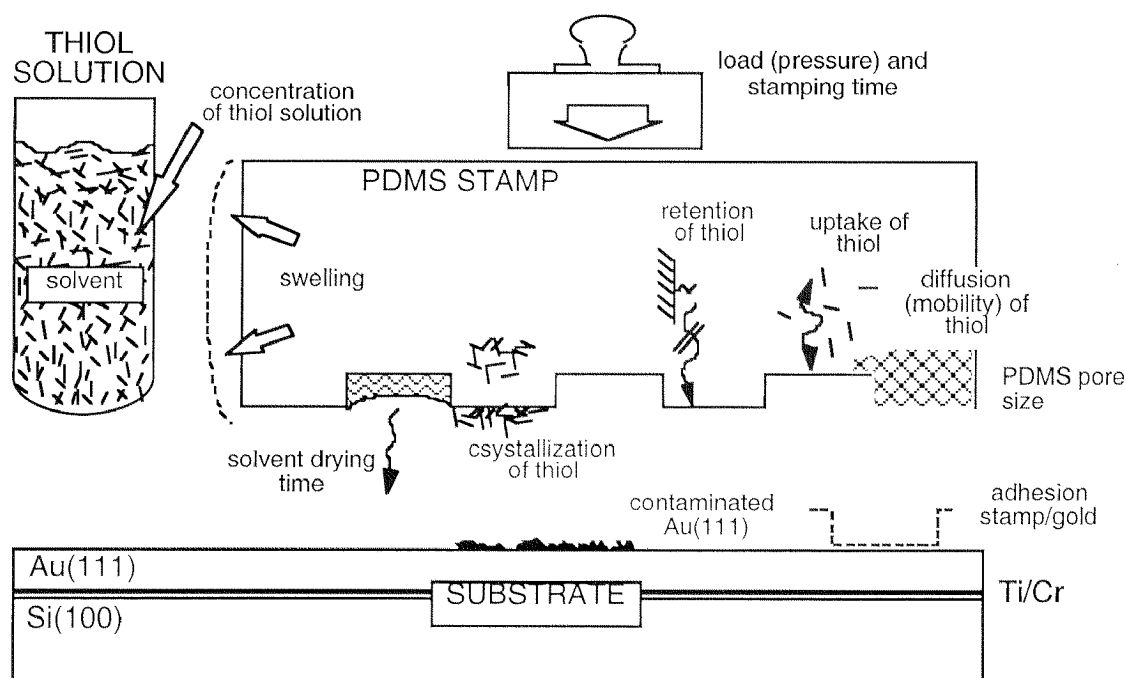


Figure 47: The processes involved in μ CP

The following things should be kept in mind when performing μ CP:

- 1) The solvent used for the alkanethiols should completely dissolve the thiol, but too good a solvent will lead to a reduced affinity of the thiol to the substrate.
- 2) The chosen solvent has to penetrate into the PDMS but must not swell the stamp too much. Swelling would lead to distortion of the micropatterns and of the whole stamp, making a good seal (adhesion) to the substrate impossible. A relatively strong adhesion of the stamp to the substrate is crucial, as the slightest movement of the stamp during stamping will lead to distorted micropatterns.
- 3) It is important to choose an appropriate drying time between the application of the solution to the stamp and the stamping per se. If the surface of the PDMS is not dry, it will smear alkanethiols between the micropatterns. If, on the other hand, the chosen drying time is too long, no solvent will remain entrapped in the pores of the stamp, and the alkanethiols will not be able to diffuse out again to form the SAM. Very much care has also to be taken that no thiol crystallizes on the PDMS.
- 4) The degree of polymerization of the PDMS may gain in importance when large molecules are to be stamped. The molecules must be able to penetrate the polymer and be mobile therein. The amount of thiol species entrapped must be large enough to lead to a complete SAM on the Au after stamping.

- 5) The nature of the functional group on the alkanethiol will determine whether or not the thiol can penetrate into the PDMS (electrostatic repulsion/steric hindrance/hydrophobicity, hydrophilicity etc.). Thereafter, the interaction of the functional group with the PDMS must not be too strong, or else the thiol will not be free to diffuse out onto the substrate.
- 6) Usually, the stamp is not really pressed onto the substrate with a defined load, but it is rather carefully laid down onto it and then only lightly pressed to assure an effective seal over the whole stamping area. If, on the other hand, the adhesion between the stamp and the substrate is weak, application of some pressure will be inevitable. Of course, the stamping time must be long enough for a full SAM to be developed upon stamping.
- 7) Concerning the substrate, too large contamination layers on the gold can not any more be swept away by the SAM formation process and will therefore lead to badly resolved patterns and defects in the SAM. Very importantly, contamination is also constantly being taken up from the air by the drying solvent after the stamp has been “inked“. It is therefore of importance, in which room (laboratory) the stamping is performed.

Using micro-contact printed substrates for the covalent immobilization of biological objects

Many aspects have to be taken into account when developing interfacial devices involving native biological molecules and inorganic, microstructured surfaces: Biological objects, due to their sensitivity and complexity, need a well-defined, mild “physiological” environment for their structural integrity and activity. On the other hand, these systems have to be rendered convenient, making them accessible to experimental research or applications in artificial devices. In this regard, an important tool is the spatial direction of the site of immobilization of biomolecules on microstructured surfaces. However, one has to take care not to denature the biological systems upon immobilization and to make sure that the attachment is strong enough to resist changes in the chemical and physical composition of the liquid environment, which can substantially impair the strength of immobilization of, for example, physisorbed membranes or proteins. Structured and chemically defined surfaces based on the alkanethiolate-SAM chemistry offer several advantages for the purposes mentioned above: alkanethiolate monolayers on gold are stable under aqueous conditions and they are ideal crosslinkers between biomolecules and the inorganic substrate. Moreover, the densely packed arrangement of the hydrocarbon chains with a defined spacer length provides a mechanical as well as a chemical barrier protecting the

underlying substrate from direct contact with the environment. There are also no chemical limitations with respect to the synthesis of alkanethiols having complex end-group functionalities.

We have produced (by micro-contact printing) and then tested two different sets of structured surfaces for the covalent immobilization of biomolecules via SAMs: on ultraflat gold (i.e., on TSG) we prepared patterned DSU/HUT monolayers and tested them using proteins such as collagen V and peroxidase (POD) (Figure 48, left). In a second strategy, we prepared structured silicon/gold surfaces with immobilized collagen (Figure 48, middle).

While hexadecanethiol has been used in innumerable μ CP studies and has been shown to be readily printable as a complete monolayer, it is not suited to the applications described in this chapter, since its hydrophobic character is likely to induce protein adsorption with subsequent denaturation. Stamping the reactive SAM first, appropriate monolayer end-group chemistries can be chosen at will for the remaining, free gold areas, and the reactivity of the surface can either be tuned towards the immobilization of a specific ligand or to minimize non-specific adsorption of contaminants.

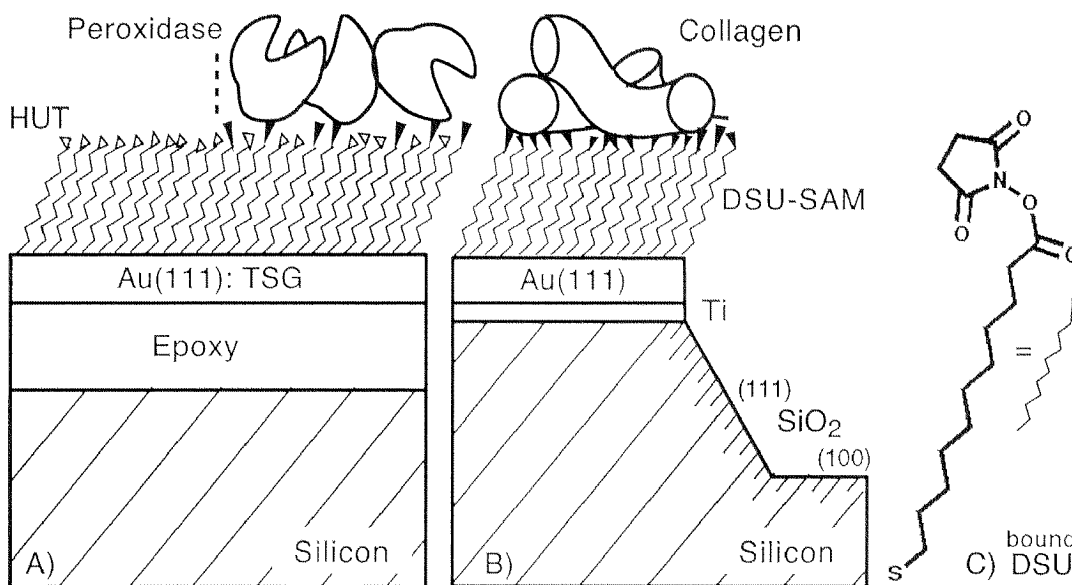


Figure 48: Left: Schematic section through a chemically microstructured TSG sample after μ CP with reactive DSU, formation of a HUT SAM and immobilization of proteins. Primary amines of proteins react with the end groups of the DSU crosslinker (11,11'-dithio-bis(succinimidylundecanoate; Right: bound DSU (thiolate form)) with the formation of an amide bond. Middle: Schematic section through a microstructured silicon/gold structure after μ CP, etching the gold, titanium and silicon, removal of the etch-resistant monolayer, formation of a reactive monolayer and finally reaction with protein.

We have concentrated on functionalization by stamping the reactive DSU disulfide. The higher polarity and increased size of this molecule compared to the n-alkanethiols used in standard μ CP techniques also changes the stamping performance; ellipsometric measurements show that after stamping, on average a mean layer thickness of 0.48 ± 0.19 nm is obtained, compared to 1.7 nm for a fully formed DSU SAM after incubation (Wagner et al., 1996a). Thus, only 1/4 of a monolayer is transferred to the substrate, on average. Subsequent rinsing with HUT, which adsorbs between the DSU molecules, gives rise to a SAM composed of mixed DSU and HUT molecules. The smaller amount of reactive sites available in the resulting mixed SAM may be counterbalanced by an increased reactivity of the DSU molecules—due to a reduced steric hindrance by neighboring DSU molecules towards nucleophilic attack (Wagner et al., 1996a, Wang et al., 1997b). Additionally, it is beneficial to embed the reactive species into a matrix with non-adsorbing surface chemistry, leading to reduced nonspecific adsorption on the reactive areas.

First, amino-modified fluorescently labeled latex microspheres and Semliki Forest viruses with diameters of 200 nm and 70 nm respectively were chosen as test-objects for the immobilization on the chemically patterned SAMs, because they are easy to identify in the LSM (beads) or AFM (virus) and react with DSU through the same amide-bond formation process as proteins. Then, the study was extended to the macromolecular collagen V monomer - a filamentous, extracellular protein and finally the enzyme horseradish peroxidase (POD) was immobilized to assay, whether proteins are completely denatured or not through the covalent linkage to the substrate.

Latex beads on chemically patterned surfaces

Fluorescent latex beads with a diameter of 200 nm were chosen for fast, general testing of (1) the patterning performance by micro-contact printing, (2) the homogeneity and reactivity of the patterned SAM, and (3) the binding selectivity of the two different monolayer head-groups after the adsorption of DSU, and HUT. Figure 49 shows a scheme and Figure 50 a laser scanning fluorescence microscopy image of covalently bound microspheres on a monolayer pattern obtained from DSU. Fluorescence is only detected where DSU had been transferred to the gold surface by direct contact with the elastomeric stamp and thus formed a tightly packed monolayer arrangement. Images with higher magnification reveal the round shaped, individual, randomly adsorbed microspheres on the DSU-monolayer areas (data not shown). Importantly, only very few or no spheres at all are attached to areas where HUT, instead of DSU covered the gold surface.

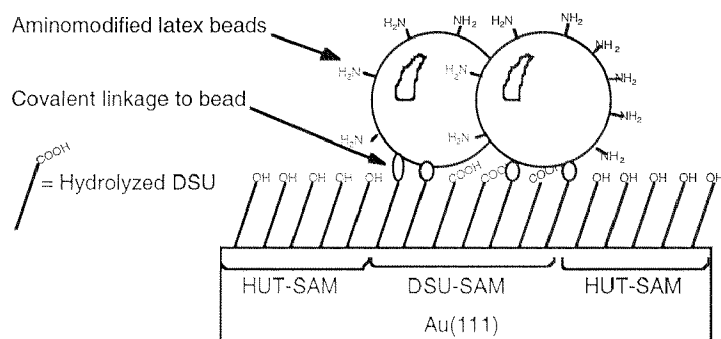


Figure 49: Scheme of fluorescent, aminommodified latex beads covalently immobilized on micropatterned DSU-SAM areas between HUT-SAM.

The edge resolution of these objects on patterned DSU is highly satisfactory. Thus, by using elastomeric stamps with sharply edged patterns, the combination of amino-reactive monolayers and μ CP should be applicable to produce patterns of proteins or other biomolecules with dimensions in the sub-micron range. Fluorescent spheres are specially suitable for very fast optical testing of the remaining binding capacity of reactive SAMs. Moreover, latex beads are very easy to handle, because they are stable, do not aggregate or "denature", etc., making them superior to biological objects for many methodological investigations.

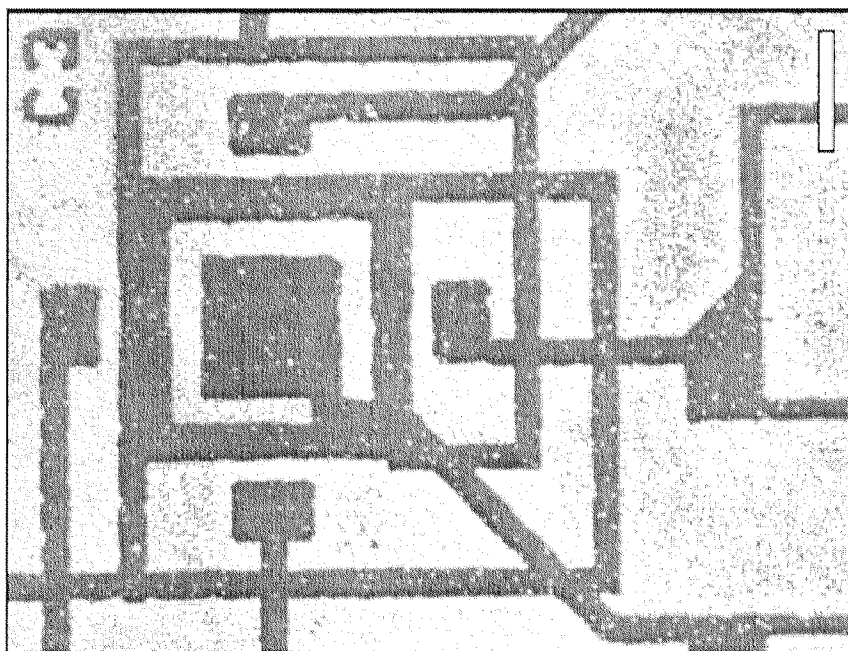


Figure 50: Fluorescent latex microspheres covalently immobilized on a chemically structured gold surface and imaged by laser scanning fluorescence microscopy. First, a pattern of DSU-monolayer was transferred onto the gold by μ CP with subsequent rinsing with a solution of HUT. Light areas: DSU monolayer on Au(111) with immobilized microspheres. Dark areas: Au covered with HUT-SAM. Bar = 100 μ m.

The clear-cut difference between areas of DSU and HUT in Figure 50 was obtained only after efficient removal of the latex beads that had physisorbed on HUT. In fact, immediately after the immobilization step, latex beads covered both the DSU areas (chemisorbed) and the HUT areas (physisorbed). Selective bead removal could be accomplished by a very strong jet of water, other procedures such as washing with concentrated ammonium sulfate, vigorous shaking in concentrated buffers and rinsing with streams of buffers at extreme pH-values failing to efficiently remove physisorbed beads with any degree of selectivity. Brief sonication of the samples removed all the latex beads, no matter whether covalently bound to DSU or physisorbed to HUT, probably because of the destruction of the beads. ω -terminated alkanethiols other than HUT (i.e., amino-, carboxyl-, or methyl-terminated) were also tried as fill-in monolayers for DSU patterns, but none proved superior to HUT. We are currently exploring the use of a polyethylene-glycol-terminated SAM, which was shown to resist physical adsorption of many proteins and even of cells, as a better alternative to HUT, where protein immobilization is not desired.

Immobilization of Viruses on the patterned surfaces

The possibility to covalently immobilize protein assemblies was tested in the next step using Semliki Forest viruses, which belong to the family of α -viruses and which expose a densely packed protein layer (envelope proteins) on their surface. A model of the virus which was reconstructed from cryo-electron microscopy images (Fuller et al., 1995) is shown in Figure 51 (right). On the left, a general scheme of an α -virus is shown.

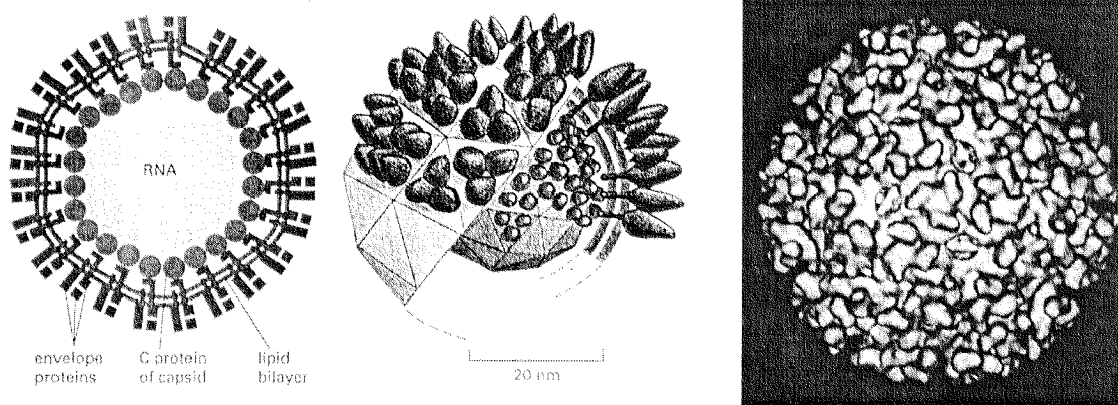


Figure 51: Left: Schematic drawing of a cross-section and an exploded three-dimensional view 3-D of a SFV. Right: Three-dimensional reconstruction of the surface of the virus derived from cryoelectron micrographs. Source: (Fuller et al., 1995).

The viruses were selectively immobilized on a μ CP DSU monolayer pattern on Au(111) through the lysine-side chains of their protein envelope. No strong adhesion of the viruses occurs on the dodecanethiol-SAM covered gold areas, from which physisorbed viruses could be washed away with buffer. The DSU-SAM areas with immobilized viruses appear more granular and brighter on the AFM image in Figure 52 (left). These areas are roughly 30 nm higher with respect to the areas covered with dodecanethiol-monolayer corresponding to strongly bound and therefore flattened viruses. On non-patterned, ultraflat TSG surfaces, the round shaped viruses can be imaged very nicely by AFM (Figure 52 (right)). The viruses on this preparation were obtained after centrifugation of 300 μ l of a SFV solution diluted 1/48 for 30 min. at 100'000 g onto a DSU substrate.

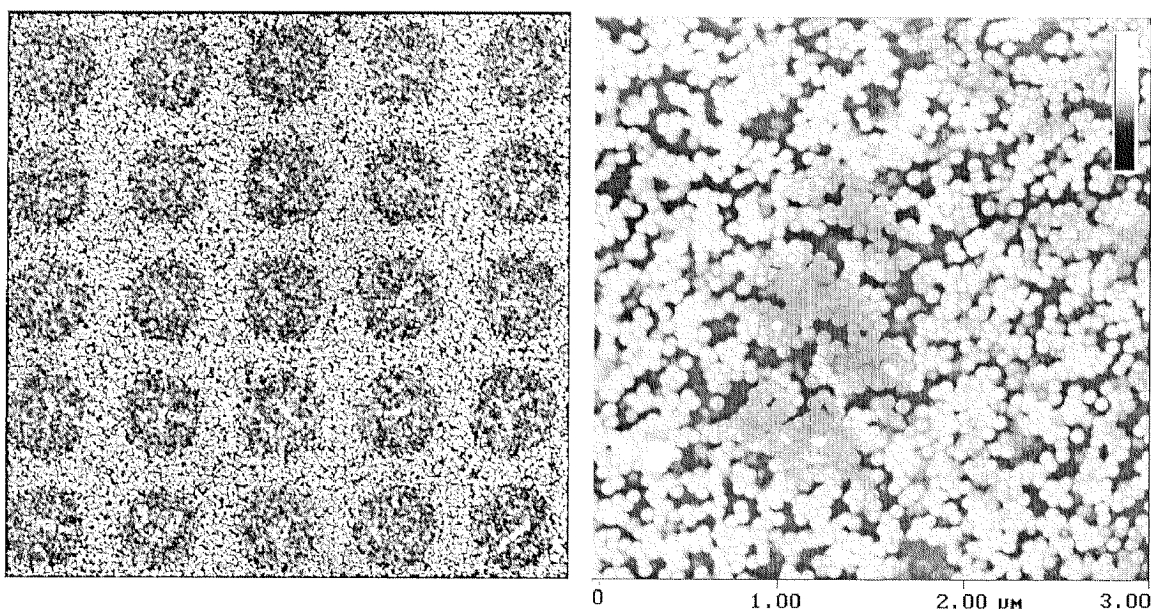


Figure 52: Left: AFM image of Semliki Forest virus particles immobilized on a patterned DSU monolayer on a gold surface. On the lighter areas, a dense layer of covalently immobilized viruses is visible, with a height of 30 nm with respect to gold areas covered with dodecanethiol (darker circles, no bound viruses). The background structure on this thermally evaporated gold surface appears rather rough compared to the ultraflat (TSG) gold in Figure 53. The diameter of the darker, circular areas is 4.5 μ m. Right: AFM tapping-mode image at higher magnification of a dried preparation of SFV immobilized on DSU-SAM on TSG. Single, globular SFV virus are visible. Height scale: 150 nm.

Collagen V immobilization

Collagen V is a typical extracellular matrix protein with a triple helical, 300-nm-long and 1.4-nm-wide structure consisting of 3042 amino acids. 152 lysine residues are fairly

homogeneously spread over its surface, enabling the protein to develop multiple bonds with the NHS-ester groups of a DSU monolayer.

Individual (i.e. three-subunits) molecules of collagen V were applied to a pattern of DSU and HUT monolayers. Figure 53 shows an AFM image at high magnification of collagen V molecules immobilized only on those areas covered by DSU resulting in a network of single collagen monomers while no protein is observed on ultraflat-gold areas covered by HUT molecules. The amount of covalently immobilized collagen monomers on this system can be controlled by using different pH values and collagen concentrations in the buffer solution (Wagner et al., 1996a). Densities ranging from a few molecules per square micron to dense networks of collagen can be obtained. The very characteristic filamentous shape of these proteins makes them clearly distinguishable from the template-stripped gold morphology in the background of the AFM images. They are visibly flexible and often follow the boundaries of HUT/DSU patterns. Interestingly, despite its size and shape, collagen V forms very sharp boundaries between patterned DSU and the protein-resistant, OH-terminated monolayer. Conceivably, once a collagen molecule has bound with one lysine to a monolayer-site close to the DSU/HUT-SAM border, the non-bound triple-helical strand may be induced to zip-like binding also. In other words, being unable to create covalent bonds with HUT-SAM regions, the protein is thermodynamically forced to find its final location upon reaction with the NHS headgroups of the DSU monolayer. Contact-mode AFM revealed the very strong binding of the covalent (amide) bond between the proteins and the monolayer: an increased loading force on the scanning tip did not sweep aside the collagen until the protein chain itself was ruptured by the strong lateral forces applied. Physisorption of collagen on a HUT monolayer is also fairly stable, but can be overcome by special washing procedures, as described in “Materials and Methods“. Other ω -terminated alkanethiols (i.e., amino-, carboxyl-, or methyl-terminated) were also tried as fill-in monolayers for DSU patterns, but none proved superior to HUT. A better approach would be the use of a polyethylene-glycol-terminated SAM, which was shown to resist physical adsorption of many proteins and even of cells (Prime and Whitesides, 1991, Harris and Zalipsky, 1997, Du et al., 1997), as an alternative protein-resistant monolayer coating.

Immobilization of Peroxidase

In order to investigate the influence of the monolayer immobilization method on the activity of a model-protein, we adsorbed horseradish peroxidase on a similar pattern as described above and detected its enzymatic activity. Survival of the enzymatic activity at the solid-liquid interface cannot be taken for granted, since proteins often suffer large

conformational changes with partial or complete loss of their activity —when adsorbed at surfaces (Rialdi and Battistel, 1996). Non-covalently adsorbed peroxidase could be very efficiently removed by washing with a buffer solution containing 0.1 % (v/v) Tween 20. This mild, nonpolar detergent is known not to interfere with the activity of most proteins. The AFM image in Figure 54 demonstrates that peroxidase molecules were exclusively adsorbed on those areas in the monolayer containing DSU. The height of these regions determined by contact mode AFM was 3.3 ± 0.6 nm, which is a realistic size if compared with X-ray structural data of the enzyme (Banci et al., 1994), taking into account some degree of compression and convolution caused by the interaction of the tip with the sample. A quantification of bound peroxidase can be attempted on the basis of tapping mode AFM images, on which individual immobilized peroxidase molecules can be distinguished as globular structures which can be counted and thence an average surface-coverage determined. Figure 54 (bottom) shows a typical TSG surface with individual POD molecules.

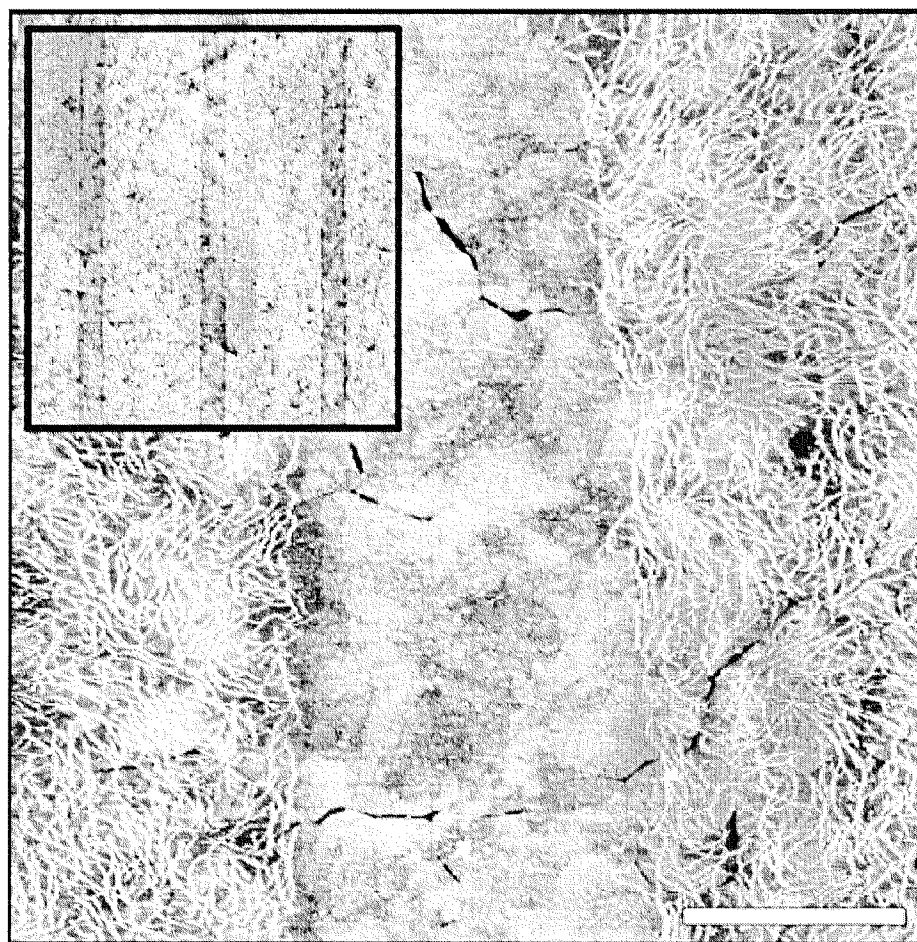


Figure 53: Immobilization of proteins on ultraflat Au(111): A patterned network of collagen V single molecules covalently immobilized on a DSU monolayer. Due to the very low roughness of the ultraflat, template-stripped gold surface, the molecular structure of the immobilized proteins can be resolved over large areas. Inset: the same surface at 18 x lower magnification. Bar = 1 μ m.

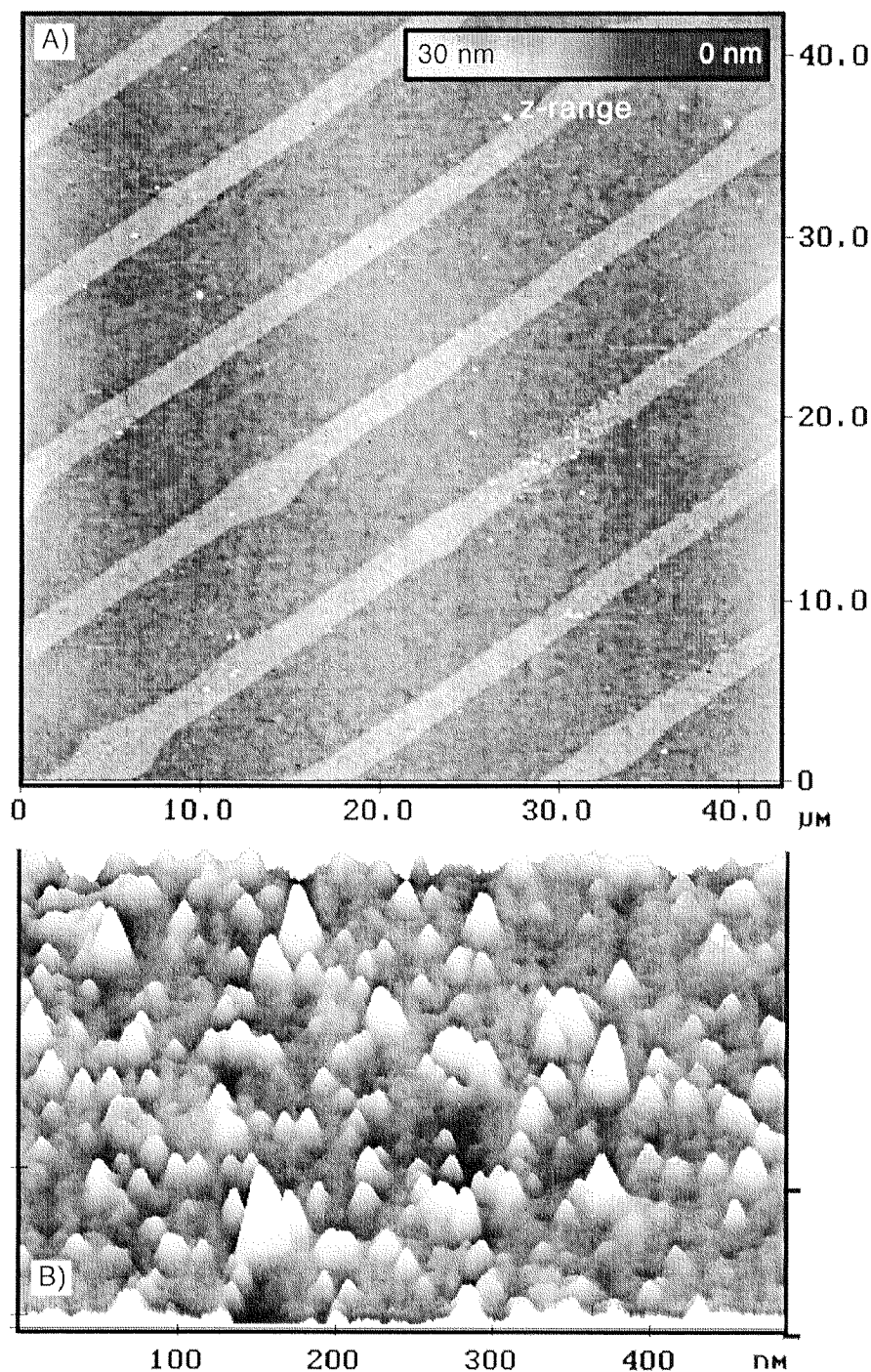


Figure 54: AFM image of bands of covalently immobilized horseradish peroxidase (A, light, higher areas) on ultraflat Au(111). Prior to the attachment of peroxidase, the gold was micro-contact printed with a solution containing DSU and then rinsed with a solution of HUT, which covers the areas that appear dark in the image. B) Individual POD molecules can be distinguished - and counted- at higher magnification on the tapping-mode AFM image. z-Bar = 5 nm.

A peroxidase surface density of 0.13 pmol/cm^2 peroxidase could be calculated for an immobilization time of 10 hours in PBS pH 7.5 at 4°C , on ultraflat gold. X-ray data show (Banci et al., 1994) that the size of the enzyme is approximately $4 * 4 * 6 \text{ nm}$. A

maximal density of 3 pmol/cm² can thus be expected for a tightly packed protein monolayer on ultraflat gold, assuming an exclusion radius of half the diameter around each protein. The enzymatic activity of the covalently bound peroxidase was estimated using 3,3'-5,5'-tetramethylbenzidine (TMB) (see "Materials and Methods") and Figure 55. Three different surfaces have been examined for activity of the attached peroxidase after removing physisorbed enzyme by washing with PBS containing detergent (Tween): (i) surfaces totally covered by DSU binding the enzyme covalently (ii) surfaces covered by a HUT monolayer, (iii) surfaces with DSU/HUT monolayer patterns. In three control experiments, the peroxidase activity was always the highest in the first case (i; 6.2 mU/cm² activity on TSG) and the lowest in the second case (ii; 1.4 mU/cm² activity on TSG), while the patterned samples (iii; 3.3 mU/cm² activity on TSG) displayed intermediate activities. As expected, the enzyme activity correlates at least roughly with the amount of DSU present on the respective gold surface and, thus, with the number of bound enzyme molecules.

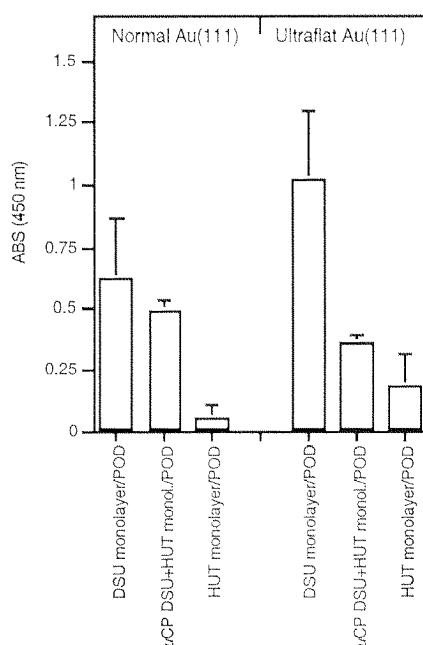


Figure 55: The relative activity of covalently immobilized peroxidase on two different Au(111) substrates pre-coated with three different SAM compositions: Au(111) normal = gold thermally evaporated on a Ti-primed Si(100) wafer; ultraflat Au(111) = ultraflat, TSG gold (see "Materials and Methods") with a mean roughness of 0.2 - 0.5 nm/25 μm²; DSU monolayer = the gold was incubated with the aminoreactive DSU-SAM prior to the immobilization of Peroxidase (POD); HUT monolayer = the gold was incubated with 11-hydroxyundecanethiol prior to the immobilization of POD; μCP DSU+HUT monol. = the gold was first micro-contact printed with DSU followed by rinsing with a solution of HUT, prior to POD incubation.

The influence of roughness of the gold surface on the amount of bound enzyme was investigated by comparing two types of surfaces: (i) a substrate prepared by thermal

evaporation of gold on silicon wafers having a roughness of approx. 2-6 nm and (ii) ultraflat gold surfaces having mean roughness values one order of magnitude lower. Bound POD proved to retain enzymatic activity in both cases (Figure 55), but only half as much activity was detected on the rather rough surface of the first substrate compared to the second type consisting only of mono-atomic steps over cm^2 areas. Increased peroxidase activity on smooth surfaces was observed for the DSU-, HUT- and DSU/HUT-monolayer samples mentioned above. This may be explained by preferential adsorption of the protein in the (more reactive) grooves of the rougher substrate, which might lead to a different protein conformation due to multiple binding with concomitant loss of activity; and/or to unstirred layers during testing, which are known to result in an apparent increase of K_m and decrease in V_{\max} . An equivalent activity of 0.08 pmol dissolved POD was found immobilized on 1 cm^2 of a TSG surface covered with DSU.

Determination of the amount Alkanethiol transferred by μCP onto a substrate

Due to the transfer of less than a monolayer amounts of e.g. DSU by micro-contact printing, surface analytical methods are at their limits in terms of measuring the properties of such layers. Here, the different approaches which were used and the problems which arose are briefly discussed. The basic question was: How many % of a complete DSU-SAM are transferred by μCP onto a surface.

Ellipsometry

This technique is particularly suited for thickness measurement of thin layers in the angstrom to micrometer range. In the lower thickness limit (sub-nanometer range), some difficulties arise due to the fact that for high accuracy measurements, usually the sample must consist of a clean area for reference measurements and an area with the adsorbed layer of which the thickness is to be determined. Especially in the case of gold surfaces however, fast adsorption of (organic) contamination from the atmosphere (in the 1-5 \AA range) leads to incorrect determinations of the optical parameters for clean Au, leading to incorrect thickness for the layer. For thin layers it is therefore very important to measure the reference on the same sample as already very small variations in the evaporation angle of the gold - or small differences in the gold-nanoroughness lead to significant differences in Δ and Ψ for the substrate.

The layer thickness calculations for stamped DSU SAM are given in the chapter “Using micro-contact printed substrates for the covalent immobilization of biological objects“. These results could only be obtained taking many precautions to avoid sample contamination: Incubation of SAM or micro-contact printing was performed immediately after gold evaporation, the samples were always transported under argon and ellipsometry was carried out immediately after stamping.

Contact-angle

The contact angle measurements - although they are extremely sensitive to changes in surface chemistry - were not performed in this case as they would not be able to distinguish between adsorbed contamination and DSU SAM.

XPS

When measuring the thickness of sub-monolayer films, the XPS reaches its limits. The detection limit is about 0.1 ppm. At low coverages, therefore only elements with a very high sensitivity factor can be detected. Unfortunately, our compound of interest was fully made of the elements C, O, and N (H can not be detected by XPS) which either have a low sensitivity factor or which are also main components of contamination layers. To enhance the signal of bound DSU, therefore a trifluorinated molecule containing a primary amine (3-(trifluoromethyl)benzylamine) was allowed to react with the DSU SAM after stamping. Fluorine has a relatively high sensitivity factor and it is an element which certainly cannot commonly be found in organic species. XPS spectra showed the presence of a fairly strong fluorine peak on the stamped DSU samples, but unfortunately also the samples on which 1,4-dioxane alone had been stamped showed a huge amount of adsorbed fluorine. Gold has a strong affinity for the trifluoroamine compound making the discrimination of DSU-bound and physisorbed species impossible. So, XPS proved to be not useful in this case.

Indirect tests: Enzyme and fluoroprotein immobilizations

A measure of the relative protein immobilization capability of the stamped DSU SAM compared to a DSU-SAM formed in liquid was attempted by the immobilization of the naturally fluorescent protein “Green fluorescent Protein (GFP)“(Chalfie and Kain,

1996). On silicon surfaces monolayers of this protein can readily be seen in the fluorescence microscope after excitation at 480 nm and detection at $\lambda > 500$ nm. On Au or SAM coated Au surfaces, however this protein is probably either denatured or the fluorescence excitation energy is transferred to the gold layer. In any case, we never observed any fluorescence emitted by this protein once it has been adsorbed onto a Au surface. This observation has also been confirmed by other groups.

Another protein was therefore used with a catalytic activity which can be used to detect the amount of bound protein. These experiments were quite successful and they are described in the chapter “Immobilization of peroxidase“.

Generation of etch-patterned surfaces with immobilized biomolecules: SAM exchange technique and collagen V immobilization.

The creation of 3-D structured gold/silicon surfaces was achieved by transferring a hydrophobic SAM onto gold using μ CP, followed by gold-etching, removal of the Ti layer and finally Si-etching.

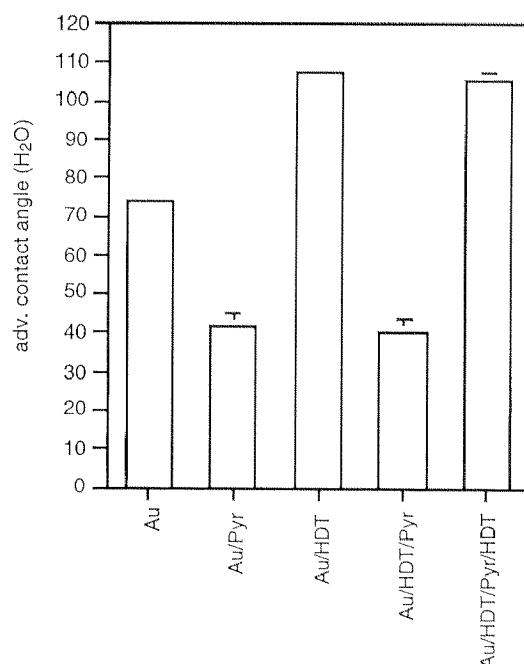


Figure 56: Changes in contact angle related to the process of oxidative SAM removal with piranha solution. Legend: Au: pure Au(111) with natural contamination layer; Au/Pyr: Au treated with hot Piranha solution for 2 min.; Au/HDT: Au(111) after 2 h exposure to hexadecanethiol (5 mM in ethanol); Au/HDT/Pyr: Au after the removal of the hexadecanethiolate-SAM (hot piranha for 2 min.); Au/HDT/Pyr/HDT: new-formation of a hexadecanethiolate-SAM on Au(111) after piranha removal of a previous SAM (5 mM in ethanol).

The procedure is described in chapter “Micro-contact printing (μ CP)/etching“. This surface had then to be rendered chemically active in order to immobilize proteins - or in the future to immobilize supported membranes. The non-reactive and certainly damaged (by the action of the etching solutions) hexadecanethiolate monolayer still left on the gold areas had therefore to be removed by exposing the surface to hot "piranha" solution (30% H_2O_2 /conc. $\text{H}_2\text{SO}_4 = 3:7$; 60°C) for 5 min. (caution: this solution can explode in contact with organic matter !).

Contact angle measurements on non-etched test Au samples (Figure 56) confirm the removal of the hydrophobic etch-resist SAM upon 2 min. exposure to piranha. This treatment leads to a bare gold surface which is now again accessible to the adsorption of a new SAM, as can be seen from the recovery of hydrophobicity upon exposure to a 5 mM hexadecanethiol solution.

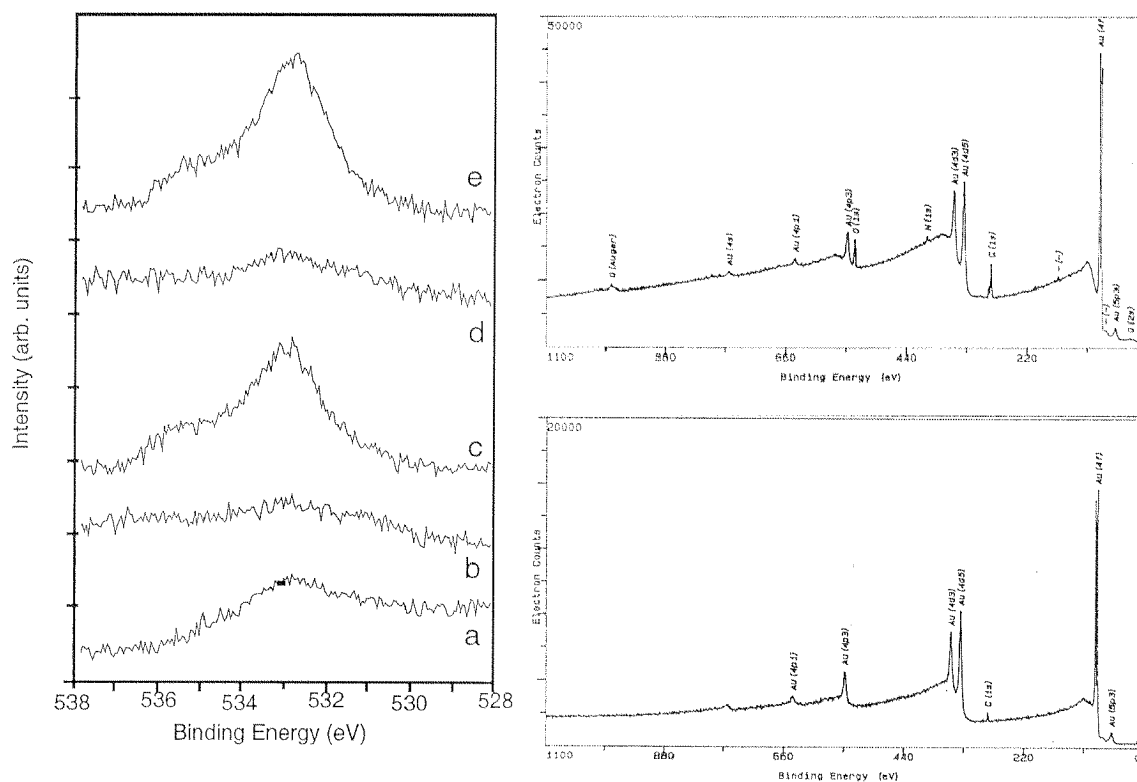


Figure 57: Left: O(1s) X-ray photoelectron spectrum progression of a gold sample at different stages of functionalized-SAM replacement. a: fresh, naturally contaminated gold; b: gold after exposure to 2 min. piranha (60°C); c: DSU-SAM on gold (0.5 mM in 1,4-dioxane for 18 h); d: sample c exposed to 2 min. piranha (60°C), e: sample d upon repeated exposure to DSU. Right, top: XPS spectrum of a DSU SAM on gold with clearly visible O(1s) and N(1s) bands and a strong carbon peak. On a clean Au sample (bottom, right), no O and N is visible, and the small C(1s) peak indicates the presence of small amounts of adsorbed hydrocarbon contamination on the gold.

The same behavior can also be demonstrated for functionalized SAMs, such as DSU: Figure 57 shows XPS spectra of a non-modified gold surface, gold coated with a monolayer of DSU the progression of the O(1s) peak after the different reaction steps: Only a very weak oxygen contamination peak can be detected on freshly deposited gold, which then disappears after immersion in hot piranha solution. After formation of a DSU SAM, the O1s envelope of the succinimidyl-ester functionality appears as a strong band showing two shoulders at 532.2 ± 0.5 eV (C=O) and 534.3 ± 0.13 eV (C-O-C). The peak shape is similar for DSU chemisorbed on Au(111) as for a powder-spectrum of N-succinimidyl palmitate, a commercial compound containing the same succinimidyl-ester group (data not shown). Nevertheless, in no case a good 1/1/2 curve-fitting for the oxygen peak could be obtained. This was probably due to partial hydrolysis of the succinimide ester, which leads to the appearance of carboxylate and hydroxy peaks within the same binding-energy region.

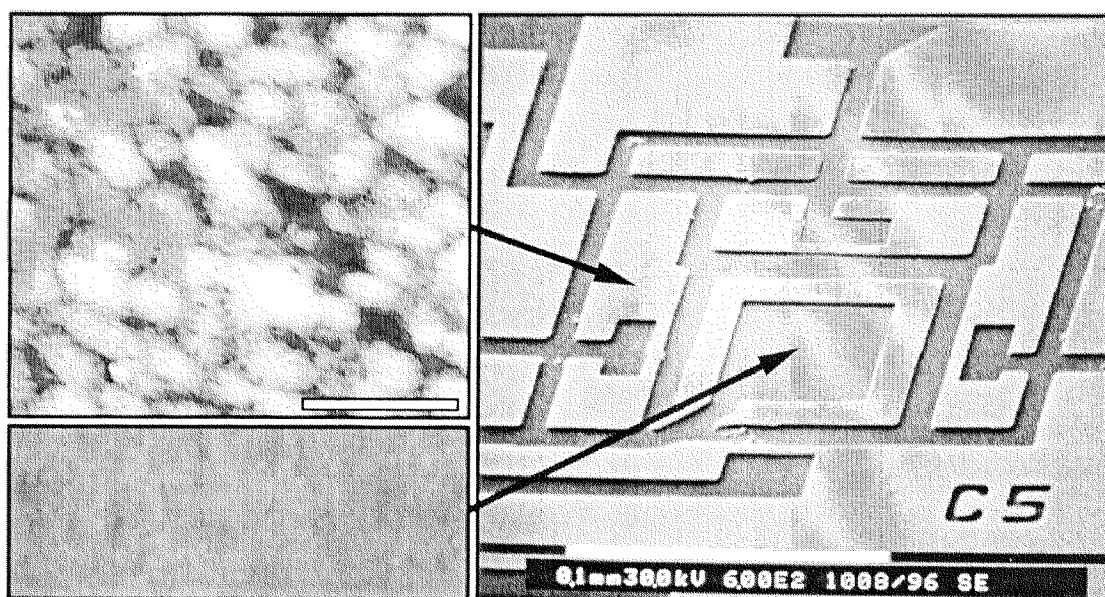


Figure 58: Covalently immobilized proteins on microstructured Au/Si surfaces: (right), SEM image of a structured Au/Si surface produced by μ CP, etching, SAM replacement and covalent collagen immobilization (top, left; bar = 200 nm; z-range = 30 nm): An AFM (tapping mode in air) zoom of the Au/DSU-SAM areas reveals the presence of a two-dimensional network of covalently bound collagen V molecules. The resolution is lower than in Figure 53 because the round-shaped (rough) morphology of this Au(111) impairs AFM measurements. (bottom, left): No collagen is visible on the silicon areas on the surface (same scales as top, left).

Exposure of the DSU-covered substrate to piranha solution leads to a complete disappearance of the oxygen peaks, whereas upon repeated formation of a DSU SAM, these peaks reappear in the original shape, demonstrating the reversibility of the SAM formation. After removal of the hexadecanethiolate etch-resist and formation of a DSU

SAM, the quality and specificity of this aminoreactive DSU pattern was examined again by immobilization of collagen V molecules on the 3-D samples. Figure 58 shows a SEM image of such a topographically and chemically patterned sample. AFM imaging of the monolayer-free silicon oxide areas reveals no physisorbed collagen, while a network of single, covalently bound collagen monomers can be distinguished on the Au(111) islets. Collagen immobilized on the gold tracks of etch-patterned surfaces shows the same characteristics as that on chemically patterned surfaces. However, the apparent edge definition of the collagen on this kind of surface (Figure 58) is much lower than on TSG (Figure 53), because AFM imaging is negatively affected by the rough substrate morphology of Au(111) surfaces prepared by standard thermal evaporation of gold on titanium-primed silicon.

Many materials are processable by the sequence described above, since gold layers of well-defined thickness and topography can easily be deposited on a large number of substrates by vacuum-evaporation techniques. Subsequent structuring steps in the micrometer range can be performed by applying traditional wet-etching procedures. The possibility of removing a SAM from gold either by means of an electrical field, or heating above 80 °C in a suitable solvent (Bain et al., 1989a), or by oxidation (Huang et al., 1994) allows the specific replacement of one monolayer by another. Interesting applications of this include the described possibility of using inert alkanethiols to pattern and etch a surface by μ CP and then - through SAM exchange - to impart a desired chemical reactivity to it. Additionally, the process allows monolayer-immobilized proteins that have become non-functional to be replaced by fresh ones: Silicon devices containing enzymes on small gold areas could be regenerated through a simple three-step procedure: removing the damaged monolayer/protein layer by photo-oxidation; formation of a new monolayer by rinsing with reactive compounds, and finally binding native enzyme. This kind of surface recycling can be of use in biophysical research applications where complex devices can only be produced in small numbers.

Conclusions for this chapter

In this chapter, a mild procedure for the covalent immobilization of proteins on microstructured gold surfaces has been presented. The use of ultraflat, template-stripped gold (TSG) as a substrate opens the possibility of making patterned biomolecule structures accessible to scanning probe methods on a background with defined surface chemistry. On microstructured Si/SiO₂/Ti/Au surfaces produced by μ CP and etching,

the immobilization site of proteins could also be spatially controlled using an amino-reactive SAM. The production of these micro-patterned substrates including SAM-exchange and protein immobilization, can all be performed in one day, thus providing a high degree of flexibility in experimental work. Although most biological samples have amino groups on their surfaces and can thus be immobilized via DSU, the need may arise for other ω -substituted alkanethiols with chemical reactivity directed towards other functional groups. For example, aryldiazonium-terminated alkanethiols (Wagner et al., 1996b) selectively bind activated aromatic hydrogens of, e.g., histidine and tyrosine residues; Ni^{2+} -chelating monolayer-headgroups bind histidine-tagged fusion proteins (Sigal et al., 1996). We are currently exploring the use of this technology for the immobilization of cells and biological bilayer membranes.

BILAYER FORMATION

As described in the introduction, there were several demands to the technique for creating supported bilayer membranes: First, the technique must be able to produce a homogeneous and complete bilayer membrane on a support with dimensions not smaller than 4 mm². At the same time, the lipid composition of the bilayer should be able to be chosen at will, and thirdly, the method should be able to suspend the bilayer over nanometer-sized holes in the support. Based on these considerations, four different methods were taken into consideration and were tested with respect to their suitability for our approach: black lipid membranes, langmuir blodgett films, liposome fusion and oocyte membranes.

Black Lipid Membranes (BLM)

Very early in the history of biochemistry, scientists began to be interested in biological membranes and the proteins related to them. Soon, they discovered that many membrane proteins were incorporated in the membranes and that they often function as tiny channels or pumps, controlling the flux of molecules and transporting ions, molecules or proteins from one side of the membrane to the other.

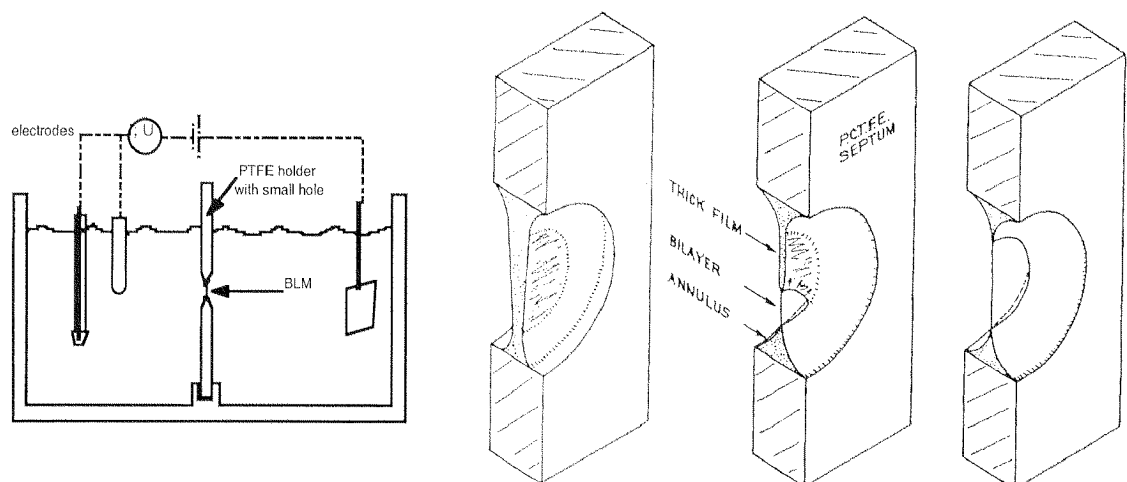


Figure 59: Left: Standard setup for electrochemical experiments with black lipid membranes (BLMs): The membrane is suspended over a hole in a PTFE plate between two aqueous compartments, and the electrical current through the membrane-, or the voltage over the membrane is measured using a three-electrode setup. Right: Scheme of the thinning mechanism of the lipid/solvent mixture which was spread over the PTFE hole under water: A bilayer-thick membrane is formed by expulsion of the solvent from the central part of the aperture. Source: (Hanke and Schlue,).

In order to make the “cellular-membrane system“ accessible to scientific research under defined conditions, a method was developed to produce artificial membranes separating two electrically isolated water compartments. After incorporation of proteins into these membranes, ion-fluxes as well as transport mechanisms could be studied via electrochemical studies (Miller, 1982).

The BLM method can be described as follows:

A small hole with a diameter of some hundred microns to several millimeters was carefully micromachined into a piece of a hydrophobic polymer plate (usually PTFE). This plate was then tightly fit between two aqueous compartments in a specially machined holder (see Figure 59, left). After filling with water, an organic solvent containing a defined lipid mixture was carefully drawn over the aperture using a paintbrush or an air bubble attached to a pipette. Under the influence of the Plateau-Gibbs border suction as well as the van der Waals attraction between the aqueous phases on both sides of the film (Hanke and Schlue,), the initially thick „soap-like“ film suspended over the opening thins rapidly down, until all the solvent is squeezed into the annulus of the holder. A membrane composed of only two adjacent lipid monolayers is obtained (Figure 59, right). This process can be optically followed using a microscope: Due to light diffraction, the soap-like film is very colored in the first thinning steps. But as soon as the thickness of the film gets smaller than the wavelength of visible light, the membrane turns black (say invisible) and a few seconds later the bilayer state is reached (the invisible part of the membrane thinning process is usually monitored by impedance measurements).

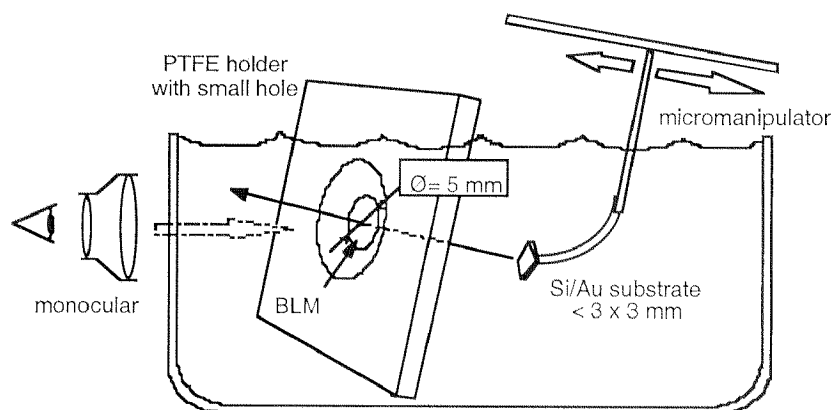


Figure 60: Our setup for the transfer of black lipid membranes to solid supports.

It has been pointed out in several publications that extreme care has to be taken to work in a very clean environment as the method is very sensitive to moisture. Any small

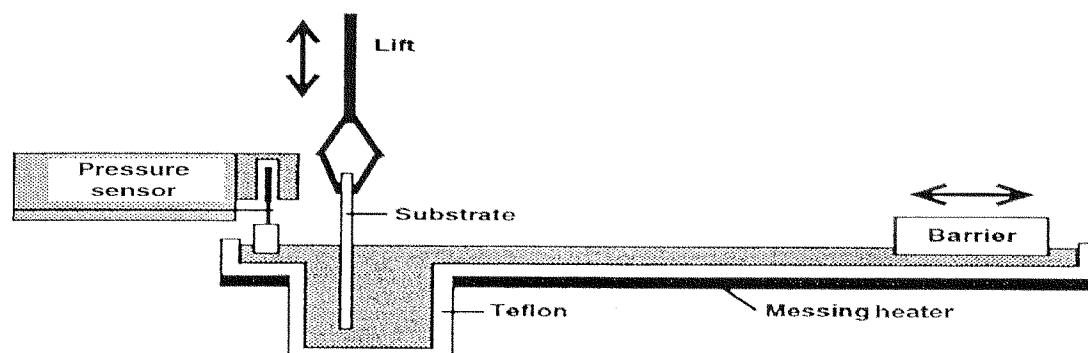
contamination will destabilize the membrane. It is also important to avoid vibrations or else the membrane will vibrate and break.

For our applications, we proceeded as follows: A BLM was formed as described above, using a teflon holder with a hole of 5 mm in diameter. Then, the $\sim 4 \text{ mm}^2$ substrate was carefully pushed through the opening containing the suspended membrane. Another possibility was to position the substrate very close to the BLM and then a positive pressure was applied to the opposite water compartment by adding additional water. Using this strategy, the membrane is automatically “pressed” onto the substrate.

Using a small teflon piece and tweezers, it was reproducibly possible to suspend the lipid-film over the very big opening. Unfortunately, the film always literally exploded (tore up) after a few first areas of the film had thinned to the “black” state, or the film stopped thinning after a few minutes. Also the pushing-through of the extremely small, gold coated sample could not be done with the needed control and precision, although a motor-driven x,y,z-micropositioner was used. The technical handling therefore was very tricky. In addition to these difficulties, other groups reported that BLMs could not be obtained free of small, lense-like inclusions of solvent. These facts finally led to abandoning this strategy for the creation of supported bilayer membranes.

Langmuir Blodgett films (LB)

The LB method is most often used for the preparation of mono- and multilayers of surface active molecules (e.g. lipids). Summarized, this technique consists of transferring a well ordered monolayer of an amphiphile at the water/air interface under controlled pressure onto a substrate which is slowly inserted into- or extracted from the water. A scheme of a LB trough is shown below:



A large and heatable trough made out of teflon contains water over which a solution of e.g. lipids in CHCl_3 is carefully applied. The organic solvent then evaporates leaving behind well oriented amphiphile molecules on the water surface. By means of a movable teflon barrier, the surface area which is at disposal for the amphiphiles can be varied. This way the pressure within the amphiphile layer can be influenced manually or controlled by means of a feedback loop fed by actual surface-tension measurements done using a Wilhelmi-plate surface-pressure meter fixed over the trough. The surface which is to be coated is attached to a stepper motor by which it can be lowered or raised into and out of the trough - each time (in the best case) a monolayer of amphiphiles being transferred onto it.

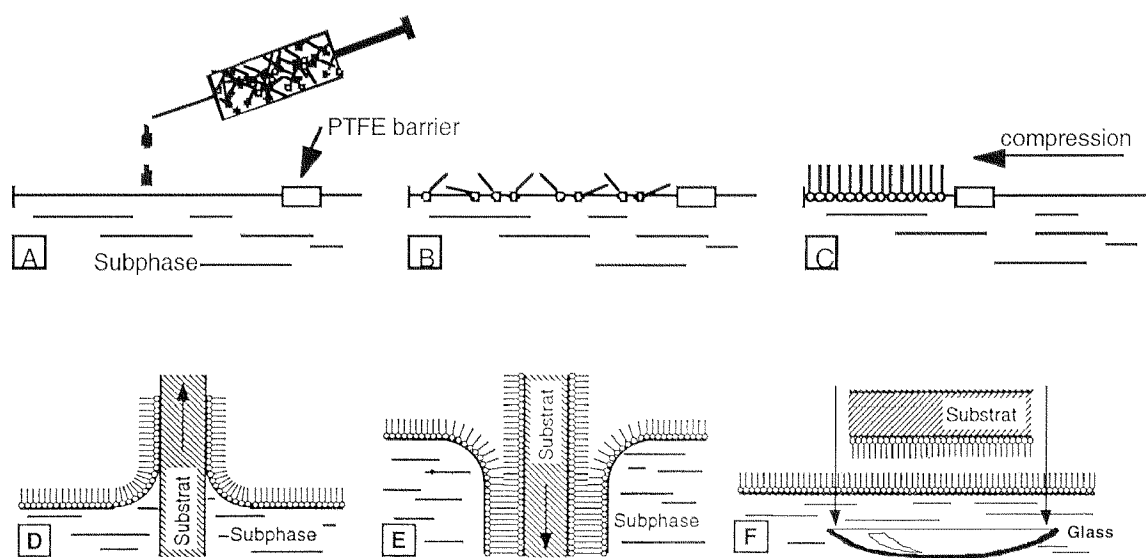


Figure 61: Formation of a phospholipid Langmuir-Blodgett monolayer on the air/water interface of a LB-trough and transfer of the ordered lipids onto a substrate to produce supported membranes: A) deposition of a defined amount of lipid in a volatile solvent onto the water; B) Evaporation of the solvent and equilibration of the film; C) Compression of the monolayer leading to a 2D-crystalline lipid monolayer; D) Withdrawal of the substrate through the compressed monolayer at constant pressure; E) Deposition of the second monolayer by either (E) reinsertion of the preloaded substrate through the hydrophobic lipid layer or (F) horizontal dipping of the substrate. Source: Image modified from (Spratte, 1994).

A scheme of the transfer mechanism is given in Figure 61: For the creation of a lipid bilayer on the substrate, first the Au(111) substrate coated with a SAM is lowered completely into the water phase, then the desired lipid solution is spread on the water surface and after which the lipids are compressed until the desired transfer pressure is reached as described below. The sample is then withdrawn from the solution at constant speed whereby the surface pressure is kept constant by automatic adjustment of the teflon barrier. After a very defined drying-time, the sample is lowered again into the solution and the second monolayer transferred with inverted orientation. After this step,

the remaining lipids on the surface of the trough are removed by aspiration and the substrate inserted (under water) into a sealable container which can be used to transport the sample to other applications.

Prior to the deposition, it is very importantly that the orientation and phase of the lipid monolayer on the water must be adjusted. This can be done by changing the surface area which is available for the lipids and monitoring the surface pressure of the system with a Wilhelmi-plate. In the best case, a pressure-versus-area curve (isotherm) is obtained as shown in Figure 62.

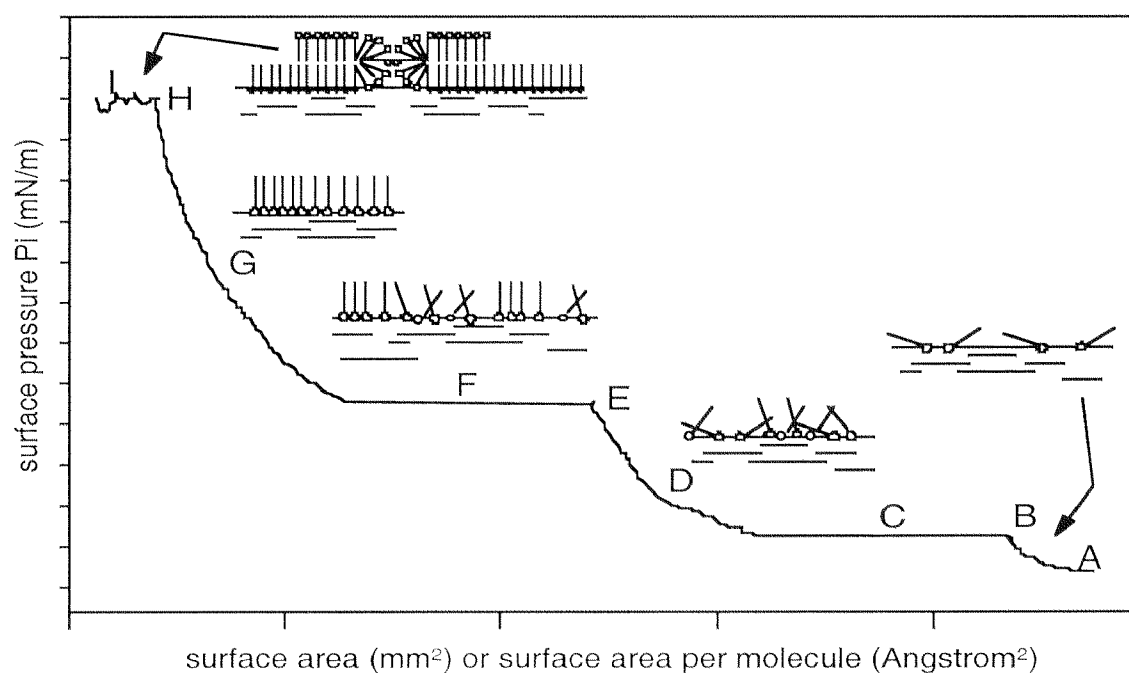


Figure 62: A classical pressure-versus area per molecule (Π/A) isotherm including schemes of the phases of the amphiphiles. the curve is explained in the text.

Usually, only a small amount of lipids is applied to the LB trough, such that the single lipid molecules at the beginning are very far away from each other on the water surface (A). At this point, the molecules are in a kind of “gaseous“ state and virtually do not “see“ (interact with) each other. Then, the surface area which is available for the lipids is slowly lowered by moving the LB-barrier. The pressure in the film increases due to the molecules coming into closer contact with each other, restricting their diffusion. This corresponds to a reduction of their degree of freedom, which in turn is an energy consuming process and which at constant temperature leads to an increase of the film pressure. The so called liquid state (or expanded monolayer phase) is reached, in which the hydrophobic chains interact with each other. In C, the gaseous and the liquid phases

coexist and no rise in pressure is observed. As soon as the whole monolayer is in the liquid state, further compression leads to a situation in which there is not enough space any more for the sidechains of the molecules to lie “flat“ on the water surface. The aliphatic side-chains then begin to stand up and order (D). At a certain threshold pressure (E), domains of crystalline amphiphile areas begin to condense which again leads to a pressure plateau (F) in which the liquid and the crystalline (condensed) phase coexist. Very often during this process, geometrically shaped crystallization structures (stars, circles, meanders) are formed - two dimensional analogues of e.g. the salt- and snow crystal in our environment (McConnell et al., 1984). In the step that follows, a very fast increase of pressure is detected, due to the mutual colombic repulsion of the molecules. Finally, at the collapsing point, the monomolecular layer is forced to fold into the third dimension - a process for which nearly no energy is needed, but which destroys the order in the film (H). Most often, the LB monolayer is transferred near (but below) this collapsing point. The molecules are then well ordered and tightly packed.

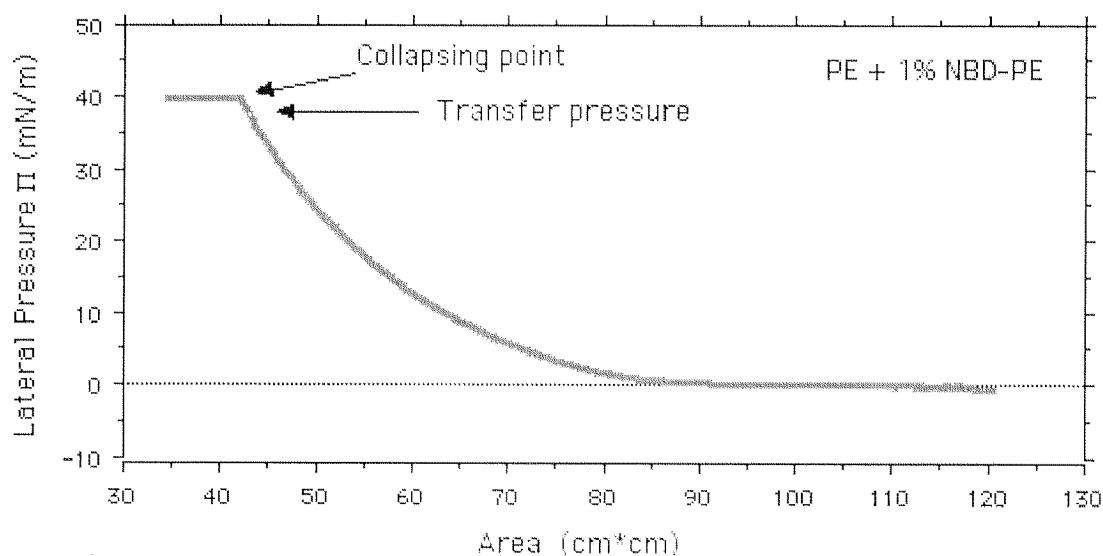


Figure 63: Standard pressure-versus-area isotherm for a lipid mixture obtained with our LB trough. Due to the complex lipid mixtures we used in our experiments, the different phase transitions are smeared out, leading to a constantly increasing pressure curve. This monolayer collapsed at a pressure of 40 mN/m.

With our phospholipid systems (Table 8), more likely isotherms as shown in Figure 63. were obtained. The very small pressure changes related to the first phase transitions can anyway only be detected with very sensitive electronic balances. But more importantly, we were using mixtures of different lipids with varying fatty-acid chains, for which the condensation and crystallization temperatures are smeared out, leading to isotherms without the complex substructure as drawn in the isotherm before. The present curve

was obtained by compressing a lipid mixture composed of Egg-PE with 1% NBD-PE, for which a collapsing pressure of about 40 mN/m is found. For each new lipid composition, the collapsing pressure had first to be determined, in order to set the optimal LB pressure for the transfer of the lipids onto the substrate.

The major problem related to the LB transfer of lipids is their bad adhesion to substrates. From the point of view of nature, this behavior makes sense since a cellular membrane must avoid unspecific adhesion to surfaces or must avoid being contaminated by the adhesion of molecules of any kind. If the strength of the binding between the polar head-group of the lipid and the hydrophilic substrate is not strong enough, either no monolayer or only part of it will be transferred, resulting in a bad transfer ratios. Specially the major components of natural membranes, phosphatidylcholine or -ethanolamine are non charged species and are therefore prone to such a behavior because they can only develop weak electrostatic interactions. Experiments A, B etc. in Table 8 show, that PC bilayers cannot be transferred well on gold coated with COOH-SAM nor Si or mica surfaces. Addition of uranyl-acetate ($\text{UO}_2(\text{OCOCH}_3)_2$ (UAc is weakly radioactive !)) to the subphase increases the monolayer adherence to substrates. UO_2^{2+} strongly sticks to the phosphate species in lipids leading to a positive net charge of the lipid which then more readily adsorbs to negatively charged surfaces. All the further depositions therefore were made in the presence of 0.1 mM UAc at pH 4.4 in the subphase. On glass - the most frequently used substrate in literature for LB depositions - good transfer ratios for the first monolayer are obtained even in the absence of UAc. But, as soon as the sample is lowered again through the LB layer, instead of depositing the second monolayer, the first monolayer simply floats off again (this is visible by an increase of surface area at constant pressure (Experiment E, Table 8)). The adhesion of the first layer was therefore not strong enough and UAc has to be added to avoid this floating-off. Another approach is to deposit the second layer by dipping the substrate horizontally into the LB film (Experiment O, done at the Institute of Biochemistry at the University of Zurich). The air-drying time after the deposition of the first monolayer and prior to the deposition of the second layer is very crucial. Too short drying times will lead to a wet substrate on which the second layer will not stick adequately, and too long drying times will lead to deterioration of the monolayer structure. Drying for 2-5 minutes proved to give acceptable results.

A further, problematic thing happened: After the deposition of the second monolayer, the sample usually is in the water phase.

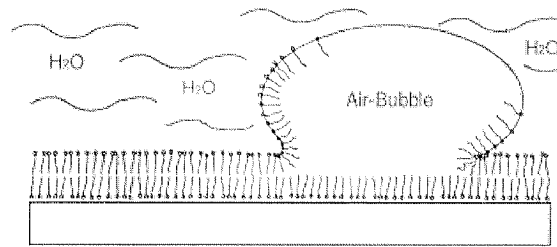
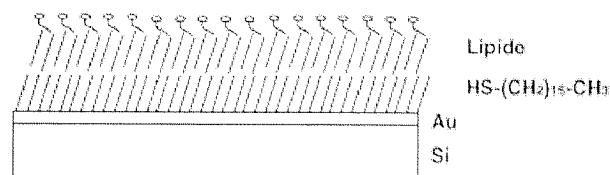


Figure 64: Destruction of a supported bilayer membrane by exposure to an air bubble.

Independently on whether lipid is present on the water phase or not, the second lipid monolayer on the sample will readily come off the surface as soon as the sample is lifted through the water/air interface (Experiments E and F, transfers 3). This is an indication that hydrophobic forces - and not only van der Waals forces - play a very important role in the bilayer stabilization. Experience showed, that this zip-like breaking-up of the membrane cannot be avoided and always occurs when a lipid bilayer is pushed through an air/water interface or when it comes into contact with air (Figure 64). Bilayers on a substrate therefore have to be always kept under water and even exposure to small air bubbles has to be avoided. This point increases enormously the demands on the experimental setup and makes it difficult to handle membranes.

During LB deposition, hydrophobic substrates lead to good transfer ratios in the first downward dip. In Experiment D, a gold sample was coated with a hexadecanethiol SAM and then immersed into the LB trough. Close to 100 % of a lipid monolayer were thereby transferred leading to a layer geometry as shown below.



Such systems have been widely used to study adsorption phenomena onto lipid layers (Ding et al., 1996, Ding et al., 1997, Plant et al., 1994), but they are not useful for our applications as membrane proteins obviously cannot be inserted into these strongly bound artificial "bilayer" architectures.

By LB deposition, it is possible to suspend membranes over small voids. The van der Waals forces within the alkyl chains stabilize the monolayer until the second layer is deposited. In the experiments G, J and K, a phosphatidylethanolamine bilayer was deposited over etched Si/Au microstructures coated with a DSU-SAM. Relatively high transfer ratios were obtained in all three cases and the presence of a homogeneous layer of lipid on the surface could be proven by LSM photobleaching experiments. The bleached areas did not recover which is an indication for a strong binding of the lipids to the substrate.

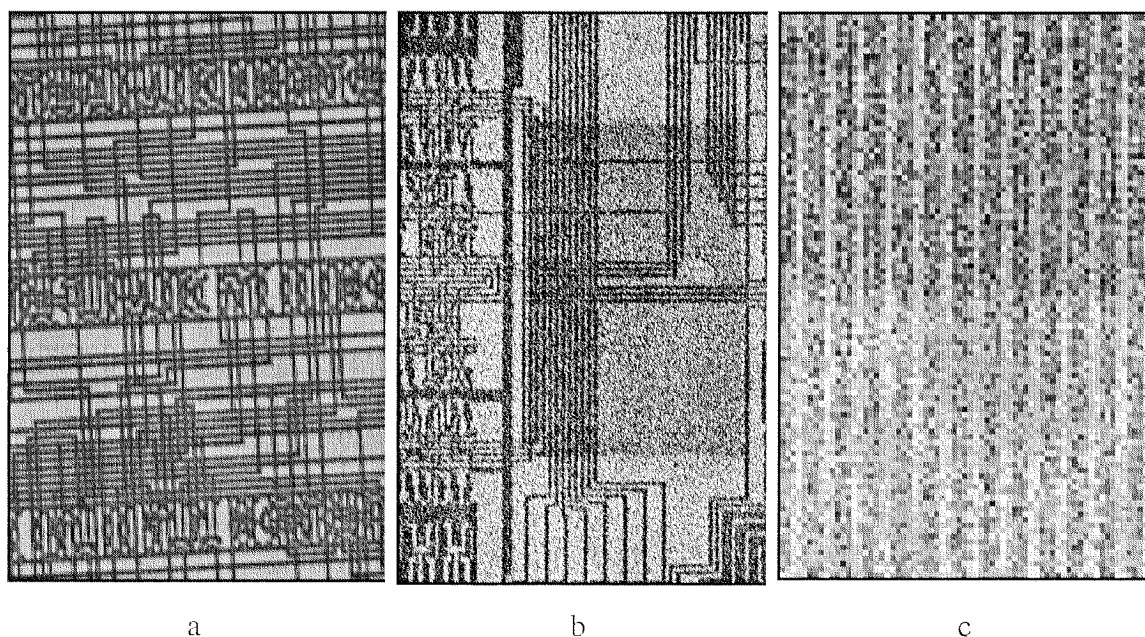


Figure 65 a-c: LSM images of etched Au/Si surfaces coated with DSU SAM. In “b” and “c”, a PE bilayer was deposited over the structures and then locally bleached. The width of the dark lines is 2.6 μm .

The very strong contrast in Figure 65 a-c is not due to the presence of a bilayer exclusively on the gold areas of the patterned sample, but is merely due to the much higher reflectivity of an Au surface compared to a silicon surface. In Figure 65a, no fluorophore is present and still very clearly the Au/Si Pattern is visible. In Fig. b, the central part of the image was bleached and indeed the presence of lipid can be seen. Finally, in a zoom of Fig. c, where the upper part of the image shows a bleached area, it can be seen that both Si as well as Au areas are covered with bleachable lipid.

	Substrate	Lipid	Subphase	Transfer 1	Transfer 2	Transfer 3
A	Au-COOH	Egg-PC	H ₂ O	↓ 22%	↑ 4.5%	↓ 13%
B	Si	Egg-PC	H ₂ O	↓ 11,9%	↑ 20%	↓ -6%
C	Glass	Egg-PC	H ₂ O	↓ 6%	↑ 86%	
D	Au-CH ₃	Egg-PC	H ₂ O	↓ 93,8%		
E	Glass	Egg-PC	H ₂ O	↓ 1%	↑ 112%	↓ -84%
F	Mica	PE	H ₂ O 0,1 mM UAc, pH 4,4	↑ good	↓ good	↑ -100%
G	Etched Au/ DSU	PE + BODIPY	H ₂ O + 0,1 mM UAc, pH 4,4	↑ 150 % dry 10'		
H	Au-DSU	PE + BODIPY	H ₂ O + 0,1 mM UAc, pH 4,4	↑ 210% dry 10'	↓ 200%	
I	Au	PE + NBD-PE	H ₂ O + 0,1 mM UAc, pH 4,4	↑ 131% dry 3'	↓ 118.2%	
J	Etched Au/ DSU	PE + NBD-PE	H ₂ O + 0,1 mM UAc, pH 4,4	↑ 93% dry 2'	↓ 107.9%	
K	Etched Au/ DSU	PE + NBD-PE	H ₂ O + 0,1 mM UAc, pH 4,4	↑ 96.7% dry 2'	↓ 91.3%	
L	Etched Au/ DSU	PC 66% Chol. 33% NBD-PE 2%	10 mM Tricine 100 mM NaCl pH 7.4	↑ No data	↓ No data	
M	Etched Au/ DSU	PC 66% Chol. 33% NBD-PE 2%	10 mM Tricine 100 mM NaCl pH 7.4 0.1 mM UAc	↑ 190%	↓ 124%	
N	Etched Au/ DSU	PC 66% Chol. 33% NBD-PE 2%	10 mM Tricine 100 mM NaCl pH 7.4 0.1 mM UAc	↑ 114%	↓ 100.2%	
O	SiO ₂ UniIrchel	PE NBD-PE 2%	UAc	↑ No data	↓ No data	

Table 8: Table of the performed LB depositions under varying conditions and using different substrates and lipid mixtures. The arrows indicate the deposition direction of the layer: ↑: withdrawal from the aqueous phase; ↓: transfer into the aqueous phase.

Summarizing, it can be said that the LB technique can be used to create bilayer membranes on Au/SAM substrates, but the method is very time consuming and prone to many difficulties: The method is extremely sensitive to moisture, non-natural substances have to be added to the subphase to get good transfer ratios and the different deposition parameters have to be optimized for each new lipid composition or substrate. The big difficulties related to the handling of supported bilayers make it very important that the LB-trough is located near the instruments used for the bilayer characterization or near the laboratory where the further experiments are to be performed. In our case, the samples had to be transported under air exclusion and in liquid from the EMPA St. Gallen to Zurich. It could therefore never be excluded with certainty, that the bilayer was destroyed all the same due to presence of small air bubbles during the transport.

Liposome Fusion

Supported lipid bilayers - in a third approach - were produced using the “liposome spreading“ technique. This method which could be called a “bilayer-self assembling“ system is illustrated in Figure 66:

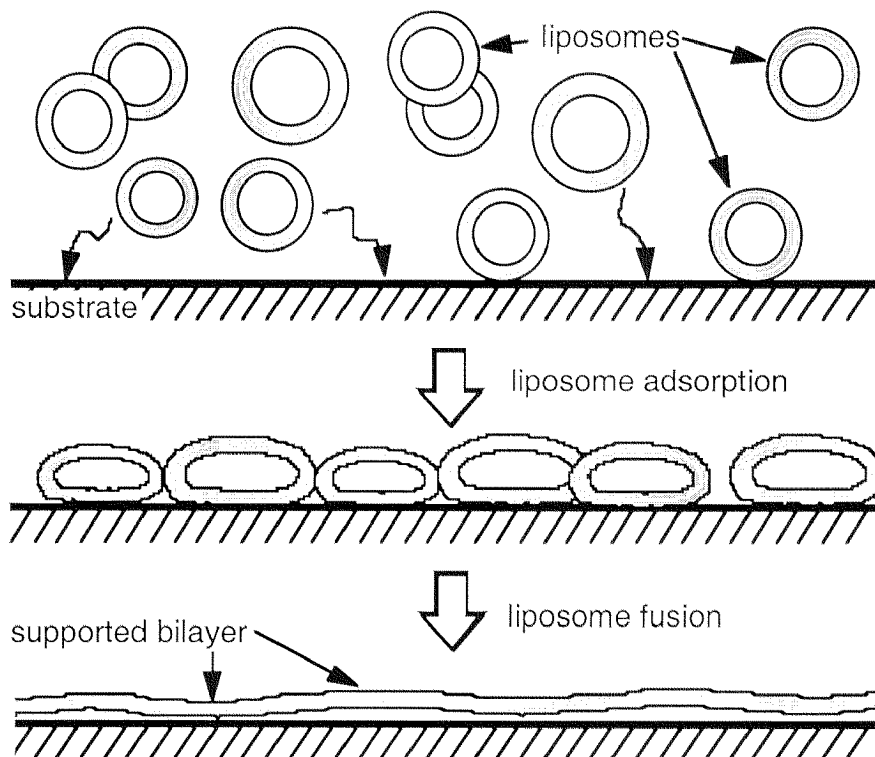


Figure 66: Formation of a supported bilayer membrane by liposome fusion.

Liposomes, if brought into contact with a substrate, can adsorb onto the surface and form a liposome-monolayer. Under certain conditions, the liposomes then fuse together and form a homogeneous, supported bilayer membrane. There are different approaches to produce such membranes. Vesicles are either directly fused onto hydrophilic substrates (Nollert et al., 1995, Pearce et al., 1992, Groves et al., 1996) or first a hydrophobic, long-chain monolayer is deposited onto a substrate onto which the liposomes are then allowed to fuse. The hydrophobic priming layer can either consist of self-assembled alkanethiol molecules on a gold surfaces (Plant et al., 1994, Stelzle et al., 1993, Steinem et al., 1997a, Wetzer et al., 1997, Ding et al., 1997, Ding et al., 1996, Plant, 1993), of a long-chain silane (Heyse, 1995, Brian and McConnell, 1984) or of a lipid monolayer transferred using the LB technique (Kalb et al., 1992). More complex surface modification strategies have also been reported, comprising dextran coated silane layers (Elender et al., 1996), thiolipids with a PEG spacer (Lang et al., 1994a, Heyse et al., 1998a), (Lang et al., 1993), thiopeptide spacers (Bunjies et al., 1997), cholesterol-modified PEG thiols (Williams et al., 1997), PEG-like disulfides (Cornell et al., 1997) and phosphothioethanol-lipids (Steinem et al., 1997b)

Membranes with integrated or adsorbed proteins have also been studied (Steinem et al., 1997a, Lang et al., 1993, Wetzer et al., 1997, Steinem et al., 1997b). They are very promising substrates for biosensor devices which make use of the substrate-selectivity of membrane proteins.

As can be seen above, most of the literature is concerned with bilayers formed by liposome fusion onto preformed hydrophobic monolayers. - Although this approach is very straight-forward due to reproducible fusion conditions, it could not be used for our approach, because it is not suited for the study of transmembrane proteins. The non-lipidic nature of the surface bound layer as well as the strong binding to the substrate does not allow proper insertion of such proteins. The fusion of a liposome directly onto a hydrophilic substrate is unlikely more complex: Nollert et al. (Nollert et al., 1995) studied the adsorption of negatively charged *Escherichia Coli* lipid vesicles and palmitoyl-oleoyl-phosphatidylcholine (POPC) vesicles onto glass surfaces, using fluorescence measurements. They could show that the negatively charged *E.-Coli*-vesicles do not fuse onto the surface but form an adsorbed vesicle layer. This is probably due to the electrostatic repulsion from the negative charge of both the vesicles and the surface. On the other hand, neutral POPC vesicles formed well-fused and spread lipid bilayers. Addition of Ca^{2+} to the adsorbed *E.-Coli* vesicles induced their fusion. A large dependence of the fusion kinetics on the lipid composition of the vesicles was

demonstrated by Pearce et al. (Pearce et al., 1992): The more negatively charged lipids were present in the liposomes, the slower was the adsorption kinetics. A short, mechanistic description of the fusion process is given in the article of Sackmann (Sackmann, 1996). Summarizing, the surface chemistries of both the substrates and the liposomes have to be made consistent with each-other in order to get good spreading (fusion) behavior, and attractive interactions enhance the formation of supported planar bilayer membranes.

A study of the fusion of positively charged dioctadecyldimethylammonium bromide (DODAB) vesicles onto hydrophilic, carboxylated alkanethiol SAMs was presented by Stelzle et al. and Steinem et al. (Stelzle et al., 1993, Steinem et al., 1997a).

Despite the fact that the liposome-fusion has to be optimized for each new lipid composition of the vesicles, the vesicle-fusion technique was finally chosen as standard methodology for the creation of supported and suspended membranes for our applications. The advantages of this approach are:

- The bilayers can be spread on any surface by simply incubating them in, or under a liquid drop containing the liposomes.
- The fusion conditions can be varied very easily (temperature, humidity, mechanical agitation, buffer composition, etc.) as only extremely small sample volumes are needed and no apparatus is needed for the deposition.
- Unlike after LB depositions, the liposome-fused bilayer is deposited at a natural lipid-pressure. This may be very important for subsequent incorporation of biological species.
- The time needed to obtain a bilayer is usually very fast (10 min.), and no special machines are needed.
- No specially clean conditions are needed for this way of bilayer formation.
- If necessary in the future, the real-time adsorption kinetics and -behavior could be monitored by means of Surface-Plasmon Resonance (SPR) or Optical Waveguide Lightmode Spectroscopy (OWLS).

The technique

For the preparation of a lipid bilayer, the following procedure was developed, as is summarized in Figure 64: First, the substrates (SiO_2 , SAM coated Au, etc.) were cut into small squares of a few millimeters in diameter. These were then thoroughly cleaned using ethanol in the case of SAM/gold or piranha solution to make SiO_2 hydrophilic.

The small substrates were then glued onto a PTFE/glass holder using 10 min. epoxy-glue, allowed to dry and then a small drop of concentrated liposomes solution was applied to the substrates. The adsorption of the vesicles was allowed to proceed over 60 min. in a humid environment. Then the liposome fusion was induced by addition of a large drop of water, using a wide glass-pipette. After 2 minutes, the sample was rinsed with several milliliters of water, proceeding as described in “Requirements on the sample-holder“. The homogeneity of the bilayer and its phase state were then each time verified in the LSM, followed by AFM or further washing steps in case that the liposomes did not fuse well. The sample must be never allowed to dry out during the entire process !

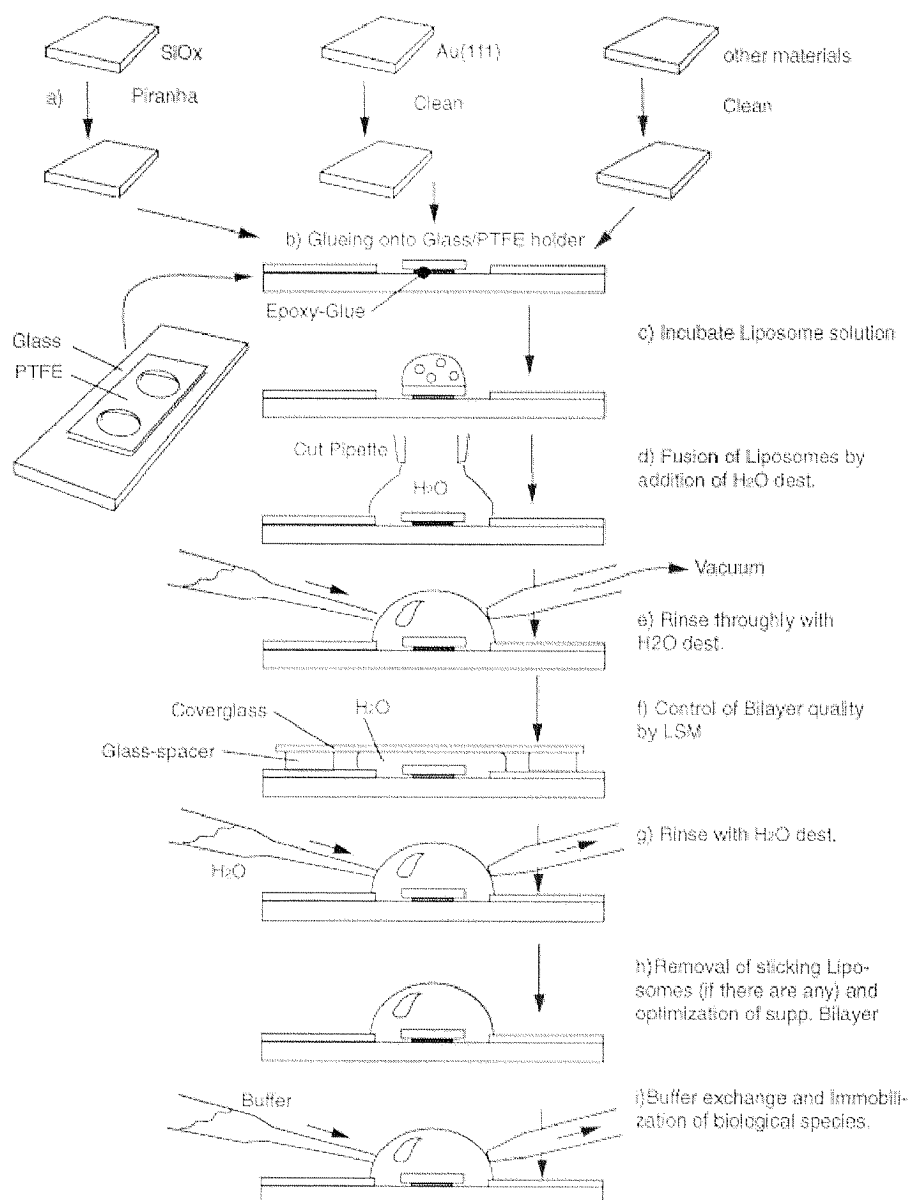


Figure 67: Liposome fusion procedure

For the fusion of liposomes with a $T_c >$ room temperature, the same procedure was used, but the incubation of the liposomes, their fusion and the rinsing steps were performed in an oven at $T_{\text{oven}} = T_{c_{\text{liposomes}}} + 7^\circ\text{C}$ (approximately). The washing solutions were preheated to above the T_c of the lipids. Very often, several washing steps were needed to fuse these liposomes.

Requirements on the sample-holder

In order to make the sample amenable to different analytical- and preparation techniques, a special glass holder was developed. The factors which had to be taken into account are many:

- Small Si-wafer plates as well as glass and Au-coated substrates must be able to be used as substrates for liposome spreading.
- Only very small amounts of liposome solution should be needed for each sample (50 μl maximum per sample).
- The sample must never dry during the whole process.
- The sample must be compatible with optical-, laser scanning- and atomic-force microscopy.
- For AFM, the sample needs to be immobilized firmly and no swelling of the glue should occur in buffer environments.
- No contamination should result from the sample holder. The whole setup must be stable in saline solutions for days.
- The sample must be very accessible in order to be able to perform many washing and immobilization steps on the same sample.

The fabrication of an useful holder was extremely important and it was achieved by glueing a single-sided oxygen-plasma treated PTFE-foil with two holes in it onto a cleaned microscope slide using epoxy-gluе (Figure 67 b). The small samples are then glued into the holes after the cleaning step, upon which they are ready for the spreading step. Due to the hydrophobicity of the surrounding PTFE, a water droplet will always remain confined over the glass area covering the sample. This setup is directly amenable to AFM microscopy (Bioscope), and for laser scanning microscopy, simply two rectangular glass pieces are laid onto the sides of the holder over which a large microscope cover-glass is deposited (Figure 67 f). If the cover-glass is removed carefully, the sample will not dry. For this very critical step, the cover-glass is best slid

horizontally over the sample until one of its edges is vertically over the sample. Then, the opposite edge is carefully lifted until the slide is in a normal position relative to the holder surface (If needed, more liquid has to be added to the sample to avoid drying). After this, the sample can vertically be lifted off the holder and a water drop will remain on the sample.

For washing steps and the exchange of buffers, it has proven most practical to use a plastic pipette tip attached to the vacuum tube which can be adjusted at a defined height over the sample (3-4 mm). If the pipette is positioned over the sample as indicated in Figure 67 e, it will remove liquid from the sample drop as soon as the drop exceeds a certain liquid volume. Washing solutions can simply be applied from the opposite side using hand-held pipettes. Neither wax-pens nor silicon rubber proved to be able to replace the PTFE foils, for neither show long-term stability in buffer solutions. Completely hydrophobic glass slides make it impossible to avoid sample drying when, after LSM, the cover-glass has to be removed.

Vesicle-fusion onto different substrates

In the following section, the different substrates which have been tested for liposome spreading are discussed and the characteristics of the resulting supported bilayer are reviewed:

Gold samples coated with different SAMs were exposed to fluorescent liposome solutions and then analyzed in the LSM.

Au/COOH-SAM:

PC/PE liposomes (Lip 1) diluted 1/4 in PBS pH 7.4; incub. 20 min.	Very low fluorescence in the LSM and “grainy“ aspect. Bleaching works, but no fluorescence recovery.
Lip7, incub. 2 h	Very low fluorescence on the substrate and a very grainy distribution. Addition of Ca ²⁺ does not change the appearance.
Lip5, incub. 75 min.	Homogeneous fluorescence visible on the substrate. Bleaching OK, No recovery.
PC/PE lipos (Lip6) incub. 75 min.	No fluorescence visible on the surface.

Au/OH-SAM

PC/PE liposomes (Lip 1) diluted 1/4 in PBS pH 7.4; incub. 20 min.	Very much and homogeneously spread fluorescence on the substrate. But also a grainy structure. Bleaching works, but no fluorescence recovery.
Lip5, incub. 75 min.	Homogeneous fluorescence visible on the substrate but large patches of brighter fluorescence present. Bleaching OK. No recovery.
PC/PE liposomes (Lip6) incub. 75 min.	Homogeneous fluorescence visible, maybe a very little grainy. Bleaching OK, No recovery.

Au/DSU-SAM

PC/PE liposomes (Lip 1) diluted 1/4 in PBS pH 7.4; incub. 20 min.	Very much and homogeneously spread fluorescence on the substrate. But also a grainy structure. Bleaching works, but no fluorescence recovery.
PC/PE liposomes (Lip3)	Homogeneous fluorescence with some brighter stripes at certain locations. Bleaching OK, no recovery just after the spreading step, but fast and complete RECOVERY in H ₂ O at 60°C (!).
PC/PE liposomes (Lip4)	Very homogeneous fluorescence Bleaching OK, no recovery. 36 hours later, very slow recovery of half of the lipid-bilayer after bleaching.

The increase in bilayer fluidity observed many hours after the formation of the covalently bound Lip4 bilayer could possibly be attributed to the slow hydrolysis of the succinimide-ester bond (of non lipid binding alkanethiol species) leading to a change in surface chemistry. Very interestingly, the fluid phase can also be induced at elevated temperatures which should not be possible if a vesicle layer is present.

Au/CH₃-SAM

PC/PE liposomes (Lip 1) diluted 1/4 in PBS pH 7.4; incub. 20 min.	No fluorescence detectable. But sample did shortly dry prior to the LSM measurement due either to the presence of no lipid layer or to an extremely bad adhesion between the lipid monolayer and the SAM.
---	---

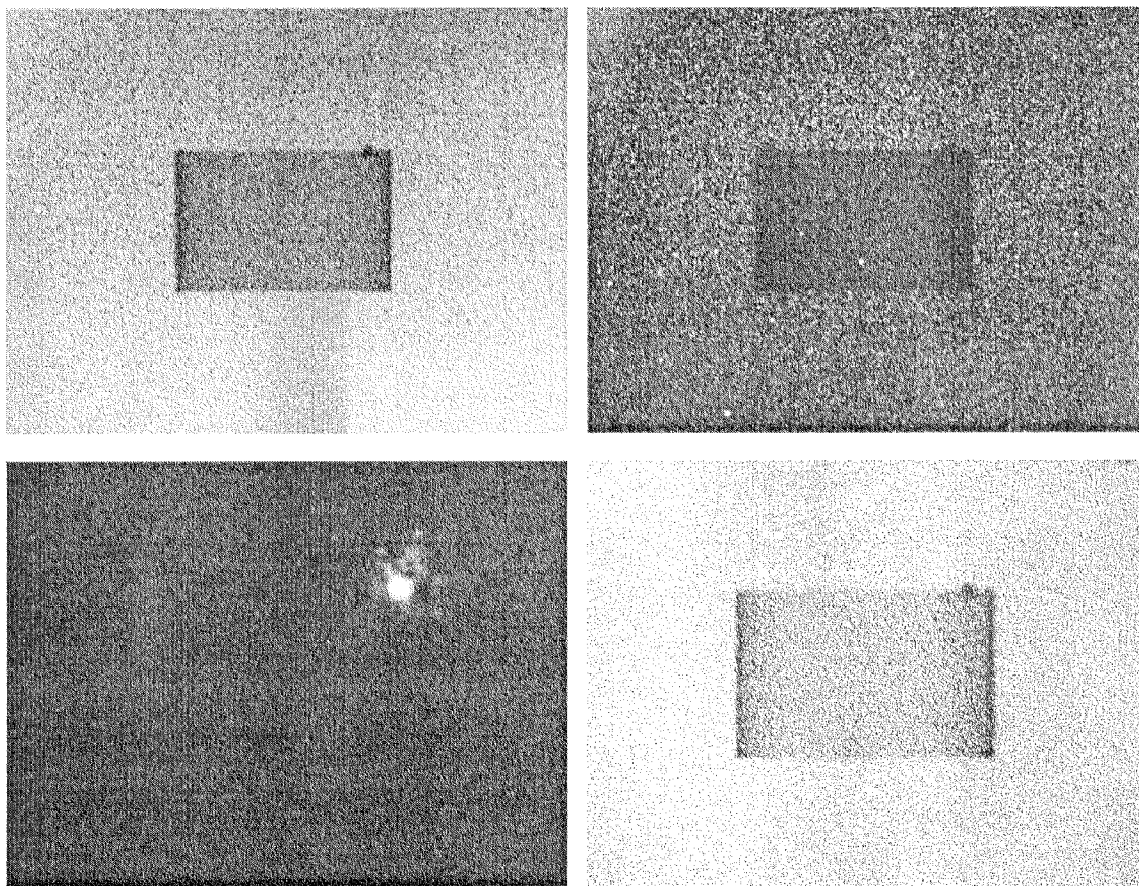


Figure 68: LSM images of supported, fluorescent bilayers or vesicle layers after vesicle fusion of Lip1 liposomes on Au(111) substrates functionalized with four different, ω -terminated alkanethiols: Top, left: Au/OH-SAM (HUT); Top, right: Au/COOH-SAM (MHA); Bottom, left: Au/CH₃-SAM (HDT) and bottom, right: Au/DSU-SAM.

Au/NH₃-SAM

PC/PE liposomes (Lip 1) diluted 1/4 in PBS pH 7.4; incub. 30 min.	Extremely strong and homogeneous fluorescence visible. Vesicle-layer? Bleaching OK. No recovery even after exchanging the buffer for pH 11 (non positively charged amine).
TSG-Au, Lip 1; incub 10 min.	Very strong and homogeneous fluorescence Bleaching OK, no recovery.
Lip5, incub. 75 min.	Very homogeneous fluorescence visible on the substrate. Bleaching OK, No recovery.
PC/PE liposomes (Lip6) incub. 75 min.	No fluorescence visible on the surface.
TSG-Au, Lip 1; incub. 15 min. (10 min. at 70°C).	Homogeneous, but at higher magnifications slightly grainy fluorescent layer. Bleaching OK, no recovery.

TSG-Au, SAM incubated in EtOH/dioxane 1:1. Lip 1; incub. 90 min.	Grainy and non-homogeneous fluorescent layer. Bleaching OK, no recovery.
TSG-Au, SAM incubated in H ₂ O. Lip 1; incub 90 min.	Very homogeneous, bright fluorescent layer. Not grainy ! Bleaching OK, no recovery.
Au sputtered on polycarbonate filter, SAM incubated in H ₂ O. Lip 1 ; incub 9 hours	Homogeneous, but slightly grainy fluorescent layer. Bleaching OK, Recovery !

According to the experiments mentioned above, the aminoterminated SAM proved to be the best substrate for liposome spreading, even though the bilayer is not in a fluid state on the surface. Figure 69 shows a fluorescently labeled PC/PE (Lip1) bilayer spread on the aminoterminated SAM. The fluorescence is extremely homogeneous and AFM measurements on this substrate showed the absence of any topography on the surface, ruling out the presence of a vesicles-layer.

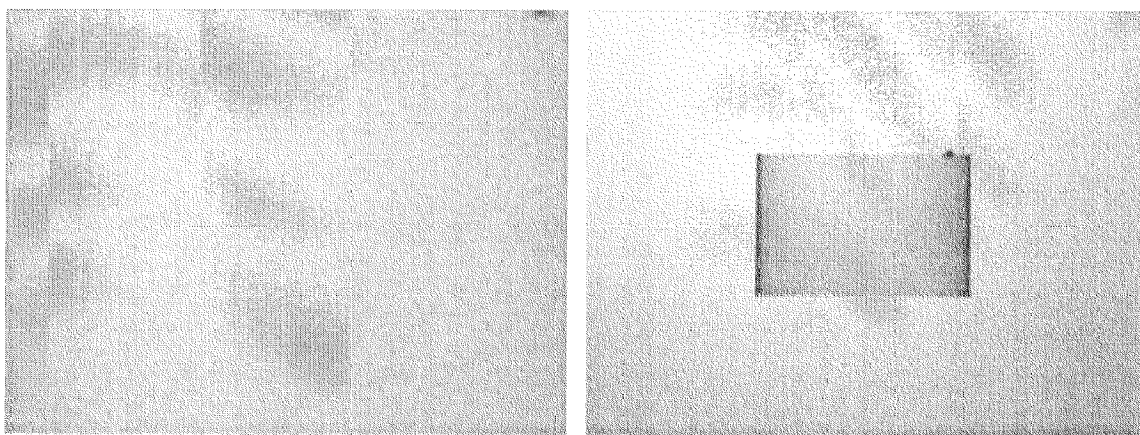


Figure 69: Left: LSM image of a supported Lip1 bilayer on an aminoterminated Au(111) surface. Right: The same bilayer after photobleaching. No fluorescence recovery.

Small structural differences within SAMs of the same alkanethiol species can have important consequences for the bilayer structure after fusion. Lip1 vesicles spread on an aminoterminated SAM assembled from water gave a supported bilayer which was very homogeneous and bright. On the other hand, the same SAM assembled from an Ethanol/Dioxane 1:1 solution showed a very grainy texture and was not homogeneous. The solubility of the self-assembling molecules in the assembling solvent has a big influence on the final structure of the SAM as well as on the assembling kinetics. Probably the aminoterminated alkanethiol is more soluble in water which gives better equilibrium conditions for a slow, controlled and well packed assembly.

Glass

Glass is a very good and cheap substrate for liposome spreading and for this reasons it has widely been used in literature (Pearce et al., 1992, Nollert et al., 1995). Due to the need for defined, nanostructured surfaces which can not be produced using glass, this material was not used. For the same reason, cleaved mica sheets, which have similar properties and which additionally are atomically smooth, were not considered. A short note concerning the use of mica: If the cut edges of the mica sheets are not properly sealed, liposome solution can penetrate between loose mica layers. In the LSM, such “inclusions“ behave like supported bilayers for they are equally highly fluorescent, bleachable and recovering.

Oxidized silicon wafers

PC/PG liposomes (Lip2) diluted 1/4 in PBS, followed by washing with 100 mM CaCl ₂ and H ₂ O	Complete but not homogeneous fluorescence with many liposomes still attached to the surface. Bleaching OK, and good fluorescence recovery. Complete recovery after 70 minutes at room temperature in H ₂ O. Bil7 and 10
PC/PE liposomes (Lip6) diluted 1/6 in PBS pH 7.4	Homogeneous fluorescence on the substrate. Bleaching OK, fast recovery.
Cholesterol-containing liposomes concentrated, in PBS pH 7.4.	Very homogeneous fluorescence Bleaching OK, fats recovery.

On silicon oxide surfaces, the divalent cation Ca²⁺ is used to promote a good adhesion between negatively charged liposomes and negatively charged substrates. Indeed, liposomes containing PG do spread well on SiO₂ if CaCl₂ is added prior to osmotically swell the vesicles. On the other hand, the sticking of non-fused liposomes onto the already supported bilayer is promoted by this ion which leads to a non-flat bilayer architecture. By washing with a solution containing EDTA, a Ca²⁺-complexing agent, most of these attached vesicles are readily released from the surface and also an extreme increase in bilayer fluidity is observed according to LSM fluorescence recovery data (Total recovery after 7 minutes). This can either be explained by the assumption that Ca²⁺ very strongly reduces the mobility of PG lipids in a bilayer by crosslinking - or by

a reduction of the binding force between the surface bound lipid layer and the substrate, if Ca^{2+} is removed.

Neutral vesicles (composed of PC and/or PE) as well as cholesterol-containing vesicles do also nicely spread on SiO_2 substrates leading to fluid supported bilayers. The fluidity is higher compared to PG containing bilayers immobilized via Ca^{2+} .

Substrate	Roughness Ra (nm) (last digit not relevant)
SiO_2	0.095
SiO_2 /Bilayer (fluid)	0.10
SiO_2 /Bilayer/ GA fixation	0.11
SiO_2 /Bilayer/ GA fixation/ OsO_4 fixation.	0.10

Table 9: Mean Roughness (Ra) data obtained with an AFM on SiO_2 substrates covered with a supported bilayer membrane, before and after fixation. The roughness was determined over areas of $4 \mu\text{m}^2$

If the spreading and fusion of liposomes which do not contain any proteins is done properly, very homogeneous supported bilayers are obtained. Contact-mode AFM images taken at minimal forces of such bilayers show extremely flat areas with almost no topography. Dirt on these surfaces will result in small, spot-like elevations of a few angstroms to nanometers in height. Only very rarely, holes of some tens of nanometers in diameter are observed. They are probably due to the presence of contaminations on the substrate prior to bilayer fusion. These perturbations are usually 3-6 nm deep. The roughness of the bilayers, as measured by AFM, is in the range of 1 \AA , which is very close to data obtained for a bare SiO_2 substrate. Table 9 summarizes the roughness measurements obtained on fixed or unfixed supported membranes. Figure 70, below, shows typical AFM images and corresponding line-sections obtained on a Bioscope with commercial cantilevers and in solution of a bare SiO_2 surface (a) and of an unfixed- (b), a glutaraldehyde (GA) treated(c), and a GA- and OsO_4 -fixed, supported bilayer. According to evidence obtained on samples with bilayer patches (see chapter “Bilayer fixation“), on non fixed samples, the AFM-tip has to be thought of as sometimes penetrating the bilayer during scanning -a kind of “combing“ of the lipid chains. After Osmium-fixation, the bilayer is hard enough to withstand the tip-pressure.

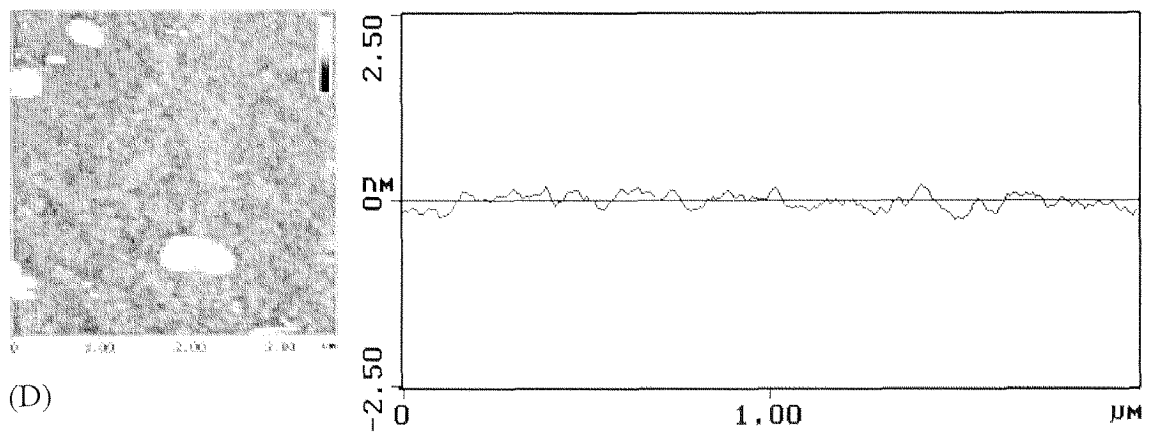
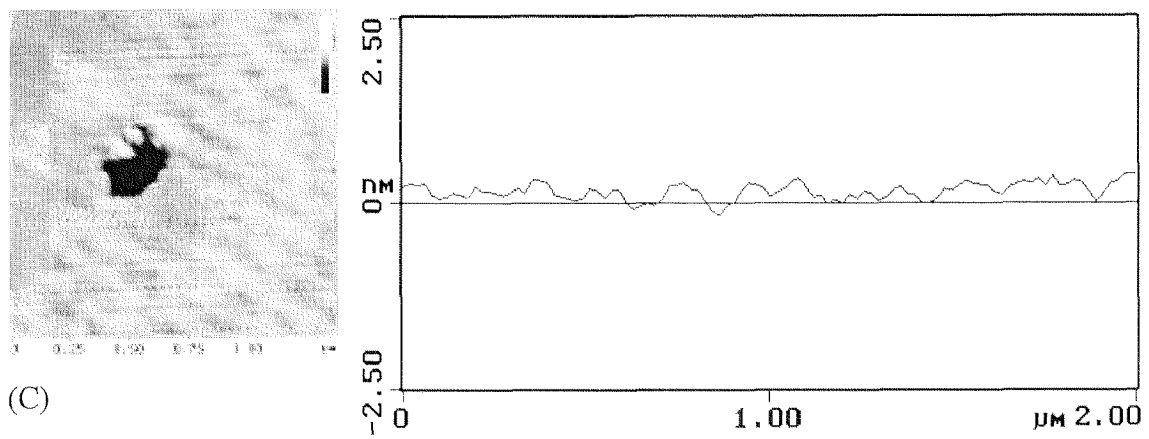
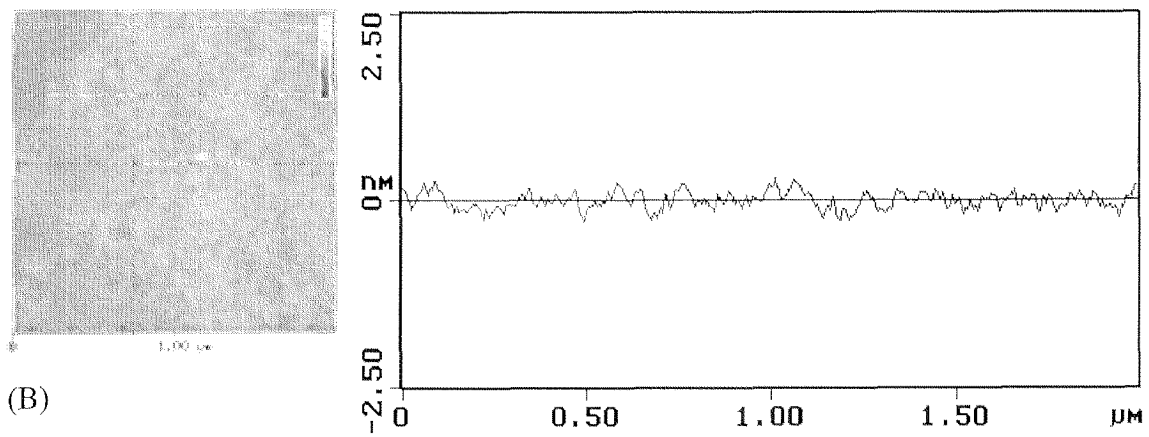
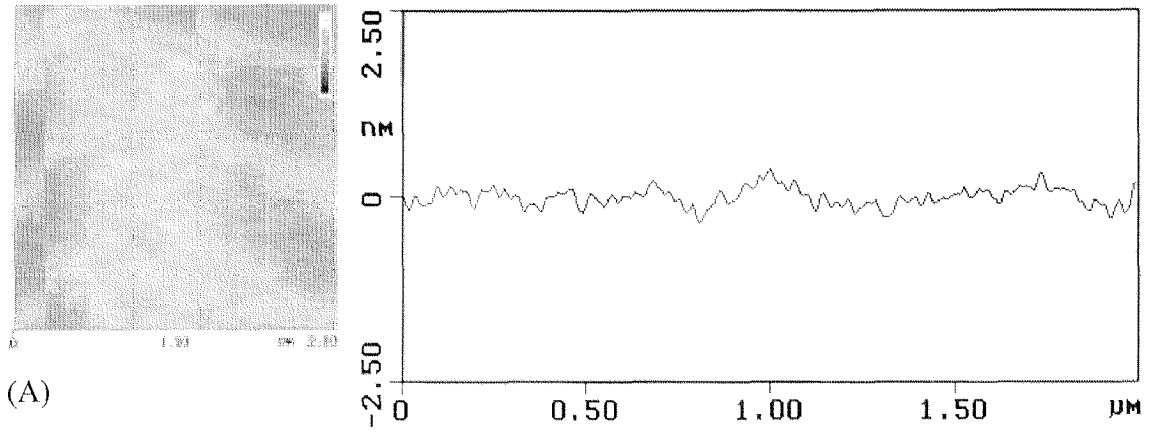


Figure 70: (previous page) AFM images of a SiO_2 substrate covered with bilayer membranes before and after fixation: A) bare SiO_2 ; B) fluid bilayer; C) bilayer fixed with GA (the black hole is an inhomogeneity in the membrane) and D) bilayer fixed with glutaraldehyde and OsO_4 (some non-fused liposomes are visible). On the right, a line-scan of the images is presented: the roughness of the surfaces is small compared to the thickness of a bilayer (5 nm) and it is nearly independent of the fixation conditions.

Good evidence for the presence of a bilayer at a certain locations of a sample is obtained by measuring the relation between the deflection of the cantilever and the distance of the tip to the surface, at a defined location. These so-called “force-versus-distance curves“ can be used to measure forces acting between single molecular species and also to obtain data about the mechanical properties like hardness, elasticity and plasticity of a surface ((Vinckier and Semenza, 1998).

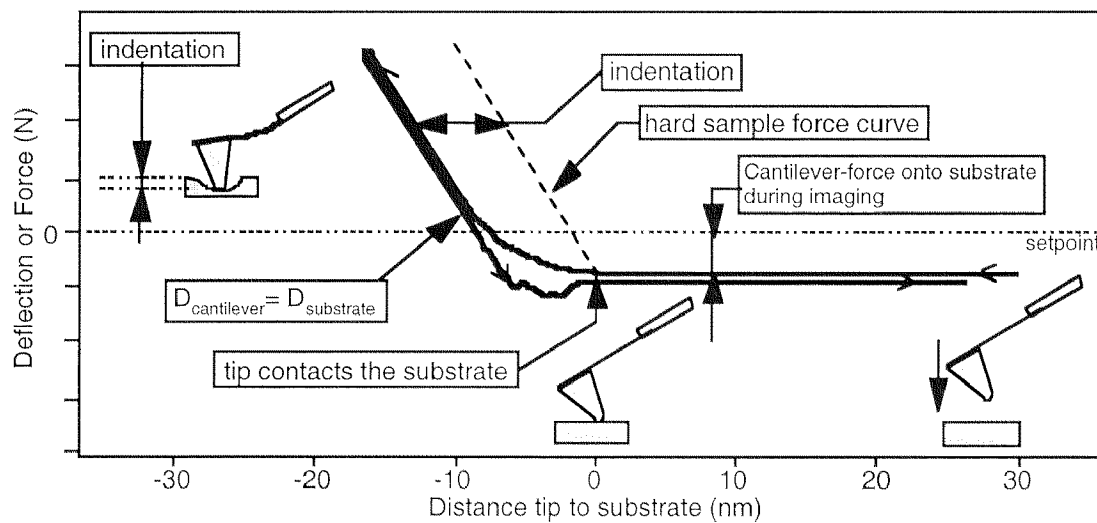


Figure 71: Classical force-versus-distance curve obtained with an AFM on a soft (elastic) surface.

Figure 71 shows a theoretical curve obtained on a soft substrate and includes schematic drawings of the cantilever position at selected points of the measurement. Additional information about AFM force measurements can be found in the Appendix in chapter “Atomic force microscopy detects changes in the interaction forces between GroEL and substrate proteins.“. The presence of a bilayer definitively changes the surface chemistry of a SiO_2 substrate and also introduces an elastic term. Figure 72 shows typical force-curves obtained on a bare SiO_2 substrate (A) and on the same substrate covered with a lipid-bilayer (B and C). On the hard sample, after the tip comes into contact with the substrate, the deflection versus distance curve follows Hooke’s law which predicts a proportionality between the force applied to the cantilever and its deflection. On the elastic membrane however, the deflection of the cantilever is reduced by the indentation into the bilayer which is dependent on the Young’s modulus of the

membrane. The force-versus-distance curve is then expected to be curved from the point of contact to the maximal distance interval (x-axis) of the diameter of the membrane (See Figure 71). In our experiments and also on the curve shown below, however, the indentation exceeds the thickness of the membrane for which a strong, long-range repulsive force between the tip and the bilayer must be acting in the presence of a bilayer. As van der Waals forces show an exponential decay of strength with distance, only electrostatic forces can account for the strong, long-range repulsion in our experiment. Lip20 bilayers are net negatively charged (due to the presence of dicetylphosphate) - which is also the case for the tips which have isoelectric points of 2.5 - 3.5 (for Si-tips) and 4 - 5 (for silicon nitride (Si_3N_4) tips). The differences in the force-curves between bilayer and non-bilayer samples is therefore not mainly due to a change in the elastic properties, but rather due to a change of the surface polarity. A net positively charged bilayer (e.g. containing Dioctadecyldimethyl-ammoniumbromide (DODAB)) according to this theory would be expected to produce a long-range attractive force on the tip combined with a visibly elastic-like behavior after contact with the substrate (if the spring constant of the cantilever exceeds the Young's modulus of the membrane).

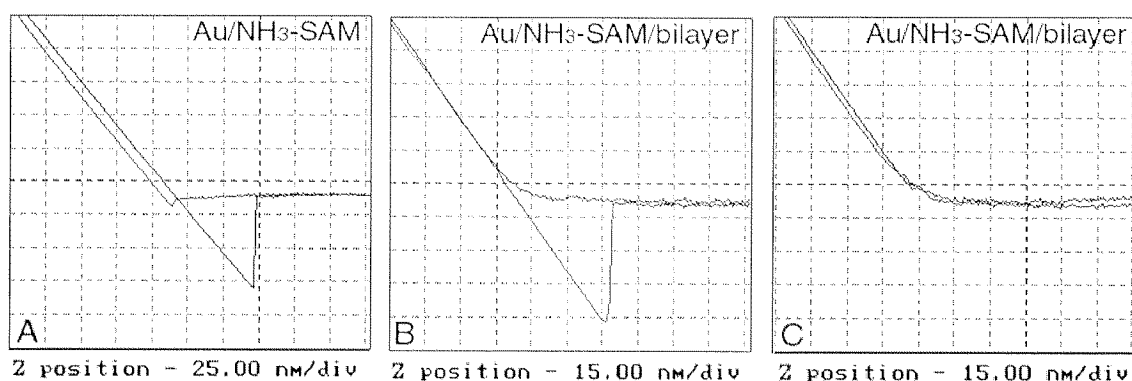


Figure 72: Typical force-versus-distance curves obtained under water on Au covered with an amino-terminated-SAM (A), and on the same substrate covered with a fluid bilayer (B and C). In fig. A, a strong adhesion between the positively charged SAM and the negatively charged tip is visible (the tip jumps into contact before having reached the substrate). On the membrane covered samples (B,C), a strong repulsion between the tip and the also negatively charged bilayer is visible (curved approach curve). As usual there is nothing there to hold back the tip after it touches the bilayer, no adhesion hysteresis is observed (C). If however the tip is pressed onto the bilayer with increasing force, it can penetrate the membrane and reach the positively charged SAM, which leads to the attractive force visible in the retraction curve in B.

Very interestingly, the force-curve obtained on a bilayer slowly transforms into a curve obtained on SiO_2 if many (10-50) curves are measured without changing the position of

tip on the surface. This is an indication that the bilayer integrity deteriorates by the successive “hacking“ of the AFM tip until finally the complete bilayer is displaced.

Bilayer fixation

A very important tool in membrane research is the stabilization (fixation) of membranes. This process makes the membranes less fragile and therefore better accessible to a variety of analytical methods. Fixation will result in substantial or complete loss of biological activity and, in some cases, it can even lead to membrane cracking or bursting. Biological membranes containing huge amounts of proteins can be fixed using glutaraldehyde. This compound will crosslink amino-groups which are close to each other in space. In bilayers, the primary amines of the phospholipids PE and phosphatidylserin can be linked too, if they are present. Direct crosslinking of the lipids is usually achieved by exposing the bilayer membrane to OsO_4 (Burck, 1969). This compound will bind to double-bonds in the fatty-acid chains and make a bridge to the next double bond. If there is more than one double bond per lipid molecule, polymerization will occur. This approach is very efficient for crosslinking lipids from biological sources as they are very unsaturated. No crosslinking, however, will occur if the membrane is made out of synthetic, double-bond free lipids.

For our applications - usually to check whether a certain AFM resolution on a native bilayer can be increased by fixation - the samples covered by a drop of water were exposed to OsO_4 vapor for one hour and then rinsed with buffer solution or water. The fluorescence is irreversibly and completely destroyed by this process, for which the sample cannot anymore be subjected to LSM analysis. For AFM imaging, fixation has clearly positive effects: As can be seen in Figure 73 (left and middle), unfixed bilayer patches are likely to be cut by the sharp AFM tip even at very small vertical forces. Note the dependence of the cutting on the scanning direction: This cutting only occurs where the tip crashes into the border of a bilayer area,. On the OsO_4 treated sample on the right, the bilayer survives the scanning process very well. The membrane became hard enough and resists penetration of the tip.

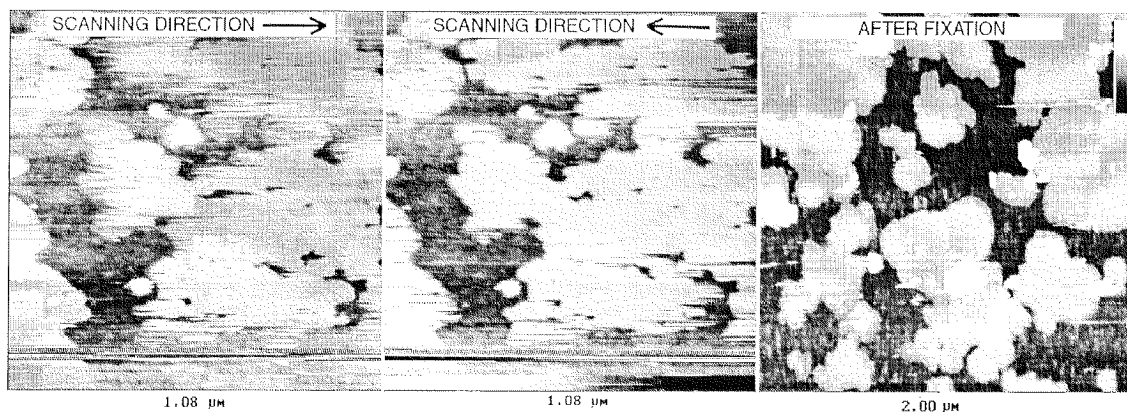


Figure 73: AFM image of supported bilayer patches scanned at a minimal force in contact mode. a) Unfixed sample, tip scanning to the right; b), unfixed sample, tip scanning to the left and c), OsO_4 fixed sample.

A huge variety of other bilayer-stabilizing techniques exist (Ringsdorf et al., 1988), but the need for such alternative techniques did not arise during this thesis as it was rather aimed to preserve the bilayer in its natural integrity and dynamics.

Inhomogeneities on the supported bilayers

The amount of non-fused or attached liposomes could not very reproducibly be controlled during the preparation of the membranes. These unwanted liposomes as shown by AFM in Figure 74 are also easily visible in the LSM as spots of bright fluorescence (see Figure 76).

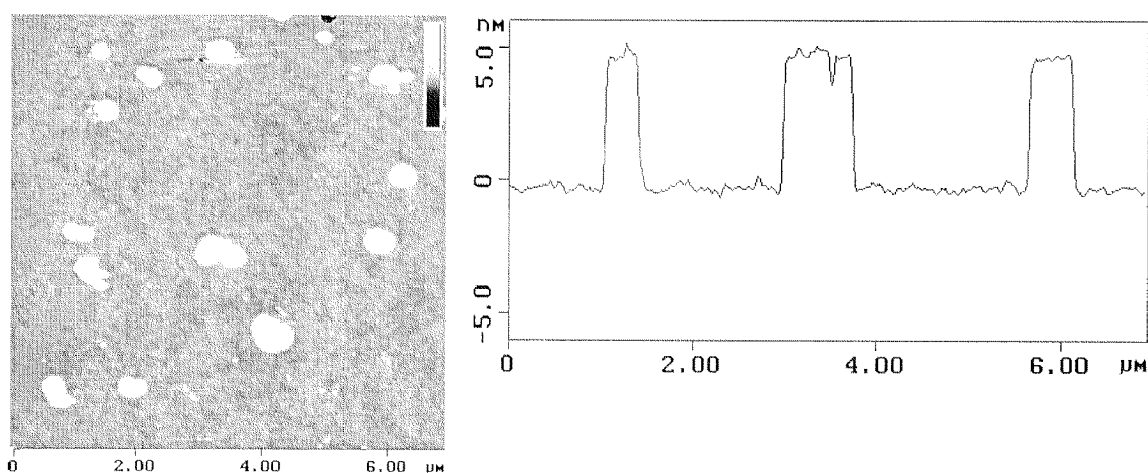


Figure 74: AFM image of a OsO_4 fixed sample which showed attached liposomes within-, or on a fluid Lip8 bilayer, in the LSM. The round shaped islands extend from the background by one bilayer thickness for which a model as shown below must be assumed.

They correspond either to non-fused liposomes which are attached directly to the inorganic substrate between the supported bilayer - probably at a site where the substrate was dirty (Figure 75), or to liposomes attached onto the spread bilayer itself.

Very interestingly, small multiwalled liposomes of the same composition have a quite different topography when adsorbed on a surface. This behavior is discussed in more detail in the chapter dealing with sonicated liposomes, below.

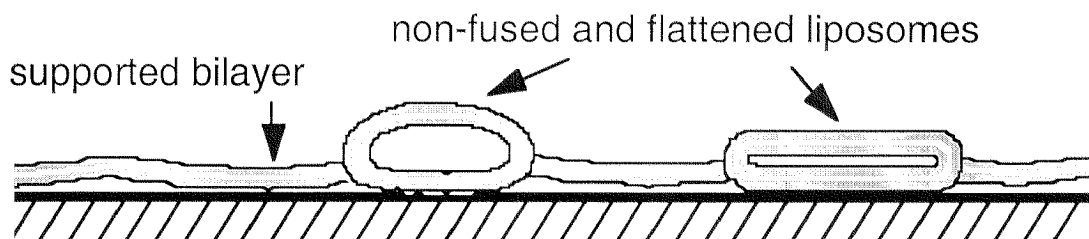


Figure 75: Scheme of a non-fused liposome attached on a substrate between a fused bilayer membrane.

Several strategies have been used to get rid of these vesicles: Additional washing steps with buffer or bidistilled H₂O or high-salt solutions (0.5-0.8 M NaCl) usually did not reduce the amount of attached liposomes (indicating that the liposomes are not only adsorbed on the bilayer). Treating the sample with a high-pressure water jet produced by purging water through the needle of a syringe proved to be more efficient. Of course, extreme care has to be taken not to dry the sample during this procedure and not to produce air bubbles which would damage the bilayer. Figure 76 shows how efficiently the non-fused liposomes can be removed by the water jet.

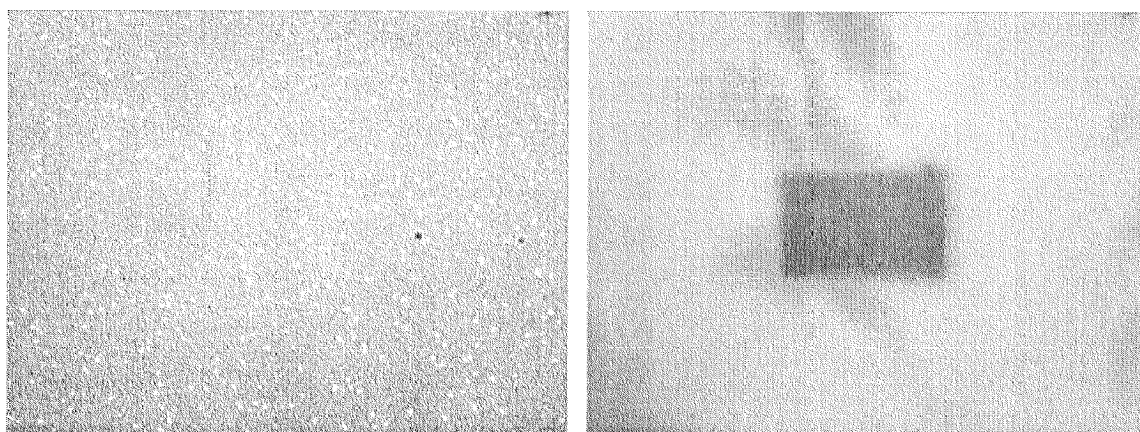


Figure 76: LSM image of a Lip16 bilayer on SiO₂ before (left) and after (right) treatment with a high-pressure water jet. The bilayer on the right was photobleached to test its integrity and fluidity.

A further, successful, mechanical method for liposome removal consists of a short sonication step. This procedure was also employed to bring persistent vesicle layers to fuse. The samples are, in a first approach, completely immersed in a beaker containing water and sonicated therein. The drawback of this method is that it will be extremely difficult to remove the sample from the sonication water bath again without drying the sample. A better approach is therefore simply to put the sample covered with a liquid drop onto some wet paper-towels in a flat-bottom glass petri-dish, and to sonicate it this way. Usually a 2 min. exposure will not damage the bilayer integrity but huge sonication energies or too long exposures will result in partial loss of the bilayer. Very interestingly, LSM images of too strongly sonicated samples firstly show hole-like structures followed by circle-shaped areas of weaker fluorescence at longer exposure times (Figure 77). These structures may be the consequence of cavitation- or air bubble implosion phenomena occurring in the proximity of the surface at high sound-wave amplitudes (Mason, 1990). Repeatedly, long, filamentous and fluorescent objects were observed on the surface after vesicle incubation and washing (see Figure 78, middle). The real nature of these structures, which are very mobile but seem to be attached to the substrate at one of their extremities could not yet fully be determined. Bacteria or rather large liposomes would be possible, which are forced to transform into long tubular lipid-structures due to the strong changes in osmolarity and ion composition of the solution. The latter hypothesis is supported by the observation that high-salt solutions will lead to filament shortening and finally reduce the filaments to single sphere-like structures on the substrate (Figure 78, right).

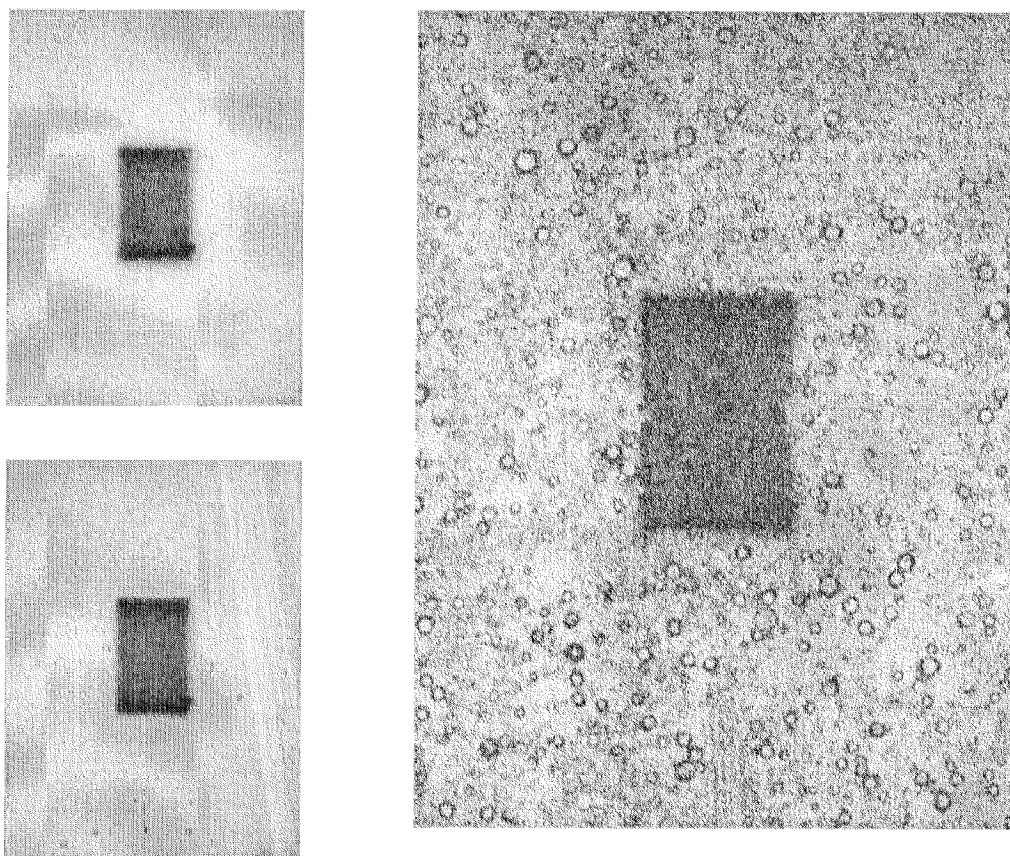


Figure 77: LSM image of a supported Lip16 bilayer on SiO₂ before (top, left) and after strong sonication for 1 and 8 minutes (bottom left, and right respectively). The bilayer after sonication (right) still recovers after photobleaching, but the process is slower compared to before sonication.

At very high magnification in the AFM, the filamentous objects did contaminate the surface of a supported bilayer in some cases (Figure 79). These extremely thin and rope-like structures were only clearly discernible if the AFM tip was scanned at absolute minimal force in contact mode. Under slightly non-optimal scanning conditions - as often is the case - , the presence of these tiny structures probably would not even be noticed. There are three possible explanations for them: Most likely, these structures are polymerization products of glutaraldehyde. The storage of this fixation solution is very critical and polymerization can occur. It can however also not be excluded that these structures are very slim phospholipid-tubes (their observation in a larger scale was described above) or DNA and collagen contamination from bacteria or animal species (compare with the AFM images of collagen-monomers in Figure 53 !).

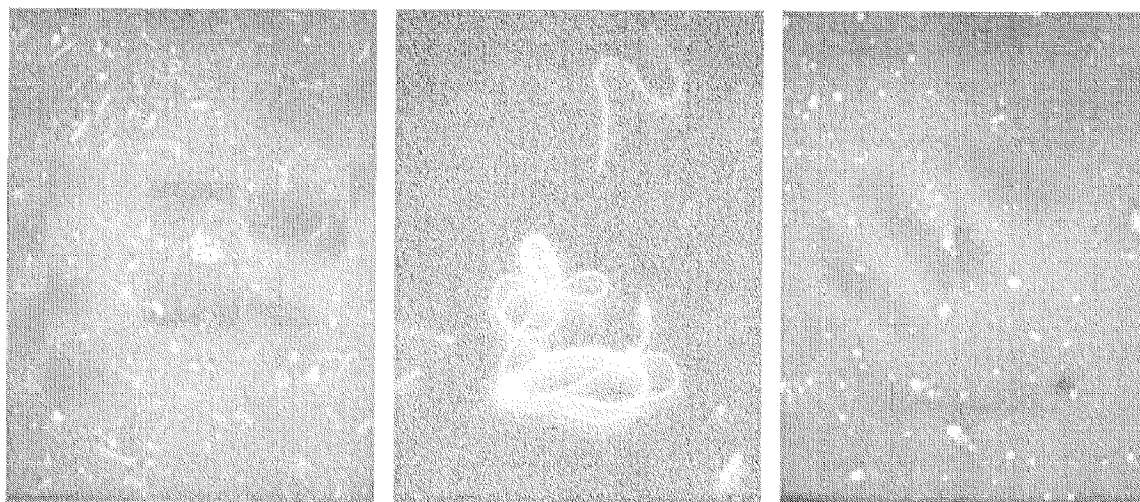


Figure 78: Fluorescent, filamentous structures extending from a supported Lip9 bilayer as observed in the LSM. Upon addition of high salt solution, they retract forming spherical structures.

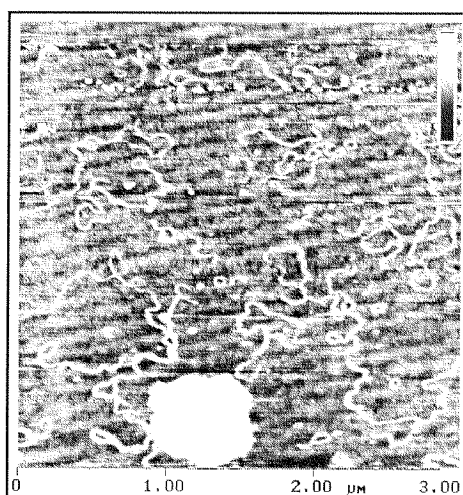


Figure 79: AFM image showing filamentous contaminations on a supported bilayer membrane. These structures with a height of about 1 nm were only visible at optimal feedback settings and minimal scanning forces (height bar: 10 nm).

Behavior of liposomes obtained by vortexing and sonication: Multiwalled vesicles

Liposomes produced using different methodologies do have different fusion behaviors on SiO₂. Usually, liposomes were produced by freeze-thawing cycles followed by extrusion. But often, research groups dealing with liposomes use liposomes produced by simply vortexing and sonication of a lipid-in water emulsion, instead. Such vesicles have a broader size distribution and more importantly, they are often multiwalled

(multilamellar). In our hands, these vesicles did not adsorb at all onto a SiO_2 surface until they were post-treated by freeze-thawing and extrusion. We assume that the multiwalled character of these vesicles made them very stiff and not accessible to osmotic swelling, and that therefore they were neither sticky to surfaces nor accessible to induced fusion.

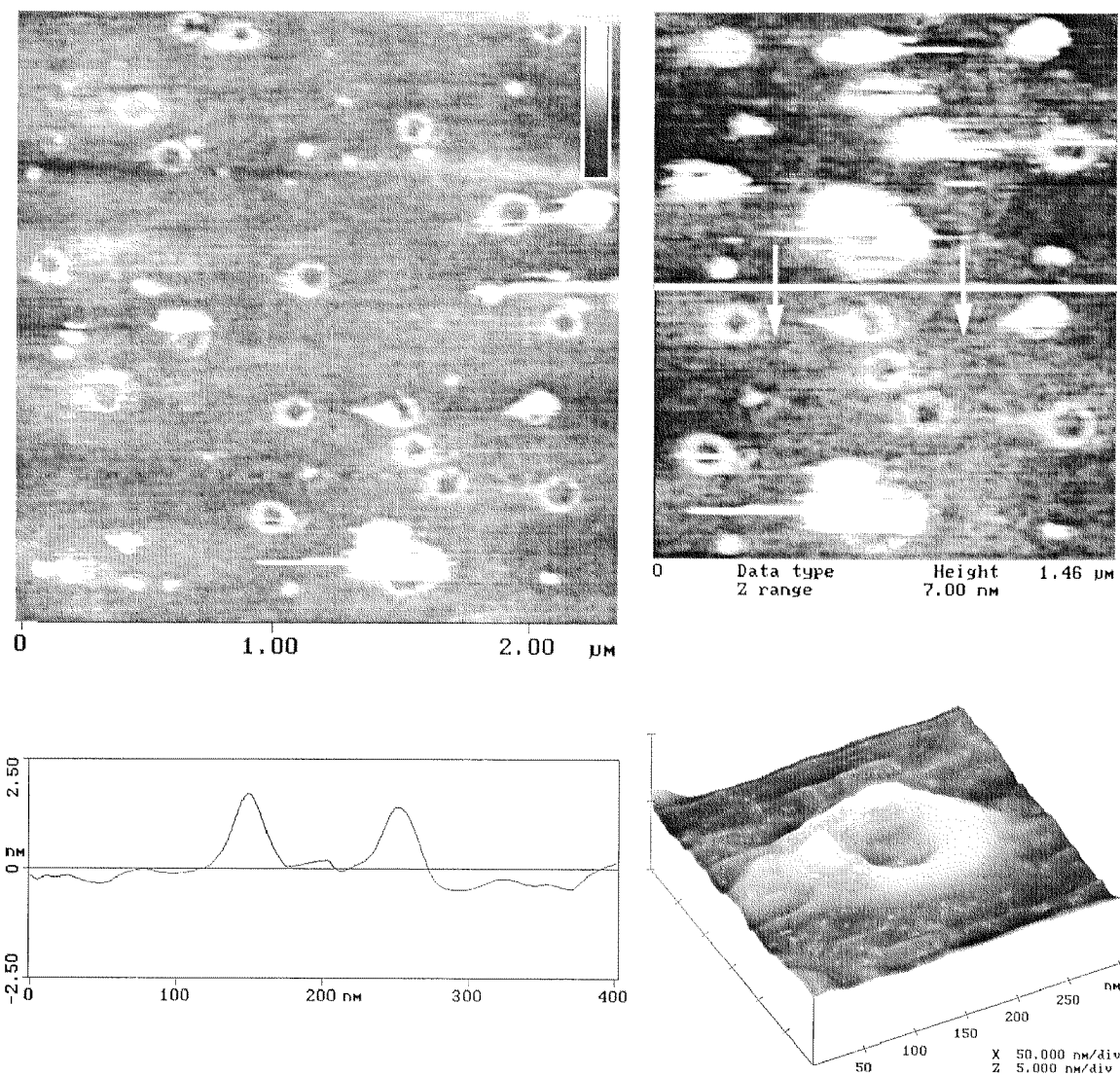


Figure 80: Top. left: Doughnut like, ring-shaped lipid structures in a fixed (GA and OsO_4) bilayer, after fusion of sonicated vesicles. Top, right: In the very first AFM scan, the structures appear as globular structures, which are then kind of decapitated by the AFM tip, leading to the doughnut-like structures. In the images below, a selected structure is shown in a 3-D representation and the section on the left gives informations about the height and width of the structure. Note the similarity of the shape with SLO-rings. The diameter of the small rings here is however larger, in the range of 120 nm.

After the post-treatment, they did form bilayers, but these had bad recovery properties and a multitude of liposomes remained attached to the surface. AFM images of such samples show extremely “dirty” surfaces on which very soft objects are being smeared over the surface. After glutaraldehyde fixation, nothing changes, but fixation with OsO_4 ,

which polymerizes unsaturated fatty-acid chains, reveals the presence of small, doughnut-shaped lipid structures on the surface (Figure 80).

How can these “doughnuts“ be explained ? Comparison of TEM images (not shown) of sonicated liposomes with the shape of liposomes of the same lipid composition but produced by vortexing, shows that the sonicated vesicles must be stiffer (they do not rupture on the TEM-grid) which can only be explained by assuming that they are multiwalled. During sonication, the large, crude vesicles are reduced in size until - at too long exposure - they become micelles. Very small but still multiwalled liposomes were therefore probably present after sonication which then were not affected by the extrusion post-treatment. These liposomes do not fuse on substrates even under harsh conditions, but are fixed as intact liposomes together with the supported bilayer membrane surrounding them, and giving rise to circular structures in the AFM according to the mechanism shown in Figure 81. The sonication method to produce liposomes is therefore not suited for the preparation of planar supported membranes by the liposome fusion technique.

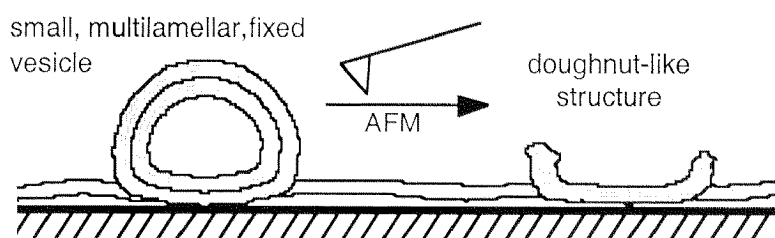


Figure 81: Formation of doughnut-like lipid structures by the “decapitation“ of fixed, multilamellar vesicles with the AFM.

Creation of bilayers at defined areas on a surface

The experiments above on gold surfaces show that the spreading and fusion behavior of vesicles is very much dependent on the surface chemistry of the substrate. E.g., on aminomodified surfaces liposomes do form a well-fused supported bilayer membrane, while on hydrophobic surfaces they do not. In the chapter “Chemical Patterning“, on the other hand, a technique was presented which allows to confine chemical functionalities with micrometer resolution on a gold surface. Combining these concepts, a patterned, site directed immobilization of a bilayer membrane was expected to be feasible. To test this, a TSG Au(111) surface was micro-contact printed with hexadecanethiol followed by rinsing with 11,11'-dithiobis(1-aminododecane).

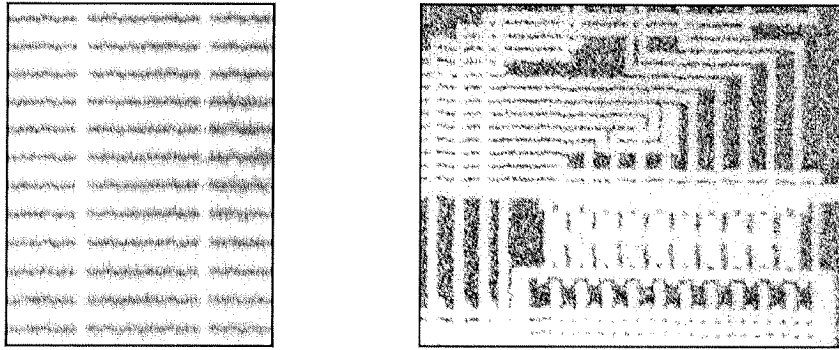


Figure 82: Site-directed immobilization of a supported bilayer on a TSG Au(111) surface patterned with two different SAMs. The bright areas are covered with a fluorescent bilayer membrane. Width of the bright patterns: approx. 2.5 μm .

This surface was then exposed to a liposome solution (Lip1) for 60 min., followed by carefully rinsing with distilled water and then examined - the sample did never dry. In the laser scanning microscope, the fluorescent replica of the master stamp was very clearly visible: the aminomodified areas were bright whereas the areas covered with the hydrophobic SAM were dark. As expected, the liposomes therefore only spread on the hydrophilic areas and it is thus possible to direct the localization of a bilayer in the micron scale on a substrate. Figure 82 shows the fluorescent image of such a structured bilayer and Figure 83 A) shows a scheme of the same sample.

After the LSM experiments, the patterned sample was rinsed with water, dried (by which the upper lipid monolayer is lost) and then imaged with the AFM in contact mode (Figure 70, left). Although the homogeneity of the lipid monolayer has suffered from the drying of the sample, it is clearly visible, that the lipid must have been confined to defined areas on the surface.

The possibility to control the site of immobilization as well as the phase of a supported bilayer by means of chemically patterning of a surface with SAMs, as described above, opens many applications in the field of controlling the behavior of membrane proteins in artificial membranes. One can think of immobilizing two different kinds of membranes, one after the other, to create a continuous supported bilayer with alternating areas of differing lipid composition. The composition of the lipid environment around membrane proteins can trigger or influence their activity and is therefore very crucial for their function. Alternatively, a continuous, supported bilayer could be created which is in different phase-states at defined microdomains. An additional tool is also the possibility to influence the lipid repartition within a supported, patterned bilayer by means of an electrical field (Groves et al., 1996). A method to locally influence the insertion of proteins into a supported bilayer was recently published by Heyse et al. (Heyse et al., 1998a).

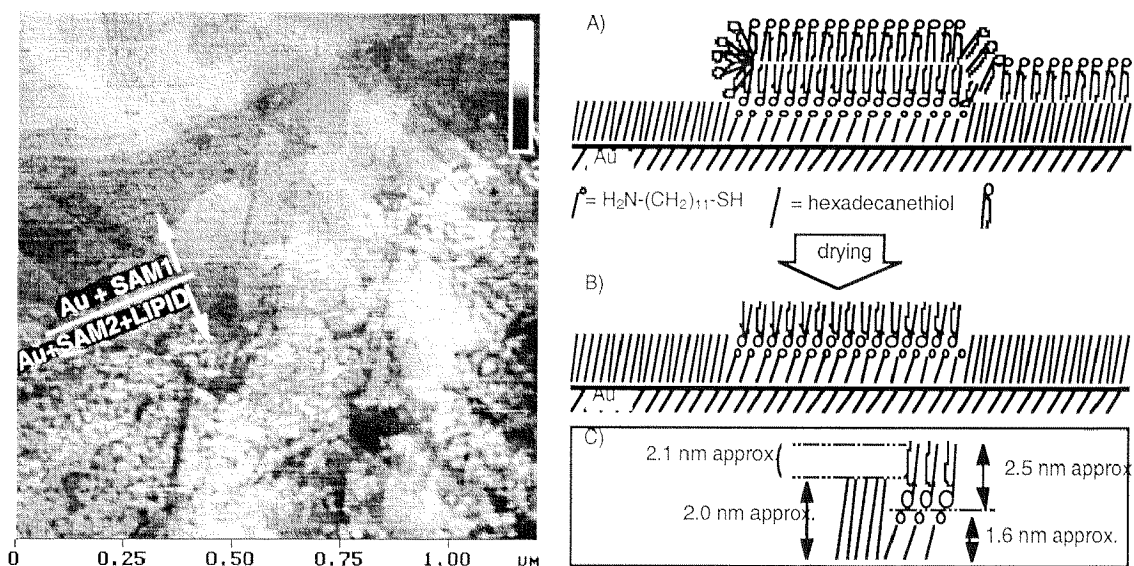


Figure 83: Left: Very high magnification AFM image of a dried, bilayer-patterned Au(111) (TSG) /SAM surface showing gold-atom high, triangular, crystalline domains on the bare gold areas. The white domains below are 1.6 nm high remains of a phospholipid monolayer. The homogeneity of the monolayer was negatively affected by the drying procedure (height-bar: 10 nm). Right: Scheme of a the patterned gold substrate in liquid (A), with a bilayer supported exclusively over the aminoterminated SAM areas), after drying (B), the upper phospholipid layers are lost) and theoretical heights expected for the described system (C).

Oocyte membranes

In the very beginning of the work with membranes, the use of biological membranes from a living source was also taken into consideration for making supported membranes. Specially the eggs of the frog *Xenopus laevis* which have a size of about 1 mm³ were potential candidates for this undertaking.

The oocyte bilayer membrane is protected and stabilized by an additional follicular layer as well as a vitelline membrane which are superimposed to the bilayer itself (Figure 85). They have to be removed to be able to access the cellular membrane. Figure 84 (left) shows a SEM image of dried and gold sputtered oocyte. At higher magnification (right), the very aesthetically shaped vitelline membrane can be seen. These protecting layers can be removed mechanically with tweezers (Bertrand et al., 1991), but very often, the bilayer membrane is injured during this process, making the egg unusable. We firstly tried to make AFM measurements directly on eggs prepared by air-drying or critical point drying followed by different fixation strategies.

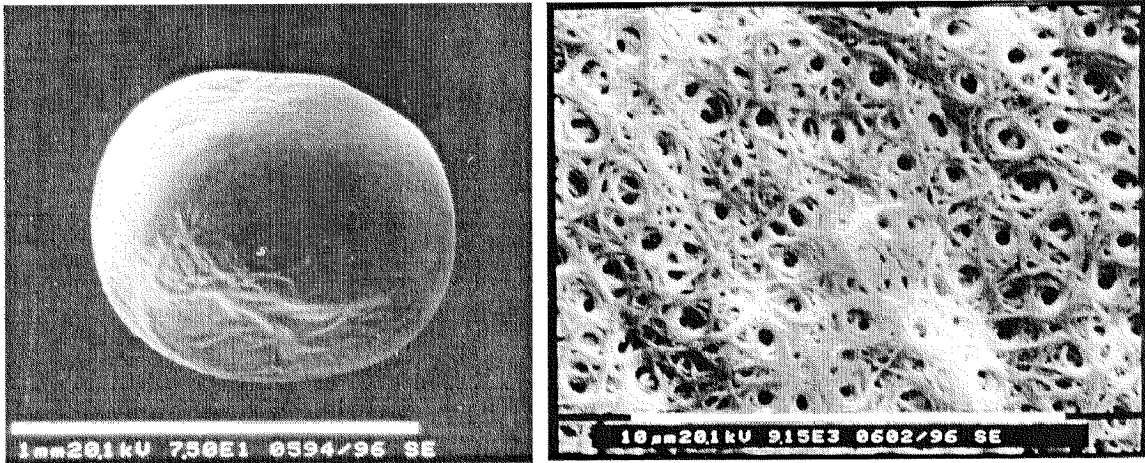


Figure 84: Left: SEM image of the surface of a dried oocyte. Right: higher magnification showing the beautiful porous structure of the vitelline membrane (A. Vinckier).

A very rough and hilly surface was visible in the AFM. The reason for this was soon after discovered by looking at oocyte sections in the TEM, and at SEM images of eggs after removal of the protecting outer layers: To increase the nutrient exchanging surface with the environment, oocytes form microvilli on their surface. These tiny membrane tubes are several microns in length and less than a micron in diameter and cover the whole of the cell (Figure 85, right).

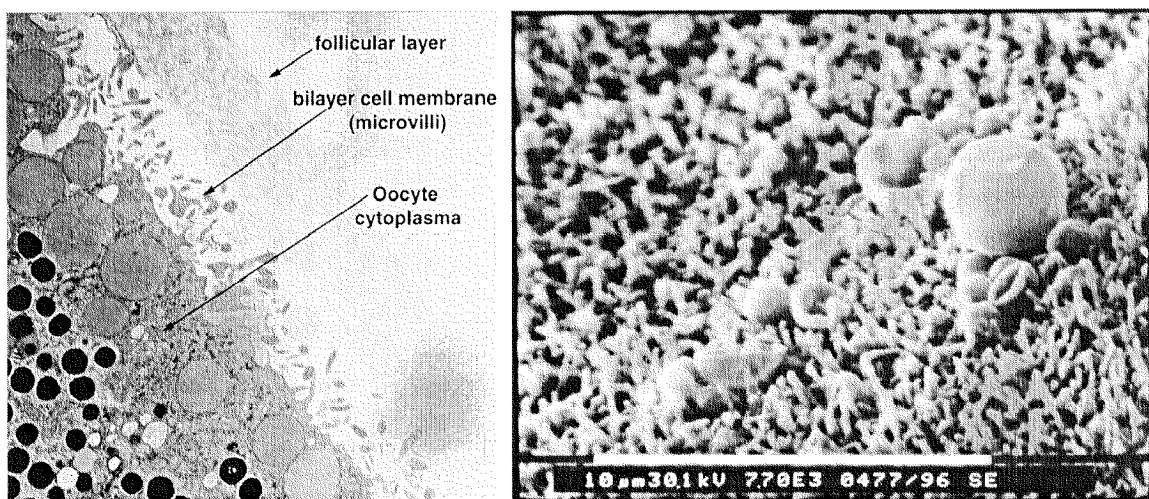


Figure 85: Left: TEM image of a section through an oocyte (U. Ziegler). Right: SEM topography at high magnification showing the bilayer cell-membrane of the oocyte. The phospholipid membrane of this egg is not flat, but organized in microvilli, which enhance the cellular surface. The round-shaped objects on the microvilli are storage structures from the interior of the oocyte (compare with left image) which accidentally escaped and adsorbed to the membrane.

Such structures are clearly not at all suited for AFM measurements. Attempts were made by A. Vinckier, U. Ziegler and P. Kernén to flatten the cells enzymatically or by

the action of drugs. This led to some improved membrane topography but finally they abandoned the oocytes for cultured cell-lines which naturally have smoother and better accessible membranes ((Ziegler et al., 1998a)). Two interesting experiments involving cell-membranes were later published by two groups: the measurement of the elastic properties of a patched membrane fragment excerpted from an oocyte (Hoerber et al., 1995) and high resolution images of membrane-patches from MDCK cells transferred onto a mica substrate (Lärmer et al., 1997).

PROPERTIES OF LIPID BILAYERS ON SURFACES

The phase state and morphology of bilayers adsorbed on substrates

Depending on chemical and physical properties of a homogeneous and clean substrate, the adsorption of liposomes can follow three different routes leading either to a supported bilayer, an adsorbed vesicular layer or no adsorption at all (See chapter “Bilayer Formation”). If a lipid bilayer has adsorbed, it can still exist in different phase states described as the solid, crystalline phase (L_c or L_β , which is often also referred to as “gel-state”), the gel state with tilted alkyl-chains (L_β'), the undulated transition gel-state (P_β' ; “ripple-phase”) and finally above the melting temperature of the alkyl chains, the liquid crystalline state (L_α) (Figure 86). The actual state depends on the temperature and on the water content in the system. Figure 86 (right) shows a phase diagram for 1,2-Dimyristoyl-sn-glycero(3)phosphocholine. For a supported bilayer, a water excess can be assumed, for which the phase transitions at 60% water are significant.

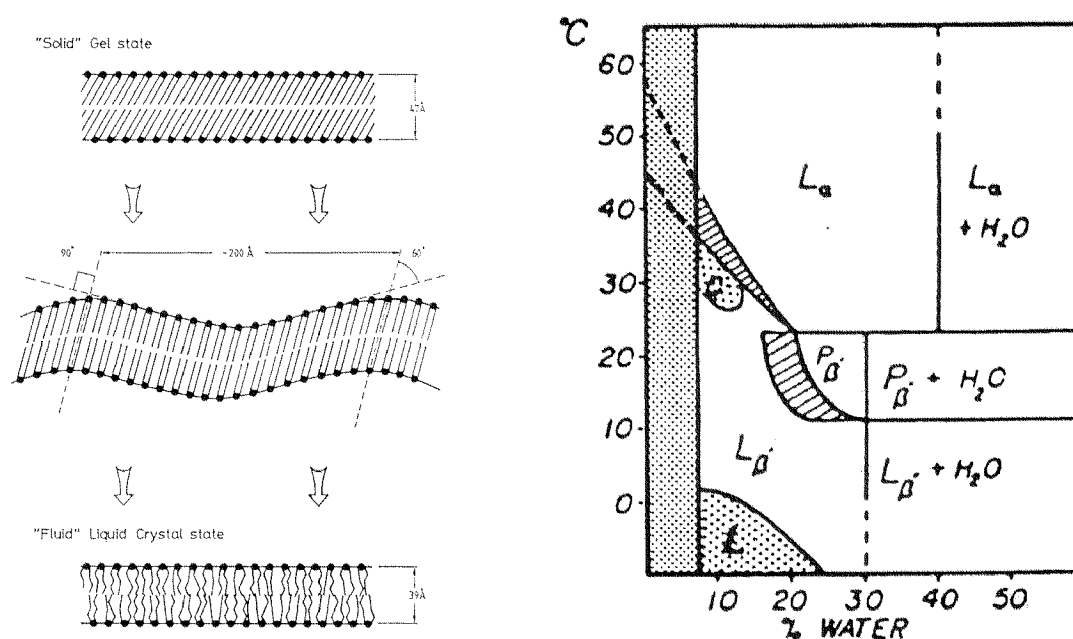


Figure 86: Left: The main phases of a bilayer membrane: the solid, crystalline phase (L_c or L_β), the undulated transition gel-state (P_β' ; “ripple-phase”) and the liquid crystalline state (L_α). Right: Phase diagram for 1,2-Dimyristoyl-sn-glycero(3)phosphocholine in water.

On the other hand, the interaction of the bilayer with the substrate gives rise to additional forces in the system, leading to shifts in the transition temperatures. In

supported membranes, furthermore phase separations have to be considered, leading to coexisting lipid-patches in two different phases. This can even occur if only one lipid species is present in the bilayer, and (accidentally), in the presence of only a monolayer of lipids ((Spratte, 1994)).

For our applications, the differentiation of a vesicular layer (which does not show long-range mobility of lipids above T_c , due to the restriction of their motion within the boundaries of the liposome), a bilayer in the liquid or crystalline phase or a lipid monolayer are important. All these states can to some extent be differentiated in the LSM, if fluorescent lipids are incorporated into the liposomes. An sample showing the lipid behavior on the surface, is the one presented in Figure 87, where two of the above mentioned states coexist: After the incubation of Lip5 liposomes on a SiO_2 substrate, areas of different fluorescence intensity were observed on the sample. Both areas could be bleached, proving the presence of lipids (the dark area on the left is the border of the sample with no fluorescence at all). Recovery of fluorescence, however, was only observed in the area of weaker fluorescence. This phenomenon could be understood, if a non-fused vesicle-layer forms the brighter areas and a fused, supported bilayer is responsible for the areas of weaker fluorescence.

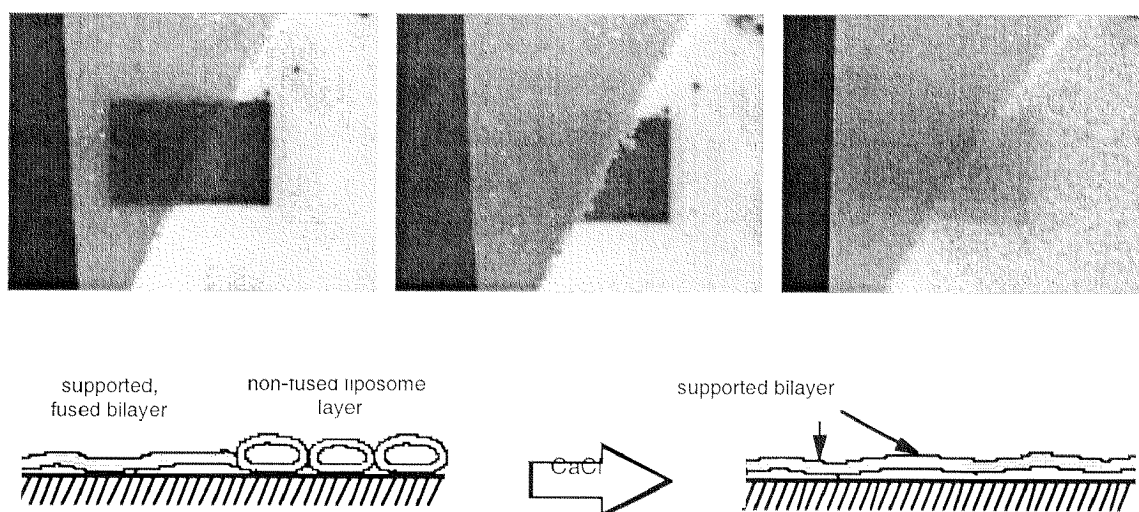


Figure 87: Lip5 liposomes incubated on a SiO_2 substrate, after washing; LSM images under water: Areas of different fluorescence intensity can be discerned. **Left:** Substrate after photobleaching. **Middle:** The same surface, 20 min. later. **Right:** Same sample after the addition of 10 mM CaCl_2 and washing: Loss of fluorescence intensity on the right side and induced recovery of fluorescence. The bilayer in the right image shows two different fluorescence intensities, although a bilayer is present in both areas. This is due to the left area of the sample having been exposed to larger bleaching intensities than the right area (which was protected by the second bilayer when still in the “attached liposomes“ state).

Direct addition of Ca^{2+} in the fluid cell of the LSM, indeed, led to weakening of fluorescence on the before brighter areas and improved fluorescence recovery. This indicates that the liposomes now did fuse. The differentiation of bilayers and vesicle-layers can thus be made on the basis of fluorescence recovery- and fluorescence intensity measurements (if suitable reference-samples are available for the latter).

On another sample, presented in Figure 88, a similar behavior of a lipid bilayer and a lipid monolayer can be studied. Due to an accident after successful liposome spreading and fusion, the right half of the sample dried out for a second but was immediately rehydrated. According to experience, half of a bilayer is always removed if a bilayer contacts the gaseous phase. The sample was then immediately transferred to the LSM.

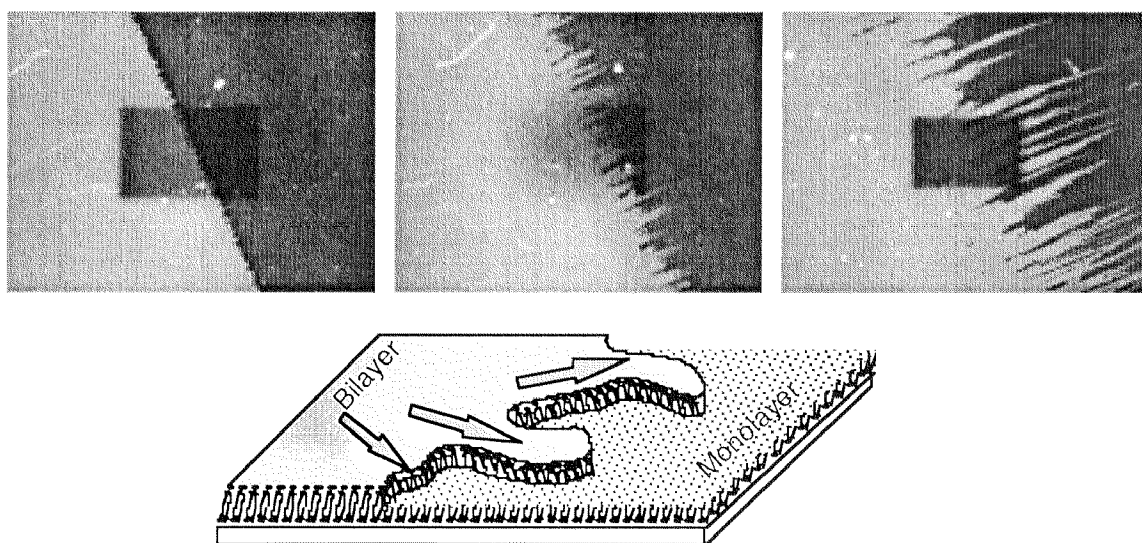


Figure 88: Supported bilayer which was allowed to dry for a short period of time on the right half: Lipid-finger growth into the hydrophobic monolayer areas. Left: Photobleached bilayer/monolayer. Middle: 15 min. later (at room temperature): fluorescence recovery and finger-growth. Right: 8 hours later at 4°C : newly photobleached sample with the upper monolayer still advancing into the monolayer areas.

At the non-dried/dried boundary, two different fluorescence intensities were observed, both of which could be bleached. Recovery, however was only found to happen with the brighter bilayer areas. The monolayer area—exposing the very hydrophobic fatty acid chains towards the water—collapses and sticks together due to the hydrophobic force, leading to loss of fluidity. AFM images of such a collapsed layer show a highly rough surface compared to bilayers, due to the paint-brush-like arrangement of the lipid-tails searching to minimize the contact area with water (Figure 89). Very interestingly, the upper bilayer slowly began to re-expand over the hydrophobic layer in finger-like structures (Figure 88).

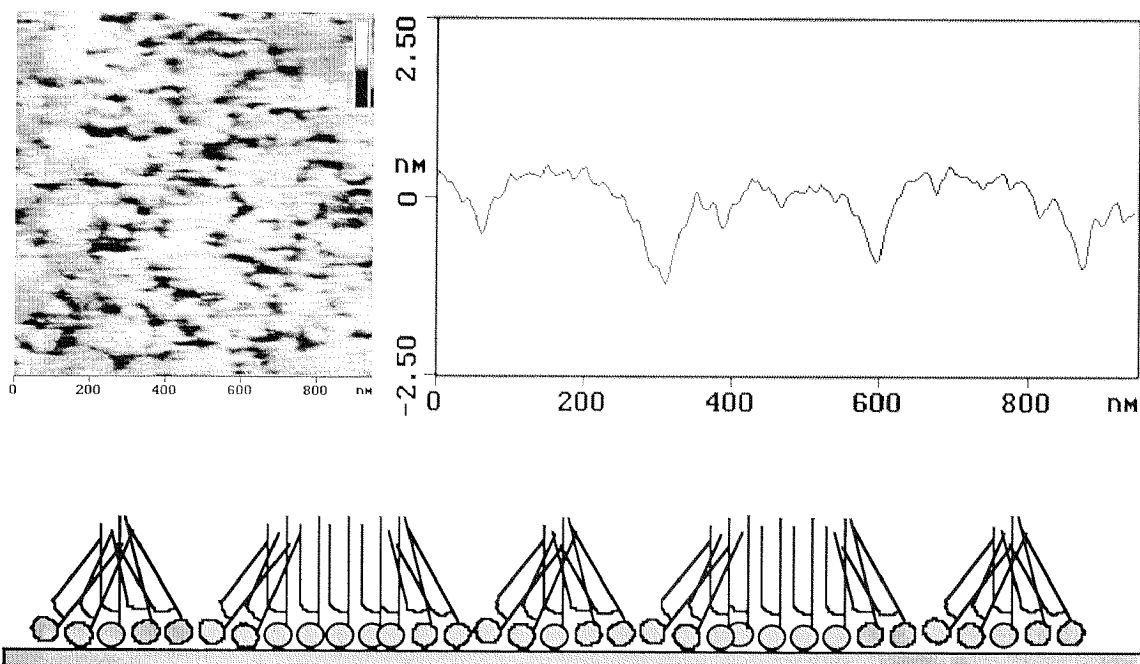


Figure 89: Roughening of a lipid monolayer exposing the hydrophobic tails upward when contacted with water. Left: AFM image. Right: Section through the image on the left. Bottom: Scheme of the brush-like collapsed lipid monolayer (domain-size not to scale!).

Regarding different states of the supported bilayer, AFM images of a supported bilayer in the $P\beta'$ “ribble-phase“ were published by (Mou et al., 1994b), which shows, that under defined conditions, also this non-flat phase can be induced in surface-bound membranes. Further, we would like to point out that an alternative scenario after drying of a bilayer is that the remaining, surface bound lipid monolayer simply floats-off the surface as soon as the sample is reintroduced into a liquid. This phenomenon often happens when lipid bilayers were intended to be transferred onto a hydrophilic substrate using the LB technique (see chapter “Langmuir Blodgett Films“).

The best and most useful method to monitor on-line the adsorption and fusion behavior of liposomes on surfaces would be the use of “Optical Waveguide Lightmode Spectroscopy“ (OWLS) in the case of oxide surfaces (Garland, 1996) and “Surface Plasmon Resonance (SPR)“ for Gold/SAM substrates (Pharmacia Biosensor AB company, Uppsala, Sweden). These techniques give direct evidence of the adsorption kinetics of species and the thickness of the adsorbed layer as well as its mass can be determined. No such measurements were performed for oxide surfaces, because the liposomes usually fused well on them and LSM imaging - in addition to proofing the presence of bilayer - gave data about the phase-state of the membrane. Also, using the LSM, the homogeneity of the bilayer over the whole substrate can be verified, instead of

making a single-point measurement. In the case of SAM-coated Au substrates, evanescent field measurements of the vesicle fusion process could have been a valuable completion to LSM data. We tried to produce gold-coated optical waveguide grating couplers by evaporation of extremely thin Ti and Au coatings. Unfortunately, even the thinnest metal coating (1 nm Ti and 1 nm Au) led to no measurable signals in the OWLS detector due to the absorption of laser-intensity by the heavy Au atoms. SPR measurements were not undertaken, as in the second part of the thesis, the interest moved more towards oxide substrates.

Control of bilayer fluidity and heat induced morphologies

Especially for AFM measurements, control of the mobility of proteins inserted in a supported bilayer is crucial. Good resolution cannot be obtained if the proteins move around during scanning, but on the other hand, the membrane must be kept in the fluid state, if one aims to give the protein an environment which mimics the situation of nature. On our artificial, supported systems, we therefore were searching for a tool to tune the fluidity of the membrane by an external factor. The possibility to switch from the crystalline to the fluid state would allow to freeze a certain protein conformation or to stop a protein interaction study at a certain configuration.

Supported bilayer composition: [Cholesterol content in % ^{w/w} of total lipid] (Liposome sample names (see Table 2))	Transition temperature (T _c)
PC/DP/NBD-PE/Cholesterol [31.2%] (Lip10)	T _c < room temperature
DPPC/DP/NBD-PE/Cholesterol [31.2%] (Lip9)	T _c < room temperature
DPPC/DP/NBD-PE/Cholesterol [7.8%] (Lip12)	T _c ≈ 35°C
DPPC/DP/NBD-PE/Cholesterol [1.5%] (Lip13)	T _c ≈ 45°C

Table 10: Transition temperatures T_c (“crystalline to fluid“ transition temperatures) for supported bilayers composed of different lipid mixtures. PC: egg phosphatidylcholine; DP: dicetylphosphate; NBD-PE: fluorescent lipid.

The three main factors influencing the transition temperature (T_c = melting point of the hydrophobic lipid chains in a bilayer) of a membrane are: the lipid composition, the water-to-lipid ratio and the temperature. On our supported bilayers, there is always excess water, for which the “water to lipid ratio“ can be neglected. On the other hand, the bilayer is in close contact with a substrate which greatly influences the mobility of the lipids. Therefore, the surface chemistry in our case plays an important role in controlling the bilayer phase-state. On most of the substrates tested in this thesis, the

surface chemistry must however be thought of as being inert. This means that it will not be possible to change this parameter to control protein mobility.

The most practicable way to influence the fluidity was the combination of vesicles with a very refined lipid composition along with switching the substrate temperature around the T_c of the bilayer. The established lipid composition used for the insertion of streptolysine was carefully redesigned, such that the T_c was positioned near but just above room temperature. Table 10 shows the different lipid compositions which were tested and the resulting solid-to-fluid transition temperatures of a corresponding supported bilayer

As can be seen, replacement of the PC from a natural source ($T_c < 0^\circ\text{C}$) by the synthetic DPPC ($T_c = 41^\circ\text{C}$) did not result in the expected rise of T_c above room temperature, although usually DPPC bilayers have very high melting temperatures. The reason for this is the presence of huge amounts (31%) of cholesterol - a well known membrane-softening component which also removes the sharp enthalpic transition at the lipid melting point (Chapman, 1993, Bloch, 1985). Reduction of the cholesterol content in the bilayer finally led to the desired increase of T_c . Lipid compositions with T_c around 35° and 45°C were obtained as described in Table 10.

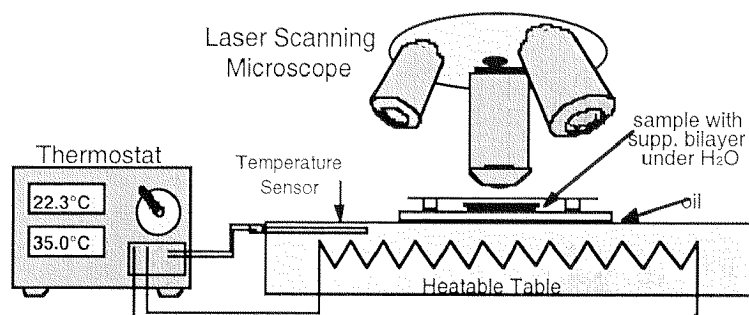


Figure 90: Experimental setup for the determination of the transition temperature (T_c) of a supported bilayer.

Usually, the transition temperatures of lipids can be determined using Differential Scanning Calorimetry (DSC). This technique measures the heat absorbed (or released) by lipids as they undergo an endothermic (or exothermic) phase transition. For our liposomes, which were composed of four different lipids and which additionally entrap PBS buffer molecules, a quite broad transition temperature range has to be expected for which this technique probably is not sensitive enough. The determination of the melting temperatures for the different liposomes was therefore made by slowly heating a thermostated microscopy-table on which a photobleached supported bilayer on SiO_2 was observed using the LSM. Recovery of fluorescence initiated as soon as $T_{\text{supp}} > T_c$.

The setup is schematically shown in Figure 90. This approach, unlike DSC, takes into account the deviation of T_c produced by the presence of the substrate.

Liposome fusion of these high- T_c vesicles required special immobilization protocols. After 4 hours incubation of the liposomes on the SiO_2 substrate at room temperature, the samples were post-incubated for an additional 15 min. in a wet-chamber at 50°C . They were then rinsed with 10×100 ml H_2O dest. at also 50°C . This led to heat induced fusion of the liposomes and very homogeneous bilayers with only a few attached liposomes were obtained. On a sample, which had been exposed to the liposome (Lip13) solution for too short a time, a full vesicle layer had been formed.

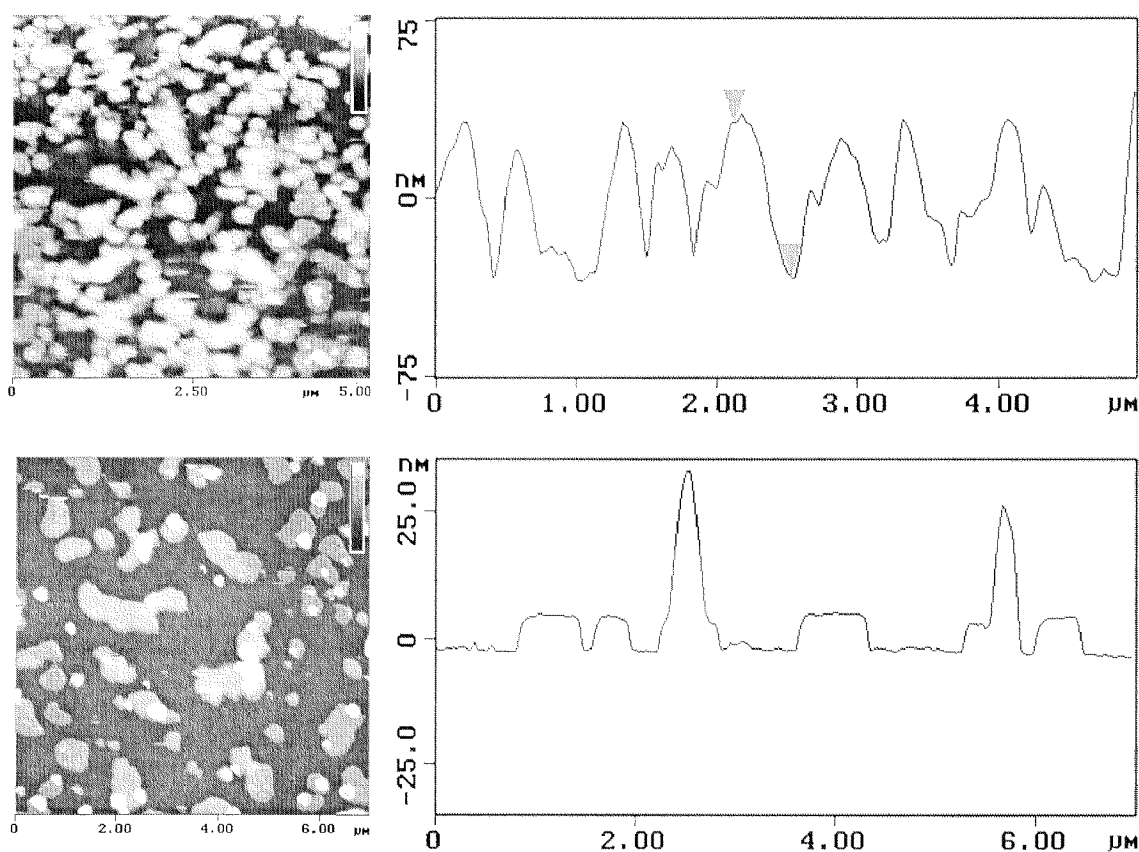


Figure 91: Top: Non-fused liposomes on SiO_2 , after incubation of high- T_c Lip13 vesicles and water rinsing. Bottom: Islands of supported bilayer patches are obtained after heat-induced fusion of the individual liposomes shown above. Note the different z-scales of the sections on the right.

The effect of heat-induced fusion can be demonstrated: In the AFM, the sample showed the presence of single, non-fused liposomes. After exposure to 65°C for 60 min., most of the vesicles fused onto the surface, leading to round-shaped, individual membrane patches of a thickness of exactly one bilayer (Figure 91).

In a future step, we were planning to introduce proteins in a bilayer. For this, it is important to use vesicles with a T_c close to but just above the usual temperature range for the proteins. There are 3 reasons: Firstly, inserted membrane proteins may denature or not behave naturally if heated above 37°C . Secondly, it is very practical if only small temperature changes are needed to switch the bilayer between the two phase states. The third reason is due to the thermal expansion coefficient of lipid bilayers. The observation was made that if a spread, supported bilayer which had been equilibrated at 4°C was heated above 40°C , a mottled fluorescence appeared in the LSM (Figure 92, middle). This phenomenon can be interpreted as budding of small vesicle-like structures, due to bilayer-folding in order to compensate its expanded surface area at elevated temperature, as shown in the scheme below.

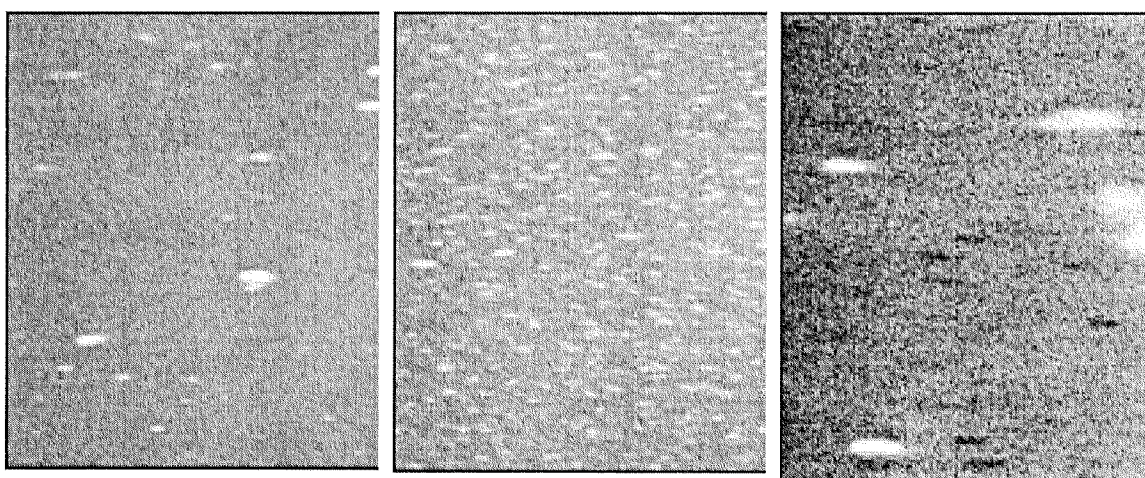
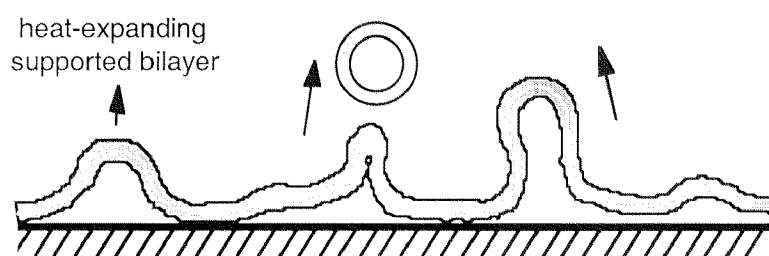


Figure 92: Effect of temperature on the morphology of a Lip9 bilayer on SiO_2 . **left:** Bilayer after equilibration to room temperature (from 4°C). **B:** after heating to 45°C and **C:** Holes visible in a Lip12 bilayer after cooling from an elevated temperature back to 4°C .

This behavior is very unwanted as it introduces inhomogeneities into the flat bilayer and more importantly, if the bilayer is cooled again to room temperature or below, the lost lipid fraction due to budding will lead to lack of lipids and the membrane will develop holes (Figure 92, right).

As a rule or within the possibilities, high temperature variations should be avoided if working with supported bilayers.

Suspended bilayers

The formation of bilayer membranes on nanocavity substrates was one of the central steps of the dissertation. Three topics which had been treated separately before, had now to be combined giving rise to a system of higher complexity: the bilayer membrane suspended between two aqueous compartments. In a first step, the etched nanohole substrates which were described in the last chapter had to be chemically modified with SAMs described in the chapters “CHEMICAL MODIFICATION OF SURFACES“ and “CHEMICAL PATTERNING“. Then, for suspending the membranes, we could build the experience acquired in the chapter “BILAYER FORMATION“. A scheme of the architecture which we were trying to build is shown in Figure 93.

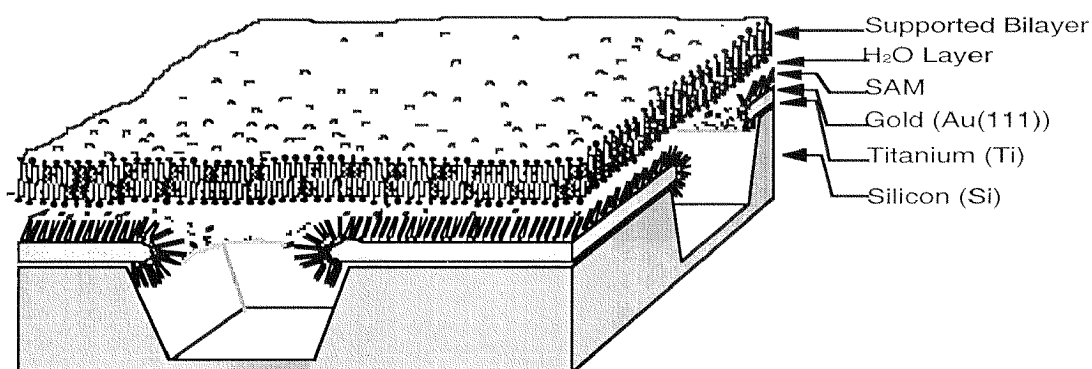


Figure 93: Scheme of an idealized nanoholes substrate with a supported/suspended membrane.

Several points had to be taken into consideration for the preparation of these structures:

- The demands on the choice of an appropriate SAM for the modification of the gold areas of the nanostructures were several: In the first place, a SAM had to be chosen which leads to good vesicle adsorption and spreading. During the bilayer formation experiments, amino-terminated SAMs proved to be the best regarding the homogeneity and reproducibility of the bilayers.

But there was an even stronger argument for the choice of the amino-terminated SAM: As already mentioned in the introduction, the nanohole surfaces were composed of two components, Au and Si, in order to get different surface properties on the outside and inside of the nanocavities. The reason for this was that the surface of the substrates had

to be lipid-adsorbing in order to induce liposome fusion, while the interior of the cavities had to be lipid-repulsive. Otherwise the very flexible bilayer membrane would probably penetrate into the cavities leading to the situation shown in Figure 94 (left). Given that silicon, and therefore the cavity, is negatively charged by nature, we chose a positively charged coating for the gold, and negatively charged liposomes, to produce the needed chemical anisotropy between the two surfaces.

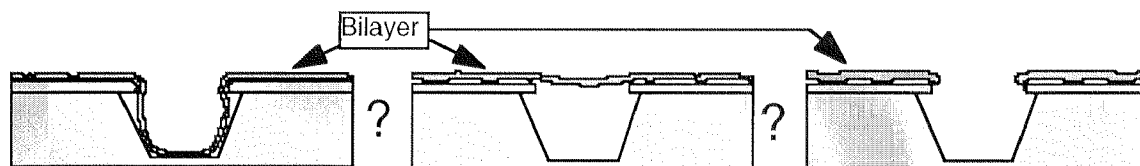


Figure 94: The three most probable configurations of the lipid membrane after spreading of the liposomes.

Using this strategy, the supported membrane would bind to the gold surface, but it would be hindered from penetrating the nanohole due to strong electrostatic repulsion.

These were the two reasons why we did chose the amino-terminated alkanethiols to coat the gold.

- Until now we always spread the bilayers on flat, homogeneous substrates. In this case however, the bilayers had to be suspended over nanocavities. According to Figure 95, this can only be achieved by using liposomes which have a larger diameter than the nanocavities. Because we did usually extrude our pre-liposomes through 100 and 200 nm filters, we produced vesicles with a mean diameter of about 130 nm - an unfortunate diameter therefore for 100 - or 200 nm cavities. We consequently tried to produce larger liposomes by extrusion through 450 nm filters, but, this did not work well in the case of the Lip22,23 and 24 preparations. Liposomes up to 6 μm in diameter were obtained which certainly were not unilamellar. Repeated extrusion of these larger liposomes through a 200 nm filter reduces their size to between 1000 and 1800 nm. This was better, but not very satisfying, because we did not understand this phenomenon. However, these large liposome preparations were used all the same, and the LSM revealed, that despite their unknown lamellarity, homogeneous bilayers were formed on the amino-SAM coated gold substrates.

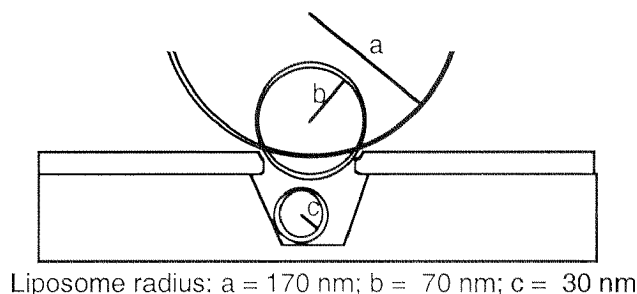


Figure 95: The size of the liposomes must exceed the diameter of the nanoholes to stretch over the cavity.

We proceeded as follows for suspending the membrane: The etched nanohole substrates were prepared according to chapter “Nanospheres“. They were rinsed with isopropanol, dried with nitrogen and then incubated in water containing 2 mM 11-aminoundecanethiol. The samples were then washed with water and ethanol, broken into small squares and glued onto the glass/teflon holders described previously. The liposomes were then incubated, fused and then the suspended bilayer was washed as described in chapter BILAYER FORMATION. As soon as a homogeneous, bleachable bilayer was visible in the LSM covering the substrate, the sample was analyzed by AFM.

Due to the extremely small dimensions of the nanocavities (100 nm) and the fact that the suspended membranes had to be kept immersed in water, AFM is the only technique which allows to answer the following questions: (i) whether a homogeneous bilayer covers the substrate being suspended over the nanoholes, (ii) whether the bilayer penetrates the nanocavities or (iii) whether the suspended bilayer does spread over the cavities but breaks on contact with the tip (see Figure 94).

At the same time, we were also seeking to learn more about the stability of such suspended membranes under AFM scanning conditions.

In the best case we expected to see no holes at all on the surface, if a minimal force is applied by the tip, and then to see indentations of the same diameter as the nanoholes, if the force is increased. The following results, summarized in table 12, were obtained:

The following conclusions could be drawn from these experiments: (i) According to LSM images, very homogeneous, supported bilayer membranes could be created on the nanostructured surfaces modified with the aminoterminated SAM. This was also confirmed by force-versus-distance curves and AFM images. The last revealed the presence of a flat, clean membrane. Crystalline ($T_c > \text{room temperature}$) liposome preparations did not fuse to 100%, but flat bilayer areas large enough were obtained. (ii) On supported membranes formed by liposomes which have a T_c below room temperature, the suspended membrane areas over the nanoholes were indented by the

vertical force of the AFM, even if AFM tips with small spring constants (in the range of 0.12 N/m) were used.

Sample Nr./nanohole-geometry	Liposomes used for spreading	Bilayer-aspect in the LSM	Bilayer morphology in the AFM
A) Not etched 50 nm nanoholes	Lip20 (PC/Chol/DP/BODIPY) Negatively charged.	Homogeneous fluorescence. Good bleaching No recovery	Nanohole positions well visible. Small tipload dependence of the membrane-shape. negative control did dry out
B) Etched 100 nm nanoholes	Lip20 (PC/Chol/DP/BODIPY) Negatively charged.	Homogeneous fluorescence. Good bleaching No recovery	No difference between this membrane sample and the negative control sample without bilayer.
C) Not etched 100 nm nanoholes	Lip20 (PC/Chol/DP/BODIPY) Negatively charged.	Homogeneous fluorescence. Good bleaching No recovery	Small tipload dependence of the membrane-shape. Negative control: No tipload dependence of the membrane-shape.
D) Not etched 100 nm nanoholes	Lip23 PC	Homogeneous fluorescence Good bleaching No recovery	Small tipload dependence of the membrane-shape.
E) Not etched 100 nm nanoholes	Lip24 DPPC T _c >room temperature !	Not very homogeneous Difficult to bleach No recovery	Mixture of non-fused liposomes (height 50-250 nm!) and fused membrane patches. Nanoholes visible. Small tipload dependence of the membrane-shape.
F) Not etched 100 nm nanoholes	Ditto, after additional extrusion step. Heat induces fusion (55°,2h)	Homogeneous fluorescence and some few vesicles attached	Partly large liposomes attached to the surface, but on flat membrane areas, the nanoholes can be seen. Large tipload dependence of the membrane-shape! See Figure 96 and Table 12. Negative control: No tipload dependence of the membrane shape (Table 13)!

Table 11: Results of the membrane suspension experiments. The nanocavity substrates were modified with an aminoterminated SAM, liposomes were incubated on the substrates, washed and then analyzed in the LSM and AFM.

The holes usually had a shape very similar to the negative controls without membranes. Only a very weak dependence of the section through the middle of a hole on the load

applied to the tip could be detected, indicating that the elasticity of these membranes was higher than the spring constant of the used tips.

On the other hand, suspended bilayer membranes made of synthetic lipid (DPPC, with a T_c above room temperature), were not indented by the AFM tip at small vertical forces. The 5 nm thick bilayer in this case did show stretching all over the nanohole, at a depth corresponding to the gold layer thickness below the bilayer plane (see Figure 96 (right)). A scheme of this situation is shown in Figure 97. The “staggered” arrangement of the suspended bilayer relative to the bilayer plane could be explained by a strong attraction between the DPPC bilayer and the amino-terminated SAM covering the gold. This adhesive strength seems to be strong enough to bend the bilayer down onto the rim of the gold (Figure 97 (left)).

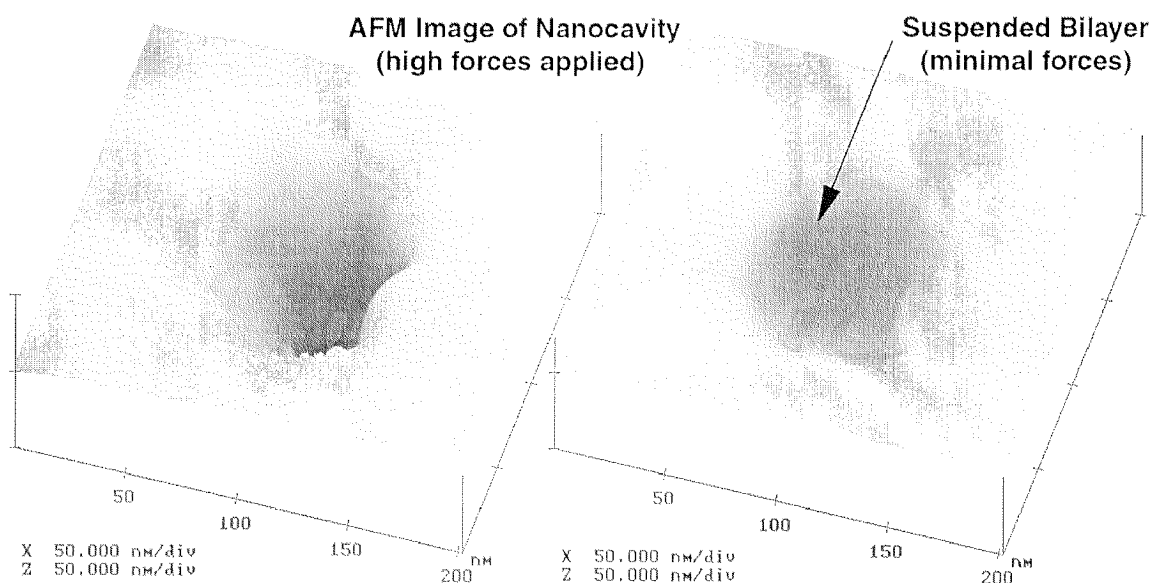


Figure 96: 3-D AFM images of nanocavities covered with a supported/suspended bilayer membrane. Right: At minimal contact forces between the tip and the substrate, the bilayer membrane can be seen suspending over a nanocavity. Left: Same place after increasing the setpoint (load) of the AFM tip. The membrane is elastically indented into the liquid-containing cavity. Due to the small dimensions of the hole, the AFM tip can not reach the bottom of the cavity as shown schematically in Figure 97 (right).

Increasing the load onto the tip successively leads to a deeper indentation of the tip into the suspended bilayer, until finally the cone of the tip comes into contact with the membrane coated Au edges (Figure 97, right). This behavior is completely reversible, meaning that the membrane will recover the non-indented state, at lower forces. Table 12 shows a series of single line scans through the middle of a nanohole covered by a

Lip24 bilayer membrane with changing forces (setpoint) applied between the tip and the supported membrane. The reversibility of the process is clearly visible.

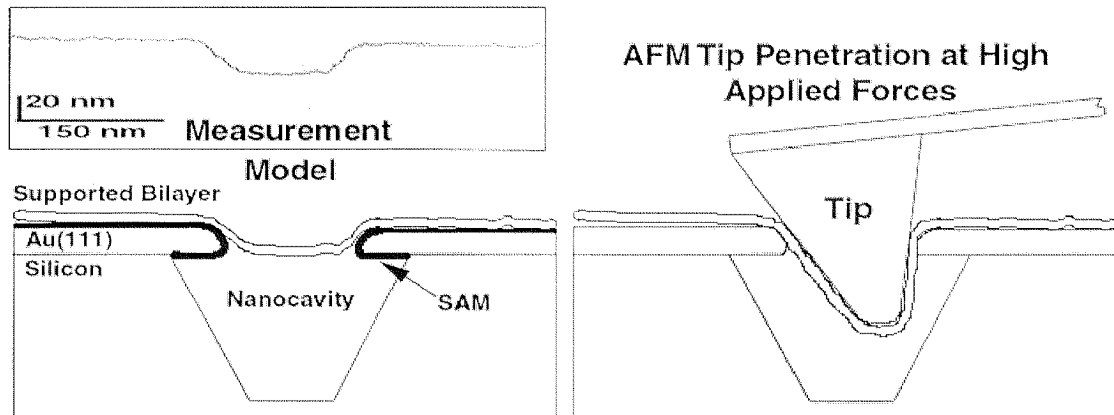


Figure 97: Top, left: Single line topography obtained with AFM of a bilayer-covered nanohole at low forces. Bottom, left: Schematic section through the same nanocavity, explaining the shape of the AFM image. Right: Indentation of the AFM tip into the nanohole if large scanning forces are applied.

These results show that it is indeed possible to control the spreading of vesicles over nanohole substrates, obtaining small, suspended membrane-areas with nanometer dimensions. These bilayer membranes stretch between the small water volume entrapped in the nanocavity and the bulk solution. Using appropriate lipid compositions and AFM tips with small spring constants, these suspended membranes can resist the tipforces exerted by a scanning AFM tip. This makes the bilayer substrates useful tools for scanning-probe microscopy investigation of membrane proteins.

Setpoint (Tip force)	AFM line-scan	
- 3.17 minimal force		
+ 1.00 huge force		
- 2.00 small force		
- 3.25 contact to surface lost.		
-3.22 minimal force		
+ 1.00 huge force		

Table 12: AFM linescan through a nanohole covered with a suspended bilayer membrane. The lineshapes as well as the penetration depth of the tip change depending on the applied tip-force.

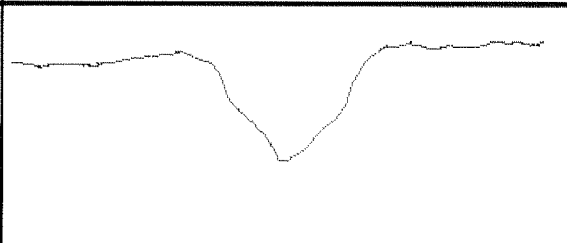
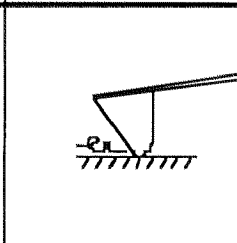
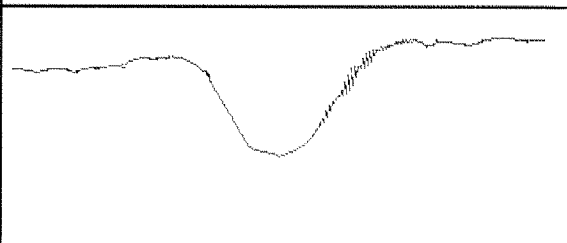
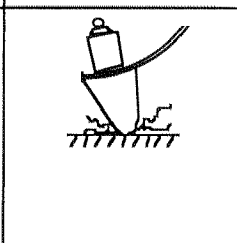
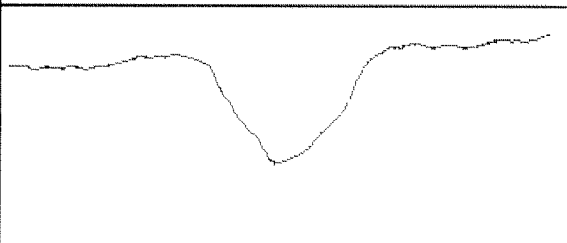
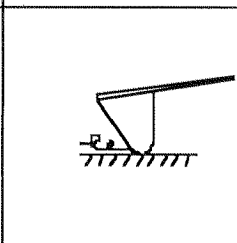
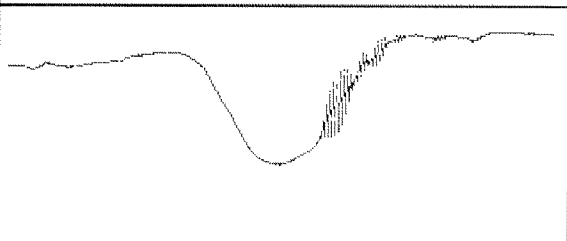
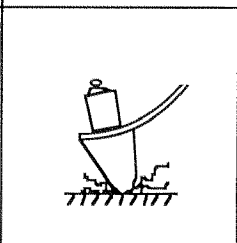
Setpoint (Tip force)	AFM linescan over a nanohole (without suspended bilayer membrane)	
- 0.45 minimal force		
+ 2.00 huge force		
- 0.40 small force		
+ 3.00 huge force		

Table 13: AFM line scans obtained on the negative control sample for the series in Table 12 (NH_3 -SAM coated nanocavity substrate without membrane): The depth of the cavity is, as expected, not a function of the tipload.

INSERTION OF PROTEINS IN BILAYERS

As already discussed in “Control of bilayer fluidity and heat induced morphologies“, we want to insert proteins into the bilayers. The supported bilayers are very useful model systems which mimick fairly well the natural environment of membrane proteins in nature. The advantage of supported membranes - compared to natural membranes, is that the complexity of the natural systems can be reduced. It is not possible (or extremely difficult) to distinguish different proteins in a natural membrane. In a supported bilayer however, with only a single or a few proteins inserted, this is possible.

Streptolysine (SLO) as a model protein

To evaluate how membrane proteins can be inserted into the supported bilayers and how the inserted proteins behave, a well-characterized membrane protein was searched for which is available in large quantities and which has a well-defined morphology. The latter is necessary to be able to easily distinguish the protein from the bilayer morphology in the AFM. Streptolysine O (SLO) fulfills these requirements. It is a toxic, pore forming protein which is produced by the bacterium *Streptococcus pyogenes* to permeabilize animal cell membranes. The 60 kD protein can be bought in huge amounts, is quite stable in buffer solutions and forms vary large pores in bilayer membranes by the aggregation of dozens of SLO monomers.

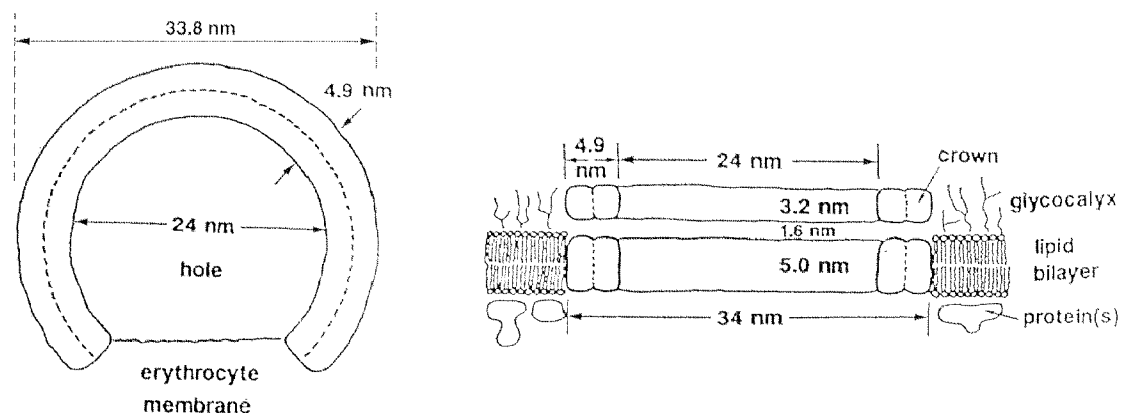


Figure 98: Structure and presumed dimensions of the streptolysine O pore in erythrocyte membranes, derived from electron micrographs. Left: Top view; Right: Section. Source: (Sekiya et al., 1993).

The quaternary structure of these pores is clearly visible in negative stained (Bremer et al., 1998) TEM images of liposomes containing the protein (Duncan and Schlegel, 1975b) and a 3-D model has been proposed based on these data (Figure 98). An SLO

pore is thought to be composed of two rings of about 22 SLO monomer units each. A closed ring-pore can have varying diameters, but usually they have a size of about 39 nm, which is extremely large compared to other membrane pores. therefore, this protein is very well suited for AFM studies. Not fully closed SLO rings seem to be stable too, being the precursors for the closed-ring pores.

A more detailed study of the SLO monomer, its tertiary structure and allosteric behavior was made by Palmer et al. (Palmer et al., 1998b, Harris et al., 1998). A crystal structure of the protein has not yet been obtained but the structure of the homologous protein *Perfringolysin O* can give a good impression of how SLO probably looks like. Figure 99 shows three 3-D views of this protein from different angles. The protein is made out of 4 domains, which are connected by thin hinges, (Palmer et al., 1998b). These hinges make large conformational (allosteric) changes possible by modification of the conformation of only a few aminoacids. The anisotropic shape of the monomer is very apparent: It is extremely flat, diametrically opposed to the globular shape of standard proteins.

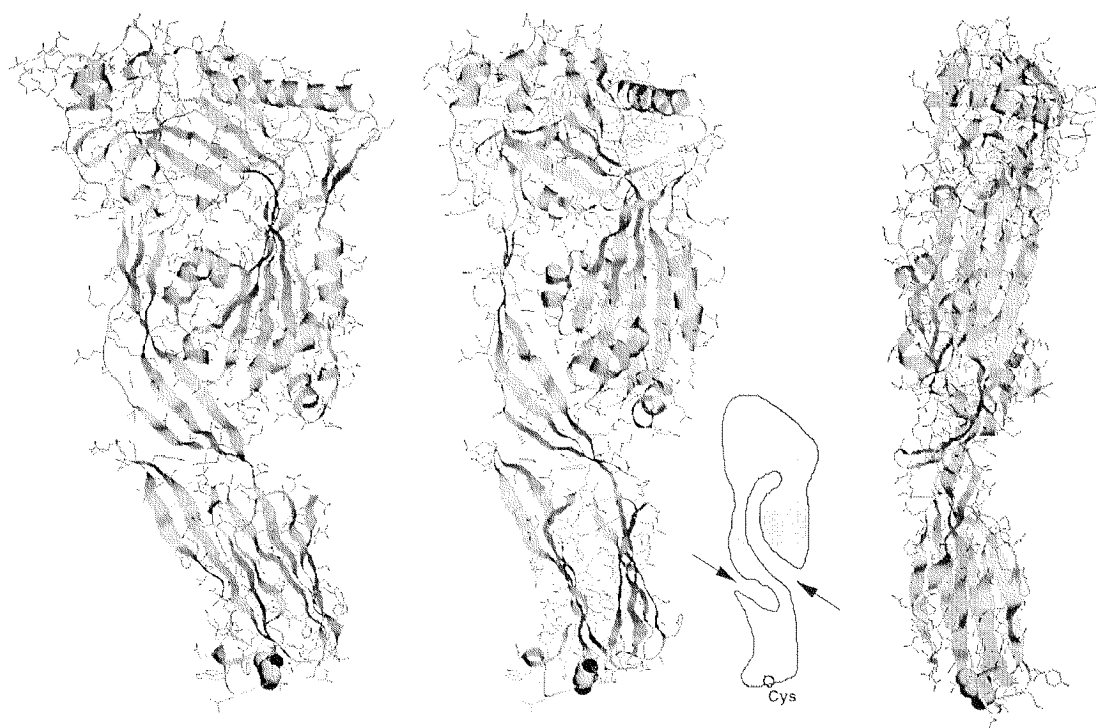


Figure 99: Three 3-D views of the SLO-homologue *Perfringolysin O* monomer from different angles (data obtained from the “Brookhaven Protein Data Bank, PDB Structures“). The protein has the shape of an elongated, very flat slice. The picture in the middle and the corresponding schematic presentation reveals the different sub-domains of the protein which are interconnected by thin, hinge-like protein chains. Also the position of the aminoacid cysteine is highlighted. A discussion of the tertiary structure of the protein can be found in (Palmer et al., 1998b).

A tryptophan-rich region in the lower end of the SLO binds selectively to cholesterol which then triggers large allosteric changes by which the protein then induces oligomerization and insertion into the membrane. It is not yet known whether oligomerization or membrane insertion takes place first. Also, the formation of a pore in the membrane has not yet completely been understood, although there is some evidence to believe that upon polymerization, the inner part of the SLO ring turns hydrophilic by which the hydrophobic bilayer is expelled from the ring-interior during ring-formation (Palmer et al., 1998a).

A scheme of an intermediate state during pore formation is shown in Figure 100, giving an idea of the proposed pore formation mechanism.

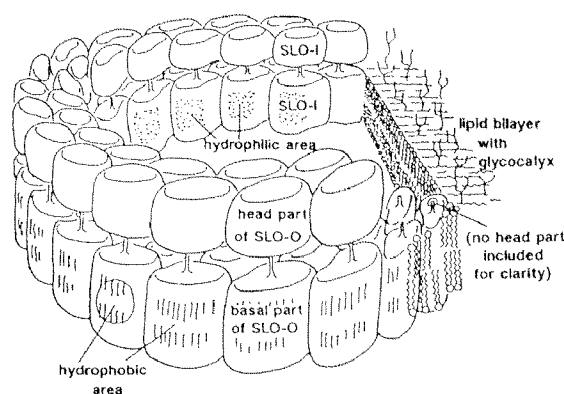


Figure 100: Schematic drawing of a SLO pore during the expulsion of the lipid bilayer. The appearance of hydrophilic domains in the interior of the pore forces the hydrophobic bilayer membrane out of the ring. Source: (Sekiya et al., 1993).

An important requirement of the SLO protein is that cholesterol is needed in the target membrane in order to allow SLO binding. Low concentrations of cholesterol in solution strongly and competitively inhibit SLO integration. Also filipin and alfalfa saponin, which both bind to cholesterol in the membrane, inhibit SLO binding (Shany et al., 1974). Besides the presence of cholesterol, SLO has to be activated by thiol-compounds like mercaptoethanol or cystein and is therefore oxygen labile (although contact with ambient air has not to be specially avoided during the experiments). At low temperatures (4°C), the SLO monomers do bind to target membranes, but no ring formation is observed. At high temperatures, on the other hand, the protein is inactivated (95°C, 10 min.). GA or OsO₄ fixation of the membrane does not influence pore formation (Duncan and Schlegel, 1975b).

For our experiments, vesicles were prepared with the lipid composition described in Duncan et al. (Duncan and Schlegel, 1975b), but the liposomes were made in the same manner as the other liposomes described in the chapter “Liposome Fusion“. Usually, the

frozen (-70°C) SLO stock solution in Tris-buffer was thawed and then activated for 30 min. at 37°C after addition of 25 mM cystein. Then, the SLO was directly pipetted into the PBS drop covering a supported bilayer membrane. In another approach, the activated SLO solution is pipetted into a solution of vesicles, which are then afterwards allowed to fuse with a substrate.

Reactivity tests

Testing the ring-structure formation capability

Prior to testing SLO on supported membranes, its aggregation capability was monitored on a suspension of our liposomes by TEM imaging of negatively stained liposomes which had been exposed to a SLO solution. SLO “pores“ can very easily be seen as rings of relatively constant radius and thickness on these preparations (Figure 101). However, it cannot be concluded from these images whether the SLO rings are only attached to the bilayer surface or if they are inserted into it. It can also not be decided with certainty, whether the pores still contain lipid or not. Liposome preparations without SLO did not show the defined round shaped membrane inhomogeneities. Two images of “negative controls“ are shown in Figure 103.

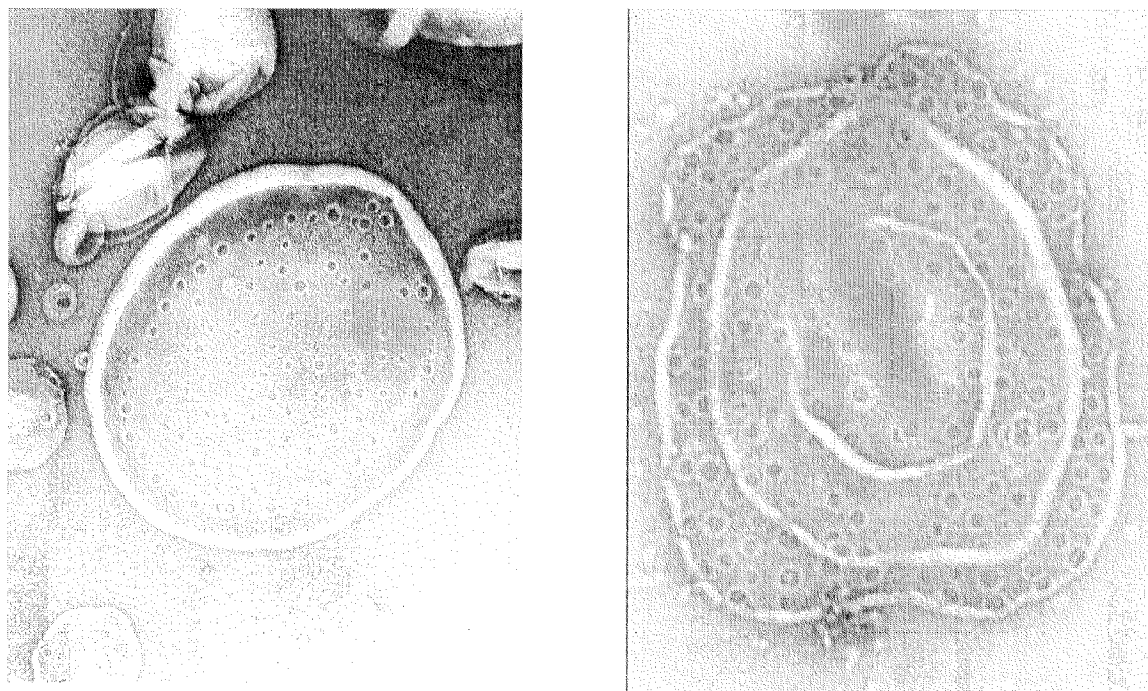


Figure 101: TEM images of several SLO pore-rings in adsorbed liposomes. These pictures are “best-of’s“ rather than the norm.

Usually, a slightly diluted vesicle-suspension was exposed to a solution of highly concentrated, cystein-activated SLO. The pore formation was allowed to proceed for several minutes to hours at 37°C or above the transition temperature of the liposomes used. Then, a carbon/PVC/Copper TEM grid was exposed to the vesicles/SLO solution for a short time, rinsed by dipping in water, heavy-metal stained in a 1% uranyl acetate (UAc) solution, and finally, after drying, directly analyzed in the TEM. Figure 101 shows two TEM pictures of adsorbed liposomes which contain several copies of SLO pore rings. The negative staining and immobilization technique had to be optimized in order to get such clean and contrast-rich images. Water-rinsing of the TEM grid after exposure to the liposome buffer solution was crucial because otherwise UAc would stain thousands of salt-aggregates on the liposomes which did look similar to dark pores in the membrane (Figure 102). As soon as this artifact was avoided, the SLO pores with their very characteristic shape were visible on the samples. Fixation of the liposomes with GA and/or OsO₄ prior to negative staining was not necessary but did in some cases give some more stable liposome preparations.

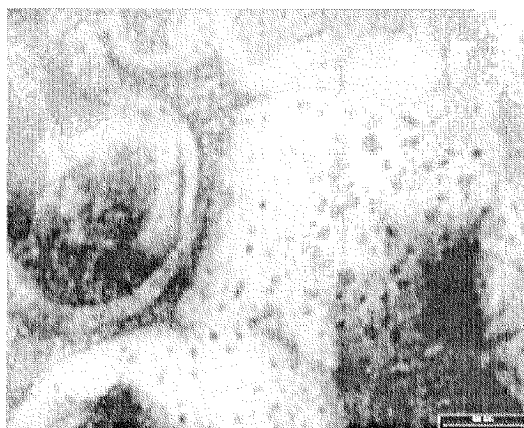


Figure 102: Pore-imitating artifacts visible on a liposome preparation due to UAc staining of buffer-salt crystals. These structures can be avoided by rinsing the TEM grids with water after the liposome incubation step.

We did follow two possible ways to incubate the SLO on the membranes. Either the liposomes were first spread on the grids - similar to the liposome fusion on the substrates discussed in chapter “Liposome Fusion” - or the liposomes were first brought into contact with the SLO, followed by incubation on the grids. Table 14 summarizes the results obtained on the different liposome fractions.

According to the data in Table 14, SLO rings inserted quite successfully into the different liposome fractions composed of PC, cholesterol, DP and a fluorophore. Very importantly, the SLO solution had to be applied in very high concentrations in order to get satisfactory formation of SLO pores.

Table 14: SLO ring-formation on liposome fractions analyzed by TEM: Experimental conditions and results. (“↑“ means, “the same conditions as mentioned in the field above“).

Nr.	Lip. fraction	Experimental conditions	TEM results
1	Lip 10	10 μ l Lip10 (1/10) + 3 μ l SLO (activated) , 38°C, 60 min.	Very few SLO rings visible
2		Lip10 (1/50) on grid/H ₂ O wash/ + 5 μ l conc. SLO (activated), 37°C, 10 min.	Very few denatured SLO rings visible
3		“↑“, but 30 min. SLO incubation.	Very few SLO rings visible
4		5 μ l Lip10 (1/20) + 5 μ l SLO (activated), 24°C, 150 min.	Quite a lot of SLO rings visible.
5		“↑“, but SLO incubation at 38°C	Some more SLO rings visible compared to at 24°C.
6	Lip12	10 μ l Lip12 (1/10) + 3 μ l SLO (activated), 46°C, 60 min.	No SLO rings visible
7		5 μ l Lip12 (1/20) + 5 μ l SLO (activated), 24°C, 150 min.	No SLO rings visible
8		“↑“, but SLO incubation at 44°C	Quite some SLO rings visible.
9	Lip13	10 μ l Lip12 (1/10) + 3 μ l SLO (activated), 54°C, 60 min.	No SLO rings visible
10		5 μ l Lip12 (1/20) + 5 μ l SLO (activated), 38°C, 150 min.	No SLO rings visible
11		“↑“, but SLO incubation at 55°C	No SLO rings visible
12	Lip14	Lip14 (1/20) on grid/H ₂ O wash/+ 5 μ l conc. SLO (activated), 37°C, 10 min.	Very few, (denatured?) SLO rings visible. No liposomes visible.
13		5 μ l Lip14 (1/20) + 5 μ l SLO (activated), 37°C, 30 min.	Very few SLO rings visible. Liposomes are very small.
14		“↑“, but Lip14 diluted (1/200)	Some more SLO rings visible.
15		“↑↑“, but shaking during SLO incubation	Quite some SLO rings visible.
16	Lip15	Lip15 on grid/H ₂ O wash/+ 5 μ l conc. SLO (activated), 40°C, 30 min.	Many SLO rings visible.
17		5 μ l Lip15 (1/20) + 5 μ l SLO (activated), 37°C, 120 min.	Many SLO rings visible
18		“↑“, but Lip15 diluted (1/500)	Few liposomes but fully covered with SLO rings.
19		15 μ l Lip15 (1/20) + 15 μ l SLO (activated), 37°C, 330 min.	Some SLO rings visible in very large liposomes.

20	Lip16	Lip16 on grid/H ₂ O wash/Tris/+ 10 μ l conc. SLO (activated), 37°C, 456 min./GA + OsO ₄ fix. Sample was never dried before fixation !	Few liposomes but fully covered with SLO rings. (Figure 104, right).
21		15 μ l Lip16 (1/10) or (1/30) + 15 μ l SLO (activated), 37°C, 330 min.	Some SLO rings visible
22		5 μ l 100 μ M cholesterol + 5 μ l SLO (activated), 37°C, 180 min.	No SLO rings visible

Compared to cells as SLO targets, liposomes are much smaller and therefore a much higher SLO concentration is needed in order to obtain that enough SLO monomers inserted in each liposome to create a pore. Very interestingly, it often was observed that within one liposome sample, many vesicles did not contain any rings, while a few others contained many. This could be explained if the SLO membrane-binding kinetics are very fast, such that the few liposomes which come first into contact with the SLO solution take up all the protein, not leaving any for the other liposomes. According to measurements with erythrocytes, the binding kinetics is indeed very fast (see next chapter).

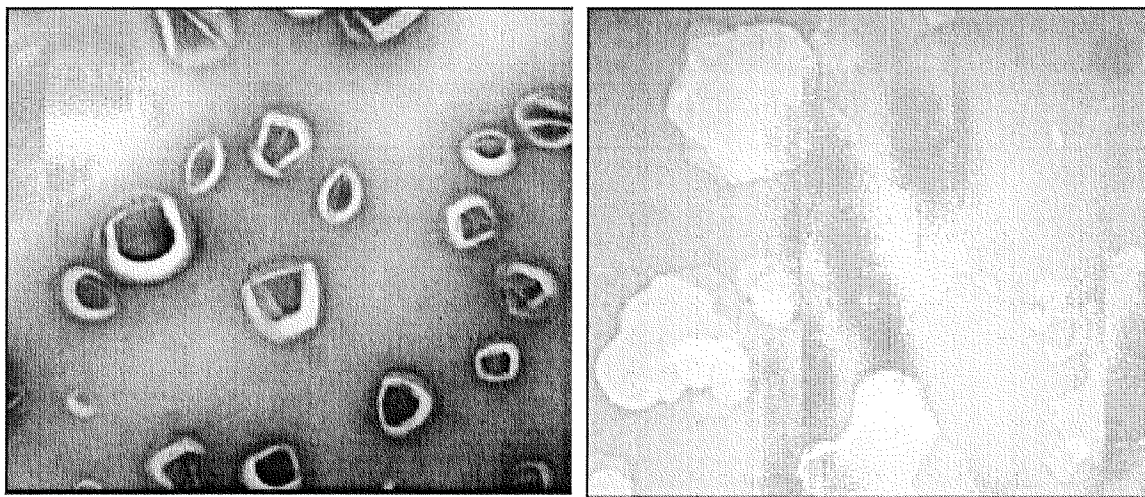


Figure 103: TEM image of negatively stained, non-fused (left) and fused (right) vesicles without SLO on a carbon grid

Both large unilamellar vesicles (LUVs) prepared according to the standard preparation technique in this thesis as well as those prepared by simple sonication, were equally accessible to pore formation. But, for the creation of supported bilayers, the latter proved much less useful as discussed in chapter “Behavior of liposomes obtained by vortexing and sonication: Multiwalled vesicles“. A reduction of the amount of liposomes exposed to the same SLO activity leads to larger amounts of rings per liposome, which in extreme cases can even lead to liposome ghosts of which the hole surface area is covered with SLO (Figure 104, right).

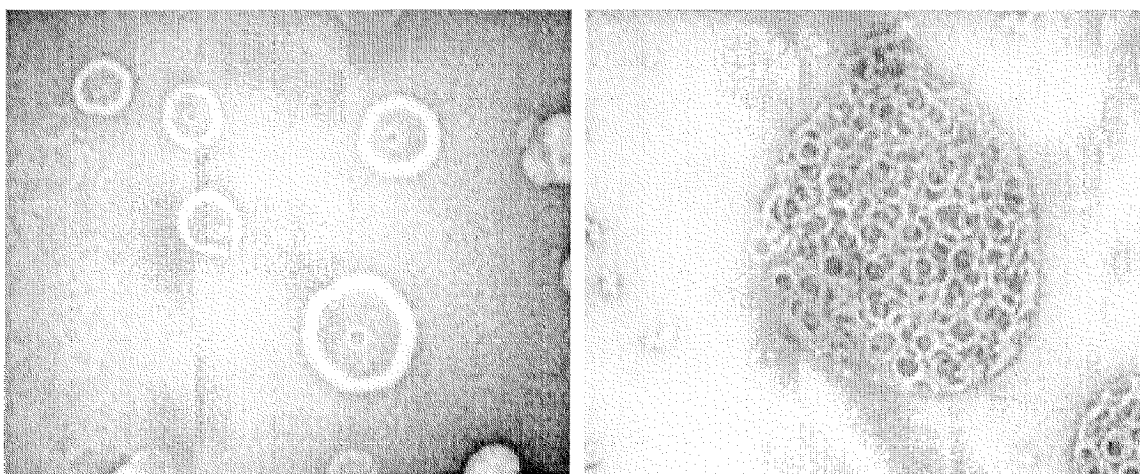


Figure 104: Left: TEM image of negative stained liposomes containing one SLO pore each. Right: Vesicle with a maximal density of pores resulting from an incubation with locally very high SLO/vesicles ratios.

On the other hand, in this case, also only very few vesicles are available for the creation of a homogeneous, interfused bilayer on the substrate leading to rather single, adsorbed liposome patches. Shaking during SLO incubation also leads to some improved SLO integration.

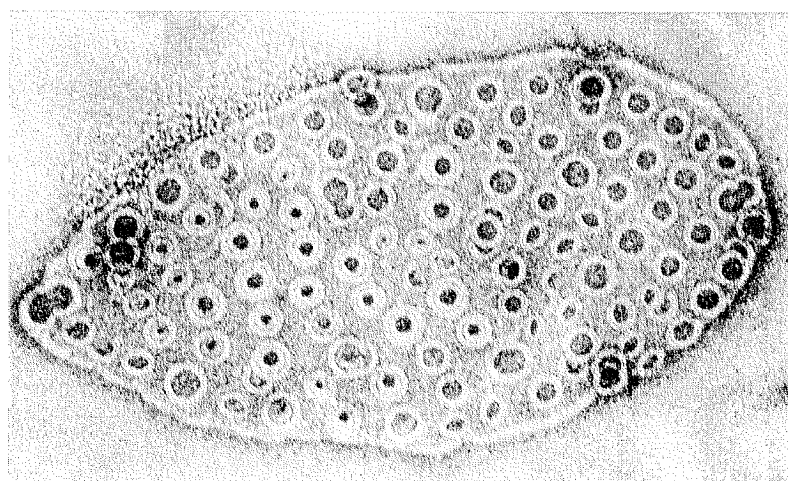


Figure 105: Large, spread liposome fully covered with SLO holes including some double-walled specimens.

Integration of SLO was only observed if the incubation temperature was above the T_c of the liposomes. E.g., In the Lip12 vesicles with a T_c of about 35°C , no SLO rings were observed at room- temperature, but at 45°C , rings did form. In liposomes with even higher T_c (Lip13, T_c of about 45°C), SLO neither integrated at 38°C nor at 55°C . Probably, 55°C is simply too hot for the biological activity of SLO or the cholesterol content of these liposomes was too low. In the “normal“ liposomes with a T_c far below

room temperature, an increased pore formation was observed at 37°C compared to room temperature.

Testing the pore-formation capability

The TEM experiments performed above can show whether a certain liposome fraction is accessible to SLO ring formation and under which conditions (temperature, concentration) this is the case. On the other hand, these images cannot really prove whether the formed SLO rings are really pores or just SLO sitting on top of the membrane. This cannot completely be excluded, as it is not yet known, how the integration and assembly process takes place and very surprisingly, SLO ring formation was also reported in the absence of lipid, on cholesterol dispersions (Duncan and Schlegel, 1975b). However, huge amounts of cholesterol seem to be necessary for such a behavior, as we could not detect any rings in the TEM in a similar experiment using more standard cholesterol concentrations (see Table 14, line 22).

An assay which really tests the pore formation capability of SLO in a membrane is based on the use of red blood cells (erythrocytes, EC) (Duncan and Schlegel, 1975a). These cells contain huge amounts of the red-colored hemoglobin which can only escape from the cells if these are injured. Another important remark is that the cells contain an amount of 28 % cholesterol, which makes them good targets for testing the SLO activity. We performed this experiment to test the influence of the cystein-activation and the incubation temperature on the pore forming capability of SLO.

For the preparation of the EC's, fresh human blood was collected and immediately centrifuged. The coagulated fibrin-clot was removed with tweezers and the supernatant discarded. The blood-cell pellet was then washed three times with buffer solution (PBS pH 7.4) and then stored at 4 °C. Non-activated and activated SLO solutions were then added to the fresh erythrocyte preparation and incubated at room temperature or 37°C respectively. The SLO was allowed to permeabilize the cells during several hours, after which the cell suspensions were centrifuged again and the absorption of the red color in the supernatant was measured at 540 and 575 nm - the main absorption bands of hemoglobin. Figure 106 shows the absorption measured for the different preparations which give a good illustration of the pore formation capabilities of the SLO in the different samples.

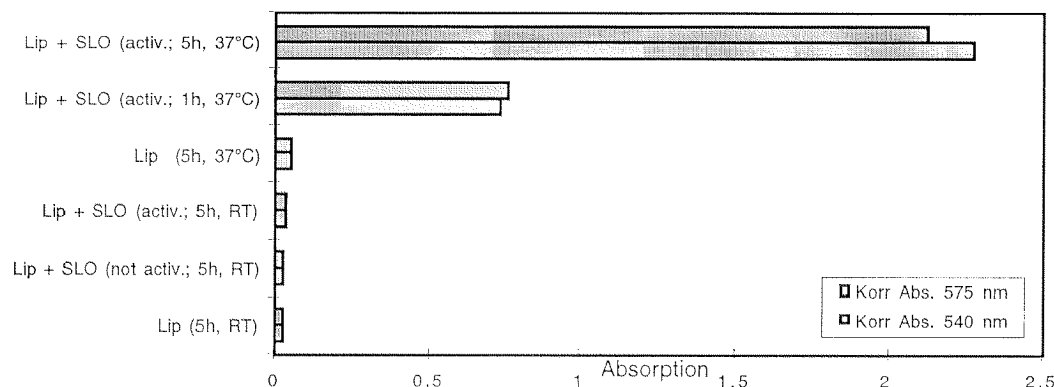


Figure 106: SLO activity test using erythrocytes as target cells. 30 μ l of a fresh erythrocyte suspension in PBS pH 7.4 was exposed to 75 U (activated and non-activated) SLO. The permeabilization of the EC's was allowed to proceed at room temperature or at 37°C for the time indicated. The suspensions were then centrifuged and the amount of hemoglobin in the supernatant determined by measuring the absorbance at 540 and 575 nm.

Very interestingly, neither non-activated nor activated SLO permeabilizes the cells at room temperature. By increasing the incubation temperature to 37°C, an about 200-fold increase of lytic activity is detected. It is therefore very important to perform membrane incubations with SLO using activated toxin and at elevated temperatures.

Duncan et al. reported in their paper (Duncan and Schlegel, 1975b), that no escape of internal Markers was detected if liposomes containing K_2CrO_4 or glucose were exposed to SLO. The authors make the lipid composition responsible for this behavior, which is not the same as in erythrocytes. The nature of liposome lipids may not allow the pore to open, despite the fact that SLO rings were observed in the TEM on these liposome fractions. In our opinion, this observation could be explained more easily, if multiwalled- instead of unilamellar - vesicles were used by Duncan et al. In this case, of course, no escape of the markers would be observed, even if the outermost membrane contains opened pores. It is further therefore very unlikely that the SLO is unable to form opened pores in the liposome lipid membrane, because on high-resolution TEM images, sometimes the missing bilayer within the boundaries of the protein ring could be seen (see Figure 107). In the negative stained picture shown, even the expulsion of the membrane out of a half-moon pore is visible, in agreement with the pore-formation model proposed in Figure 100. Therefore we conclude that there is strong evidence that opening of the pores is also possible in lipid membranes composed of non-natural lipid compositions.

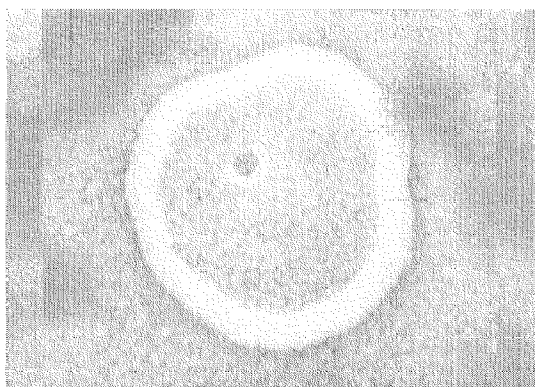


Figure 107: TEM image of a single SLO pore in a small, supported vesicle. The lack of membrane within the pore is clearly discernible. Compare this negative stained sample with the scheme in Figure 100.

The liposomes used by Duncan et al. were produced by the sonication method. This procedure leads to vesicles with very large size distributions and often, multiwalled vesicles are obtained. It is therefore very possible that the above mentioned problem did arise. An attempt was made to repeat the permeabilization experiment on our freeze-thawed and extruded (unilamellar) vesicles containing K_2CrO_4 or glucose. Unfortunately, these internal markers had already escaped from the liposomes before the experiment could be started, and with the remaining amount of internal markers, no meaningful test-results were obtained.

Insertion of SLO in a supported bilayer

In a next step, the insertion of SLO in a homogeneous, flat and fluid bilayer including cholesterol was investigated. These experiments on non-suspended bilayers were made in order to get a feeling for this toxin and to learn about the AFM resolution which can be achieved on the SLO pores. The presence of the inorganic SiO_2 support directly behind the bilayer membrane (probably separated by a 0.3 nm water layer) was expected to interfere with the protein dynamics within the membrane and thus with the aggregation and pore formation of SLO - if the pore-aggregation takes place within- and not on the membrane. On the other hand, according to the TEM model presented in Figure 98, the SLO does not seem to have large extramembraneous domains on the membrane side adjacent to the insertion direction, for which there was a chance that pore formation would work all the same. This approach was made to collect data about the behavior of SLO on these standard supported bilayers in order to be later able to compare the results with the SLO integration into free-suspended bilayers spanning the nanohole architectures developed in this dissertation.

For most of the experiments, firstly a lipid bilayer membrane was produced on a SiO₂ substrate glued onto a glass/PTFE holder as already described. After LSM verification of the bilayer integrity and fluidity, if needed, further purification steps to remove excess amounts of adsorbed, non-fused vesicles were made. Then, the distilled water on the bilayer was exchanged by SLO incubation buffer (usually PBS pH 7.4 or SLO-Tris), and then diluted or concentrated, activated SLO solutions were added and incubated at different temperatures for minutes or hours. The samples were then rinsed with fresh incubation buffer to remove non-bound toxin, sometimes followed by water rinsing. In most of the cases, the sample was fixed with GA and/or OsO₄ in order to stabilize the system for ulterior AFM imaging. Due to the high stability of the bilayers, the samples could be measured over several days and the buffer, fixation or temperature conditions could be varied in between AFM measurements. Due to the specially designed glass/PTFE sample holder, the membranes could be moved back and forth between the LSM and the AFM, giving the possibility to control the integrity of the bilayer at any stage of the experiment. The sample was never dried during the entire process. However, it must be said that - due to the fact that very small liquid volumes had to be handled and up to 30 liquid exchange processes had to be performed on one and the same sample - at the beginning 6 of 10 and later 1 of 10 samples accidentally dried on average.

As in the precedent chapters, a table summarizing the most important experiments and results is first presented, followed by a discussion.

Nr.	Liposomes used to produce bilayer	LSM of the bilayer	Experimental conditions: SLO added
		Results	
23	Lip5 (NBD-PE)	very homogeneous fluid	50 µl SLO act. in 100 µl SLO-TRIS, room temperature, 30' glutaraldehyde fixation (1%, 60')
		AFM: Extremely flat (Ra=0.1 nm) + clean surface. Small holes in the bilayer with Ø ≤ 40 nm. Depth: 1 nm. Deterioration after OsO ₄ fix. (25').	
24	Lip7 (BODIPY)	homogeneous liposomes, fluid	10 µl SLO act. in 100 µl SLO-TRIS, room temperature, 30' glutaraldehyde fixation (1%, 70')
		Bilayer covered with undefined objects After OsO ₄ fixation, some nice SLO rings visible.	

26	Lip7 (BODIPY)	homogeneous liposomes fluid	+	10 μ l SLO act. in 100 μ l SLO-TRIS, room temperature, 30' glutaraldehyde fixation (1%, 70'), OsO ₄ fixation (30')
Bilayer very flat (Ra=0.11 nm) but undef. objects on the surface which can be removed by the Tip, leading to 3.5 - 4 nm deep holes in the bilayer. After additional glutaraldehyde fixation (120'), no change, no rings.				
27	Lip7 (BODIPY)	homogeneous filaments; fluid	+	10 μ l SLO act. in 100 μ l SLO-TRIS, room temperature, 30' SLO incubation for 215', 36°C. glutaraldehyde fixation (1%, 120')/OsO ₄ fix.
AFM: Bilayer flat, containing undef. objects. 12 h later with hydrophobic tip: Very nice, thin filaments cover the substrate (see Figure 79).				
29	Lip8	homogeneous some large liposomes, fluid.	+	10 μ l SLO act. in 100 μ l SLO-TRIS, room temperature, 60' glutaraldehyde fixation (1%, 70'), OsO ₄ fix.
AFM: Stiff bilayer with 5 nm high, round shaped lipid-islands on bilayer. No SLO visible.				
31	Lip 10 and 12 and 13, T>Tc	homogeneous some liposomes, fluid.	+	10 μ l SLO act. in 100 μ l PBS pH 7.4, 42°C, 345'.
AFM: Bilayer flat containing \pm 5 nm deep, large holes due to the thermal treatment. Undefined objects and some small holes. After glutaraldehyde fixation and/or OsO ₄ : No significant change. Surface still containing objects and holes.-				
42	Lip16 (extruded)	homogeneous some liposomes, fluid.	+	A: 50 μ l SLO act. in 50 μ l PBS pH7.4, 39°C, 240' then room temperature, 10 h. B: 20 μ l SLO act. in 50 μ l PBS pH7.4, 39°C, 120'. No fixation in both cases.
Many and very nice SLO rings cover the hole surface in both preparations ! \emptyset -Reference: Very flat and clean bilayer surface.				
43	Lip16 (extruded)	No data.		A: 15 μ l SLO act. in 50 μ l PBS pH7.4, 40°C, 120'.
A few very nice and extremely sharp SLO. \emptyset -Reference: Very flat and clean bilayer surface (Probe A). After highsalt-wash (60', NaCl 1M): Extremely strange Bilayer aspect: Surface very clean (No more SLO visible), but homogeneously distributed large (250 nm \emptyset) hole-like depressions. After glutaraldehyde and OsO ₄ fix. : Very contaminated surface due probably to glutaraldehyde polymerization products.				

45	Lip16 (extruded)	homogeneous some liposomes fluid.	+ A: 12.5 μ l SLO act. in 50 μ l PBS pH7.4, 37°C, 2.5 days.
		AFM: flat bilayer with some holes in the bilayer. No SLO visible	

Topography of SLO inserted in the bilayer

Supported bilayers which have not been exposed to SLO (the control/reference samples) in case of a successful spreading did not show any features or topography on the contact-mode AFM images obtained under buffer solution. A roughness (R_a) for these substrates of 1.1 nm over surface areas of several microns was reproducibly found. This is flat enough to be able to distinguish 0.3 nm objects which rise above the bilayer or holes of the same dimension in the bilayer. Often, however, less optimal background topographies were encountered, due to the presence of non-fused vesicles which, because of their softness, were disturbing the scanning tip, making it impossible to achieve SLO resolution. Upon OsO_4 fixation, these liposomes converted into more stable, flat, bilayer thick islands (see Figure 91) which interfered less with scanning, but still reduced the possible resolution. A further source for surface contamination, which made it impossible to resolve SLO were the strange filamentous structures shown in Figure 79. When such structures were present, SLO rings were never seen in the bilayers, for which they probably also negatively influenced the scanning.

The topographies obtained for SLO attached to or inserted into a bilayer were manifold. The very first insertion experiment - for which no control sample was measured - gave very promising results: AFM images of the bilayer exposed to SLO showed a very flat surface with occasional, small holes in it with diameters ranging from 25 to 55 nm (Figure 108)- which is in good agreement with SLO ring diameters observed in TEM studies. No such small holes have ever been observed before in a supported bilayer preparations without SLO, which is a strong evidence, that we were not dealing with bilayer artifacts. No large domains rising above the membrane plane were observed, something which would not be expected according to the SLO model proposed in Figure 98. The same experiment repeated (using vesicles containing the fluorochrome BODIPY instead of NBD-PE) revealed a very contaminated surface after GA fixation with non-stable objects being smeared over the surface during AFM scanning. Fixation of the membrane with OsO_4 , which crosslinks the unsaturated fatty-acid chains, led to the appearance of ring-like structures rising above the membrane in between of some

other aggregated objects in which no ultrastructure could be observed. On average, these rings rose 2.9 - 5.3 nm above the bilayer and had an outer diameter of 39 - 65 nm.

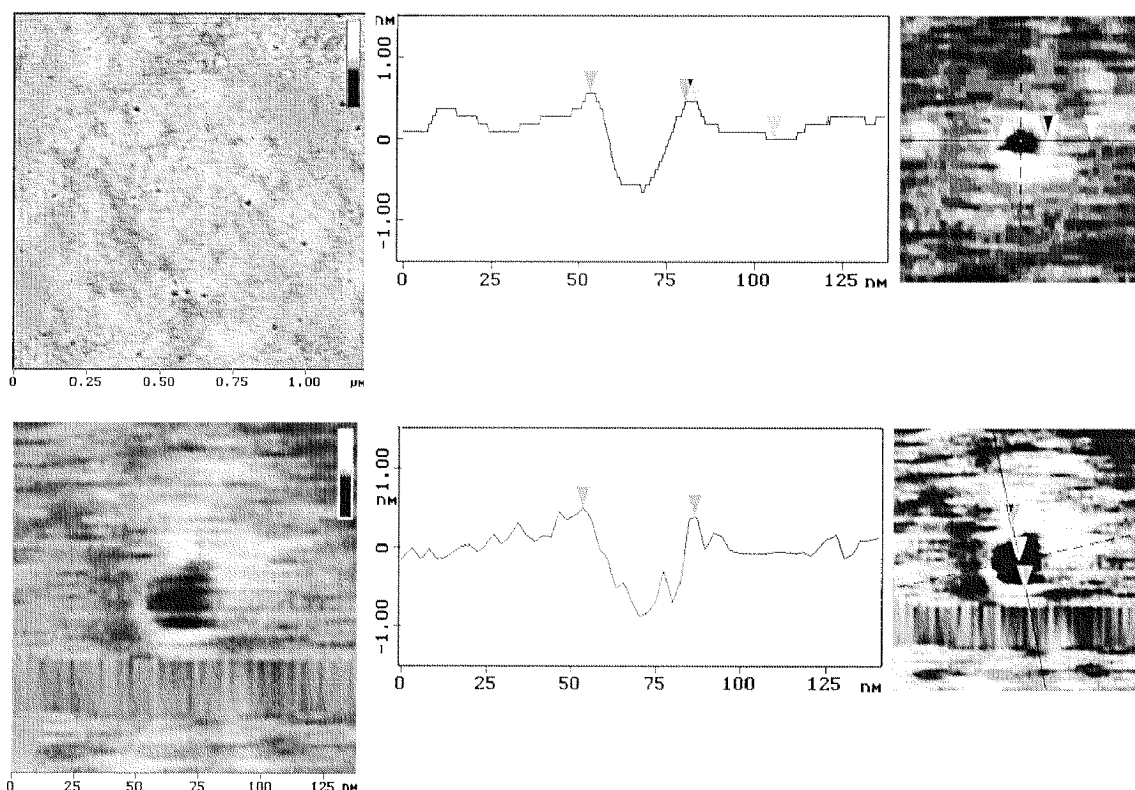


Figure 108: Round-shaped pores with the right dimensions for SLO rings in a supported Lip5 bilayer on SiO₂. The interior of the pores seems not to contain lipid, but the AFM tip can nevertheless not reach the SiO₂ substrate because it is not sharp enough to penetrate the SLO.

In addition to the good agreement of these dimensions with those expected by the SLO model, no such structures were observed on a bilayer not exposed to SLO, which are good indications that these structures corresponded to SLO rings. The expected height for the SLO is 9.8 nm (see model). In our case we observed on the maximum 5.3 nm high structures for which it must be assumed, that indeed the observed SLO is inserted in - and not only lying on - the surface. Very interestingly, the GA fixed SLOs were extremely mobile on the surface prior to the OsO₄ fixation (due to unhindered surface diffusion; making AFM imaging impossible) or the OsO₄ additionally stabilized the protein. So, the mobility of the protein seems not to be completely restricted in the presence of the SiO₂ substrate just below the bilayer.

We then performed experiments to test the influence of the fixation methods on the AFM scanning results: When the bilayer was only fixed by OsO₄ and not with GA after the SLO incubation, very soft but locally immobilized structures were observed which

could easily be removed by the scanning tip, leaving small holes in the bilayer of a depth of 3.5 - 4 nm and diameters ranging from 50 to 200 nm.

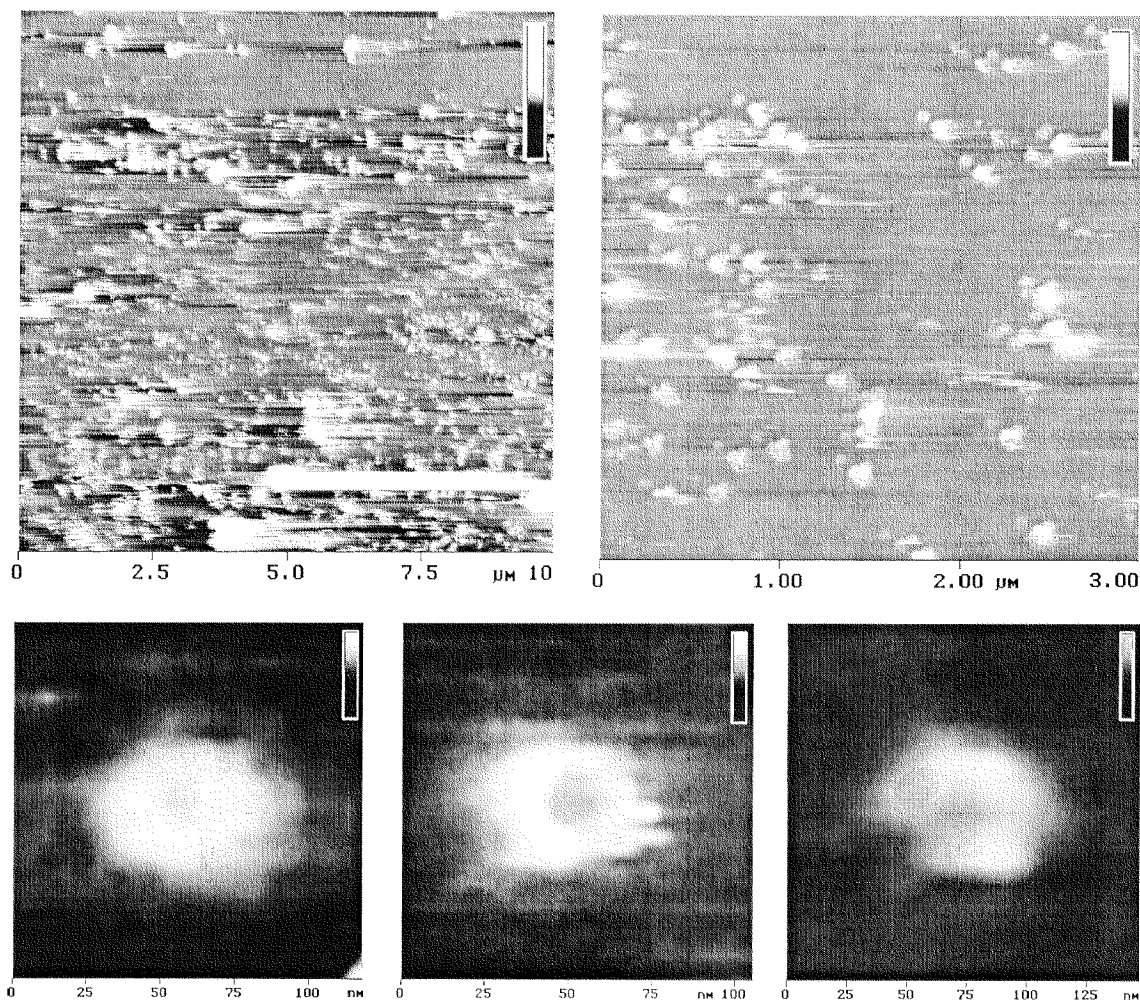


Figure 109: AFM images in water of a Lip7 supported bilayer exposed to SLO. Top, left: GA fixed sample after intensive washing with water. Undefined, globular structures are visible, attached to the bilayer which are partially swept away by the AFM-tip. Top, right: Same substrate after additional fixation with OsO_4 . Between larger structures, very clearly, small ring-like structures are now visible. The three images at higher magnification of single pores, below, reveal the well expected circular- or semicircular - structure for SLO.

Most probably, this phenomenon can be explained by soft and to some extent sticky, nonfixed SLO rings or ring aggregates being removed by the AFM tip out of a crosslinked, stiff bilayer membrane. Additional GA fixation did not lead to a better resolution on the structures observed. Maybe SLO needs to be stabilized first in order to withstand an in-plane bilayer pressure caused by the OsO_4 crosslinking process.

Very opposed to these results, on a bilayer produced using Lip16 vesicles (the liposomes were sonicated prior to freeze-thawing and extruding), nice images of SLO rings covering the hole of the bilayer were obtained without any fixation (Figure 110, top, right). In the LSM, however, also these supported membrane showed to be in a fluid state for which the sharp images of the SLO rings could only be explained assuming a model in which the protein-rings are strongly attached to the SiO_2 surface but embedded in a fluid bilayer membrane. To our surprise, at non-minimal scanning forces, the SLO rings could be moved around on the surface indicating either a weak binding to the substrate (and good mobility within the bilayer) or indicating that the SLO were only attached to the bilayer instead of being inserted into it. The measured height of the rings standing out from the membrane was 4-6 nm, better compatible with the membrane inserted model. If the “SLO attached to the membrane“ model is assumed, then - due to the mobility of the membrane - no stable imaging of the SLO should be possible as the diffusion of the proteins could not be restricted by anything. At the end, careful analysis of the SLO shapes gave evidence that the observed SLO rings were probably attached to the AFM tip instead of being on or in the bilayer. This effect, known as “tip-artifact“ and being recognizable by a repeated appearance of the same pattern in a very same orientation on AFM images (Figure 110, bottom), was very badly visible in this case. When this assumption is true, something quite sharp - and at higher scanning forces mobile - extending from the bilayer must have existed which was responsible for imaging the SLO on the tip. As nothing other than SLO, liposomes and buffer solution were present in our experimental setup and the same behavior was observed on membranes glued onto a completely different glass support, most probably membrane integrated SLO (or fractions of it) did image the SLO on the tip. The fact, that the observed height of the rings is equivalent to the expected height for a membrane integrated SLO supports this theory (Figure 110, middle, scheme). Changing the tip did not help getting rid of the attached SLO's, because immediately after a very short scanning times, new SLO (obviously stemming from the bilayer surface) attached to the new tip. A strong interaction between the tip and the SLO was already assumed in a previous experiment due to the observation that the tip was readily able to pull SLO out of a OsO_4 fixed bilayer. After washing the aforementioned samples with high-salt solutions (1 M NaCl, 60 min., room temperature), no more SLO rings could be seen on the surface, but very strange, 100-300 nm large areas of a changing depth depending on the applied load were observed. These areas had a maximal depth of 2,5 nm at minimal load. At strong applied forces between the tip and the surface, the areas were hardly visible. Probably half of the bilayer was removed during high-salt washing and maybe the large holes are due to areas where SLO was previously sitting on the SiO_2 . Summarizing, it is quite unclear what happened.

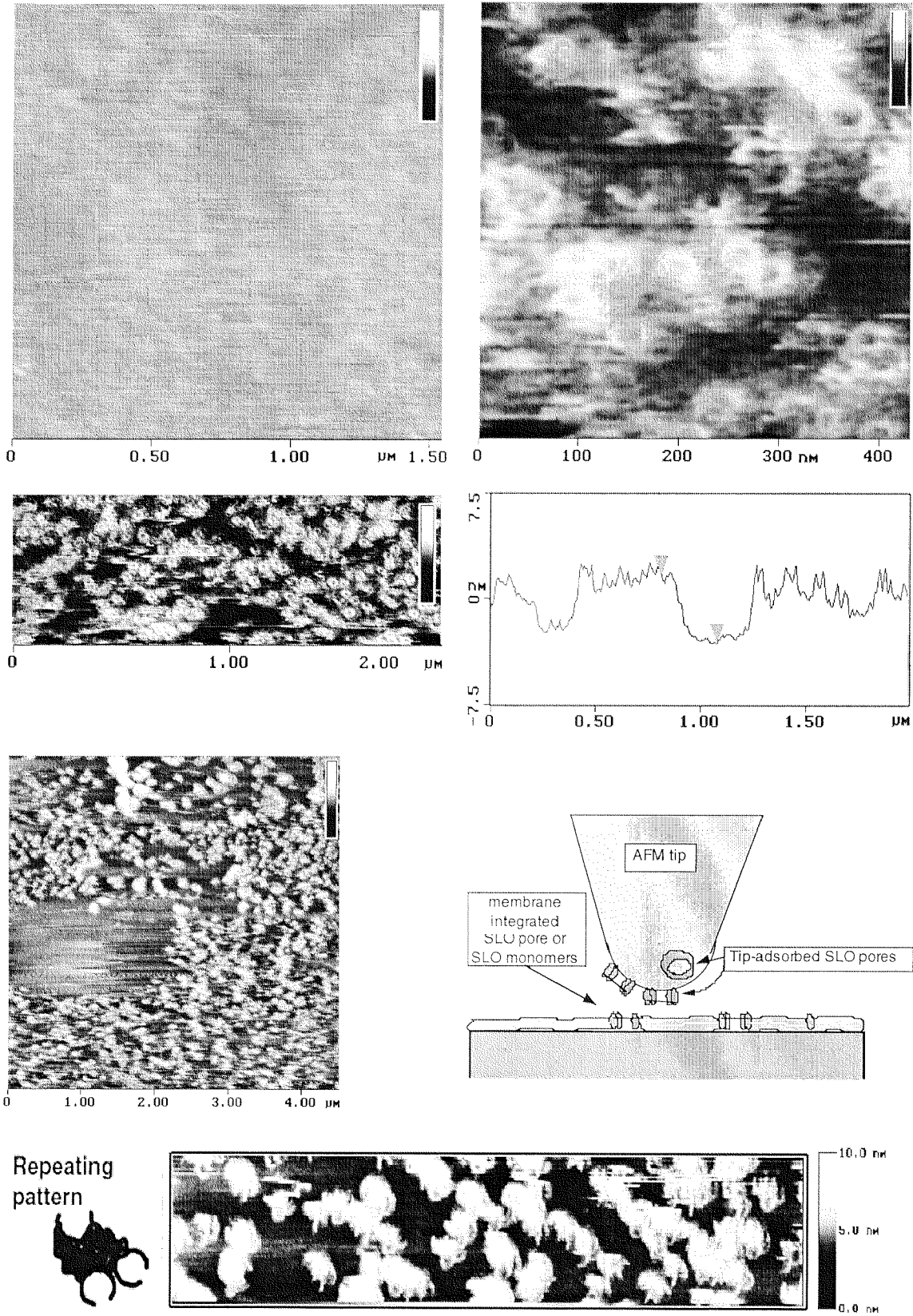


Figure 110: (Previous page) SLO pores imaged by AFM in water in a supported Lip16 bilayer on SiO₂. Top, left: Negative control showing the flat and homogeneous bilayer which had not been exposed to SLO. Top, right: Bilayer after SLO incubation. Round pores cover nearly the hole of the surface. A section of the image is shown below. On the detail shown in the bottom, clearly visibly, a tip artifact is responsible for the multiple pores which are imaged. These structures can either be explained assuming SLO pores being attached to the tip of the AFM (see scheme), or assuming a tip with multiple asperities. Left of the scheme in the large scale AFM image, it can be seen that the SLO pores are not strongly attached to the substrate (or that they are very mobile in the membrane), for which they can be swept away by the tip at higher scanning forces.

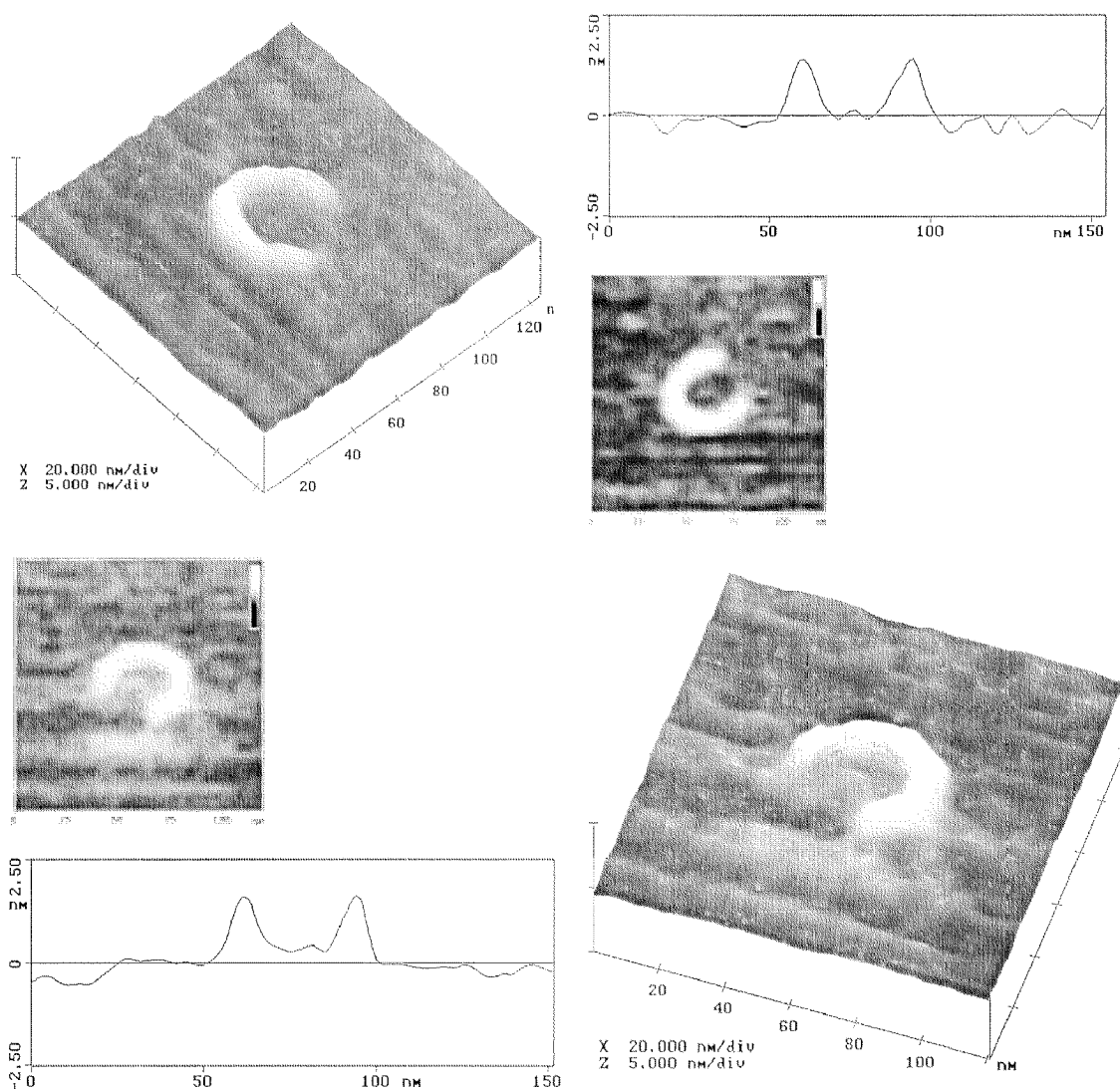


Figure 111: AFM images of two selected, well-resolved, native SLO pores in a Lip 16 supported bilayer. The sections through the images show that these pores did still not expel the bilayer membrane from their interior.

The best resolved topographical AFM images of native SLO pores in a Lip16 bilayer are shown in Figure 111. The pore-rings had an outer diameters of 41 nm and a height above the membrane of 1.7 nm. In contrast to the images shown before, these pores

seem to still contain a lipid bilayer in their interior, which may be the reason for their high structural stability leading to good AFM resolution. These images show that a reasonable resolution for structural and protein-interaction studies can be obtained on single protein pores inserted in a supported membrane, without fixation.

For a reason which is not yet understood, bilayers prepared using sonicated (and then freeze-thawed and extruded) vesicles behave differently from those prepared using standard liposome preparations. SLO inserts into standard supported membranes and it even seems to be free to diffuse within the membrane, although very high concentrations of SLO are needed. For good AFM imaging, the proteins have to be fixed with GA followed by fixing the bilayer with OsO_4 . SLO in the unfixed state strongly adheres to the AFM tip which makes it necessary to carefully check whether a SLO in the membrane or a SLO attached to the tip is imaged. On “sonicated vesicles” bilayers, there is some evidence to believe that SLO also inserts into these membranes but at the same time it can more easily be removed from it.

Insertion of SLO in a bilayer before bilayer formation

The very sharp images of liposomes containing SLO obtained with the TEM (see Figure 104 and Figure 101) suggest to use the same preparation procedure for the AFM. Namely to expose the liposomes to SLO before they are spread on a substrate. However one has to keep in mind, that such beautifully spread liposomes containing many copies of SLO rings were rather the exception. Most often, the liposomes did not fuse on the substrate but were attached in a collapsed state. Furthermore, SLO in bilayers formed by preincubation of the toxin has an inverted orientation (see Figure 112).

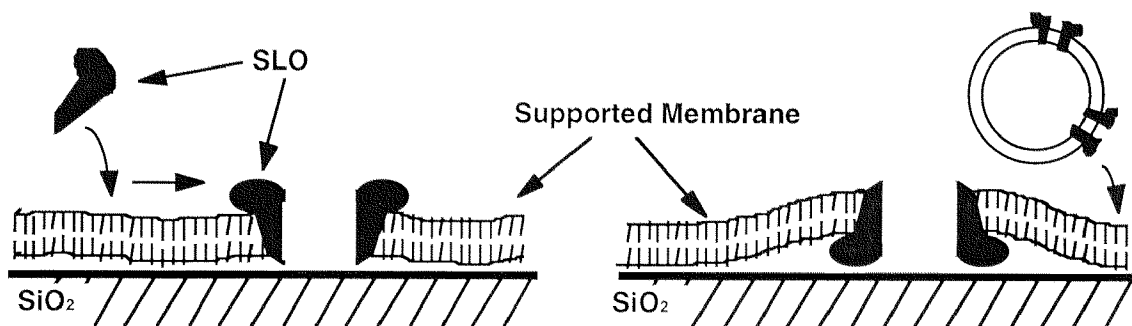


Figure 112: Scheme of the SLO pore orientation in supported membranes. Left: Insertion of the SLO after the membrane formation. Right: Insertion of the SLO into the liposomes prior to liposome fusion onto the substrate.

Using high concentrations of (SLO preincubated) liposomes and allowing them to adsorb on the well known SiO_2 substrate, we hoped to be able to form a homogeneous

and flat bilayer membrane, easily accessible for AFM experiments. But there were two reservations: Liposomes containing SLO pores cannot be induced to fuse using distilled water, as no osmotic pressure can be built up across their membrane. Further will the same problem arise as we already encountered when preparing the samples for the TEM: The higher the concentration of the liposomes, the fewer SLO rings will be formed - and - the lower the liposome concentration, the fewer liposomes will be available for the attachment to the surface. For the formation of a bilayer, large amounts of liposomes are needed (Figure 113).

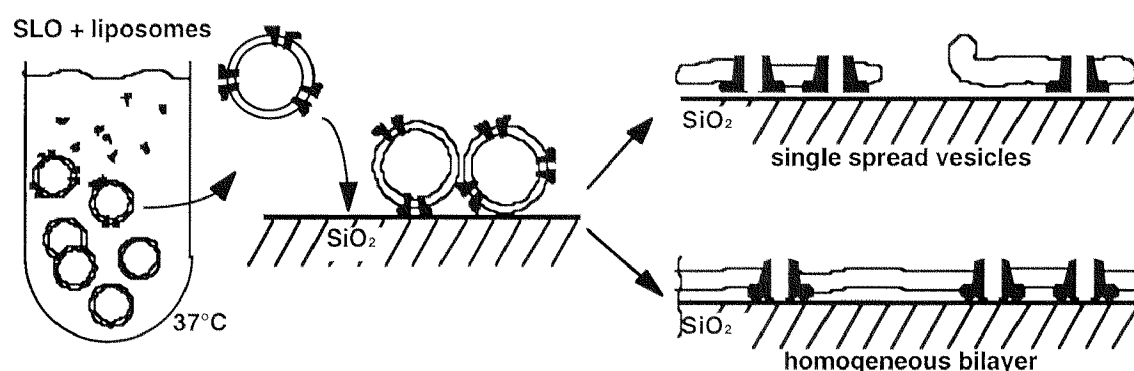


Figure 113: Formation of a supported bilayer with liposomes which have been pre-exposed to SLO.

The general procedure in these experiments to overcome the problem mentioned above was to incubate diluted solutions of liposomes with huge amounts of activated SLO. After a few hours at 37°C, this solution was then added to freshly piranha-treated SiO₂ substrates. The samples were rinsed with distilled water after an incubation time ranging from 2 to 10 hours. Subsequently, they were analyzed in the LSM and then in the AFM.

The first observation made on samples after the immobilization of liposomes containing SLO was, that while there was fluorescence on the SiO₂ substrates, no recovery could be observed after photobleaching. This did not change even after incubation of these samples for 10 hours at 40°C. In the AFM, many unfused liposomes could still be observed. Images of these substrates revealed the presence of mostly individual, only partially fused liposomes on the surface. Only very few liposomes had fused together leading to membrane patches of larger size. Very interestingly, the height of flat areas of these membrane patches was only 3.3 nm.

In a similar, but different experiment, somewhat larger membrane patches were observed, but the areas between these patches were very rough, as if the SiO₂ substrate

was covered with something between the membrane patches. Here, the thickness of the membrane-like areas was only 2.6 nm (Figure 114).

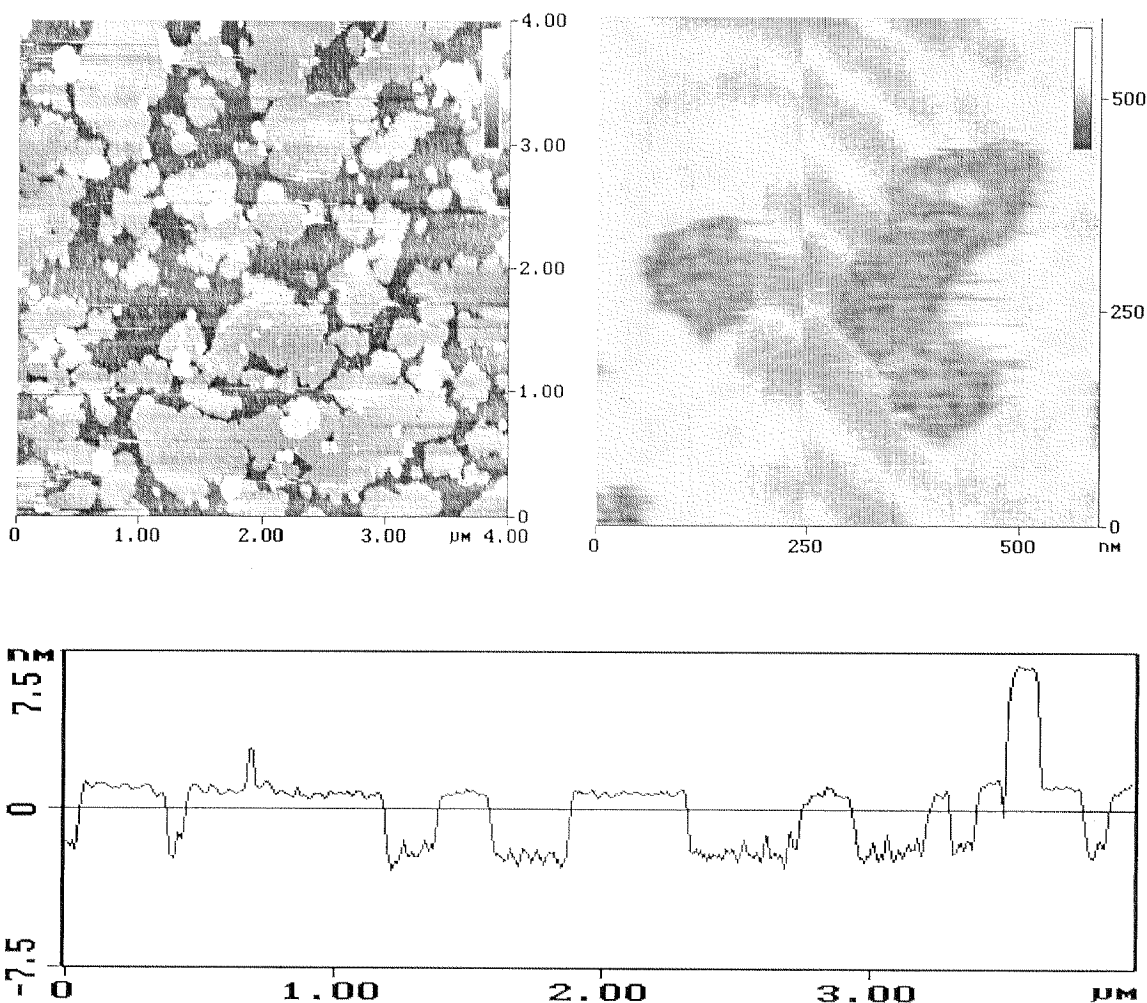


Figure 114: Left: Partly fused vesicles on a SiO₂ substrate after incubation of a liposome solution previously exposed to SLO. Right: Higher magnification showing that something (SLO monomers) is adsorbed on the SiO₂ between the fused membrane patches. Beneath: Section through the left image showing an apparently reduced bilayer thickness due to the adsorbed protein layer between the membrane patches. The height of the rough (presumed) protein layer is 2.6 nm. The attached liposome, visible as an elevation on the right, as expected towers above the supported bilayer by exactly one bilayer thickness (5 nm).

Because these samples have never been dried, it was very unlikely that membrane monolayers had been formed on the substrate. Much more likely, the nano-roughness of those areas could be explained by the adsorption of SLO monomers from the solution onto the SiO₂ surface, which occurred in competition with liposome-adsorption. A scheme of such a situation is shown in Figure 115.

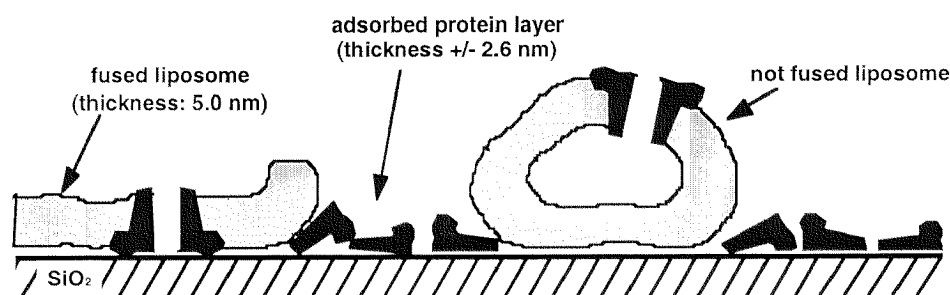


Figure 115: Section through a SiO₂ surface covered with adsorbed- or fused vesicles and protein layers.

The presence of non-membrane inserted SLO therefore prevented the formation of a homogeneous bilayer. For this reason, a size-exclusion chromatography step was added after the SLO incubation to remove non-inserted protein. The SLO/liposomes solution was passed through a small (1 ml bed volume) Sephadex G-100 column which was pre-washed with a solution of liposomes to saturate possible lipid binding sites. 1 μ l of all the collected eluate fractions was then allowed to dry on a cover-slide of which the fluorescence intensity was examined in the LSM after rehydration. The samples containing the largest fluorescent intensities - and therefore the liposomes - were then mixed together and used for bilayer formation. During this column-purification, the liposome solutions were diluted by a factor of about 10.

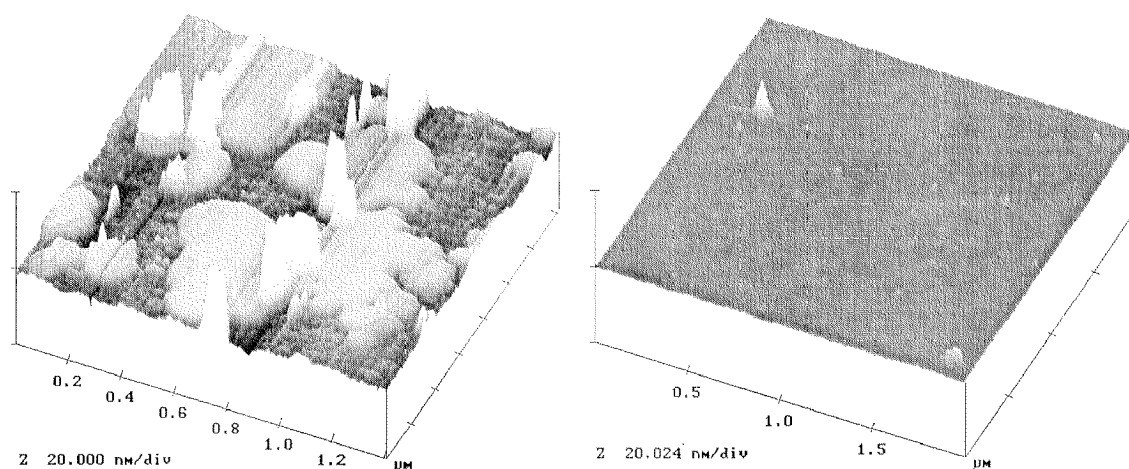


Figure 116: 3D-AFM image projections of SiO₂ substrates after the spreading of SLO/liposome solutions before (left) and after (right) size exclusion chromatography. A non confluent supported bilayer is obtained in the first case due to competitive adsorption of proteins from the solution. In the second case, a homogeneous bilayer is obtained, because non-membrane integrated proteins have been removed prior to liposome fusion.

After incubation of these purified liposome fractions on SiO₂, homogeneous bilayers were obtained which recovered after photobleaching. The non-integrated SLO monomers were therefore successfully removed by the column. AFM images of the

supported membranes did not reveal individually adsorbed liposomes surrounded by areas with adsorbed SLO (as obtained with non-cleaned liposome/SLO fractions; Figure 116, left) anymore, but continuous bilayers with some attached liposomes (Figure 116, right). No SLO rings could be seen, however, in the supported bilayer. A possible cause could be the high fluidity of the membrane. After OsO_4 and glutaraldehyde fixation, filamentous objects partially contaminated the surface and only very few and badly resolved SLO rings were visible in the best case (Figure 117).

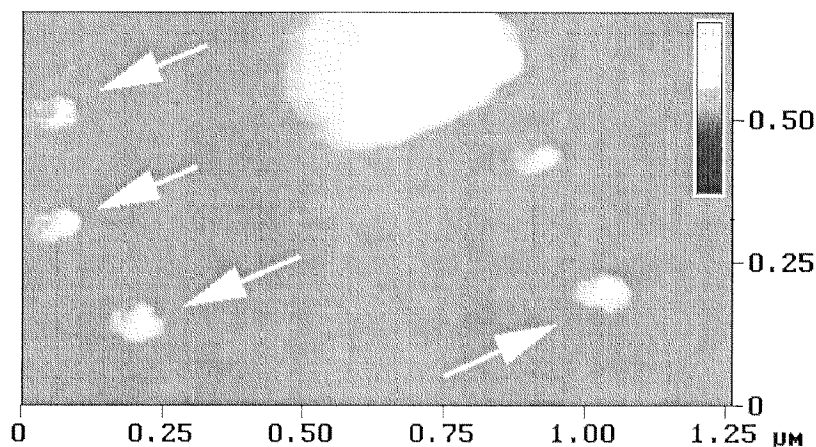


Figure 117: Badly resolved SLO rings in a supported bilayer prepared from column purified liposomes containing SLO.

According to TEM images, vesicles passed through the Sephadex column did contain (but not many) SLO pores. The same was observed for the liposome solutions before the column purification.

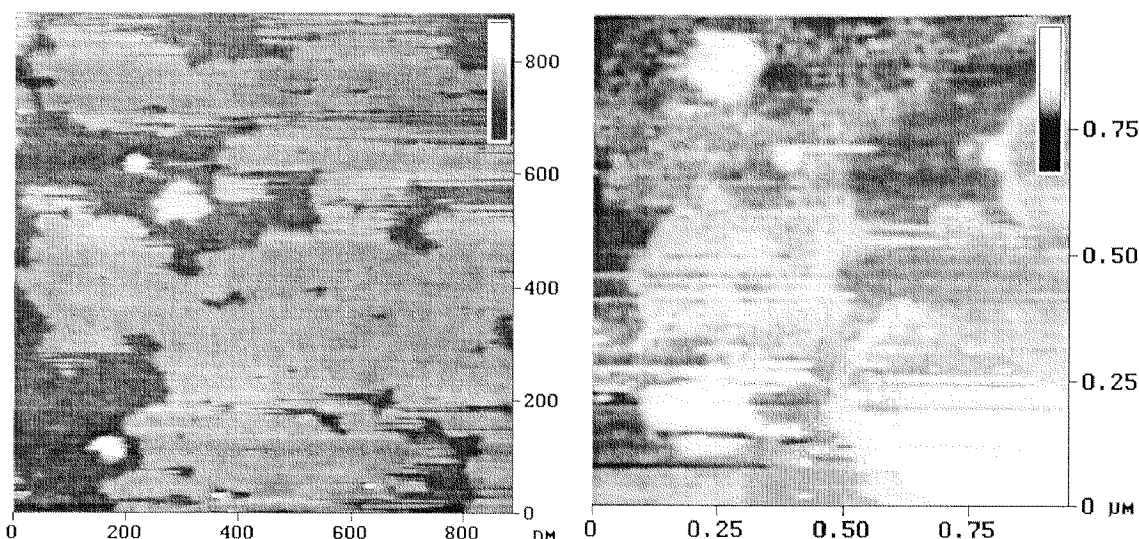


Figure 118: AFM image of very badly visible SLO rings on the samples prepared with non-purified SLO/liposomes. The non homogeneous substrate reduces the achievable resolution.

Taking the previous observation into account, that many SLO monomers still remained in solution even-though they were exposed for a long time to large amounts of cholesterol containing membranes, one has to suppose that a large fraction of the SLO is not active. It is also possible that huge amounts of non-SLO proteins are present in the SLO solution, which would lead to the same results. On the membrane patches obtained after fusion of non purified SLO/liposome solutions, SLO rings could only be suggested by the presence of badly defined ring- or hole like structures on the bilayer background (Figure 118). Due to the badly spread liposomes, no good resolution could be obtained of the SLO rings. A homogeneous and flat supported bilayer is therefore a prerequisite for successful high-resolution AFM imaging of membrane proteins.

Thus, the most successful approach is to produce a supported bilayer first, followed by incubation of SLO. We are very much looking forward to seeing AFM images of membrane proteins integrated in membranes suspended over nanocavities.

Summary and Outlook

In this dissertation, a suitable support was designed for making protein-containing biological membranes accessible to scanning probe microscopy. Methods coming from very different fields were first optimized and then combined to produce a bilayer architecture.

This work can be subdivided in the following 5 sections

Production of nanocavity substrates:

Flat gold/silicon substrates, containing a defined density of nanohole structures with diameters ranging from 50 - 200 nm and a depth varying between 5 and 200 nm have been successfully prepared. The geometrical dimensions of the small cavities could be completely controlled, making them adaptable for different applications. The presence of different materials in and out of the nanocavities could be taken advantage of to direct the interaction site of biological species with the holes.

Chemical modification of the substrates and chemical patterning:

We were able to tune the physical and/or chemical properties of the substrates hydrophilic and hydrophobic, positively- and negatively charged, inert and amino-reactive by modifying the gold surfaces with alkanethiol SAMs having different end-group functionalities. This allows the surface chemistry to be made compatible with the demands of a specific application.

By using micro-contact printing (μ CP), we could direct an aminoreactive, chemical functionality to predefined, micrometer-sized areas on the gold surfaces. With this technique, the (covalent) immobilization site of proteins and biomolecules could be controlled. The fusion of liposomes on a similar support composed of hydrophobic and hydrophilic SAM areas did lead to the formation of a supported bilayer exclusively on the hydrophilic areas. Thus, the final localization of a bilayer could be directed by chemical means.

As an alternative to alkanethiols, a new route for the chemical modification of metal- and metal-oxide surfaces was studied, based on hydrosilanes and a catalyst. We were mainly interested in knowing whether this system leads to SAM formation or to multilayer films. Indeed, stable, thin organic layers were obtained on gold using the hydrosilane approach, but the thickness of such layers proved to exceed one monolayer and to be a linear function of the incubation time, ruling out the SAM hypothesis.

Formation and suspension of supported membranes and influencing of their phase behavior

Out of four different methods to produce a supported bilayer membrane on gold or SiO_2 surfaces, the liposome spreading approach was the most reproducible and best suited for our applications. The influence of different parameters, which affect the spreading behavior of liposomes (composed of different lipids) was investigated. Among these parameters, the choice of the substrate appeared to play a crucial role. Very homogeneous supported bilayers were obtained on SiO_2 surfaces and on amino-SAM modified gold surfaces, according to laser scanning microscopy (LSM) and atomic force microscopy (AFM).

The phase behavior of fluorescently labeled, supported bilayers was then investigated using photobleaching experiments. On SAM-modified gold surfaces, crystalline lipid bilayers were mainly obtained, whereas on SiO_2 surfaces, the bilayers retained their fluidity. By fine-tuning the lipid composition of liposomes containing cholesterol, the crystalline-to-fluid phase transition temperature of the supported bilayers could be adjusted from below room temperature to 60°C . This leads to the possibility of switching the bilayer-state from solid to liquid in an experimental setup, making it possible to precisely control the lateral diffusion of inserted membrane proteins.

Integration of a model membrane protein into the supported bilayers

To test the resolution which can be obtained with the atomic force microscope on proteins integrated in the supported membranes, a model, pore-forming protein was inserted in a bilayer spread on SiO_2 . After optimization of the integration conditions, the round shaped Streptolysine O (SLO) pore with a diameter of about 39 nm could be well resolved in the AFM, under aqueous conditions and without fixation of the membrane. Compared to liposomes or erythrocyte membranes, however, the pore formation of SLO

in supported membranes seems to be more hindered. This is probably due to the presence of the support just beneath the membrane, sterically hindering the protein.

Suspension of bilayer membranes over nanocavities and determination of the mechanical properties of these architectures by AFM

The creation of flat, AFM accessible bilayer areas suspended between two aqueous compartments was finally achieved using a substrate with etched nanocavities of 100 nm diameter. This substrate was chemically modified with 11-aminoundecanethiol to promote the formation of a homogeneous bilayer, and for the liposome fusion, extra-large lipid vesicles were produced to make sure that they could not penetrate into the nanoholes.

Using the AFM, images of the suspended membranes stretching over the nanoholes were obtained. But very importantly, AFM cantilevers with very small spring constants had to be used combined with lipids of a transition temperature above room temperature, as else the suspended membrane would be (reversibly) elastically deformed by the vertical AFM-tip force.

These results show, that by controlling the chemistry and the topography of a substrate, biological bilayer membranes can be handled down to very small dimensions. The nanocavity/bilayer substrates are now ready for the integration of proteins and atomic force microscopy.

Outlook

We are very much looking forward to seeing the first images of a protein inserted in the membranes suspended over the small nanocavities, and to observe its behavior therein. As the chemistry as well as the geometry of the nanoholes can be designed at will, it should be possible to adapt the environment surrounding the proteins, such that it does not interfere with their function.

Even more interesting will be the observation of a nanocavity containing two or more different proteins simultaneously, as this will allow the interaction of membrane proteins to be studied in a native membrane environment for the first time.

If needed, a still more elaborate chemical definition of the nanoholes can be achieved by using micro-contact printing to form a defined SAM on flat gold surface areas only, and then by rinsing the sample with another alkanethiol, which will cover the small gold-edge-areas at the entrance of each nanocavity. Using a SAM which has the same charge as the liposomes, in the latter case, this should then allow completely flat supported bilayers to be produced, which are not sucked towards the interior of the hole, as we observed in our present experiments.

A very interesting, further development of the present system would be the implementation of an electrode into the nanocavities, which would make possible the simultaneously study of electrochemical and dynamic processes occurring in membranes.

APPENDIX

Hydrosilane thin films

This Hydrosilane topic was already introduced in a sub-chapter of “CHEMICAL MODIFICATION OF SURFACES“. Here, a short abstract dealing with the chemistry behind hydrosilanes is given, followed by the experimental results obtained for the hydrosilane system we studied.

As it was already mentioned in the introduction to this dissertation, self-assembled monolayers are finding more and more applications for the chemical functionalization of substrates. We did use thiol-based SAMs with a variety of ω -functionalities to tune the interaction of supported bilayers with the substrate. Due to the fact that gold substrates are needed for thiol-based monolayers, we mainly concentrated on the development of nanostructured Au surfaces. Of course, many other materials are also well suited for the production of the nanohole-structures, some of which were presented in the chapter “B) Nanostructuring“. Namely polymer- as well as Si/SiO₂ based substrates would be interesting alternatives. Controlling the spreading behavior and physical state of the supported bilayer on these other materials would then however require non-thiol SAM based approaches to tune their surface chemistry. For SiO₂ as well as for oxygen containing plastic substrates, this can be achieved by silanization techniques. But, using this approach, most often non-monolayer surface coatings are obtained of which the thickness can not very reproducibly be controlled. Finding surface modification routes leading to “self-assembled monolayer“ coatings on these substrates would be a big progress. Because of that, it seemed worthwhile to test a novel compound, based on a chemistry patented by Dr. M. Hirayama, which was very promising in sight of leading to SAM layers on metal- and metal-oxide surfaces.

Dr. Hirayama did discover in her dissertation, that PDMS-based polymers containing Si-H bonds could strongly be attached to many substrates in a reaction catalyzed by cis-Dichlorobis(styrol)platinum(II) ((Hirayama, 1997)). A polymer coating not exceeding a monolayer coverage is obtained and mechanistically it was observed, that the Si-H bond is lost upon immobilization. The question, whether or not the platinum compound is directly involved in the binding to the substrate could not definitively be answered. But very importantly, the range of substrates on which these coatings can be formed are not limited to metals like Au, Al, Ti, Cr, Fe and Cu, but also stone, wood and silicon etc. can be coated.

In this work we wanted to take advantage of the broad range of substrates which are accessible to this new chemistry and test whether a long chain alkylsilane (an alkyl chain with a Si-H functionality attached to one end) could be immobilized by the same catalyzed process (see Figure 41 on page 79). We did expect, that due to the presence of the long alkyl chain (not present in the PDMS polymer compounds), the immobilization would be governed by self-assembly and would lead to a more or less ordered monolayer - or at least to a stable organic layer which would not exceed the thickness of a monolayer. For these experiments, we did chose gold substrates, as we were most familiar with this kind of surface and also because gold does not have a native oxide layer. The absence of oxygen on the substrate as well as in the hydrosilanes leads to the possibility to study the involvement of this important element in the film-formation process.

Hydrosilylation in organic chemistry

In this context, it is worthy to have a closer look at the role of the organoplatinum catalyst, cis-Dichlorobis(styrol)platinum(II). In organic chemistry, transition metals are very well known to catalyze “hydrosilylation“ reactions in which silicon-hydrides are added to double-or triple bonds like olefins etc. (Barton and Ollis, 1979, Jones, 1979, Pawlenko, 1986). A typical reaction is shown in Figure 119. In our case, however, no such groups were added to the reaction mixture, and therefore a different, unknown mechanism must account for the activation of the hydrosilane compound. Also a direct participation of the platinum in the bond to the substrate can not be excluded with certainty.

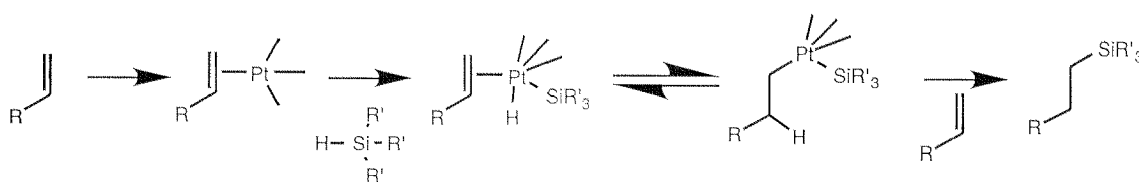


Figure 119: Hydrosilylation: Reaction of an olefin with a Si-H compound (Barton and Ollis,)

The hydrosilane bond is quite inert and thermally stable. 377 kJ/mol are needed to dissociate the Si-H bond. In aqueous media, on the other hand, catalytic amounts of base (nucleophiles) will lead to hydrolysis under creation of a silanol species and H₂ (Pawlenko, 1986). This reaction, which does not occur with C-H bonds (no hydrolysis), is possible in the silicon case since the electronegativity of Si is smaller than that of H. Radical substitution (pyrolysis) of the Si-H bond only occurs at very elevated temperatures due to the above mentioned high binding energy. In the presence of

catalytic amounts of radicals, however, the hydrosilanes are readily attacked, giving silyl radicals which convert to silanols in the presence of oxygen. To our knowledge, no radical starter was present in our reaction mixture. The exact fate of the platinum compound during these kinds of reactions could not yet definitively be elucidated. However, the initially transparent reaction solution slowly turns dark red and then black as the reaction goes on or if the reaction is exposed to oxygen. The black color could be attributed to colloidal Platinum. Therefore, the Platinum (II) is probably reduced to Platinum (0) in this reaction - there being some evidence for the latter to be the really active, catalyzing species (Caseri, 1988). A very detailed study of Pt catalysts and also an overview over hydrosilylation reactions can be found in Caseri (Caseri, 1988). Figure 41 on page 79 shows the hydrosilane compounds which were used in our study as well as the catalyst involved.

Methods

Production of the gold substrates and reaction with the hydrosilane compound: 18 x 40 mm silicon wafer substrates were cleaned from possible adhesive contamination by incubation in technical toluene for 10 hours, followed by rinsing with spectroscopic grade toluene. Then, 5 nm of Cr and 200 nm Au were thermally evaporated onto these substrates, after which they were directly inserted in a glass holder and immersed in 160 ml degased (with Ar) toluene in the reactor. The reactor consisted of a specially designed, wide-neck glass beakers with a glass cover, in which the Si/metal samples could be hung into the organic solvent, 2 cm above a magnetic stirrer. 10 Min. prior to the insertion of the substrates, 3.79 mg (50 μ M) cis-Dichlorobis(styrol)platinum(II) were dissolved in the stirred toluene solution, and after the submersion of the substrates, the hydrosilane compound was added to a final concentration of 1 mM. Then, the hole reactor was immediately purged with argon and the reaction was allowed to proceed for different time-length under a steady flow of fresh argon. Upon removal of the samples, they were immediately thoroughly rinsed with toluene and then stored in argon. After the reaction, the toluene solution was discarded and the reactor cleaned by rinsing with acetone, water, acetone, toluene and finally with UV-grade toluene.

In all the experiments, a parallel reactor was run under exactly the same conditions as the main reactor, but without addition of catalyst.

In order to remove possible chlorosilane contamination from the octadecylsilane compound, the following cleaning procedure was applied:

1 g of silane was dissolved in 20 ml dioxane. Then, 1 ml of water and 2 g silica gel 60 were added and the solution stirred for 9 hours at room temperature. The reaction mixture was then passed through a paper filter leading to a transparent solution, from which the solvents were removed by rotary evaporation. 0.805 g white crystals were obtained with a melting point between room temperature and 37 °C. These distilled in a 4-segment glass oven at 240°C and slightly reduced pressure (60 min.). Some silane from the glass-segment containing the largest amount of substance was then analyzed using IR-spectroscopy and the spectrum compared with the non-cleaned, commercial compound. No difference could be detected between both spectra and the Si-H absorption peak at 2165 cm⁻¹ clearly showed that the hydrosilane was not hydrolyzed during the cleaning procedure.

Optical evaluation of the Au samples after reaction with ODSil, and contact angle measurements

The gold samples, after exposure to the ODSil and rinsing, were bright and clean at a first glance. Under special laboratory-light conditions however, very faint, white schlieres could be observed on the substrate, which could not be washed away with solvents ranging from water to hexane, chloroform and ether.

The ODSil films had advancing contact angles between 102 and 108 ° after incubation times exceeding 60 min. (On octadecanethiol SAMs, angles ranging from 108 to 112 ° were measured). These data show, that indeed very hydrophobic layers are produced by ODSil on gold, which did encourage us to pursue further the investigations on this system.

FT-IR-Spectra of octadecylsilane in CHCl₃

In a next step, we did evaluate, whether the cleaning procedure to remove chlorosilane contamination from the commercial compound did affect the substance and a first reactivity study was performed to evaluate the influence of the catalyst on the ODSil. IR spectra of ODSil before and after cleaning were recorded, together with a spectrum of the ODSil which had been exposed to DBSP (cis-Dichlorobis(styrol)platinum (II)) for 20 h. No difference could be detected between the spectra of the commercial ODSil before and after cleaning, proving that neither the presence of water nor heating the compound to 250°C for 60 min. did destroy the Si-H bond (ppm chlorosilane-contaminations can not be detected in IR spectra). The long exposure of the silane to the catalyst DBSP did not visibly lead to a disappearance of the Si-H bond. However, very

small, broad peaks do appear between 1014 and 1138, the region where siloxanes and Si-O-C absorption bands are situated.

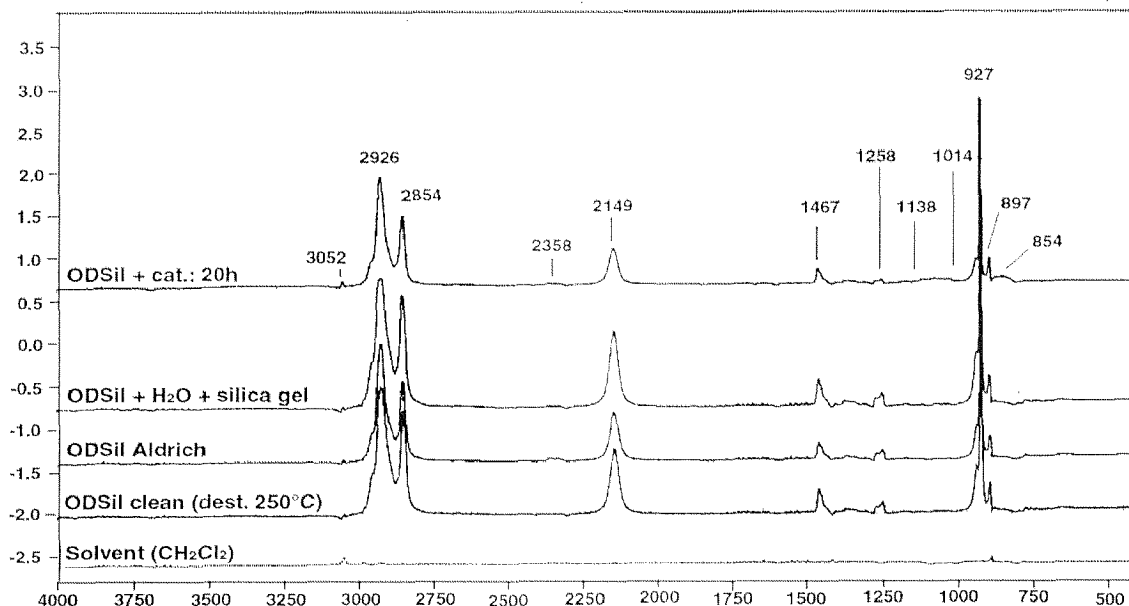


Figure 120: IR-spectra of ODSil after different treatments. These are solution spectra obtained in CH_2Cl_2 . Legend: “ODSil Aldrich“: the commercial ODSil obtained from Aldrich (Buchs, Switzerland); “ODSil + H_2O + silica gel“: ODSil after exposure to silica gel 60 and water, in dioxane, as described in “Methods“; “ODSil clean (dest. 250°C)“: The cleaned ODSil after glass-oven distillation; “ODSil + cat.: 20h“: ODSil after exposure to $50 \mu\text{m}$ DBSP in CH_2Cl_2 .

The broad peak appearing at 854 cm^{-1} may be attributed to a Si-C vibration mode, but this is only a speculation. The following list gives an overview over relevant IR-band frequencies and their assignments for ODSil systems.

Frequency (cm^{-1})	Mode assignment
854	Si-C stretching (?)
897-950	Si-H
1010	Si-O-C asym. stretching
1138	Si-O-Si asym. stretching
1465	CH_2 scissor bending
2149	Si-H stretching
2358	CO_2 from the air
2854	CH_2 sym. stretching
2877	CH_3 sym. stretching
2926	CH_2 asym. stretching
2964	CH_3 asym. stretching
3052	?

Comparison of IR spectra of ODSil, octadecanethiol and octadecyltrichlorosilane

Grazing-angle FT-IR spectra were then recorded of gold samples which had been exposed for up to 60 min. to an ODSil solution containing catalyst or not.

For comparison, samples covered with an octadecanethiol SAM a thin film based on octadecyltrichlorosilane were recorded (Figure 121).

The most conspicuous differences between the spectra were visible at low wavenumbers, where the octadecanethiol SAM did not show any peaks. As expected for the chlorosilane film, a very strong and broad absorption band could be seen at 1133 cm^{-1} , corresponding to Si-O-Si stretching vibrations of the siloxane, which is formed through polymerization of the silanizing agent. This peak was accompanied by a broad peaks at 918 cm^{-1} , which can be attributed to Si-OH or SiO-H vibrations, proving, that not all the available silanol-groups had been hydrolyzed in this organic film. Very interestingly, also the catalyzed ODSil films did show the presence of large amounts of siloxanes, although a priori no oxygen is expected in these films. The silanol modes on these surfaces are however much less pronounced than on the chlorosilane surfaces. The organic ODSil layer adsorbed to the gold in the absence of catalyst shows only rudiments of a siloxane absorbency, but has an additional, unique peak at 1373 cm^{-1} , which could not be assigned yet. The information which can be extracted from the carbon chain IR-vibrations of these layers is described below.

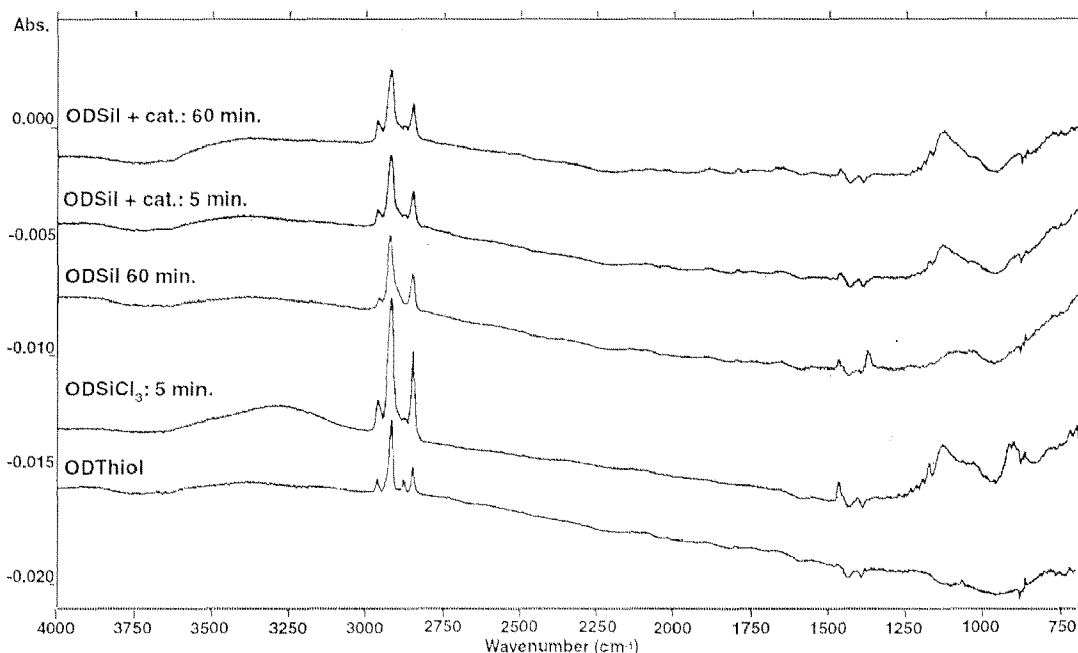


Figure 121

Spectral details giving information about the orientation of the molecular layers are:

- A well resolved C-H stretching region between 2850 and 2967 cm^{-1} . In solution, this region is made out of 2 broad, main peaks (Figure 120) which do split in 4 sharp and well separated modes if the alkyl-chains of the molecules do vertically extend from the surface as in the case of a well ordered alkanethiol SAM (ODThiol in Figure 121) (Allara and Nuzzo, 1995). According to this argument, the spectrum of ODSil reveals a chain orientation between these two extremes. Incubation of ODSil without catalyst reveals to lead to a less ordered organic layer compared to ODSiCl₃. However, if ODSil is reacted in the presence of catalyst, the resulting layer is slightly more ordered than the chlorosilane compound, as the CH₃ (sym.) stretching modes are weakly visible.

- The frequency shifts of some CH₂ stretching modes to lower wavenumbers, reflecting an increased crystallinity (reduced motion) of the hydrocarbon chains ((Finklea et al., 1986)). In bulk, the asymmetric CH₂ stretching mode is located at 2926 cm^{-1} . The same absorption peak is located at 2918 cm^{-1} for the oriented alkanethiol SAM - shifted 8 cm^{-1} to lower frequencies. Also here, the ODSil and ODSiCl₃ layers do absorb at wavenumbers in between these extremes, catalyzed ODSil layers being slightly more crystalline than non catalyzed, but both much more crystalline than ODSiCl₃ layers (however, these results have to be regarded with care, as the thickness of the different organic layers were not identical).

- The intensity of the CH₂ bending vibration around 1468 cm^{-1} , which weakens, the more the alkyl chains are oriented normal to the surface (the CH₂ planes - and consequently their transition dipole moments - are then oriented parallel to the surface, loosing their IR activity according to the “surface selection rule“). In the bulk spectra, this absorbency peak is strong. On the gold surfaces, the ODSil layers must be somewhat oriented in the vertical direction, as only a small absorbency is found around 1468 cm^{-1} . And, again the chlorosilane layer shows less order than the hydrosilane layers.

- The presence of wag-twist progression absorbencies shifted to higher wavenumbers from the Si-O-Si stretching mode (between 1175 and 1234 cm^{-1}). These vibrations are present if the alkyl chains are in an all-trans, fully extended conformation. As expected, these modes are not visible on alkanethiol SAM samples, but are present on ODSil layers which were formed catalytically. ODSiCl₃ films also seem to be strongly

extended, opposed to the non-catalytically produced ODSil film, which does not show the progression.

Three of the four spectral fingerprint-regions show unanimously, that in terms of order and orientation, the hydrosilane films can not reach the perfection of SAMs formed by alkanethiols. The order parameters compare more likely to organic layers obtained with a commercial silanization reagent (ODSiCl_3).

Thickness'' of adsorbed layers and adsorption kinetics

One of the basic concepts of SAMs is, that they do stop growing as soon as exactly one monolayer of molecules cover the substrate. We did check the film growth behavior of our ODSil compound on gold using ellipsometry (see "Materials and Methods". At the beginning, incubation times ranging from a few seconds to one hour were investigated, and we were lucky to discover, that indeed layer thickness in the range of what was expected for about a monolayer coating (1.9-2.5 nm) were obtained, although the standard deviation of these measurements were large. Later, the reaction time of the gold samples with the ODSil were increased, showing, that the layer formation did not at all stop at the monolayer level, but did increase linearly with time after a fast initial adsorption step. Improving the rinsing and washing of the samples after the reaction did not lead to much reduced layer thickness'. Only very intensive sonication did slowly remove material from the substrate according to FT-IR measurements. But this effect does not necessarily indicate removal of "loosely" bound material, but is more likely the result of removal of strongly bound organic molecules by cavitation effects in the sonication liquid. Also silicon would have been attacked, if it had been exposed to the mentioned sound-wave intensities. It is very unlikely that only van der Waals or electrostatic forces are responsible for the strong adhesion observed, as we were using small molecules which cannot develop multiple "physisorption sites" as polymers. Molecules of the size of ODSil are usually easily removed by non-mechanical rinsing methods. We therefore had to conclude that kind of a polymerization reaction was taking place on the gold surfaces. Very interestingly, samples exposed to ODSil only (without catalyst) were covered with strongly adhesive organic layers which were even thicker than the "catalyzed" samples. Under very similar reaction conditions, the film-formation kinetics did vary enormously, as can be seen in Figure 122. Most probably, a yet not known source of oxygen is responsible for this behavior, as this element is needed to form the siloxanes detected in the FT-IR spectra of these thin films. Varying amounts of water impurities in the toluene or infiltration of oxygen from the air (the reaction was done under argon) are the best candidates as source for this element.

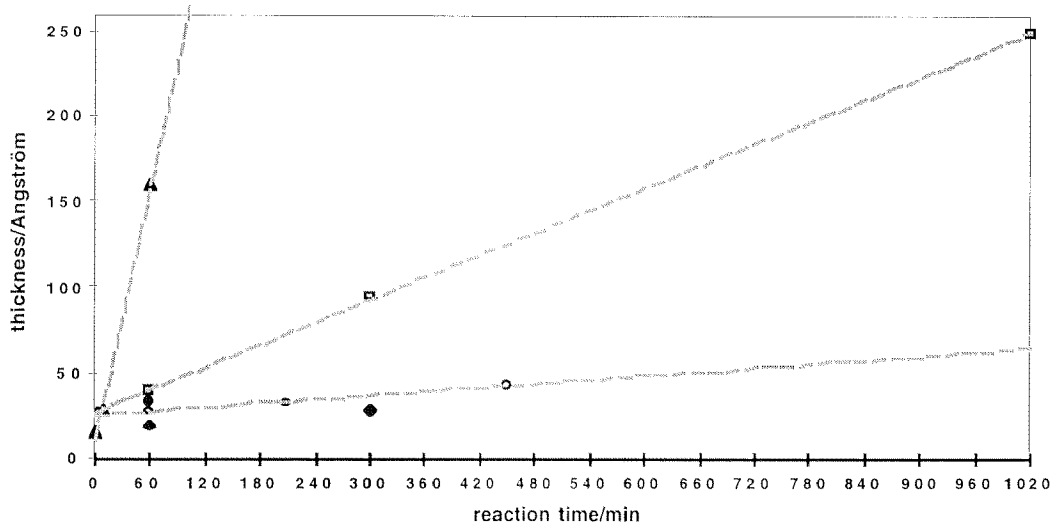


Figure 122: Film thickness (determined ellipsometrically) versus incubation time for ODSil on AU(111), in the presence of the catalyst. The different symbols represent different experiments which were performed under very similar reaction conditions. The lines are linear regressions through representative data series.

Elementary composition of the ODSil films: Confirmation of the presence of oxygen in the organic layers.

To prove the presence of oxygen in the ODSil layers and to detect, where in the films this element is located, XPS spectra of the coated gold surfaces were recorded at different electron take-off angles.

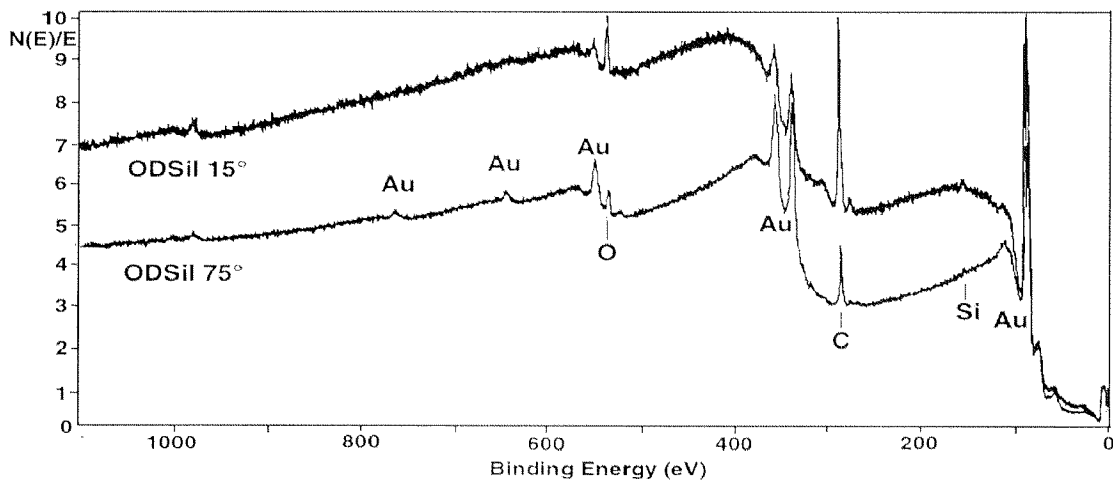


Figure 123: Survey spectrum of a 2.8 nm thick ODSil layer on gold. The electrons were collected at electron take off angles of 75 and 15°.

A typical survey spectrum is shown in Figure 123. Next to a small Si(2s) peak at 151 eV, a large C(1s) peak can be seen at 285 eV. But also, confirming the FT-IR spectra, a

large O(1s) peak is present. The ODSil layers therefore definitively contain large amounts of this element, which is neither present in the silane itself, nor in the solvent, the catalyst or on the surface. The atomic ratios between carbon (C(1s)), oxygen (O(1s)) and silicon (Si(2s)) were determined by integration of high resolution XPS spectra obtained for each element. The built-in sensitivity factors of the ESCA 5400 software were used to calculate the atomic concentration of each element. The carbon/oxygen, oxygen/silicon and carbon/silicon ratios obtained from different experiments were plotted against the reaction time of the gold samples in the toluene containing ODSil and catalyst. Not very surprisingly, also these data did very much scatter along the ratio-axis, in agreement with the ellipsometry data. For the C/O ratio, a maximum of 6 should be expected, as in the best case three oxygens can bind per alkylsilane - if a complete transformation of the Si-H bonds in Si-O bonds is assumed. This situation would correspond to each silane being attached via three oxygens to the gold surface. As the presence of siloxanes was detected in the FT-IR spectra, a C/O ratio rather smaller than 6 was expected.

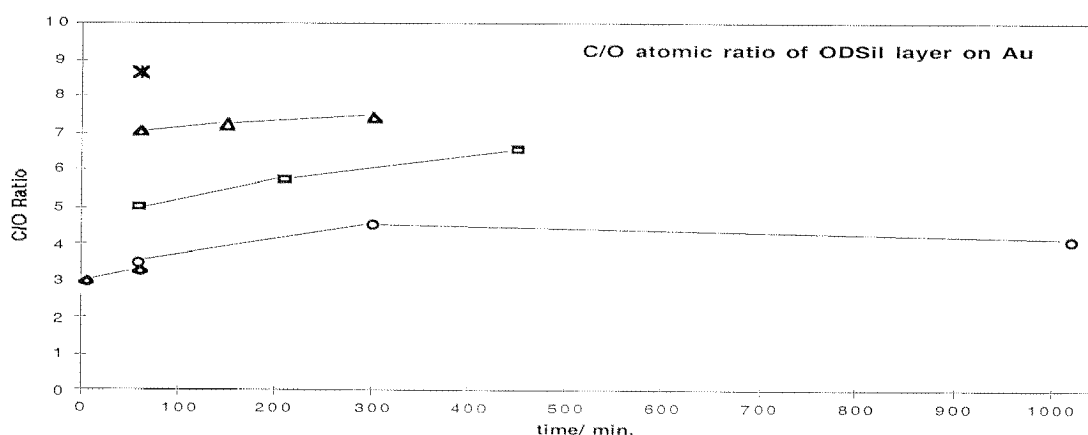


Figure 124: The ratio of carbon to oxygen (atomic %) versus reaction time, found for ODSil layers on gold, as determined by XPS. The different symbols correspond to different experiments which were performed under very similar conditions.

The results show that on average, a ratio of about 6 is found, but some samples even show a ratio of 8.7. This, to our knowledge, can only be explained if an unknown species with additional bound oxygen (e.g. the Pt of the “catalyst“ ?) is somehow involved in the binding of the silanes to the gold (On Au, the location of the main platinum peak (Pt(4f_{7/2}) at 71 eV) coincides with the location of strong Au satellites, making its detection and quantification very difficult).

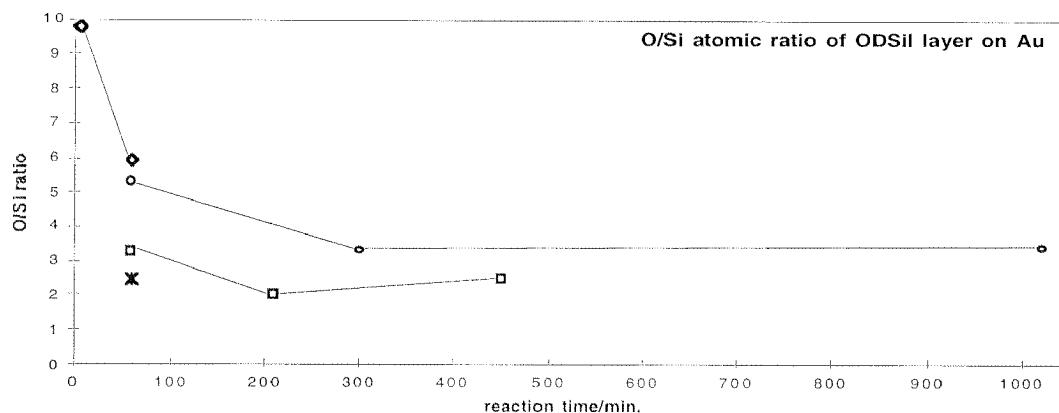


Figure 125: The ratio of oxygen to silicon (atomic %) versus reaction time, found for ODSil layers on gold, as determined by XPS. The different symbols correspond to different experiments which were performed under very similar conditions.

The O/Si atomic ratio on average lies between 3 and 4. Again, only the participation of another oxygen binding- or containing species can explain the occurrence of ratios larger than 3.

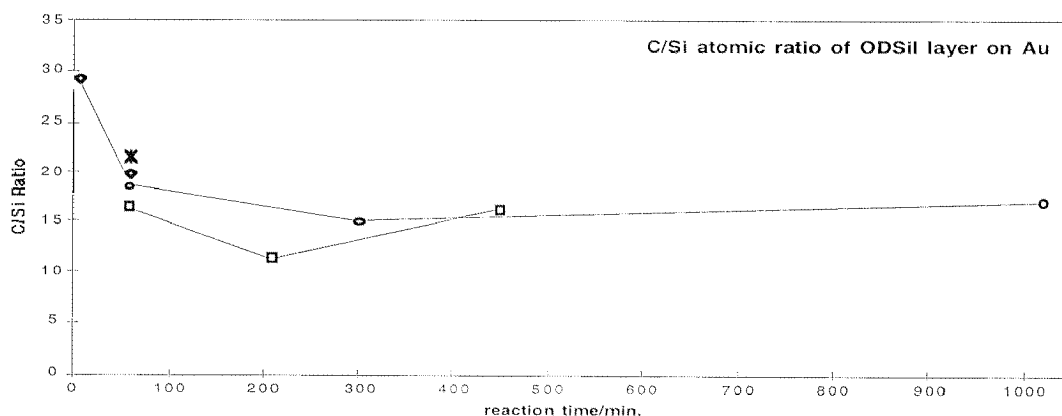


Figure 126: The ratio of carbon to silicon (atomic %) versus reaction time, found for ODSil layers on gold, as determined by XPS. The different symbols correspond to different experiments which were performed under very similar conditions.

The C/Si ratio, which should be independent of the nature of the bond between the silane and the substrate, is expected to be 18. Indeed, this ratio is found on average on our surfaces. The scattering of the results is large, not excluding the possibility that the catalyst may also be somehow directly involved in the binding, as suggested by other results.

Summary

The reader is referred to the chapter “Hydrosilanes“ on page 78 for a short summary of the results. Here, only a few closing remarks are given for this chapter:

The results of the experiments mentioned above led us clearly to conclude, that ODSil does not form an ordered, monolayer-thick film on gold. Therefore, the question which was asked at the beginning, whether hydrosilane compounds do form SAMs on surfaces in the presence of the catalyst DBSP, can be answered with NO, for the case of ODSil on gold. As we did not intend to perform an in-depth study of the hydrosilane film formation mechanism, but were merely looking for an alternative chemistry which would make oxide-containing surfaces chemically tunable for controlling the behavior of suspended lipid-bilayers, this project was abandoned at this stage.

Just as a matter of curiosity, however, and given that there were reasons to believe that the catalyst (or parts thereof) may be directly involved in the binding of the silanes, a short silicon-NMR experiment was performed:

Dimethyloctadecylsilane, dissolved in toluene, was allowed to react in a closed and argon purged container for 7 days in the presence and absence of catalyst. Then, the solutions were analyzed using ^{29}Si -NMR. As expected, only a single silicon species at -13.304 ppm was found in the solution which had not been exposed to catalyst. Opposed to that, the solution which contained the catalyst did show the presence of more than a dozen of silicon species! Which of those is (are) the surface active compound(s)? Long-chain alkylhydrosilanes combined with DBSP definitively are highly complex chemical systems. Looking back, it is therefore not amazing, that the surface analysis data were ambiguous.

Related paper:

Atomic force microscopy detects changes in the interaction forces between GroEL and substrate proteins.

Anja Vinckier^{#, §, *}, Pietro Gervasoni[°], Frank Zaugg[#], Urs Ziegler[§], Peter Lindner[°], Peter Groscurth[§], Andreas Plückthun^{°, *}, Giorgio Semenza^{#, ¶, *}

[#]Department of Biochemistry, Swiss Federal Institute of Technology, ETH Zentrum, Universitätstrasse 16, CH-8092 Zürich, Switzerland

[§]Anatomisches and [°]Biochemisches Institut der Universität Zürich, Winterthurerstr. 190, CH-8057 Zürich, Switzerland

[¶]Dipartimento di Chimica e Biochimica Medica, Università di Milano, Via Saldini 50, I-20133 Milano, Italy

Key words: force spectroscopy, molecular chaperones, tapping mode AFM, tip functionalization, citrate synthase, β -lactamase

Abbreviations: AFM, atomic force microscopy; TEM, transmission electron microscopy; (Cys-Ala) β -lactamase, Cys \rightarrow Ala double mutant β -lactamase; (Gly-Ala) citrate synthase, Gly \rightarrow Ala single mutant citrate synthase; ATP, adenosine triphosphate; ATP γ S, adenosine 5'-O-(3-thiotriphosphate); MOPS, 3-[N-morpholino]propane-sulfonic acid; GdmCl, guanidinium hydrochloride; OTS, octadecyltrichlorosilane

Running title: Interaction forces between GroEL and proteins by AFM

ABSTRACT

The structure of the *Escherichia coli* chaperonin GroEL has been investigated by tapping mode atomic force microscopy (AFM) under liquid. High-resolution images can be obtained, which show the up-right position of GroEL adsorbed on mica with the substrate binding site on top. Because of this orientation the interaction between GroEL and two substrate proteins, citrate synthase from *Saccharomyces cerevisiae* with a destabilizing Gly→Ala mutation and RTEM β -lactamase from *Escherichia coli* with two Cys→Ala mutations could be studied by using force spectroscopy under different conditions. The results show that the interaction force decreases in the presence of ATP (but not of ATP γ S) and that the force is smaller for native-like proteins than for the fully denatured ones. It also demonstrates that the interaction energy with GroEL increases with increasing molecular weight. By measuring the interaction force changes between the chaperonin and the two different substrate proteins we could specifically detect GroEL conformational changes upon nucleotide binding.

INTRODUCTION

In vivo the accumulation of misfolded species and aggregates is prevented by the action of molecular chaperones. In this context the chaperonin GroEL and its co-chaperonin GroES [Hartl, 1996; Fenton and Horwich, 1997; Xu et al., 1997] play an important role by assisting protein folding in two different ways. First, folding of the substrate proteins can occur in the central cavity of GroEL capped by GroES [Mayhew et al., 1996; Rye et al., 1997]. Second, the substrate proteins are released from GroEL and reach the final native state in solution. In this case GroEL prevents aggregation of misfolded protein molecules by releasing less aggregation prone states and keeping the concentration of folding intermediates low in free solution by rebinding them [Todd et al., 1996].

GroEL is a tetradecameric protein, consisting of two stacked rings with seven identical 57 kDa subunits in each ring [Braig et al., 1994; Chen et al., 1994]. Each subunit consists of 3 domains: apical, equatorial and intermediate. The apical domain facing the channel shows a higher percentage of hydrophobic amino acid residues than the other domains and is presumed to directly bind to the substrate. Previous studies have demonstrated that the interaction of a polypeptide chain with GroEL is based on hydrophobicity [Fenton et al., 1994; Zahn and Plückthun, 1994, Zahn et al., 1994, Itzhaki et al., 1995; Lin et al., 1995], although recent reports show that electrostatic

interactions also could be important for the (rapid) binding of the substrate protein with GroEL [Itzhaki et al., 1995; Perrett et al., 1997, Aoki et al., 1997]. When ATP cooperatively binds to seven equatorial domains of the same GroEL-ring, the apical domains rotate and move upwards and reach the so-called R-state [Roseman et al., 1996; White et al., 1997]. This structural change is the reason for the reduced affinity of unfolded (or partly folded) proteins for GroEL in the presence of ATP, since some of the hydrophobic residues of GroEL will no longer contact the substrate. This structural change is enhanced by GroES which contacts the hydrophobic residues after the equatorial domains been moved upward.

Different techniques such as the surface force apparatus [Israelachvili, 1989; Leckband, 1995], pipette suction [Evans et al., 1991] or flow chamber technology [Pierres et al., 1996a and b] have been used to measure biological interactions. Recently, the use of the AFM to detect specific interaction forces has been described by several groups and shown to be very sensitive [Hoh et al., 1992; Stuart and Hladly, 1995; Dammer et al., 1995 and 1996; Hinterdorfer et al., 1996; Roberts et al., 1996; Allen et al., 1996 and 1997; Fritz et al., 1997; Nakajima et al., 1997]. The measurements of specific interaction forces with AFM were reported for e.g., the avidin-biotin system [Lee et al., 1994a; Florin et al., 1994; Ludwig et al., 1994; Moy et al., 1994], or for complementary DNA strands [Lee et al., 1994b; Boland and Ratner, 1995; Noy et al., 1997]. The measured forces are due to non-covalent interactions leading to measured interaction force values far weaker than that of a covalent bond, which is about 1000 pN [Evans et al., 1995].

In this paper, the interaction between GroEL and two substrate proteins has been studied by measuring the interaction forces. The two substrate proteins are citrate synthase from yeast, carrying the destabilizing Gly276Ala mutation [Zahn et al., 1996, Lindner et al., unpublished] and RTEM β -lactamase in which both cysteines forming a disulfide bond have been changed to alanines (Cys-Ala β -lactamase) [Gervasoni et al., 1997a and b]. Force distributions have been obtained by measuring the interaction force from recorded force-distance curves under different conditions of pretreating the substrate protein, and in the presence or absence of ATP or ATP γ S, which enabled us to obtain information on the conformational features of the chaperonin GroEL. We have also shown that with tapping mode AFM under water highly resolved images can be obtained.

MATERIALS AND METHODS

Atomic force microscopy (AFM)

Tapping mode images under liquid have been obtained with a NanoScope III (Digital Instruments, Santa Barbara, California), modified as described in Vinckier et al. [1996a]. A frequency of 8.5 kHz, and an amplitude of 2.9 nm was applied on standard commercially available silicon tips with a cone angle of 20°. For the functionalization in the force spectroscopical experiments the same silicon tips were used as for AFM imaging. The spring constant of each individual cantilever was determined using the resonant frequency method [Cleveland et al., 1993], and also the exact length of the cantilevers was measured by TEM, and found to be indeed $450 \pm 2 \mu\text{m}$ ($x \pm \text{SD}$). The spring constants were found to be within the range of 0.02 to 0.2 N/m, with an error of about 5%. In each experiment we used the appropriate force constant for that particular silicon cantilever.

The AFM force measurements have been obtained by using a BioScope (Digital Instruments, Santa Barbara, California). A simple self-made liquid cell has been constructed by bringing a small amount of a silicone glue (Forbo-CTU AG, Schönenwerd, Switzerland) around the mica sample of interest before the start of any experiment. Many force-distance curves under buffer — as described below — have been measured at several places of the sample to obtain the force distribution. The force experiments were always performed with a scan rate of 1 Hz. This scan rate must be kept constant, because it determines the interaction time between the substrate protein and the GroEL. We found a small decrease in the interaction force at higher scan speed (32 Hz), because the molecules may have less time to interact. Slower scan rates showed a slightly higher interaction force. For example, for the GroEL- (Gly-Ala) citrate synthase interaction with a scan speed of 0.1 Hz a mean force of $620 \pm 130 \text{ pN}$ was obtained, while at 1 Hz the force was $440 \pm 100 \text{ pN}$. The mean force at 0.1 Hz is after statistical calculations different from that at 1 Hz, with $P < 0.0001$. At higher scan rates the force decreases further. This is reproducible with all the tips. Therefore, we paid great attention that a constant scan rate was used in all the experiments, in order to compare different events.

Transmission electron microscopy (TEM)

Transmission electron microscopy experiments were performed with a Philips CM 100 operated at 80 kV. The sample preparation was based on the method described in Detrich et al. [1985], and the sample was negatively stained with uranyl acetate.

Protein expression and purification

The double mutant (Cys-Ala) β -lactamase (28.8 kDa) was produced and purified by methods described elsewhere [Laminet & Plückthun, 1989; Gervasoni et al., 1997a]. The (Gly-Ala) citrate synthase, a homodimer of 100 kDa, which carries an N-terminal and a C-terminal his₅-tail, was produced and purified as described in Lindner et al. [1992]. The chaperonin GroEL was overexpressed in *Escherichia coli*-strain W3110 and purified as described in Gervasoni et al. [1997b]. Protein concentrations were measured using the bicinchoninic acid assay (Pierce, Rockford, IL, USA) and are always given for the oligomeric states. All measurements in this work, unless stated otherwise, were carried out in MOPS buffer (50 mM MOPS, 50 mM KCl, 5 mM MgCl₂, pH 7.2).

Sample preparation

GroEL (1.4 μ M) in MOPS buffer was allowed to adsorb on freshly cleaved mica (Goodfellow, Cambridge, England). In order to obtain a complete coverage of the GroEL on the mica substrate (for the force measurements) 0.2% (v/v) polyethyleneglycol 6000 and 1% (w/v) ammonium molybdate was added to the MOPS buffer [Zahn et al., 1993]. After 30 minutes the GroEL-covered mica was intensively rinsed with the MOPS buffer. When the sample was prepared for AFM images, this step was followed by a 2.5% glutaraldehyde in phosphate buffer (pH 7, 0.1 M) fixation for 5 minutes. In contrast, when the sample was prepared for the force measurements, GroEL was not fixed with glutaraldehyde. In both cases the samples were investigated under liquid and never air-dried.

For the investigation of the interaction between GroEL and the substrate protein in the presence of nucleotides, either 2.5 mM ATP or 3 mM ATP γ S was added to the solution and incubated for 1 hour. During the course of the whole experiment (1-2 h), the nucleotides were always present and kept constant in the MOPS buffer with the concentrations indicated above.

Tip preparation and functionalization

Before functionalization, the AFM tip was first flattened by fast scanning on a silicon oxide surface under a high load for 3 minutes. The tip was then cleaned with UV light ($\lambda = 254$ nm) for several hours. The tip shape at the apex was determined by TEM following the method of DeRose and Revel [1997] before and after the experiment. A typical TEM image of such an AFM tip is shown in Fig 1A.

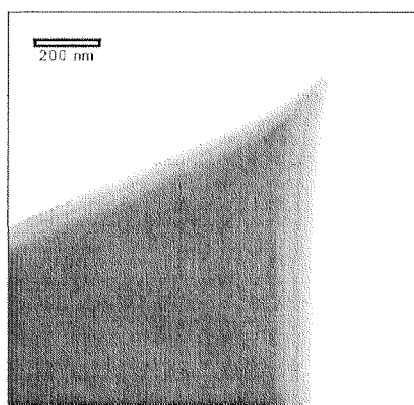


Figure 1A: TEM image of a flattened silicon tip for binding several biomolecules onto the top. The diameter of the tip at the flat area is 50 ± 1 nm and remained unchanged during the experiment.

The functionalization of the tip is based upon the method proposed by Weetall et al. [Weetall and Filbert, 1974; Weetall, 1976] and is schematically presented in Fig. 1 B. In a first step the tip was silanized with a 5% solution of 3-aminopropyl-triethoxysilane (3-APTES) (Fluka Chemie, Buchs, Switzerland) in 5% ethanol/95% water at room temperature for 15 minutes. The tip was then rinsed with the 5% ethanol/95% water solution followed by air drying for 15 to 30 minutes. In a second step, the tip was immersed into a 2.5% glutaraldehyde solution in 100 mM phosphate buffer (pH 7.0) for 45 minutes and then extensively rinsed with water.

Surface analytical investigations such as AFM roughness measurements and ellipsometry, can be found in [Vinckier, 1996b]. In the last step the proteins (Gly-Ala) citrate synthase ($10 \mu\text{M}$) and (Cys-Ala) β -lactamase ($14 \mu\text{M}$) in 50 mM MOPS pH 7.2 bind covalently onto the activated tip via their amino groups after a 30-60 minute incubation. Most likely, the proteins are immobilized randomly in different orientations.

The denaturation of these substrate proteins, covalently bound to the tip, was performed by an overnight incubation at 4°C in 8 M urea or 6 M guanidinium hydrochloride in MOPS buffer.

Hydrophobic tips were obtained by first cleaning the tip in UV light as described above and then reacting them with octadecyltrichlorosilane (OTS) (Fluka, Buchs, Switzerland). The tip was immersed in a n-hexane solution of 10% OTS during 30 minutes. Afterwards, the tip was rinsed with n-hexane and shortly air dried, followed by a 2 hour curing in an oven at 160°C .

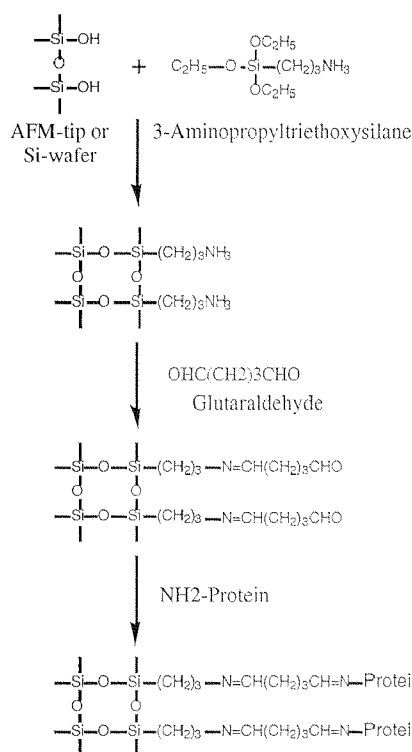


Figure 1B: Reaction scheme for the functionalization of the tip following the method of Weetall and Filbert [1974].

Since the tip modification cannot be monitored, we analyzed this reaction on pieces of a silicon wafer. Contact mode AFM showed a relatively homogeneous layer with a root mean square roughness of $6.0 \pm 0.4 \text{ \AA}$; however, a minor polymerization resulting in particle contamination cannot be excluded. The thickness by ellipsometry was $4.3 \pm 0.6 \text{ nm}$, which is a hydrophobic layer with a contact angle of $102 \pm 3^\circ$, whereas the hydrophilic SiO_2 showed a contact angle of $28 \pm 2^\circ$.

RESULTS AND DISCUSSION

Structural studies of GroEL by AFM

To study the interaction of GroEL with a substrate protein, it was first necessary to determine the orientation of the chaperonin which was allowed to adsorb onto mica. The orientational direction was investigated by atomic force microscopy (AFM). Fig. 2A shows a tapping mode (acoustically driven [Vinckier et al., 1996a]) AFM image of GroEL in water. The 'doughnut-like' structure of GroEL can be observed. The outer

diameter of the rings is 48 ± 4 nm and the height is 2.5 ± 0.3 nm. The inner diameter (the apparent 'hole') observed here was 5 ± 1 nm. The corresponding values from the x-ray structure of GroEL are 13.7 nm for the diameter, 14.6 nm for the height and 4.5 nm for the inner diameter [Braig et al., 1994].

The discrepancy between the height measured by AFM and that measured by x-rays is most probably due to squeezing the GroEL by the tip under the high vertical force. To explore this, we measured the indentation and the average height in contact mode AFM images at the same exerted force, because it has been shown that the sum of the indentation and the average height gives a height close to the true value [Vinckier et al., 1996c]. The indentation obtained was 10 ± 1 nm and the average height 4 ± 1 nm which results in a 14 nm high molecule, which is in excellent agreement with the value obtained from x-ray crystallography (14.6 nm). This result confirms that GroEL is bound in a native conformation with the two rings stacked back-to-back.

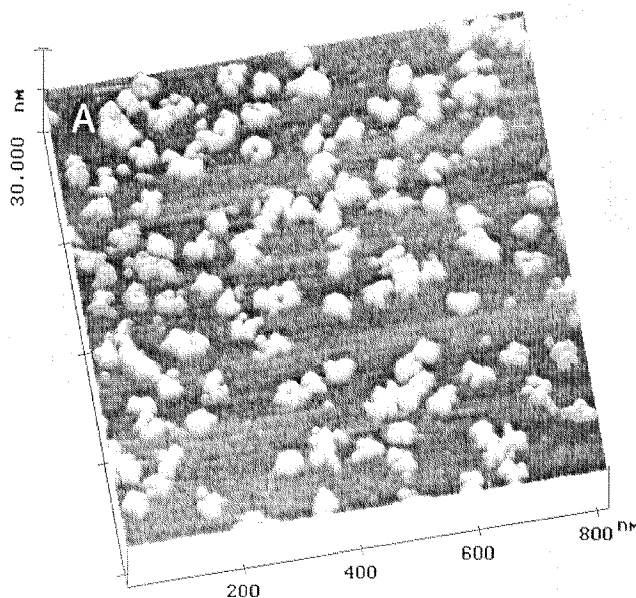


Figure 2A: Acoustically driven tapping mode AFM image under water of on mica adsorbed GroEL, which was fixed with 2.5% glutaraldehyde. The MOPS buffer did not contain polyethyleneglycol 6000 or ammonium molybdate. The characteristic ring structure is discernable, and some fine structure can be made out. The GroEL binds to mica in an up-right position.

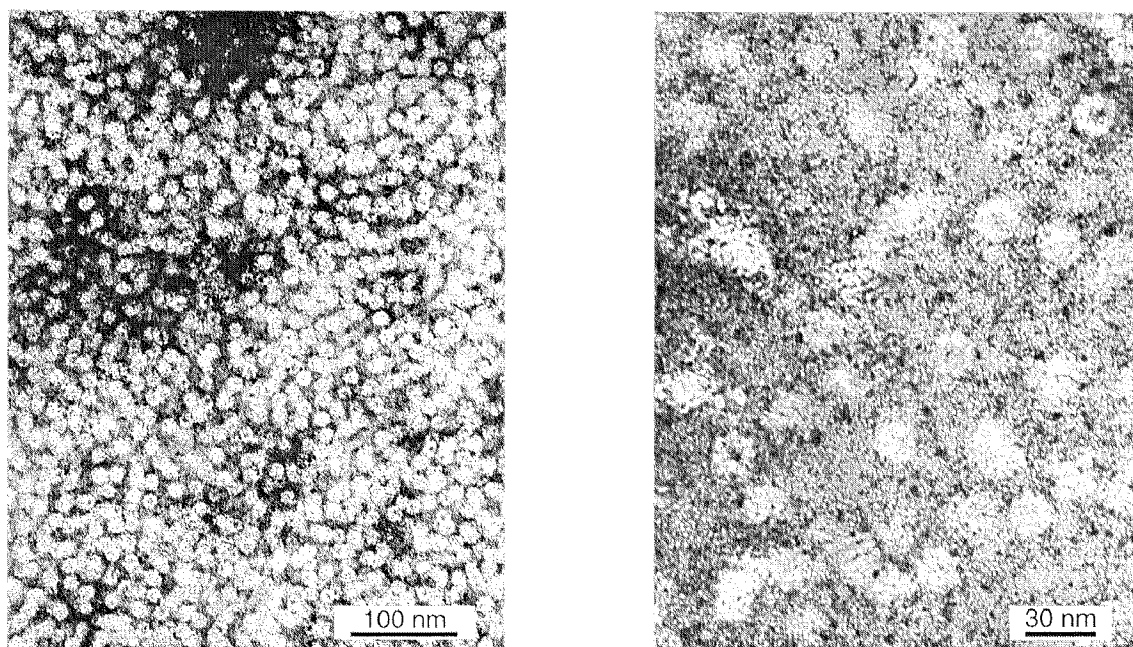


Figure 2B: Typical TEM images of GroEL (negative staining with uranyl acetate)

The apparent larger width is due to convolution because of the finite size at the apex of the tip [Vinckier et al., 1995 and references therein]. For the single molecules in Fig. 2A, a lateral resolution of 4 nm and a vertical resolution of 0.3 nm has been found. While the highest resolution has been obtained with contact mode AFM under liquid, using 2-D crystals of GroEL [Mou et al. , 1996a and b], we used tapping mode AFM for imaging in the present work despite its lower resolution to prevent the 'moving' of the molecules because we did not deal with a closely packed monolayer. In the presence of polyethyleneglycol 6000 and ammonium molybdate we obtained a relatively closely packed layer, which was used for the force measurements (data not shown).

When the structure of GroEL was investigated by TEM, the chaperonin was bound onto formvar coated grids, and negatively stained with uranyl acetate. The TEM images in Fig. 2B show the ring structure of GroEL with the subunits clearly visible. Also under these conditions there also was a tendency for an up-right orientation, as in the case of the AFM images of GroEL.

AFM images show that GroEL tends to orientate itself in the up-right position, i.e. with the channel (almost) normal to the supporting substrate. Our results are therefore in good agreement with the work of Mou et al. [1996 a and b] as well as of Scheuring [1996].

Interaction of (Gly-Ala) citrate synthase and (Cys-Ala) β -lactamase with GroEL

We used flattened tips to permit several proteins to bind, and therefore to improve the chances that a molecule on the tip will interact with GroEL. The flatness also reduces the danger of damage on the tip. Before each experiment, the shape of the flattened tip was checked by TEM, as described in Materials and Methods. Fig. 1A shows a TEM picture of the tip apex with a flat area and a diameter of 50 ± 1 nm, which was unchanged at the end of the experiment.

Due to the up-right orientation of GroEL, we investigated the interaction between GroEL and (Gly-Ala) citrate synthase, and between GroEL and (Cys-Ala) β -lactamase by recording force-distance curves under different physiological conditions with a functionalized tip. A typical force-distance curve is shown in Fig. 3.

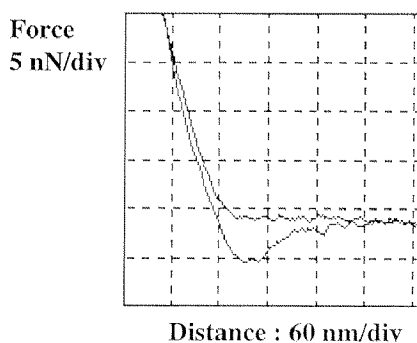


Figure 3: An example of a typical force-distance curve between a modified tip and on mica adsorbed GroEL in absence of any nucleotide. The tip was modified with 'native-like' (Gly-Ala) citrate synthase.

The resulting forces for the interaction between GroEL and (Gly-Ala) citrate synthase, and between GroEL and (Cys-Ala) β -lactamase are shown in Figs. 4 and 5 respectively. The force distributions shown in Figs. 4 and 5, however, are due to several simultaneous molecular interactions.

In Figs. 4A and 5A, the interaction of the native enzyme with GroEL was recorded in the absence of any nucleotide and it gives a distribution, whose maxima are 420 ± 100 pN for (Gly-Ala) citrate synthase and 240 ± 70 pN for (Cys-Ala) β -lactamase.

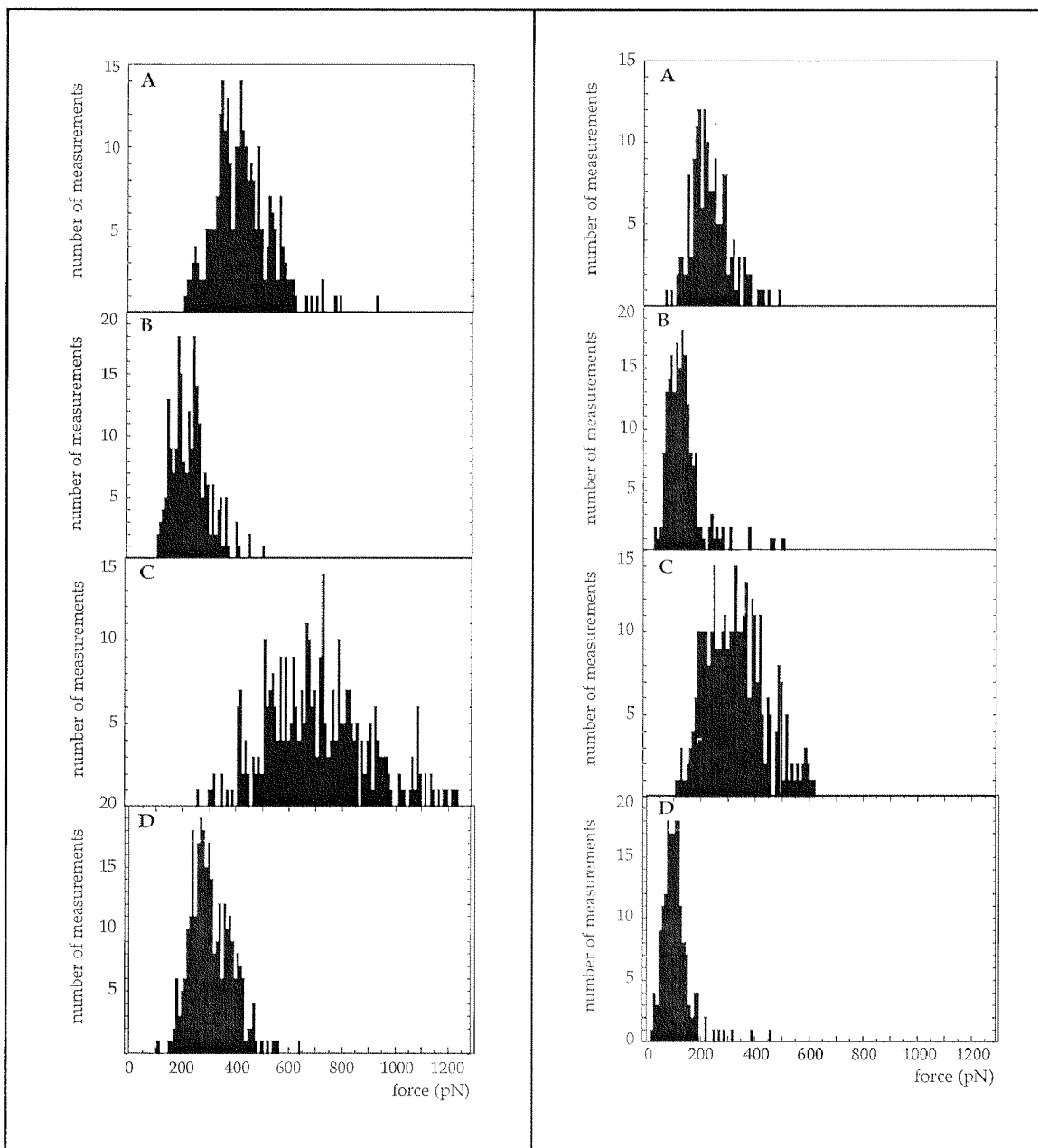


Figure 4: Force distributions of GroEL with (Gly-Ala) citrate synthase. The tip diameter was 70 ± 1 nm. In part (A) the native protein was bound onto the tip and in (B) the interaction was measured in the presence of 2.5 mM ATP. Parts (C) and (D) show the result by using denatured proteins in the absence (C) and presence (D) of ATP.

Figure 5: Force distributions of GroEL with (Cys-Ala) b-lactamase. The tip diameter was 80 ± 1 nm. In part (A) the native protein was bound onto the tip and in (B) the interaction was measured in the presence of 2.5 mM ATP. Parts (C) and (D) show the result by using denatured proteins in the absence (C) and presence (D) of ATP.

This interaction may be due to hydrophobic patches existing on the surface of the native protein, and / or involve those protein molecules which are partially denatured by either

the immobilization procedure or being compressed in the approach phase of the force measurement. In a following step (Figs. 4B and 5B) ATP was added to the solution in the cell at room temperature and incubated for 1 h. The results presented in Fig. 4B and 5B show a marked decrease in the interaction force, i.e. both proteins covalently bound to the tip interact more weakly with GroEL.

In panels C and D the same tips with (Gly-Ala) citrate synthase, or (Cys-Ala) β -lactamase molecules respectively, had been incubated overnight in urea or guanidinium hydrochloride. The force distribution between the denatured (Gly-Ala) citrate synthase or (Cys-Ala) β -lactamase and GroEL in the absence of nucleotides is shown in Figs. 4 C and 5 C. A higher maximum and a wider distribution curve was observed. For the interaction with (Gly-Ala) citrate synthase, we found a mean force of 770 ± 190 pN, for that with (Cys-Ala) β -lactamase the force was 350 ± 100 pN. In panel D the same experiment was performed in the presence of ATP, which again resulted in a marked decrease in the interaction force. Repeating this sequence of steps A through D with different tips always showed a similar, reproducible behavior (data not shown). The tip shape was controlled after each experiment by TEM to ascertain that the tip apex had not undergone alterations. Also, the packing of the GroEL-molecules on the sample before, during and after the experiments was checked by tapping mode AFM. We found that the GroEL molecules were closely packed, with almost no space between them. This densely packed layer was obtained by using polyethyleneglycol 6000 and ammonium molybdate, but no glutaraldehyde fixation has been used.

TABLE 1 Mean interaction forces in the control experiments.

tip surface	bottom surface	forces \pm SD (pN)
(Gly-Ala) citrate synthase	mica	20 ± 20
(Cys-Ala) β -lactamase	mica	130 ± 10
hydrophilic silicon tip	GroEL	80 ± 20
hydrophilic silicon tip	GroEL in the presence of ATP	970 ± 370
hydrophobic silicon tip	GroEL	430 ± 100
hydrophobic silicon tip	GroEL in the presence of ATP	140 ± 40
glutaraldehyde activated tip	GroEL	80 ± 30

Control experiments were performed by measuring the interaction between the tip and mica during all the steps of the functionalization of the tip; and the interaction of the

substrate protein, immobilized to the tip, with freshly cleaved mica, as well as the interaction between a glutaraldehyde activated tip with GroEL adsorbed on mica: almost no interaction was measured (Table 1). Thus, although we cannot totally exclude very small interactions of the mica background with the modified silicon tip, these interactions must be negligible; the force-distribution plots in Figs. 4 and 5 describe indeed the specific interactions between GroEL and the substrate proteins.

By using bovine serum albumin (BSA) or horse radish peroxidase, a behavior similar to (Gly-Ala) citrate synthase or (Cys-Ala) β -lactamase was observed. For the tip functionalized with peroxidase, we found in the absence of any nucleotide that the native-like protein feels a force of 130 ± 30 pN (tip diameter 25 nm), whereas the force between BSA and GroEL was 570 ± 60 pN (tip diameter 30 nm). It is known that GroEL interacts with exposed hydrophobic patches on many proteins and, therefore, as our results demonstrate, potentially with any partially unfolded proteins.

Comparison between native-like and unfolded substrate proteins on the interaction of GroEL.

There is a clear difference in the force distribution between the native-like and the unfolded form of both substrate proteins (Gly-Ala) citrate synthase and (Cys-Ala) β -lactamase, which is consistent with biochemical experiments [Zahn et al., 1996; Gervasoni and Plückthun, 1997a and b]. We observed a shift in the maximum of the distribution curve (770 ± 190 pN for (Gly-Ala) citrate synthase and 350 ± 100 pN for (Cys-Ala) β -lactamase), as well as a broadening of the distribution curve for the interaction forces. This can be explained by the fact that the hydrophobic amino acids of soluble, globular proteins become more exposed and therefore accessible for binding to the chaperone only in non-native states. However, it was not possible to distinguish whether there are different steps in the distribution curve, which might be due to several molecules bound to the tip or to multiple interaction steps of a single molecule. The already rather strong interaction between the native-like proteins and GroEL (420 ± 100 pN for (Gly-Ala) citrate synthase and 240 ± 70 pN for (Cys-Ala) β -lactamase) suggest that hydrophobic patches occurring on the surface of the native substrate protein interact with GroEL and / or that some partial denaturation of the proteins bound to the tip has occurred due to the immobilization step or due to the applied force during the measurements.

Effect of ATP on the interaction forces between GroEL and substrate proteins

In the presence of ATP, the apical domains of GroEL move upward, rotate and the substrate protein is released [Rye et al., 1997]. Therefore, the interaction force between GroEL and the substrate protein is expected to decrease. In the experiments shown in Figs. 4 B, D and 5 B, D the interaction force indeed decreases in the presence of 2.5 mM ATP. Under the conditions used in this work, the ATP hydrolysis by GroEL has a half life of 10 seconds, and this is also the rate limiting step of the whole ATP cycle – ATP binding, hydrolysis and ADP•P release. Therefore, the GroEL structure observed here in a steady state hydrolysis represents largely an ATP-bound state, i.e. the R-state [Burston et al., 1995; Roseman et al., 1996]. For the interaction of GroEL with native (Gly-Ala) citrate synthase we found an interaction force of 230 ± 70 pN, and for the denatured protein an interaction force of 320 ± 80 pN, both in the presence of ATP. In the case of native-like (Cys-Ala) β -lactamase the measured force was 140 ± 60 pN, and with GndCl-denatured (Cys-Ala) β -lactamase 120 ± 50 pN, also both in the presence of ATP. The minor changes can be related to the exact orientation of the molecules on the tip and to the GroEL occupation on the mica. Consequently, there is no large difference between the native and the denatured protein when ATP is present.

To test the effect of ATP hydrolysis on the interaction forces a non-hydrolyzable ATP-analogue, ATP γ S, has been used. We found that both the native and denatured substrate proteins show the same interaction force in the presence of ATP γ S as in the absence of any nucleotide. The data are summarized in Table 2. Interestingly, the x-ray structure of GroEL in the presence of ATP γ S shows that the binding of the non-hydrolyzable nucleotide analogue results in only small conformational changes, compared to the free GroEL [Boisvert et al., 1996]. This unexpected result was rationalized by Aharoni and Horowitz [1996], who showed that the negative cooperativity between the two rings of GroEL was reduced in the GroEL mutant (R13G/A126V) used in the x-ray crystallography studies. In addition, cryo-EM observations of GroEL in the presence of the non-hydrolyzable ATP analogue, AMP-PNP, also showed a conformation intermediate between the ADP- and ATP-GroEL bound state (Roseman et al., 1996). This suggests that the interaction forces between GroEL and the substrate protein are not to be necessarily effected by the presence or absence of the non-hydrolyzable ATP-analogue, ATP γ S. Taken together, these results with different nucleotides strongly support the conclusion that we are observing specific substrate-GroEL interactions.

TABLE 2 Mean forces (\pm SD) of the interaction between GroEL and (Cys-Ala) 2-lactamase in the absence of any nucleotide or in the presence of ATP or ATP_S.

(Cys-Ala) β -lactamase	without ATP (pN)	with ATP (pN)	with ATP_S (pN)
with tip 1 from Fig. 5:			
native-like	240 \pm 70	140 \pm 60	
GdmCl denatured	350 \pm 100	120 \pm 50	
with tip 2:			
native-like	260 \pm 60		280 \pm 70
GdmCl denatured	390 \pm 80		390 \pm 70

Comparison of the two substrate proteins

When comparing the interaction forces obtained for the two substrate proteins, a smaller force was always found in Figs. 4 and 5 for (Cys-Ala) β -lactamase than for (Gly-Ala) citrate synthase. Usually the interaction force between GroEL and (Cys-Ala) β -lactamase was roughly half of that obtained between GroEL and (Gly-Ala) citrate synthase, with the same tip diameter. The forces measured may be related to the molecular size and the interaction surface of the substrate protein.

In Table 3 results from several interaction experiments between GroEL and the native-like form of (Cys-Ala) β -lactamase and the varying tip diameter are listed. A tip with larger diameter can accomodate more substrate proteins which results in a higher interaction force.

TABLE 3: Mean forces in pN between GroEL and (Cys-Ala) 2-lactamase, depending on the diameter of the functionalized tip.

diameter of the tip (nm)	mean force \pm SD (pN)
35	110 \pm 30
54	220 \pm 60
80	240 \pm 70
110	280 \pm 70
160	380 \pm 100

Hydrophobic and hydrophilic tips

To check the importance of hydrophobic effects on the GroEL - substrate protein interaction, the tips were modified into hydrophilic and hydrophobic tips. We compared the interaction with GroEL on mica with a cleaned (hydrophilic) silicon tip as well as with a hydrophobic tip, i.e., a silicon tip modified with OTS, as described in Materials and Methods. These experiments were performed in order to understand the hydrophilic and hydrophobic interactions between GroEL and chemically well characterized samples (Table 1). We found that the hydrophilic tip itself interacts poorly with GroEL and gives an interaction force of only 80 ± 20 pN, whereas the hydrophobic tip shows an interaction force similar to that of the substrate proteins, immobilized on the tip. In fact, the interaction force with hydrophobic tips is 430 ± 100 pN, which lies in the range for the native-like proteins (Figs. 4 and 5). The tip diameter was also 50 nm, and thus in the same range as the functionalized tips. In the presence of ATP the hydrophilic tip shows an increased interaction with GroEL, which gives an interaction force of 970 ± 370 pN. The hydrophobic tip, however, showed a decreased interaction force of 140 ± 40 pN in the presence of ATP. Both results indicate that the interaction between GroEL and the substrate proteins is mostly hydrophobic, and that the forces measure the conformational state of GroEL.

CONCLUSIONS

In this work we show that tapping mode AFM under liquid leads to resolved images of GroEL. We were able to obtain images of the characteristic ring-structure of the chaperonin in which some fine structure can make out. Due to the up-right orientation of GroEL on mica, AFM allowed quantitative, reproducible measurements of the interaction force between GroEL and the substrate proteins, (Gly-Ala) citrate synthase and (Cys-Ala) β -lactamase by covalently immobilizing them to the surface of the tip. We could measure by AFM the changes in the interaction forces upon addition of ATP, which results in conformational changes of the GroEL apical domains: in the presence of ATP the interaction force between the two substrate proteins and GroEL decreased. Similarly, we found that denatured proteins give rise to a higher interaction force than the native-like proteins. Finally, the experiments also prove that hydrophobicity is important for the interaction of the substrate proteins with GroEL.

Acknowledgements

The authors thank P. Kernen, J.A. DeRose and P. Wagner for helpful discussions, H.-P. Lipp for the statistical advice and B. Klinger for help with the purification of the proteins.

This work was supported by SNSF (NFP 36), SNSF 31-037720.93/1 and O. Mayenfisch-Stiftung.

REFERENCES (Only for “Anja Vinckier et al.” paper)

- Aharoni, A., and A. Horovitz. 1996. Inter-ring communication is disrupted in the GroEL mutant Arg13_Gly; Ala126_Val with known crystal structure. *J. Mol. Biol.* 258: 732-735.
- Allen, S., J. Davies, A.C. Dawkes, M.C. Davies, J.C. Edwards, M.C. Parker, C.J. Roberts, J. Sefton, S.J. Tendler, and P.M. Williams. 1996. In situ observation of streptavidin-biotin binding on an immunoassy well surface using an atomic force microscope. *FEBS Lett.* 390: 161-164.
- Allen, S., X.Y. Chen, J. Davies., M.C. Davies, A.C. Dawkes, J.C. Edwards, C.J. Roberts, J. Sefton, S.J.B. Tendler, and P.M. Williams. 1997. Detection of antigen-antibody binding events with the atomic force microscope. *Biochem.* 36: 7457-7463.
- Aoki, K., H. Taguchi, Y. Shindo, M. Yoshida, K. Ogasahara, K. Yutani, and N. Tanaka. 1997. Calorimetric observation of a GroEL-protein binding reaction with little contribution of hydrophobic interaction. *J. Biol. Chem.* 272: 32158-32162.
- Boisvert, D.C., J. Wang, Z. Otwinowski, A.L. Horwich, and P.B. Sigler. 1996. The 2.4 Å crystal structure of the bacterial chaperonin complexed with ATP_S. *Nature Struct. Biol.* 3: 170-177.
- Boland, T., and B.D. Ratner. 1995. Direct measurements of hydrogen bonding in DNA nucleotide bases by atomic force meicroscopy. *Proc. Natl. Acad. Sci. USA*

92: 5297-5301.

Braig, K., Z. Otwinowski, R. Hegde, D.C. Boisvert, A. Joachmiak, A.L. Horwich, and P.B. Sigler. 1994. The crystal structure of the bacterial chaperonin GroEL at 2.8 Å. *Nature* 371: 578-586.

Burston, S.G., N.A. Ranson, and A.R. Clarke. 1995. The origins and consequences of asymmetry in the chaperonin reaction cycle. *J. Mol. Biol.* 249: 138-152.

Chen, S., A.M. Roseman, A.S. Hunter, S.P. Wood, S.G. Burston, N.A. Ranson, A.R. Clarke, and H.R. Saibil. 1994. Localization of a folding protein and shape changes in GroEL-GroES complexes imaged by cryo-electron microscopy. *Nature* 371: 261-264.

Cleveland, J., S. Manne, D. Bocek, and P.K. Hansma. 1993. A nondestructive method for determining the spring constant of cantilevers for scanning force microscopy. *Rev. Sci. Instrum.* 64: 403-405 (1993).

Dammer, U., O. Popescu, P. Wagner, D. Anselmetti, H.-J. Güntherodt, and G.N. Misevic. 1995. Binding strength between cell adhesion proteoglycans measured by atomic force microscopy. *Science* 267: 1173-1175.

Dammer, U., M. Hegner, D. Anselmetti, P. Wagner, M. Dreier, W. Huber, and H.-J. Güntherodt. 1996. Specific antigen/antibody interactions measured by force microscopy. *Biophys. J.* 70: 2437-2441.

DeRose, J.A., and J.-P. Revel. 1997. Examination of atomic (scanning) force microscopy probe tips with the transmission electron microscope. *Microsc. Microanal.* 3: 203-213.

Detrich, H.W. 3d., M.A. Jordan, L. Wilson, and R.C. Williams Jr. 1985. Mechanism of microtubule assembly. Changes in polymer structure and organization during assembly of sea urchin egg tubulin. *J. Biol. Chem.* 260: 9479-9490.

Evans, E., D. Berk, and A. Leung. 1991. Detachment of agglutinin-bonded red-blood cells. I. Forces to rupture molecular-point detachments. *Biophys. J.* 59: 838-848.

Evans, E., K. Ritchie, and R. Merkel. 1995. Sensitive force technique to probe molecular adhesion and structural linkage at biological interfaces. *Biophys. J.*

- 68: 2580-2587.
- Fenton, W.A., Y. Kashi, K. Furtak, and A.L. Horwich. 1994. Residues in chaperonin GroEL required for polypeptide binding and release. *Nature* 371: 557-559.
- Fenton, W.A., and A.L. Horwich. 1997. GroEL-mediated protein folding. *Protein Science* 6: 743-760.
- Florin, E.-L., V.T. Moy, and H.E. Gaub. 1994. Adhesion forces individual ligand-receptor pairs. *Science* 264: 415-417.
- Fritz, J., D. Anselmetti, J. Jarchow, and X. Fernàndez-Busquets. 1997. Probing single biomolecules with atomic force microscopy. *J. Struct. Biol.* 119: 165-171.
- Gervasoni, P., and A. Plückthun. 1997a. Folding intermediates of β -lactamase recognized by GroEL. *FEBS Lett.* 401: 138-142.
- Gervasoni, P., P. Gehrig, and A. Plückthun. 1997b. Two conformational states of β -lactamase bound to GroEL: a biophysical characterization. *J. Mol. Biol.* In press.
- Hartl, F.U. 1996. Molecular chaperones in cellular protein folding. *Nature* 381: 571-579.
- Hinterdorfer, P., W. Baumgartner, H.J. Gruber, K. Schilcher, and H. Schindler. 1996. Detection and localization of individual antibody-antigen recognition events by atomic force microscopy. *Proc. Natl. Acad. Sci. USA* 93: 3477-3481.
- Hoh, J.H., J.P. Cleveland, C.B. Prater, J.-P. Revel, and P.K. Hansma. 1992. Quantized adhesion detected with the atomic force microscope. *J. Am. Chem. Soc.* 114: 4917-4918.
- Israelachvili, J.N., editor. 1989. Intermolecular and surface forces. 3d ed. Academic Press Ltd, London.
- Itzhaki, L.S., D.E. Otzen, and A.R. Fersht. 1995. Nature and consequences of GroEL-protein interactions. *Biochemistry* 34: 14581-14587.
- Lamiet, A., and A. Plückthun. 1989. The precursor of β -lactamase: purification, properties and folding kinetics. *EMBO J.* 8: 1469-1477.
- Leckband, D. 1995. The surface force apparatus – a tool for probing molecular protein interactions. *Nature* 376: 617-618.

- Lee, G.U., D.A. Kidwell, and R.J. Colton. 1994a. Sensing discrete straptavidin-biotin interactions with atomic force microscopy. *Langmuir* 10: 354-357.
- Lee, G.U., L.A. Chrisey, and R.J. Colton. 1994b. Direct measurements of the forces between complementary strands of DNA. *Science* 266: 771-773.
- Lin, Z., F.P. Schwarz, and E. Eisenstein. 1995. The hydrophobic nature of GroEL-substrate binding. *J. Biol. Chem.* 270: 1011-1014.
- Lindner, P., B. Guth, C. Wülfling, C. Krebber, B. Steipe, F. Müller, and A. Plückthun. 1992. Purification of native proteins from the cytoplasm and periplasm of *Escherichia coli* using IMAC and histidine tails: a comparison of proteins and protocols. *Methods* 4: 41-56.
- Ludwig, M., V.T. Moy, M. Rief, E.-L. Florin, and H.E. Gaub. 1994. Characterization of the adhesion force between avidin-functionalized AFM tips and biotinylated agarose beads. *Microsc. Microanal. Microstruct.* 5: 321-328.
- Mayhew, M., A.C. da Silva, J. Martin, H. Erdjument-Bromage, P. Tempst, and F.U. Hartl. 1996. Protein folding in the central cavity of the GroEL-GroES chaperonin complex. *Nature* 379: 420-426.
- Mou, J., D.M. Czaykowski, S.J. Sheng, R. Ho, and Z. Shao. 1996a. High resolution surface structure of *E. Coli* GroES oligomer by atomic force microscopy. *FEBS Lett.* 381: 161-164.
- Mou, J., S.J. Sheng, R. Ho, and Z. Shao. 1996b. Chaperonins GroEL and GroES: views from atomic force microscopy. *Biophys. J.* 71: 2213-2221.
- Moy, V.T., E.L. Florin, and H.E. Gaub. 1994. Intermolecular forces and energies between ligands and receptors. *Science* 266: 257-259.
- Nakajima, H., Y. Kunioka, K. Nokano, K. Shimizu, M. Seto, and T. Ando. 1997. Scanning force microscopy of the interaction events between a single molecule of heavy meromyosin and actin. *Biochem. Biophys. Res. Commun.* 234: 178-182.
- Noy, A., D.V. Vezenov, J.F. Kayyem, T.J. Meade, and C.M. Lieber. 1997. Stretching and breaking duplex DNA by chemical force microscopy. *Chemistry and Biology* 4: 519-527.
- Perrett, S., R. Zahn, G. Stenberg, and A.R. Fersht. 1997. Importance of electrostatic

- interaction in the rapid binding of polypeptides to GroEL. *J. Mol. Biol.* 269: 892-901.
- Pierres, A., A.M. Benoliel, P. Bongrand, and P.A. van der Merwe. 1996a. Determination of the life time and force dependence of interactions of single bonds between surface-detached CD2 and CD48 adhesion molecules. *Proc. Natl. Acad. Sci. USA* 93: 15114-15118.
- Pierres, A., A.-M. Benoliel, and P. Bongrand. 1996b. Measuring bonds between surface-associated molecules. *J. Immunol. Meth.* 196: 105-120.
- Roberts, C.J., M.C. Davies, S.J. Tendler, P.M. Williams, J. Davies, A.C. Dawkes, G.D. Yearwood, and J.C. Edwards. 1996. The discrimination of IgM and IgG type antibodies and Fab' and F(ab)₂ antibody fragments on an industrial substrate using scanning force microscopy. *Ultramicroscopy* 62: 149-155.
- Roseman, A., S. Chen, H. White, K. Braig, and H. Saibil. 1996. The chaperonin ATPase cycle: mechanism of allosteric switching and movements of substrate-binding domains in GroEL. *Cell* 87: 241-251.
- Rye, H.S., S.G. Burston, W.A. Fenton, J.M. Beechem, Z.H. Xu, P.B. Sigler, and A.L. Horwich. 1997. Distinct actions of cis and trans ATP within the double ring of the chaperonin GroEL. *Nature* 388: 792-798.
- Scheuring, S. 1996. Diploma thesis. A study of the E. coli chaperonin GroEL and GroEL/GroES complexes using transmission electron and atomic force microscopy: its structure and function. Biozentrum Basel, Switzerland.
- Stuart, J.K., and V. Hlady. 1995. Effects of discrete protein-surface interactions in scanning force microscopy adhesion force measurements. *Langmuir* 11: 1368-1374.
- Todd, M.S., G.H. Lorimer, and D. Thirumalai. 1996. Chaperonin-facilitated protein folding: optimization of rate and yield by an iterative annealing mechanism. *Proc. Natl. Acad. Sci. USA* 93: 4030-4035.
- Vinckier, A., I. Heyvaert, A. D'Hoore, T. McKittrick, C. Van Haesendonck, Y. Engelborghs, and L. Hellemans. 1995. Immobilizing and imaging microtubules by atomic force microscopy. *Ultramicroscopy* 57: 337-343.
- Vinckier, A., F. Hennau, K. Kjoller, and L. Hellemans. 1996a. Low-cost

- modification of a contact atomic force microscope (AFM) into a sound-activated tapping mode AFM for use in air and liquids. *Rev. Sci. Instrum.* 67: 387-392.
- Vinckier, A. 1996b. Ph.D. thesis. Applications of atomic force microscopy (AFM): development of a tapping mode AFM and study of microtubules. Katholieke Universiteit Leuven, Belgium.
- Vinckier, A., C. Dumortier, Y. Engelborghs, and L. Hellemans. 1996c. Dynamical and mechanical study of immobilized microtubules with atomic force microscopy. *J. Vac. Sci. Technol. B* 14: 1427-1431.
- Weetall, H.H., and A.M. Filbert. 1974. Porous glass for affinity chromatography applications. *Meth. Enzymol.* 34: 59-72.
- Weetall, H.H. 1976. Covalent coupling methods for inorganic support materials. *Meth. Enzymol.* 44: 134-148.
- White, H.E., S. Chen, A.M. Roseman, O. Yifrach, A. Horovitz, and H.R. Saibil. 1997. Structural basis of allosteric changes in the GroEL mutant ARG 197_{ALA}. *Nature Struct. Biol.* 4: 690-694.
- Xu, Z.H., A.L. Horwich, and P.B. Sigler. 1997. The crystal structure of the asymmetric GroEL-GroES-ADP(7) chaperonin complex. *Nature* 388: 741-749.
- Zahn, R., J.R. Harris, G. Pfeifer, A. Plückthun, and W. Baumeister. 1993. Two-dimensional crystals of the molecular chaperone GroEL reveal structural plasticity. *J. Mol. Biol.* 229: 579-584.
- Zahn, R., and A. Plückthun. 1994. Thermodynamic partitioning model for hydrophobic binding of polypeptides by GroEL. II. GroEL recognizes thermally unfolded mature β -lactamase. *J. Mol. Biol.* 242: 165-174.
- Zahn, R., S.E. Axmann, K.-P. Rücknagel, E. Jaeger, and A. Plückthun. 1994. Thermodynamic partitioning model for hydrophobic binding of polypeptides by GroEL. I. GroEL recognizes the signal sequences of β -lactamase precursor. *J. Mol. Biol.* 242: 150-164.
- Zahn, R., P. Lindner, S.E. Axmann, and A. Plückthun. 1996. Effect of single point mutations in citrate synthase on binding to GroEL. *FEBS Lett.* 380:152-156.

REFERENCES

- Allara, D. L. and Nuzzo, R. G. (1995) *Langmuir*, **1**, 52-66.
- ANOTEC, L. (1998) Anotec Separations Ltd., Oxon.
- Bain, C. D., Evall, J. and Whitesides, G. M. (1989a) *J. Am. Chem. Soc.*, **111**, 7155-7164.
- Bain, C. D., Troughton, E. B., Tao, Y.-T., Evall, J., Whitesides, G. M. and Nuzzo, R. G. (1989b) *J. Am. Chem. Soc.*, **111**, 321-335.
- Bain, C. D. and Whitesides, G. M. (1989a) *Angew. Chem. Int. Ed. Engl.*, **28**, 506.
- Bain, C. D. and Whitesides, G. M. (1989b) *J. Am. Chem. Soc.*, **111**, 7164-7175.
- Banci, L., Carloni, P. and Savellini, G. G. (1994) *Biochemistry*, **33**, 12356-12366.
- Barton, D. and Ollis, D. W. (1979) *Sulphur, Selenium, Silicon, Boron, Organometallic Compounds*, Pergamon Press, Oxford.
- Beckmann, M., Nollert, P. and Kolb, H.-A. (1998) *J. Membrane Biol.*, **161**, 227-233.
- Bernard, A., Delamarche, E., Schmid, H., Michel, B., Bosshard, H. R. and Biebuyck, H. (1998) *Langmuir*, **14**, 2225-2229.
- Bertrand, D., Cooper, E., Valera, S., Rungger, D. and Ballivet, M. (1991) In *Methods in Neurosciences*, Vol. 4 Academic Press, , pp. 174-193.
- Biebuyck, H. A., Bain, C. D. and Whitesides, G. M. (1994) *Langmuir*, **10**, 1825.
- Binnig, G., Rohrer, H. and Gerber, C. (1986) *Phys. Rev. Lett.*, **56**, 930-933.
- Bishop, A. R. and Nuzzo, R. G. (1996) *Curr. Opinion in Coll. and Interface Sci.*, **1**, 127-136.
- Bloch, K. (1985) In *Biochemistry of Lipids and Membranes* (Eds, Vance, D. E. and Vance, J. E.) , pp. 1-24.
- Bremer, A., Haener, M. and Aebi, U. (1998) In *Cell Biology: A Laboratory Handbook*, Vol. 3 Acad. Press, .
- Brian, A. A. and McConnell, H. M. (1984) *Proc. Natl. Acad. Sci. USA*, **81**, 6159-6163.
- Buettgenbach, S. (1991) *Mikromechanik*, Teubner, Stuttgart.
- Bunjes, N., Schmidt, E. K., Jonczyk, A., Rippmann, F., Beyer, D., Ringsdorf, H., Graeber, P., Knoll, W. and Neumann, R. (1997) *Langmuir*, **13**, 6188-6194.
- Burck, H.-C. (1969) *Histologische Technik*, Thieme Verlag, Stuttgart.
- Caseri, R. C. (1988) Dissertation, ETH Zurich, Zurich.

- Chalfie, M. and Kain, S. (1996) *Green Fluorescent Protein, properties, applications and protocols*, Wiley-Liss, New York.
- Chapman, D. (1993) In *Biomembranes: Physical Aspects*(Ed, Shinitzky, M.) VHC, , pp. 29-62.
- Coles, L. E. (1976) *Analyst*, **101**, 62-66.
- Cornell, B. A., Braach-Maksvytis, V. L. B., King, L. G., Osman, P. D. J., Raguse, B., Wieczorek, L. and Pace, R. J. (1997) *Nature*, **387**, 580-583.
- Czajkowsky (1996) *Biophysical Journal*, **70**, 350.
- Dammer, U., Popescu, O., Wagner, P., Anselmetti, D., Güntherodt, H.-J. and Misevic, G. N. (1995) *Science*, **267**, 1173-1175.
- Delamarche, E., Bernard, A., Schmid, H., Michel, B. and Biebuyck, H. (1997) *Science*, **276**, 779-781.
- Delamarche, E., Michel, B., Kang, H. and Gerber, C. (1994) *Langmuir*, **10**, 4103-4108.
- Delamarche, E., Schmid, H., Bietsch, A., Larsen, N. B., Rothuizen, H., Michel, H. and Biebuyck, H. (1998) *J. Phys. Chem. B*, **102**, 3324-3334.
- Delamarche, E., Sundarababu, G., Biebuyck, H., Michel, B., Gerber, C., Sigrist, H., Ringsdorf, H., xanthopoulos, N. and Mathieu, H. J. (1996) *Langmuir*, **12**, 1997-2006.
- Ding, L., J., L., Dong, S. and Wang, E. (1996) *J. of Electroanalytical Chemistry*, **416**, 105-112.
- Ding, L., Li, J., Wang, E. and Dong, S. (1997) *Thin Solid Films*, **293**, 153-158.
- Drake, B., Prater, C. B., Weisenhorn, A. L., Gould, S. A. C., Albrecht, T. R., Quate, C. F., Cannell, D. S., Hansma, H. G. and Hansma, P. K. (1989) *Science*, **243**, 1586-1589.
- Drelich, J., Miller, J. D., Kumar, A. and Whitesides, G. M. (1994) *Colloids and Surfaces A*, **93**, 1-13.
- Du, H., Chandaroy, P. and Hui, S. W. (1997) *Biochimica et Biophysica Acta - Biomembranes*, **1326**, 236-248.
- Duncan, J. L. and Schlegel, R. (1975a) *The Journal of Cell Biology*, **67**, 160-173.
- Duncan, J. L. and Schlegel, R. (1975b) *The Journal of Cell Biology*, **67**, 160-173.
- Egger, M., Ohnesorge, F., Weisenhorn, A. L., Heyn, S. P., Drake, B., Prater, C. B., Gould, S. A. C., hansma, P. K. and Gaub, H. E. (1990) *J. of Struct. Biol.*, **103**, 89-94.
- Elender, G., Kuehner, M. and Sackmann, E. (1996) *Biosensors and Bioelectronics*, **11**, 565-577.
- Fang, Y., Cheley, S., Bayley, H. and Yang, J. (1997) *Biochemistry*, **36**, 9518-9522.
- Fang, Y. and Yang, J. (1997) *Biochimica and Biophysica Acta*, **1324**, 309-319.

- Fare, T. L., Palmer, C. A., Silvestre, C. G., Cribbs, D. H., Turner, D. C., Brandow, S. L. and Gaber, B. P. (1992) *Langmuir*, **8**, 3116-3121.
- Fenter, P., Eisenberger, P. and Liang, K. S. (1993) *Phys. rev. Lett.*, **70**, 2447-2450.
- Finklea, H. O., Avery, S., Lynch, M. and Furtch, T. (1987) *Langmuir*, **3**, 409.
- Finklea, H. O., Robinson, L. R., Blackburn, A., Richter, B., Allara, D. and Bright, T. (1986) *Langmuir*, **2**, 239-244.
- Florin, E.-L., Moy, V. T. and Gaug, H. E. (1994) *Science*, **264**, 415-417.
- Fuhrhop, J.-H. and Koenig, J. (1994) *Membranes and Molecular Assemblies*, The Royal Society of Chemistry, Cambridge.
- Fuller, S. D., Berriman, J. A., Butcher, S. J. and Gowen, B. E. (1995) *Cell*, **81**, 715-725.
- Gao, W., Dickinson, L., Gronyinger, C., Morin, F. and Reven, L. (1996) *Langmuir*, **12**, 6429-6435.
- Garland, P. B. (1996) *Quart. Rev. of Biophysics*, **29**, 91-117.
- Glockner, D. A. and Shah, S. I. (1995) *Handbook of thin film process technology*, IOP, Bristol.
- Grandbois, M., Clausen-Schaumann, H. and Gaub, H. (1998) *Biophysical Journal*, **74**, 2398-2404.
- Groves, J. T., Ulman, N. and Boxer, S. (1996) *Science*, **275**, 651-653.
- Guthold, M., Bezanilla, M., Erie, D. A., Jenkins, B., Hansma, H. G. and Bustamante, C. (1994) *Proc. Natl. Acad. Sci. USA*, **91**, 12927-12931.
- Hanke, W. and Schlue, W.-R. (1978) *Planar Lipid Bilayers: Methods and Applications.*, Academic Press.
- Hansma, H. G. and Hoh, J. H. (1994) *Annu. Rev. Biophys. Biomol. Struct.*, **23**, 115-139.
- Harris, J. M. and Zalipsky, S. (1997) *Poly(ethylene glycol)*, American Chemical Society, Washington, DC.
- Harris, J. R., Adrian, M., Bhakdi, S. and Palmer, M. (1998) *J. of Structural Biology*, **121**, 343-355.
- Hegner, M., Wagner, P. and Semenza, G. (1993) *Surf. Sci.*, **291**, 39-46.
- Herbert, C. B., McLernon, T. L., Hypolite, C. L., Adams, D. N., Pikus, L., Huang, C. C., Fields, G. B., Letourneau, P. C., Distefano, M. D. and Hu, W. S. (1997) *Chemistry & Biology*, **4**, 731-737.
- Heuberger, A. (1991) *Mikromechanik: Mikrofertigung mit Methoden der Halbleitertechnologie*, Springer, Berlin.

- Heyse, S., Vogel, H., Saenger, M., Sigrist, H. (1995) *Protein Science*, **4**, 2532-2544.
- Heyse, S., Ernst, O. P., Dienes, Z., Hofmann, K. P. and Vogel, H. (1998a) *Biochemistry*, **37**, 507-522.
- Heyse, S., Ernst, O. P., Dienes, Z., Hofmann, K. P. and Vogel, H. (1998b) *Biochemistry*, **37**, 507-522.
- Higashi, G. S., Chabal, Y. J., Trucks, G. W. and Raghavachari, K. (1990) *Appl. Phys. Lett.*, **56**, 656-658.
- Hirayama, M. K. (1997), Dissertation, ETH Zürich, Zürich.
- Hoerber, J. K. H., Mosbacher, J., Haeberle, W., Ruppertsberg, J. P. and Sakmann, B. (1995) *Biophysical Journal*, **68**, 1687-1693.
- Hoh, J. H. and Schoenenberger, C.-A. (1994) *J. of Cell Science*, **107**, 1105-1114.
- Huang, J., Dahlgren, D. A. and Hemminger, J. C. (1994) *Langmuir*, **10**, 626-628.
- Imabayashi, S., Gon, N., Sasaki, T., Hobara, D. and Kakiuchi, T. (1998) *Langmuir*, **14**, 2348-2351.
- Ingenieure, V. D. (1994) *Maskentechnik für Mikroelektronik-, Mikrotechnikbauteile*, VDI Verlag.
- John, S. A., Saner, D., Pitts, J. D., Holzenburg, A., Finbow, M. E. and Lal, R. (1995) *J. of struct. Biol.*, **120**, 22-31.
- Johnson, W. C. (1967) *Analyst*, **92**, 403-407.
- Jones, N. D. (1979) In *Comprehensive Organic Chemistry*, Vol. 3 (Eds, Barton, D. and Ollis, D. W.) Pergamon Press, Oxford.
- Kalb, E., Frey, S. and Tamm, L. K. (1992) *Biochimica et Biophysica Acta*, **1103**, 307-316.
- Karrasch, S., Hegerl, R., Hoh, J. H., Baumeister, W. and Engel, A. (1994) *Proc. Natl. Acad. Sci. USA*, **91**, 836-838.
- Kasas, S., Thomson, N. H., Smith, B. L., Hansma, P. K., Miklossy, J. and Hansma, H. G. (1997) *Int. J. of Imag. Syst. and Tech.*, **8**, 151-161.
- Kim, E., Xia, Y., Whitesides, G. M. (1996) *Advanced Materials*, **8**, 245-247.
- Kossek, S., Padeste, C. and Tiefenauer, L. (1996) *J. of Molecular Recognition*, **9**, 485-487.
- Kumar, A., Biebuyck, H. A. and Whitesides, G. M. (1994) *Langmuir*, **10**, 1498-1511.
- Kuznetsov, Y. G., Malkin, A. J. and McPherson, A. (1997) *J. of Struct. Biol.*, **120**, 180-191.
- Lal, R. and John, S. A. (1994) *Am. J. Physiol.*, **266**, C1-C21.

- Lang, H., Duschl, C. and Vogel, H. (1994a) *Langmuir*, **10**, 197-210.
- Lang, H., Duschl, C. and Vogel, H. (1994b) *Langmuir*, **10**, 197-210.
- Lang, H., Koenig, B. and Vogel, H. (1993) , Patent, Nr. G01N 33/543, 33/68, C12Q 1/00, Switzerland.
- Lärmer, J., Schneider, S. W., Danker, T., Schwab, A. and Oberleithner, H. (1997) *Pflügers Arch. - Eur. J. Physiol.*, **434**, 254-260.
- Lasic, D. D. (1993) *Liposomes: From Physics to Applications*, Elsevier, Amsterdam.
- Lee, G. U., Chrisey, L. A. and Colton, R. J. (1994) *Science*, **266**, 771-773.
- Leggett, G. J., Roberts, C., J., Williams, P. M., Davies, M. C., Jackson, D. E. and Tendler, S. J. B. (1993) *Langmuir*, **9**, 2356.
- Lehmann, H.-J., Ruiz, L. and Zaugg, F. (1998a) *Diploma thesis*, ETH Zurich.
- Lehmann, H.-J., Ruiz, L. and Zaugg, F. (1998b) *Diploma thesis*, Surface Science, Zurich.
- Lesniewska, E., Giocondi, M. C., Vie, V., Finot, E., Goudonnet, J. P. and Le Grimellec, C. (1998) *Kidney Internat.* **65**, 42-48.
- Lopez, G. P., Albers, M. W., Schreiber, S. L., Carroll, R., Peralta, E. and Whitesides, G. M. (1993a) *J. Am. Chem. Soc.*, **115**, 5877-5878.
- Lopez, G. P., Biebuyck, H. A., Haerter, R., Kumar, A. and Whitesides, G. M. (1993b) *J. Am. Chem. Soc.*, **115**, 10774-10781.
- MacDonald, R. C., MacDonald, R. I., Menco, B. P., Takeshita, K., Subbarao, N. K. and Hu, L.-R. (1991) *Biochimica et Biophysica Acta*, **1061**, 297-303.
- Mason, T. J. (1990) *Sonochemistry - The Uses of Ultrasound in Chemistry*, The Royal Society of Chemistry, Cambridge.
- McConnell, H. M., Tamm, L. K. and Weis, R. M. (1984) *Proc. Natl. Acad. Sci. USA*, **81**, 3249-3253.
- Menz, W. and Bley, P. (1993) *Mikrosystemtechnik für Ingenieure*, VCH.
- Merciniec, B. (1992) *Comprehensive handbook on hydrosilylation*, Pergamon press, Oxford.
- Michel-Choi, R. (1998) *Diploma thesis*, Laboratory of Surface Science and Technology, ETH Zürich.
- Miller, C. (1986) *Ion Channel reconstitution*, Plenum, New York.
- Miller, E. J. and Rhodes, R. K. (1982) *Meth. Enzymol.*, **82**, 33-64.
- Mittal, K. L. (1992) *Silanes and other coupling agents*, VSP, Utrecht.

- Mou, J., Yang, J., Huang, C. and Shao, Z. (1994a) *Biochemistry*, **33**, 9981-9985.
- Mou, J., Yang, J. and Shao, Z. (1994b) *Biochemistry*, **33**, 4439-4443.
- Mrksich, M., Dike, L. E., Tien, J., Ingber, D. E. and Whitesides, G. M. (1997) *Experimental Cell Research*, **235**, 305-313.
- Mrksich, M. and Whitesides, G. M. (1996) *Annu. Rev. Biophys. Biomol. Struct.*, **25**, 55-78.
- Mueller, D. J., Baumeister, W. and Engel, A. (1996) *J. of Bacteriology*, **178**, 3025-3030.
- Mueller, D. J., Bueldt, G. and Engel, A. (1995a) *J. Mol. Biol.*, **249**, 239-243.
- Mueller, D. J., Schabert, F. A., Bueldt, G. and Engel, A. (1995b) *Biophys. J.*, **68**, 1681-1686.
- Muench, W. (1993) *Einfuehrung in die Halbleitertechnologie*, B. G. Teubner, Stuttgart.
- Müller, D. J., Schoenenberger, C.-A., Büldt, G. and Engel, A. (1996) *Biophysical Journal*, **70**, 1796-1802.
- Nollert, P., Kiefer, H. and Jaehnig, F. (1995) *Biophysical Journal*, **69**, 1447-1455.
- Nuzzo, R. G. and Allara, D. L. (1983) *J. Am. Chem. Soc.*, **105**, 4481-4483.
- Oberleithner, H., Schneider, S., Lärmer, J. and Henderson, R. M. (1996) *Kidney and Blood Press Res.*, **19**, 142-147.
- Offord, D. A., John, C. M., Linford, M. R. and Griffin, J. H. (1994) *Langmuir*, **10**, 883-889.
- Palmer, M., Harris, R., Freytag, C., Kehoe, M., Trantum-Jensen, J. and Bhakdi, S. (1998a) *The EMBO Journal*, **17**, 1598-1605.
- Palmer, M., Vulicevic, I., Sawelijev, P., Valeva, A., Kehoe, M. and Bhakdi, S. (1998b) *Biochemistry*, **37**, 2378-2383.
- Pawlenko, S. (1986) *Organosilicon Chemistry*, de Gruyter, Berlin.
- Pearce, K. H., Hiskey, R. G. and Thompson, N. L. (1992) *Biochemistry*, **31**, 5983-5995.
- Plant, A. L. (1993) *Langmuir*, **9**, 2764-2767.
- Plant, A. L., Gueguetchkeri, M. and Yap, W. (1994) *Biophysical Journal*, **67**, 1126-1133.
- Porter, M. D., Bright, T. B., Allara, D. L. and Chidsey, C. E. D. (1987) *J. Am. Chem. Soc.*, **109**, 3559-3568.
- Prime, K. L. and Whitesides, G. M. (1991) *Science*, **252**, 1164-1167.

- Radmacher, M., Fritz, M., Hansma, H. G. and Hansma, P. K. (1994) *Science*, **265**, 1577-1579.
- Rakowska, A., Danker, T., Schneider, S. W. and Oberleithner, H. (1998) *J. Membrane Biol.*, **163**, 129-136.
- Rialdi, G. and Battistel, E. (1996) *Journal of Thermal Analysis*, **47**, 17-25.
- Ringsdorf, H., Schlarb, B. and Venzmer, J. (1988) *Angew. Chem.*, **100**, 117-162.
- Ros, R., Schwesinger, F., Anselmetti, D., Kubon, M., Schäfer, R., Plückthun, A. and Tiefenauer, L. (1998) *Proc. Natl. Acad. Sci. USA*, **95**, 7402-7405.
- Rothman, J. E. and Orci, L. (1996) *Scientific American*, **3**, 50-55.
- Rozsnyai, L. F. and Wrighton, M. S. (1995) *Langmuir*, **11**, 3913-3920.
- Sackmann, E. (1996) *Science*, **271**, 43-48.
- Schabert, F. A., Henn, C. and Engel, A. (1995) *Science*, **268**, 92-94.
- Schoenherr, H., Ringsdorf, H., Jashke, M., Butt, H.-J., Bamberg, E., Allison, H. and Evans, S. D. (1996) *Langmuir*, **12**, 3898-3904.
- Sekiya, K., Satoh, R., Danbara, H. and Futaesaku, Y. (1993) *J. Bacteriol.*, **175**, 5953-5961.
- Sellers, H., Ulman, A., Shnidman, Y. and Eilers, J. E. (1993) *J. Am. Chem. Soc.*, **115**, 9389-9401.
- Sellers, H. L. (1990) *Chem. Phys. Lett.*, **170**, 5.
- Shany, S., Bernheimer, A. W., Grushoff, P. S. and Kim, K. S. (1974) *Mol. Cell. Biochem.*, **3**, 179-186.
- Shao, Z. and Yang, J. (1995) *Quart. Rev. of Biophys.*, **28**, 195-251.
- Sigal, G. B., Bamdad, C., Barberis, A., Strominger, J. and Whitesides, G. M. (1996) *Anal. Chem.*, **68**, 490-497.
- Sigal, G. B., Mrksich, M. and Whitesides, G. M. (1998) *Journal of the American Chemical Society*, **120**, 3464-3473.
- Singh, S. and Keller, D. J. (1991) *Biophysical Journal*, **60**, 1401-1410.
- Singhvi, R., Kumar, A., Lopez, G. P., Stephanopoulos, G. N., Wang, D. I. C., Whitesides, G. M. and Ingber, D. E. (1994) *Science*, **264**, 696-698.
- Spratte, K. (1994) In *physics*, University Mainz, Mainz.
- St. John, P. M. and Craighead, H. G. (1996) *Appl. Phys. Lett*, **68**, 1022-1024.
- Steinem, C., Janshoff, A., Galla, H.-J. and Sieber, M. (1997a) *Bioelectrochemistry and Bioelectronics*, **42**, 213-220.

- Steinem, C., Janshoff, A., Hoehn, F., Sieber, M. and Galla, H.-J. (1997b) *Chemistry and Physics of Lipids*, **89**, 141-152.
- Stelzle, M., Weissmueller, G. and Sackmann, E. (1993) *J. Phys. Chem.*, **97**, 2974-2981.
- Stranick, S. J., Parikh, A. N., Tao, Y. T., Allara, D. L. and Weiss, P. S. (1994) *J. Phys. Chem.*, **98**, 7636-7646.
- Swalen, J. D., Allara, D. L., Andrade, J. D., Chandross, E. A., Garoff, S., Israelachvili, J., McCarthy, T. J., Murray, R., Pease, R. F., Rabolt, J. F., Wynne, K. J. and Yu, H. (1987) *Langmuir*, **3**, 932-950.
- Takeyasu, K., Omote, H., Nettikadan, S., Tokumasu, F., Iwamoto-Kihara, A. and Futai, M. (1996) *FEBS Letters*, **392**, 110-113.
- Tamm, L. K., Böhm, C., Yang, J., Shao, Z., Hwang, J., Edidin, M. and Betzig, E. (1996) *Thin Solid Films*, **284-285**, 813-816.
- Tazi, A., Boussaad, S., deRose, J. A. and Leblanc, R. M. (1996) *J. Vac. Sci. Technol. B*, **14**, 1476-1480.
- Ulman, A. (1996) *Chem. Rev.*, **96**, 1533-1554.
- Vinckier, A., Gervasoni, P., Zaugg, F., Ziegler, U., Lindner, P., Groscurth, P., Plückthun, A. and Semenza, G. (1998) *Biophysical Journal*, **74**, 3256-3263.
- Vinckier, A. and Semenza, G. (1998) *FEBS Letters*, **430**, 12-16.
- Vossen, J. L. and Kern, W. (1978) *Thin Film Processes*, Academic Press, New York.
- Wagner, P. (1995) Swiss Federal Institute of Technology Zuerich, Zuerich.
- Wagner, P., Hegner, M., Kernen, P., Zaugg, F. G. and Semenza, G. (1996a) *Biophys. J.*, **70**, 2052-2066.
- Wagner, P., Kernen, P., Hegner, M., Ungewickell, E. and Semenza, G. (1994a) *FEBS Lett.*, **356**, 267-271.
- Wagner, P., Kernen, P., hegner, M., Ungewickell, E. and Semenza, G. (1994b) *FEBS Letters*, **336**, 267-271.
- Wagner, P., Nock, S., Spudich, A., Volkmuth, W. D., Chu, S., Cicero, R. L., Wade, C. P., Linfood, M. R. and Chidsey, E. D. (1997) *J. of Struct. Biol.*, **119**, 189-201.
- Wagner, P., Zaugg, F. Z., Kernen, P., Hegner, M. and Semenza, G. (1996b) *J. Vac. Sci. Technol. B*, **14**, 1466-1471.
- Walker, P. and Tarn, W. H. (1991) *CRC Handbook of Metal Etchants*, CRC Press.
- Walz, T., Tittmann, P., Fuchs, K. H., Müller, D., Smith, B. L., Agre, P., Gross, H. and Engel, A. (1996) *J. Mol. Biol.*, **264**, 907-918.

- Wang, D., Thomas, S. G., Wang, K. L., Xia, Y. and Whitesides, G. M. (1997a) *Appl. Phys. Lett.*, **70**, 1593-1595.
- Wang, J. H., Kenseth, J. R., Jones, V. W., Green, J. B. D., McDermott, M. T. and Porter, M. D. (1997b) *Journal of the American Chemical Society*, **119**, 12796-12799.
- Weetall, H. H. (1976) *Methods of Enzymology*, **44**, 134.
- Wetzer, B., Pum, D. and Sleytr, U. B. (1997) *Journal of Structural Biology*, **119**, 123-128.
- Wilbur, J. L., Kumar, E. and Whitesides, G. M. (1994) *Adv. Mater.*, **6**, 600-604.
- Williams, L. M., Evans, S. D., Flynn, T. M., Marsh, A., Knowles, P. F., Bushby, R. J. and Boden, N. (1997) *Langmuir*, **13**, 751-757.
- Wirtz, G. P., Brown, S. D. and Kriven, W. M. (1991) *Materials & Manufacturing Processes*, **6**, 87-115.
- Xia, Y., Mrksich, M., Kim, E. and Whitesides, G. M. (1995) *J. Am. Chem. Soc.*, **117**, 9576-9577.
- Xia, Y. and Whitesides, G. M. (1998) *Angew. Chem. Int. Ed.*, **37**, 550-575.
- Yamada, H., Hirata, Y., Hara, M. and Miyake, J. (1994) *Thin Solid Films*, **243**, 445-458.
- Yang, D. F., Wilde, C. P. and Morin, M. (1997) *Langmuir*, **13**, 243-249.
- Zachee, P., Snauwaert, J., Vanderberghe, P., hellemans, L. and Boogaerts, M. (1996) *British J. of Haematology*, **95**, 472-481.
- Ziegler, U., Vinckier, A., Kernen, P., Zeisel, D., Biber, J., Semenza, G., Murer, H. and Groscurth, P. (1998a) *FEBS Lett.*, **436**, 179-184.
- Ziegler, U., Vinckier, A., Kernen, P., Zeisel, D., Biber, J., Semenza, G., Murer, H. and Groscurth, P. (1998b) *FEBS Lett.*, **436**, 179-184.

Acknowledgments

I would like to thank all the people who supported me in the last few years, especially all the people from the Laboratory for Surface Science and Technology and the Institute of Anatomy.

Special thanks go to:

Prof. Dr. G. Semenza, Prof. Dr. N. D. Spencer and Prof. Dr. P. Groscurth for giving me the opportunity to do research with the most possible freedom in a creative environment.

- Prof. Dr. G. Semenza for having given the impulse to many scientists – including me – to get involved in the new, fascinating field of Nanotechnology.
- Prof. Dr. N. D. Spencer for having adopted me in his multi-disciplinary group and letting me discover the full width of Surface Science.
- Prof. Dr. P. Groscurth for his constant interest in my project and the opportunity to work in his Institute.
- Prof. U. W. Suter for co-refereeing.
- The “old-established” Nanobiology group - Dr. Anja Vinckier, Dr. Peter Kernen and Dr. Peter Wagner – for the great time we spent together in the lab and for their friendship.
- Dr. Markus Textor for involving me in many of his very interesting projects.
- Prof. Dr. H. Murer for critical examination of my work.
- Dr. Martina Hirayama for the excellent cooperation in our joint hydrosilane project and her enthusiasm.
- Dr. Urs Ziegler for helping me in many experiments and for introducing me professionally to microscopic techniques.
- Dr. Samuel Brunner for revealing to me the secrets of ellipsometry and FTIR.
- Dr. Otte Homan for introducing me to the world of clean-room silicon technology and also Martin Lanz and Hanspeter Meier for their help in producing silicon masters.
- The Institute of Pharmacy of the ETH Zürich for allowing me to use their extruder and liposome-related equipment.
- Toni Lehmann and Bas van Wieringen for skillful technical assistance.
- Marina Balzers for her sense of humor and ever-present good mood.
- Dr. Anja Vinckier again, for the long hours she spent reading and correcting my dissertation.

Finally, I would like to thank my parents for having given me the chance and possibility to get through all the schools necessary to complete my studies, and my sister Masha for her support. The warmest thank goes to Christine Kohl for standing at my side in the good and bad times, for her many hours spent on corrections, and for her encouragement.

This Project was supported by the Swiss National Science Foundation Project NFP-36 and the O. Mayenfisch Stiftung.

Curriculum Vitae

GENERAL

Name: Frank G. Zaugg
Birthdate: January 3, 1972. Bern, Switzerland
Citizenship: Swiss

EDUCATION

1978-1983 Primary School, Bogotá (Colombia) and Solothurn (Switzerland)

1984-1990 Gymnasium Solothurn and German Gymnasium, Madrid (Spain)

1990-1995 Graduate studies in Biochemistry,
specialisation in biological chemistry
Swiss Federal Institute of Technology (ETHZ), Zürich
(Switzerland)

1995 Masters degree in Natural Sciences (Dipl. Natw. ETHZ)
Diploma thesis at the Institute of Biochemistry II (ETHZ)
(Prof. Dr. G. Semenza, Dr. P. Wagner and Dr. M. Hegner)

1995 (May-Oct.) Research assistant at the Institute of Biochemistry II (ETHZ)

1995 - 1999 Dissertation in Nanotechnology

Laboratory for Surface Science and Technology (ETH Zürich),
and University of Zürich (Switzerland).

Professors: Dr. N. D. Spencer (Surface Science, ETHZ)
Dr. G. Semenza (ETHZ, Biochemistry II)
Dr. P. Groscurth (University Zürich-Irchel)
Dr. H. Murer (University Zürich-Irchel)
